TU/e EINDHOVEN UNIVERSITY OF TECHNOLOGY

A structural investigation of supported small metal particles and the metal-support interface with EXAFS

Citation for published version (APA):
Zon, van, F. B. M. (1988). *A structural investigation of supported small metal particles and the metal-support interface with EXAFS*. [Phd Thesis 1 (Research TU/e / Graduation TU/e), Chemical Engineering and Chemistry]. Technische Universiteit Eindhoven. https://doi.org/10.6100/IR293822

DOI:
10.6100/IR293822

Document status and date:
Published: 01/01/1988

Document Version:
Publisher's PDF, also known as Version of Record (includes final page, issue and volume numbers)

Please check the document version of this publication:

• A submitted manuscript is the version of the article upon submission and before peer-review. There can be important differences between the submitted version and the official published version of record. People interested in the research are advised to contact the author for the final version of the publication, or visit the DOI to the publisher's website.
• The final author version and the galley proof are versions of the publication after peer review.
• The final published version features the final layout of the paper including the volume, issue and page numbers.

Link to publication

General rights
Copyright and moral rights for the publications made accessible in the public portal are retained by the authors and/or other copyright owners and it is a condition of accessing publications that users recognise and abide by the legal requirements associated with these rights.

• Users may download and print one copy of any publication from the public portal for the purpose of private study or research.
• You may not further distribute the material or use it for any profit-making activity or commercial gain
• You may freely distribute the URL identifying the publication in the public portal.

If the publication is distributed under the terms of Article 25fa of the Dutch Copyright Act, indicated by the "Taverne" license above, please follow below link for the End User Agreement:

www.tue.nl/taverne

Take down policy
If you believe that this document breaches copyright please contact us at:

openaccess@tue.nl

providing details and we will investigate your claim.

Download date: 04. Oct. 2023

A Structural Investigation of Supported Small Metal Particles and the Metal-Support Interface with EXAFS

Fanny van Zon

A Structural Investigation of Supported Small Metal Particles and the Metal-Support Interface with EXAFS

PROEFSCHRIFT

ter verkrijging van de graad van doctor aan de Technische Universiteit Eindhoven, op gezag van de rector magnificus, prof. ir. M. Tels, voor een commissie aangewezen door het college van decanen in het openbaar te verdedigen op dinsdag 22 november 1988 te 14.00 uur

door

Fanny van Zon
geboren te Voorschoten

Dit proefschrift is goedgekeurd door de promotoren:

prof. dr. ir. D. C. Koningsberger
en
prof. dr. R. A. van Santen

All that we see or seem
is just a dream within a dream

(E. A. Poe)

Contents

1	**Introduction**	1
1.1	Historical Development of EXAFS	1
1.2	EXAFS in Eindhoven	1
1.2.1	The Metal-Support Interaction	1
1.2.1.1	$Rh/\gamma\text{-}Al_2O_3$	2
1.2.1.2	Rh/TiO_2	3
1.2.2	The Adsorption of Gases	4
1.2.2.1	Catalysts after Evacuation	5
1.2.2.2	Adsorption of O_2	5
1.2.2.3	Adsorption of CO	6
1.3	Scope and Outline of this Thesis	7
1.3.1	The Metal-Support Interaction	7
1.3.2	Particle Morphology	8
1.3.3	H_2 Chemisorption	8
2	**Theory**	11
2.1	The EXAFS Technique	11
2.2	EXAFS Data Analysis	13
2.2.1	Data Reduction	13
2.2.2	EXAFS Formulation	15
2.2.3	Experimentally Determined Phase Shift and Backscattering Amplitude	16
2.2.4	Phase- and/or Amplitude-Corrected Fourier Transformation	18
2.2.5	The Difference File Technique	20
2.2.6	Higher Shell Analysis	20

2.3	Multiple Scattering	21
2.3.1	Adapted EXAFS Formulation	21
2.3.2	Use of Experimental References	22
2.4	References	24
3	**The Structure of Alumina-Supported Osmium Clusters after Chemisorption and Decomposition**	26
3.1	Introduction	26
3.2	Experimental	30
3.2.1	Materials and Catalyst Preparation	30
3.2.2	Infrared Spectroscopy	30
3.2.3	EXAFS	31
3.3	Results	31
3.3.1	The Os-CO Reference	31
3.3.2	Triosmium Clusters Chemisorbed on γ-Al_2O_3	35
3.3.3	Broken-up Clusters on γ-Al_2O_3	39
3.4	Discussion	43
3.4.1	Methods of Data Analysis and Reference Compounds	43
3.4.2	The Os-CO Reference	44
3.4.3	Assessment of the Structural Models	46
3.4.4	Perspectives on EXAFS of Supported Organometallics and Small Metal Clusters	47
3.5	References	49
4	**Structural Characterization of $[H_xRe_3(CO)_{12}]^{x-3}$ (x = 2 or 3) by Extended X-ray Absorption Fine Structure Spectroscopy**	51
4.1	Introduction	51
4.2	Experimental	52

4.3	Data Analysis and Results	53
4.3.1	Data Reduction	53
4.3.2	Reference Compounds	54
4.3.3	Analysis of the Data Characterizing $H_3Re_3(CO)_{12}$ and $[H_2Re_3(CO)_{12}]^-$	56
4.4	Discussion	61
4.5	References	64
5	**An EXAFS Study of the Structure of $Ir_4(CO)_{12}$ Adsorbed on Partially Dehydrated γ-Al_2O_3: Applicability as a Model for Reduced Ir/γ-Al_2O_3 Catalysts**	66
5.1	Introduction	66
5.2	Experimental	67
5.2.1	Sample Preparation	67
5.2.2	IR Measurements	67
5.2.3	TPD/MS Measurements	67
5.2.4	EXAFS Measurements	68
5.3	Results	68
5.3.1	IR Experiments	68
5.3.2	TPD/MS Experiments	69
5.3.3	EXAFS Results and Data Analysis	71
5.3.3.1	Reference Compounds	71
5.3.3.2	$Ir_4(CO)_{12}$ Adsorbed on γ-Al_2O_3	75
5.4	Discussion	79
5.4.1	Structural Changes in $Ir_4(CO)_{12}$ upon Adsorption	79
5.4.2	Model of the Surface Structure	81
5.4.3	Applicability of $Ir_4(CO)_{12}/\gamma$-Al_2O_3 as a Model for Reduced Ir/γ-Al_2O_3	83
5.5	Conclusions	85

5.6	References	85
6	**Metal Particle Morphology and Structure of the Metal-Support Interface in Ir/γ-Al_2O_3 Catalysts Studied by EXAFS Spectroscopy**	88
6.1	Introduction	88
6.2	Experimental	90
6.2.1	Catalyst Preparation	90
6.2.2	EXAFS Measurements	91
6.3	Results	93
6.3.1	Analysis of the First Shell Data	94
6.3.2	Analysis of the Higher Shell Data	100
6.4	Discussion	107
6.4.1	Nature of the Metal-Support Bonding	107
6.4.2	The Carbonaceous Overlayer in $Ir_4(CO)_{12}$-derived Ir/γ-Al_2O_3	108
6.4.3	Determination of the Particle Morphology	109
6.4.4	Structure of the Metal-Support Interface	113
6.5	Conclusions	116
6.6	References	117
7	**A Structural Characterization of the Metal-Support Interface in the Reduced Ir/MgO and Rh/MgO Catalyst Systems with EXAFS**	120
7.1	Introduction	120
7.2	Experimental	121
7.2.1	Catalyst Preparation	121
7.2.2	EXAFS Measurements	122
7.3	Data Analysis and Results	123
7.3.1	Analysis of the Ir/MgO Data	125

7.3.2	Analysis of the Rh/MgO Data	128
7.4	Discussion	131
7.4.1	Particle Size in the Reduced Systems	131
7.4.2	The Metal-Support Interface	133
7.5	Conclusions	136
7.6	References	136
8	**Determination of the Metal Particle Size in Rh, Ir, and Pt Catalysts by Hydrogen Chemisorption and EXAFS**	138
8.1	Introduction	138
8.2	Experimental	140
8.2.1	Preparation of the Catalysts	140
8.2.2	Hydrogen Chemisorption Measurements	140
8.2.3	EXAFS Measurements	140
8.3	Results	141
8.3.1	Hydrogen Chemisorption Measurements	141
8.3.2	EXAFS Measurements	144
8.3.3	Model Calculations	147
8.4	Discussion	152
8.5	References	158
9	**Determination of Metal Particle Size in Partly Reduced Ni Catalysts by Hydrogen/Oxygen Chemisorption and EXAFS**	163
9.1	Introduction	163
9.2	Experimental	163
9.2.1	Catalyst Preparation	163
9.2.2	Chemisorption Measurements	164
9.2.3	EXAFS Measurements	165

9.3	Data Analysis Results	166
9.4	Discussion	168
9.5	References	173
10	**Concluding Remarks**	175
10.1	Original Scope of this Ph. D. Study	175
10.2	The Metal-Support Interaction	175
10.2.1	Formation of the Metal-Support Interface	175
10.2.2	Metal Carbonyl Clusters as Model Systems	177
10.2.3	Other Metal-Support Combinations	178
10.3	Particle Morphology	179
10.4	H_2 Chemisorption	180
10.5	References	181
Samenvatting		182
List of Publications		186
Dankwoord		189
Curriculum Vitae		190

Chapter One

Introduction

1.1 Historical Development of EXAFS

Kronig (in 1931[1]) was the first to report the presence of fine structure in the X-ray absorption spectrum just above the absorption edge. This fine structure is called EXAFS (Extended X-ray Absorption Fine Structure). For years, EXAFS remained an interesting phenomenon of which the theoretical background was not unanimously agreed on. In fact, EXAFS became useful only in the 1970s, when Stern, Lytle, and Sayers introduced an adequate mathematical treatment of the EXAFS spectra,[2-4] which made it possible to extract structural information from the EXAFS data. Since then, EXAFS has proved to be a useful tool to obtain information about the atomic local structure of components in dilute systems, and of disordered systems. Applications are many in the fields of amorphous materials, biological systems, and catalysis.

1.2 EXAFS in Eindhoven

The EXAFS technique was introduced in Eindhoven by D. C. Koningsberger and R. Prins. Working in the Laboratory for Inorganic Chemistry and Catalysis, their attention was mainly focused on the structure of metal particles in supported metal catalysts. In 1980, the first Ph. D. students started on EXAFS research (H. F. J. Van 't Blik[5] and J. B. A. D. Van Zon[6]). J. H. A. Martens[7] followed in 1983, F. W. H. Kampers and F. B. M. Duivenvoorden in 1984.

1.2.1 The Metal-Support Interaction

Supported metal catalysts are widely used. One of the functions of the support is obtaining and keeping a good dispersion of the catalytically active metal. For many applications, it is tried to obtain metal particles

which are as small as possible, because only the metal surface is catalytically active. At higher temperatures and under the influence of gases, the small metal particles tend to coalesce, thus resulting in the loss of available surface area. Knowledge of the interaction between metal and support is essential to help solve problems in obtaining and keeping supported metal catalysts highly dispersed. EXAFS is a very suitable technique to study the metal-support interaction.

1.2.1.1 $Rh/\gamma\text{-}Al_2O_3$

As well as its advantages, the EXAFS technique has its limitations. One of the main difficulties encountered in the study of catalysts with EXAFS, is that most interesting contributions (like those from the metal-support or the metal-gas interface) are often obscured by a large contribution from the metal-metal interaction in the supported metal particles. In order to obtain accurate information about e. g. the metal-support interaction, a catalyst has to be used with very small metal particles. Such a catalyst was $Rh/\gamma\text{-}Al_2O_3$.[8,9] Rh-Rh coordination numbers as low as N = 3.7 were determined (corresponding to particle sizes as small as 7 Å). For these small particles, the metal-support contribution is large enough (with respect to the metal-metal contribution) to allow accurate determination of the coordination parameters in the metal-support interface. In the data analysis procedure, phase- and amplitude-corrected Fourier transforms were used to identify the neighbouring atoms, and the difference file technique was employed to reliably extract the contribution of the metal-support interface from the EXAFS data.[6,8,9]

The coordination parameters obtained in this way showed that the first coordination shell in the $Rh\text{-}Al_2O_3$ interface consists of $Rh\text{-}O_{support}$ neighbours. Rather unexpectedly, a bond distance of R $\sim$ 2.70 Å was determined, instead of an oxide-like Rh-O distance of R $\sim$ 2.05 Å. This long $Rh\text{-}O_{support}$ distance was then explained by a $Rh^0\text{-}O^{2-}$ interaction, the sum of the Rh^0 and O^{2-} radii being roughly equal to 2.70 Å. Since in the three-dimensional metal particles not all Rh atoms are in contact with the support, the EXAFS coordination number for the $Rh\text{-}O_{support}$ contribution (which is averaged over all Rh atoms in the sample) has to be corrected in order to yield the real coordination of the Rh atoms in the metal-support interface. Assuming that the metal particles are half-spherical in shape, the

Rh atoms in the interface were determined to be coordinated to two or three surface oxygen atoms.

Recently, theoretical calculations were performed on the Rh-Al_2O_3 interface.[7,10] Assuming an interface along the fcc (111) plane, it was shown that on a hydroxylated γ-Al_2O_3 surface with the metal particles resting on hydroxyl groups a threefold Rh-$O_{support}$ coordination is most stable, with a Rh-O distance of R $\sim$ 2.55 Å. These results compare very well with the experimental ones, because the EXAFS experiments were carried out after in situ reduction in a H_2 atmosphere, under which conditions the γ-Al_2O_3 surface is expected to be fully hydroxylated. Thus it seems that the long Rh-$O_{support}$ distance can be explained by a Rh^0-OH^- interaction. However, it is also possible that the Rh-$O_{support}$ coordination distance is influenced by electronic changes in the supported metal particles due to adsorbed hydrogen, or by the presence of hydrogen in the interface. Further experiments still must be performed in order to decide between the alternative explanations.

1.2.1.2 Rh/TiO_2

Contrary to γ-Al_2O_3, TiO_2 as a support can be reduced at moderately low temperatures (T $\sim$ 600 K). The (partly) reduced support influences the gas adsorption properties of the supported metal particles. In catalysts this effect is known as SMSI (Strong Metal-Support Interaction). Thus two kinds of systems can be studied: Rh/TiO_2 in which TiO_2 is not reduced (normal state), or partly reduced (SMSI state).

After reduction at 473 K, only the Rh metal has been reduced. Small metal particles were obtained, having a Rh-$O_{support}$ interaction (with R = 2.72 Å,[11] thus a long Rh-$O_{support}$ distance) just like Rh/γ-Al_2O_3. The first Rh/TiO_2 catalysts studied were prepared from $RhCl_3$. Especially after reduction at low temperatures, Cl atoms remain in the catalyst near the Rh particles, and their contribution in the EXAFS spectrum influences the determination of the coordination parameters for the other contributions. Therefore subsequent studies were carried out with Rh/TiO_2 catalysts prepared from $Rh(NO_3)_3$.[12,13] Very small metal particles were obtained after reduction at 473 K, with a Rh-Rh coordination number of 3.2 in the metallic particles. In this case, a Rh-$O_{support}$ contribution was detected with R = 2.78 Å. HRTEM (High-Resolution Transmission Electron Microscopy)

confirmed the average metal particle size obtained from EXAFS. It also showed that the Rh particles were present on the edges of the TiO_2 anatase crystallites and their (101) faces. The edges may perhaps be considered as small (001) faces. Thus, assuming that the metal particles rest on the anatase (001) and (101) faces, and using the EXAFS results, a Rh-TiO_2 interface could be modelled in which the Rh atoms are fourfold coordinated by support oxygen atoms at R = 2.78 Å.

Evidence for Rh-Ti contributions was not found until after reduction at 723 K. The catalyst was then in the SMSI state. The Rh-Ti contributions apparently were not due to Rh-Ti alloy formation, and therefore were attributed to Rh-Ti^{n+} interactions in the metal-support interface. Rh-Rh and Rh-$O_{support}$ coordination numbers had not changed significantly with respect to the sample reduced at 473 K. This indicates that coverage of the Rh particles with TiO_x suboxides does not take place to a significant extent. The enhanced presence of Ti neighbours after reduction at 723 K was explained by assuming that preferably TiO_2 near the metal particles is reduced to TiO_x. This process involves removal of TiO_2 oxygen as water. As a result Ti ions are exposed at the surface, which will be energetically more stable if they migrate to vacant positions nearer the metal particles. Although no changes in Rh-Rh and Rh-$O_{support}$ coordination numbers were observed, the bond length of both contributions had decreased markedly (the Rh-Rh bond decreased from R = 2.687 Å to R = 2.634 Å, and the Rh-$O_{support}$ bond from R = 2.78 Å to even R = 2.60 Å). The decrease in Rh-Rh bond length may be explained by the absence of adsorbed hydrogen (see Section 1.2.2.1), the decrease in Rh-$O_{support}$ bond length clearly indicates that the metal-support bonding has become stronger after reduction at 723 K.

1.2.2 The Adsorption of Gases

Knowledge of the influence of adsorption of gases on the structural properties of supported metal particles, and especially of the different behaviour of various catalysts, may give more insight in the differences in catalytic behaviour. Since our group studied supported metal catalysts usually after reduction, in a H_2 atmosphere, also interesting information about the influence of adsorbed hydrogen can be obtained by evacuating the samples.

1.2.2.1 Catalysts after Evacuation

Evacuation of reduced Rh/γ-Al_2O_3 results in a marked contraction of the Rh-Rh bond length (from R = 2.68 Å to R ~ 2.63 Å).[13,14] The same effect on the Rh-Rh bond has been observed when the reduced sample is measured under He.[6] In both cases, the contraction can be explained by the absence of covering hydrogen. Apparently, coordination by hydrogen is very much like coordination by metal atoms. In a H_2 atmosphere the surface metal atoms, which have an unsaturated first metal-metal coordination shell with respect to the bulk, obviously are structurally compensated by chemisorbed hydrogen atoms, since the metal-metal bond distance remains approximately equal to the bulk distance. When the hydrogen is removed, however, the metal-metal bonds contract in order to counteract the effects of unsaturation.

For Rh/TiO_2, reduced at 723 K but without any evacuation, the same contraction of the Rh-Rh bond length was observed as described above.[13] Subsequent evacuation at 623 K did not change the Rh-Rh coordination distance. It can thus be concluded that already in the SMSI state the Rh particles are not covered with hydrogen.

1.2.2.2 Adsorption of O_2

Admission of oxygen at room temperature already may lead to complete oxidation of the supported metal particles for most metals. In order to study the first stages of O_2 adsorption, it is imperative that oxygen is admitted at low temperatures.

In a study of Rh/γ-Al_2O_3, oxygen was admitted at 100 K after reduction and evacuation.[13,15] Already at this low temperature, partial oxidation occurs, which can be observed in a decrease of the Rh-Rh, and an increase of the Rh-O^{2-} coordination number. Careful modelling[15] showed that the results can be interpreted as 'peeling off' the outermost Rh metal atoms. The remaining metal kernel stays in contact with the formed oxide, having the same type of metal-oxygen bonds in the interface with the oxide as with the γ-Al_2O_3 support. Subsequent heating to 300 K under oxygen resulted in nearly complete oxidation of the Rh metal particles. Only small kernels of metal atoms remain, almost completely covered by rhodium oxide, but still having surface metal atoms available for adsorption of

gases. Thus this explains why passivated supported metal catalysts can be so easily reduced, sometimes already at room temperature, since metal atoms are available for dissociation of H_2.

Entirely different results are obtained for the oxygen adsorption of a Rh/TiO_2 catalyst in the SMSI state. After reduction at 723 K, evacuation at 623 K, and oxygen admission at 100 K, no changes were observed in the Rh-Rh coordination with respect to the reduced situation, indicating that no oxidation had taken place. The only effect of oxygen admission was the presence of an extra Rh-O contribution at R = 2.09 Å. This was attributed to oxygen adsorbed on the metal surface. Heating the sample to 300 K still does not result in oxidation of the metal particles. However, the Rh-Ti contributions now have decreased, indicating that the TiO_x suboxide around the metal particles has been reoxidized.

1.2.2.3 Adsorption of CO

Chemisorption of CO is a very important aspect in the catalysis of synthesis gas (CO + H_2) reactions. Depending on the type of adsorption (dissociative or non-dissociative) mainly C_nH_m, or $C_nH_mO_q$ products are expected.

The non-dissociative chemisorption of CO on $Rh/\gamma\text{-}Al_2O_3$ catalysts at room temperature has been extensively studied by our group.[14,16] It was shown that in the case of small Rh particles, CO causes complete disruption of the metal particles.[16] As a result, $Rh^I(CO)_2$ entities are formed on the $\gamma\text{-}Al_2O_3$ surface, bonded to the surface by three $Rh\text{-}O_{support}$ bonds with R = 2.12 Å. In catalysts with a larger average metal particle size the same process does occur,[14] but now disruption is not complete because after CO admission still a Rh-Rh contribution is detected. These results can be explained if it is assumed that not all Rh particles are equal in size. In the case of a particle size distribution, small particles will still be disrupted by CO, whereas the larger particles adsorb CO without fragmentation.

For Rh/TiO_2, having the same initial average metal particle size as one of the $Rh/\gamma\text{-}Al_2O_3$ catalysts with larger metal particles,[14] chemisorption of CO was observed to have the same effect.[11,17] Disruption to $Rh^I(CO)_2$ occurred only for the smallest particles. Bonding of these entities to the TiO_2 support was of the same type as that observed in $Rh/\gamma\text{-}Al_2O_3$: three

$Rh\text{-}O_{support}$ bonds at R = 2.12 Å.

1.3 Scope and Outline of this Thesis

The results discussed in Section 1.2 are described in the Theses of H. F. J. Van 't Blik,[5] J. B. A. D. Van Zon,[6] and J. H. A. Martens.[7] Of these results, the new findings concerning the structure of the metal-support interface in $Rh/\gamma\text{-}Al_2O_3$, and the influence of CO chemisorption on the structure of $Rh/\gamma\text{-}Al_2O_3$ were the most outstanding in 1984 when I started with my Ph. D. EXAFS research. The research goals were centered on improving the knowledge concerning the metal-support interaction. It was still felt that with EXAFS data of better quality a more detailed picture could be obtained of the structure of the metal-support interface. It was also of great interest to study other metals on different types of supports, in order to investigate whether the results obtained for the metal-support interface in $Rh/\gamma\text{-}Al_2O_3$ could be generalized for other metal-support combinations.

1.3.1 The Metal-Support Interaction

Several methods were attempted to obtain more information about the metal-support interaction. In the first place, metal carbonyls were used as a precursor for supported metal catalysts. Adsorption of metal carbonyls onto a support can result in a system with uniform metal entities, for which also the metal-support interaction is uniquely defined. In principle, such a supported carbonyl system can be studied more accurately with EXAFS than the catalysts described in Section 1.2. Subsequent reduction of the supported complex provides an opportunity to follow the formation of the metal-support interface in the metal particle. Results for Al_2O_3-supported $Ir_4(CO)_{12}$, and reduced $Ir/\gamma\text{-}Al_2O_3$ obtained from this supported $Ir_4(CO)_{12}$ system, are discussed in Chapters 5 and 6. The reduced $Ir/\gamma\text{-}Al_2O_3$ catalyst proved to be an excellent system for further study of the metal-support interface, because also higher metal-support oxygen shells could be detected.

Supported metal carbonyls were also examined without subsequent reduction. Special attention has been paid here to the number of CO ligands lost in the adsorption of $Os_3(CO)_{12}$ on γ-Al_2O_3, and subsequent decomposition. Also the influence of bonding to the support on the metal-carbonyl bonds has been studied (Chapter 3). The EXAFS results on unsupported $[H_xRe_3(CO)_{12}]^{x-3}$ (x = 2 or 3) are discussed in Chapter 4. These systems have been studied in order to obtain accurate information about the effects influencing the metal-carbonyl bonding. The studies concerning the metal carbonyl complexes mentioned in Chapters 3 and 4 were carried out in close collaboration with the group of prof. B. C. Gates from Delaware, U. S. A.

In the last place, also new metal-support combinations were studied with EXAFS: as already mentioned, reduced Ir/γ-Al_2O_3 (Chapter 6), and further Rh/MgO and Ir/MgO (Chapter 7).

1.3.2 Particle Morphology

Quantification of the metal-support interaction (viz. determining the exact metal-support epitaxy) often is only possible if more is known about the particle morphology. The metal particles in supported metal catalysts are usually assumed to be half-spherical in shape. In Chapter 6, Ir/γ-Al_2O_3 catalysts derived from $Ir_4(CO)_{12}$ and $IrCl_3$ are compared. With EXAFS, differences in the higher metal-metal shells have been detected which can be attributed to a different particle morphology in the two systems.

1.3.3 H_2 Chemisorption

EXAFS analysis of the first metal-metal shell in supported metal catalysts yields a fairly accurate estimate of the average metal particle size. For many metals, the same information can be more easily obtained by measuring the H_2 chemisorption capacity. For group VIII metals like Rh, Ir, and Pt, however, the exact metal-to-hydrogen adsorption stoichiometry is not known. By correlating the H_2 chemisorption measurements with the EXAFS results, the H_2 chemisorption results can be calibrated. In Chapter 8, this has been done for fully reduced, supported systems with Rh, Ir, and Pt, while in Chapter 9 supported systems with Ni (both fully and partly reduced) are studied.

1.4 References

(1) R. de L. Kronig, *Z. Physik* **1931**, *70*, 317.

(2) D. E. Sayers, F. W. Lytle, and E. A. Stern, *Adv. X-ray Anal.* **1970**, *13*, 248.

(3) D. E. Sayers, E. A. Stern, and F. W. Lytle, *Phys. Rev. Lett.* **1971**, *27*, 1204.

(4) E. A. Stern, *Phys. Rev. B* **1974**, *10*, 3027.

(5) H. F. J. Van 't Blik, *Thesis*; Eindhoven University of Technology, Eindhoven, The Netherlands, 1984.

(6) J. B. A. D. Van Zon, *Thesis*; Eindhoven University of Technology, Eindhoven, The Netherlands, 1984.

(7) J. H. A. Martens, *Thesis*; Eindhoven University of Technology, Eindhoven, the Netherlands, 1988.

(8) D. C. Koningsberger, J. B. A. D. Van Zon, H. F. J. Van 't Blik, G. J. Visser, R. Prins, A. N. Mansour, D. E. Sayers, D. R. Short, and J. R. Katzer, *J. Phys. Chem.* **1985**, *89*, 4075.

(9) J. B. A. D. Van Zon, D. C. Koningsberger, H. F. J. Van 't Blik, and D. E. Sayers, *J. Chem. Phys.* **1985**, *82*, 5742.

(10) J. H. A. Martens, R. A. Van Santen, D. C. Koningsberger, and R. Prins, *Catalysis Lett.* submitted.

(11) D. C. Koningsberger, H. F. J. Van 't Blik, J. B. A. D. Van Zon, and R. Prins, *Proc. 8th Int. Congress on Catalysis* (Berlin, 1984); Verlag Chemie: Weinheim, 1985; Vol. V, p 123.

(12) D. C. Koningsberger, J. H. A. Martens, R. Prins, D. R. Short, and D. E. Sayers, *J. Phys. Chem.* **1986**, *90*, 3047.

(13) J. H. A. Martens, R. Prins, H. Zandbergen, and D. C. Koningsberger, *J. Phys. Chem.* **1988**, *92*, 1903.

(14) H. F. J. Van 't Blik, J. B. A. D. Van Zon, D. C. Koningsberger, and R. Prins, *J. Mol. Catal.* **1984**, *25*, 379.

(15) J. H. A. Martens, R. Prins, and D. C. Koningsberger, *J. Phys. Chem.* accepted.

(16) H. F. J. Van 't Blik, J. B. A. D. Van Zon, T. Huizinga, J. C. Vis, D. C. Koningsberger, and R. Prins, *J. Am. Chem. Soc.* **1985**, *107*, 3139.

(17) D. C. Koningsberger, *EXAFS and Near Edge Structure III* (Proc. 3rd Int. EXAFS Conference, Stanford, 1984); K. O. Hodgson, B. Hedman, and J. E. Penner-Hahn, Eds.; Springer Verlag: Berlin, 1984; p 212.

Chapter Two

Theory

2.1 The EXAFS Technique

EXAFS (Extended X-ray Absorption Fine Structure) Spectroscopy is a spectroscopic technique to obtain information about the local structure around the atoms of a specific element in a sample. Its physical background is the absorption of an X-ray photon by the atoms of that specific element in the sample, which results in the removal of an electron, usually from the K or L shell. The energy of the monochromatic X-rays is determined by the absorber element.

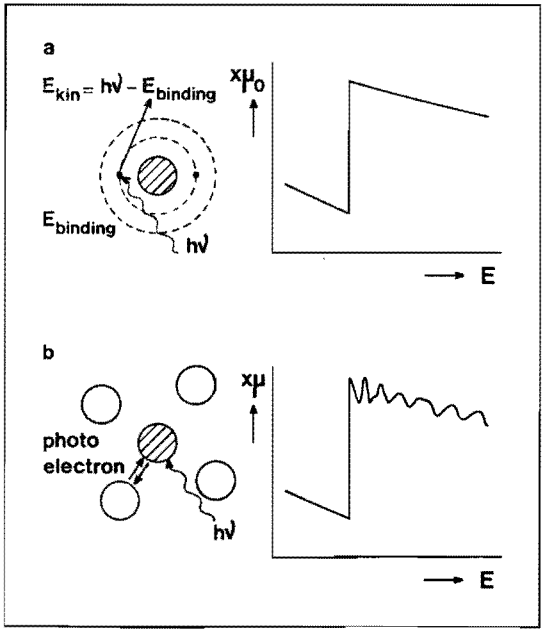

Figure 2.1. The EXAFS process: (a) absorption of X-rays by a monatomic gas: no EXAFS; and (b) absorption of X-rays by atoms in a lattice: generation of EXAFS.

A photoelectron with $E_{kin} = h\nu - E_{binding}$ is emitted by the absorber atom which is scattered by neighbouring atoms. The scattered photoelectron wave produces interferences with the original outgoing photoelectron wave. These interferences that vary as a function of E_{kin} of the photoelectron and thus with the energy of the incoming X-rays, are observed as a ripple on the high-energy side of the absorption edge. The EXAFS process is illustrated in Figure 2.1. A typical EXAFS spectrum (Pt foil, L_{III} edge = 11564 eV) is shown in Figure 2.2.

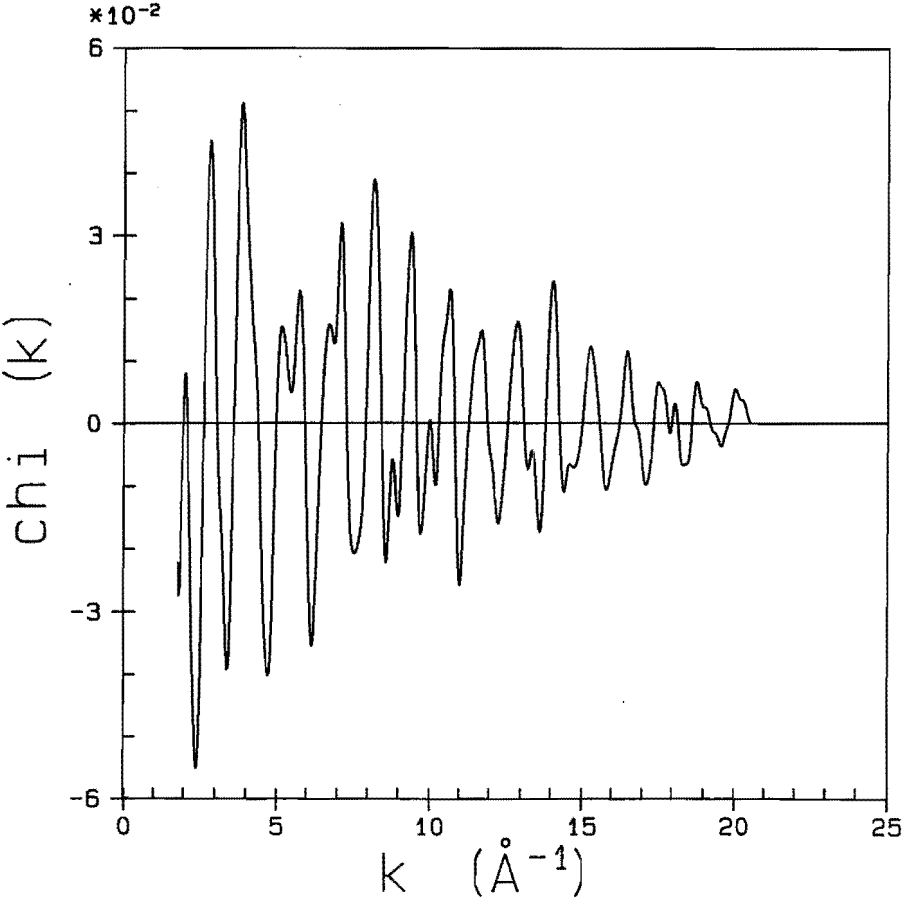

Figure 2.2. L_{III} edge EXAFS of Pt foil (E = 11564 eV) measured at 77 K, on Wiggler station 9.2 at the SRS (Daresbury, U. K.).

2.2 EXAFS Data Analysis

The method of EXAFS data analysis as used throughout this Thesis, and underlying principles, have been extensively discussed by J. B. A. D. Van Zon[1] and J. H. A. Martens.[2] For more information the reader is therefore referred to these Theses.

2.2.1 Data Reduction

To obtain structural information from the measured X-ray absorption spectrum, several steps of data processing have to be performed:

- subtraction of that part of the total X-ray absorption by the sample which does not lead to removal of the high-energy electrons, specific for the edge under study. A quadratic function is fitted to the pre-edge region (see Figure 2.3a) which is subsequently subtracted from the experimental data (Figure 2.3b).
- determination of the unperturbed absorption of the absorber atoms in the sample (i. e. the absorption profile of these atoms if they would not have any neighbours). This unperturbed absorption (called background) at the high-energy side of the edge is simulated with a cubic spline function[3] (see Figure 2.3b). The correctness of the cubic spline is determined both from the derivative of the background (which should not be too smooth, and neither should exhibit EXAFS residues), and the Fourier transform of the resultant EXAFS (in which background peaks at low r values should be minimized, while the first shell peak should be as large as possible).
- the edge position is determined as the energy at which the first inflection point in the edge occurs. The edge height is determined as the difference between the extrapolated pre-edge curve and the cubic spline function at approx. 30 eV from the edge (see Figure 2.3c). This makes it possible to normalize two files at the same energy in the same way, which is necessary if reference compounds are used for determining the phase and backscattering amplitude.
- the cubic spline curve is subtracted from the data past the edge, whereafter the remaining signal is divided by the edge height, to obtain the EXAFS signal on a per atom basis, in order to make a comparison

with other spectra possible (see Figure 2.3d).

- sometimes sudden discontinuities (jumps) and spurious sharp peaks (glitches) are observed in the measured signal that are not part of the EXAFS. They may be due to some small irregularities during the EXAFS recording, or are caused by the X-ray monochromator. These irregularities are removed as well as possible before background (cubic spline) subtraction. Jumps are removed by adding or subtracting a constant

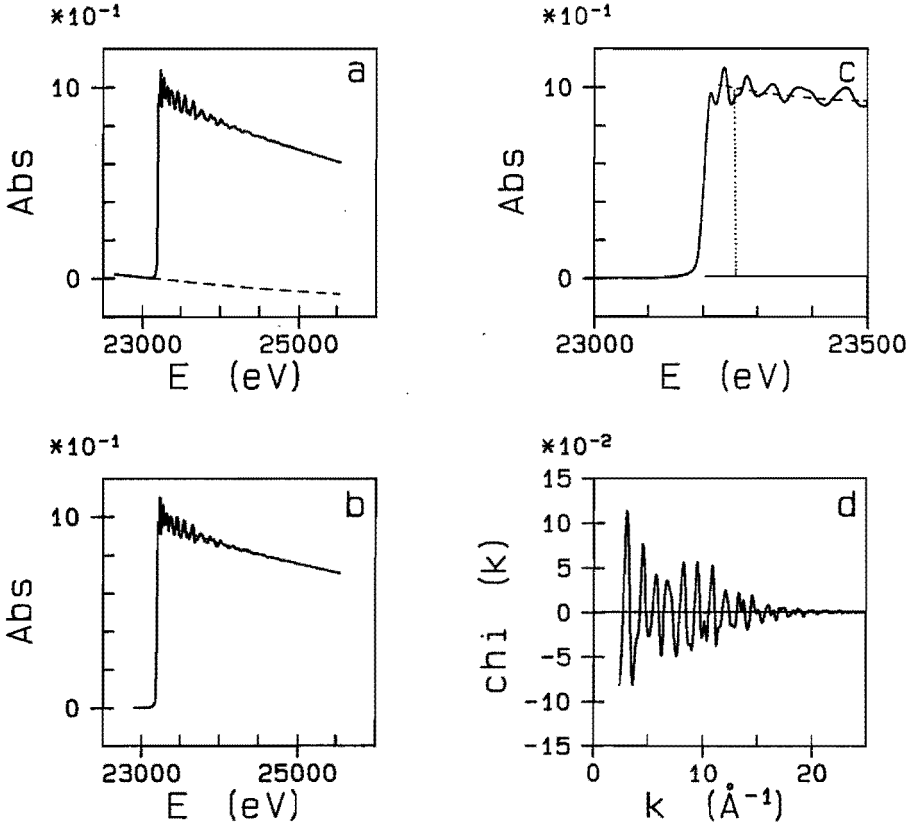

Figure 2.3. (a) The K edge EXAFS of Rh foil (—), and quadratic fit to the pre-edge region (— —); (b) Rh foil EXAFS from (a), with quadratic function removed (—), and cubic spline background (— —); (c) as (b), illustration of edge height determination (· · ·); and (d) EXAFS signal of Rh foil after all data reduction steps.

value to/from the data points after the jump. Glitches are removed by fitting a n-polynomial to good data points just before and after the glitch. The glitch data points are removed and replaced by the polynomial.

2.2.2 EXAFS Formulation

A general expression for the measured EXAFS $\chi(k)$ has been given by Stern et al.[4-6] If it is assumed that only single scattering processes are important, the EXAFS signal can be expressed by:

$$\chi(k) = \sum_j A_j(k) \sin (2kR_j + \phi_j(k)) \qquad (2.1)$$

The EXAFS function is a superposition of contributions from different coordination shells; the index j refers to the jth coordination shell. R_j is the average coordination distance between the absorbing atom and the neighbouring atoms in the jth coordination shell, $\phi_j(k)$ is the phase shift which the photoelectron experiences during the scattering process, and $A_j(k)$ is the amplitude function, which is expressed as:

$$A_j(k) = \frac{N_j}{kR_j^2} S_0^2(k) F_j(k) e^{-2k^2\sigma_j^2} e^{-2R_j/\lambda(k)} \qquad (2.2)$$

N_j is the average number of scatterer atoms in the jth coordination shell. σ_j^2 is the mean square deviation about the average coordination distance R_j (caused by thermal motion and/or static disorder). $F_j(k)$ is the backscattering amplitude characteristic of a particular type of neighbouring atom. $S_0^2(k)$ is a correction for the relaxation of the absorbing atom and multielectron excitations.[3] $\lambda(k)$ is the mean free path of the photoelectron. The expression is valid for the case of small disorder with a Gaussian pair distribution function.[7-10]

In order to separate the contributions from different coordination shells, the EXAFS function $\chi(k)$ is Fourier transformed. The Fourier transform $\theta_n(r)$ is expressed by:

$$\theta_n(r) = \frac{1}{(2\pi)^{1/2}} \int_{k_{min}}^{k_{max}} k^n \chi(k) e^{2ikr} dk \qquad (2.3)$$

A k^n weighting (usually n = 1, 2 or 3) is used to equalize the envelope of $\chi(k)$ over the transformation range, with n depending on the amplitude variation. k_{max} is determined by the signal-to-noise ratio of the measured signal. The function $\theta_n(r)$ will contain peaks which are related to the actual coordination distances R_j, but these peaks are shifted toward lower r values due to the influence of the phase shift $\phi_j(k)$ in eq 2.1.[11] Values for R and N of a shell of scatterer atoms *j* can be found when the phase shift $\phi_j(k)$ and backscattering amplitude $F_j(k)$ for the absorber-scatterer pair are known; $\phi_j(k)$ and $F_j(k)$ can be calculated theoretically,[12] or can be extracted from EXAFS data for a reference compound with known structure.

2.2.3 Experimentally Determined Phase Shift and Backscattering Amplitude

To obtain the phase shift and backscattering amplitude experimentally, the EXAFS data of a reference compound are Fourier transformed according to eq 2.3. In the resulting spectrum in r space, the peak representing the atoms for which a reference is needed is back transformed to k space between suitable values of R_{min} and R_{max}:

$$k^n\chi(k) = \frac{1}{(2\pi)^{1/2}} \int_{R_{min}}^{R_{max}} \theta_n(r)\, e^{-2ikr} dr \qquad (2.4)$$

This step requires a spectrum in r space in which the peak of interest is well separated from all other peaks. R_{min} and R_{max} values are chosen for which nodes are observed in the imaginary part of the Fourier transform. Also, it is tried to choose points at which the magnitude of the Fourier transform is as low as possible. In this way truncation effects are minimized. However, small truncation errors are always present in the first and last lobe of the back transformed EXAFS in k space due to the finite range of the Fourier transforms. Therefore we always use our reference data in a smaller interval in k space than the original forward Fourier transform. The manufacture of a typical reference (the first Pt-Pt shell in Pt foil) is illustrated in Figure 2.4. A comparison of Figures 2.4c and 2.4d shows that using the inverse EXAFS over a too long interval introduces serious errors.

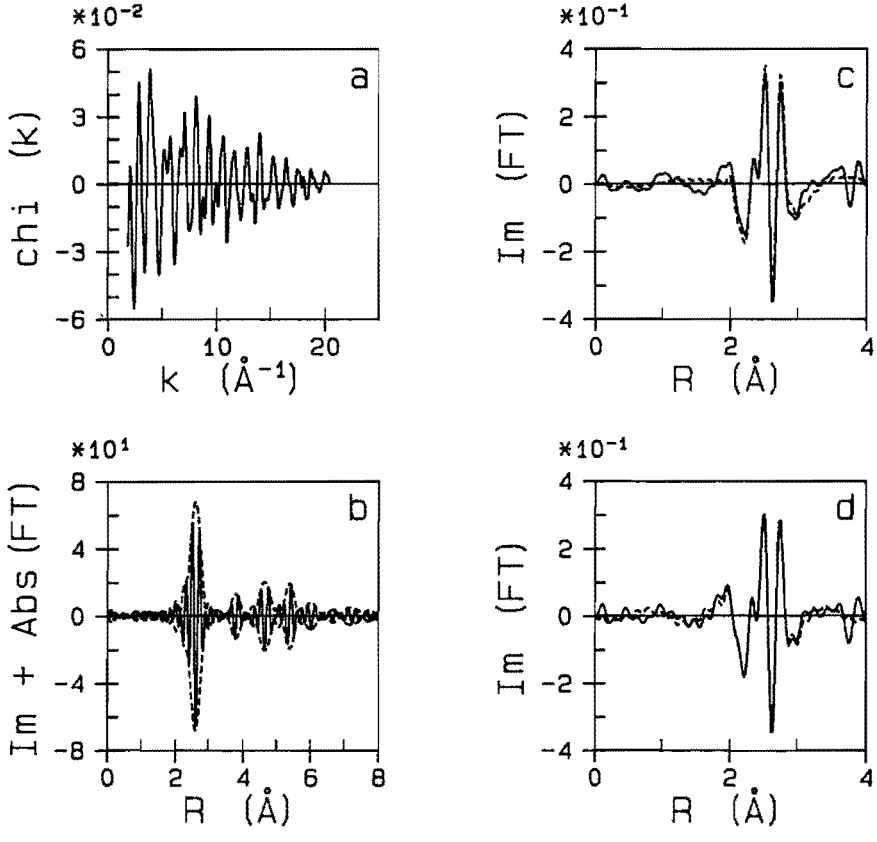

Figure 2.4. EXAFS of Pt foil (a) in k space; (b) k^3-weighted Fourier transform (Δk = 1.95-19.77 $Å^{-1}$); k^1-weighted Fourier transform of the original EXAFS (—) and the inverse EXAFS (— —) (c) with Δk = 1.95-19.77 $Å^{-1}$; and (d) with Δk = 3.03-18.60 $Å^{-1}$.

When the chemical state of the absorber-scatterer pair under observation does not differ too much in the unknown and reference compound, then only N, R, and σ^2 will differ in eq 2.1 and 2.2.[4] N_{ref} and R_{ref} are known because the structure of the reference compound is known. Thus, using a reference compound we obtain N and R of an unknown shell directly. σ^2 of the reference compound in eq 2.2 is not known; therefore we obtain the Debye-Waller factor of the unknown shell as $\Delta\sigma^2$ (i. e. relative to the reference compound).

2.2.4 Phase- and/or Amplitude-Corrected Fourier Transformation

To analyse an EXAFS spectrum composed of different contributions giving a strong overlap of the corresponding peaks in r space after Fourier transformation, one normally uses the technique of fitting in k space. In such a fitting process, a multiple-shell formula such as eq 2.1 is fitted to the experimental EXAFS signal. A large number of adjustable parameters must be estimated in this process, and it is well possible that small differences in k space, not associated with the coordination distances, may be compensated by incorrect parameter values. In order to check the reliability of the parameters obtained by fitting in k space, one has to compare the Fourier transform (the imaginary part as well as the magnitude) of the experimental results with the corresponding transform of the EXAFS function calculated with the parameter values found by fitting in k space. We have found that a reliable separation of the different contributions in an EXAFS spectrum can be obtained by applying the difference file technique[13] and using phase- and/or amplitude-corrected Fourier transforms.

A phase- and amplitude-corrected Fourier transform can be obtained when $\chi(k)$ in eq 2.3 is substituted by:[14-16]

$$\chi(k)\,\frac{e^{-i\phi(k)}}{F_j(k)} \qquad (2.5)$$

A Fourier transform, phase- and amplitude-corrected for an X-Y absorber-scatterer pair, yields the following features: (1) peaks which have a positive imaginary part of the Fourier transform (peaking at the maximum of the magnitude of this Fourier transform) are due to neighbours of atom type Y. These peaks have their maxima at the correct X-Y distance; (2) peaks which are not symmetrical are a superposition of more than one contribution. Thus, the use of corrected Fourier transforms can be a great help in the identification of different types of neighbours by application of different phase and/or amplitude corrections.

Usually phase corrections only are applied when the signal-to-noise ratio of the EXAFS signal at the end of the spectrum is comparatively small. This is the case for low-Z scatterers like C and O, and also for systems with high-Z scatterers in which the number of scatterers is low or large disorder is present (leading to a small EXAFS amplitude at higher k values). It can be seen in Figure 2.5 that in such cases, viz. when an

EXAFS signal with a small amplitude is divided by an amplitude $F_j(k)$ (also obtained from a low-Z scatterer), a phase- and amplitude-corrected Fourier transform yields a spectrum in r space in which the background level is high, while a Fourier transform, only corrected for the phase, yields a spectrum in which the background level is much lower.

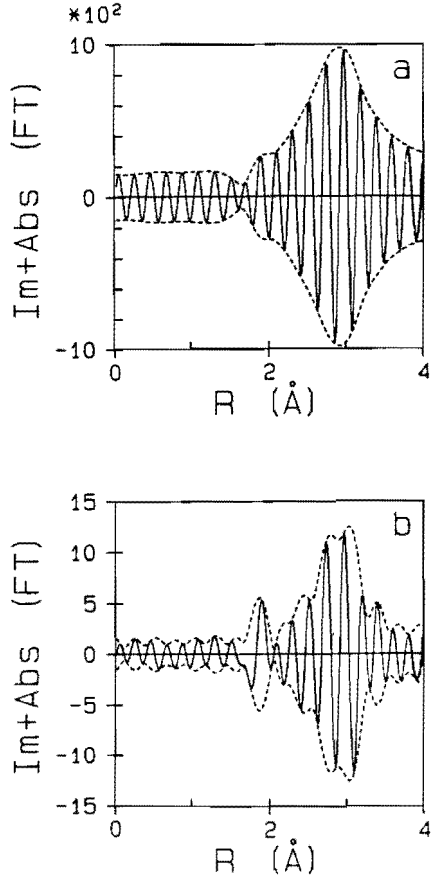

Figure 2.5. EXAFS of a physical mixture of $Ir_4(CO)_{12}$ and SiO_2 after a k^3-weighted Fourier transformation, Δk = 3.80-15.60 $Å^{-1}$ (a) Pt-O phase- and amplitude-corrected; and (b) Pt-O phase-corrected.

2.2.5 The Difference File Technique

To analyse a composite EXAFS spectrum, we further use the difference file technique.[13] In this technique, the parameters R, N, and $\Delta\sigma^2$ (relative to the reference compound) of the largest contribution in the spectrum are first estimated from a spectrum in r space (obtained by Fourier transformation, phase- and/or amplitude-corrected for the atom type which causes the largest contribution). When the estimated parameters are judged to be satisfactory, an EXAFS function calculated with these parameters is subtracted from the experimental EXAFS signal. In the remaining signal, again the largest contribution is estimated. It may be necessary, especially for superposed contributions, to alter slightly the parameters of previously calculated shells. In the end this iterative process results in a set of best parameters. During the iteration, the agreement in k space is regularly checked. The calculated EXAFS signal, composed of the different contributions, should agree as well as possible with the experimental result both in k space and in r space.

2.2.6 Higher Shell Analysis

The method of EXAFS data analysis outlined in Sections 2.2.2-2.2.5 can straightforwardly be applied in the determination of the coordination parameters for the first shells. As stated in Section 2.2.3, data analysis using experimentally determined phase shifts and backscattering amplitudes is based upon the assumption that only N, R, and σ^2 in eq 2.2 may differ between the reference shell and the shell to be analysed. In practice, one also assumes that the factor $\exp(-2R_j/\lambda(k))$ does not vary distinctly.

However this is not true when shells are analysed with the help of a reference in which R_{ref} differs more than $\sim$ 0.3 Å from the coordination distance in the shell to be analysed. The coordination number N_{unc} which is determined in the EXAFS data analysis will then differ from the actual coordination number N in the sample, and must be replaced by:

$$N = N_{unc}\, e^{2(R_j - R_{ref})/\lambda(k)} \qquad (2.6)$$

A reliable determination of the coordination numbers for higher shells (i. e. analysis of higher metal-metal shells using the first metal-metal shell as a reference) thus depends on a correct estimate of $\lambda(k)$. Although λ varies

somewhat with energy,[17] it is assumed that $\lambda \sim 6$ Å for values of $k > 3$ Å^{-1}. In Chapter 6, this assumption has been checked and proved accurate for the case of Pt foil.

2.3 Multiple Scattering

2.3.1 Adapted EXAFS Formulation

As has been mentioned in Section 2.2.2, the usual EXAFS derivations are only valid for single scattering processes. In most systems the EXAFS signal can be adequately expressed as in eq 2.1. There is one important exception however: if arrangements occur in the sample in which the absorber atom A and two scatterer atoms S_1 and S_2 are in almost colinear geometry, then the signal due to S_2 is much enhanced with respect to a similar situation in which the intervening scatterer atom S_1 is omitted (see Figure 2.6). This so-called focusing effect was first observed for the fourth Cu-Cu shell in Cu metal.[18,19] Together with the enhancement in amplitude,

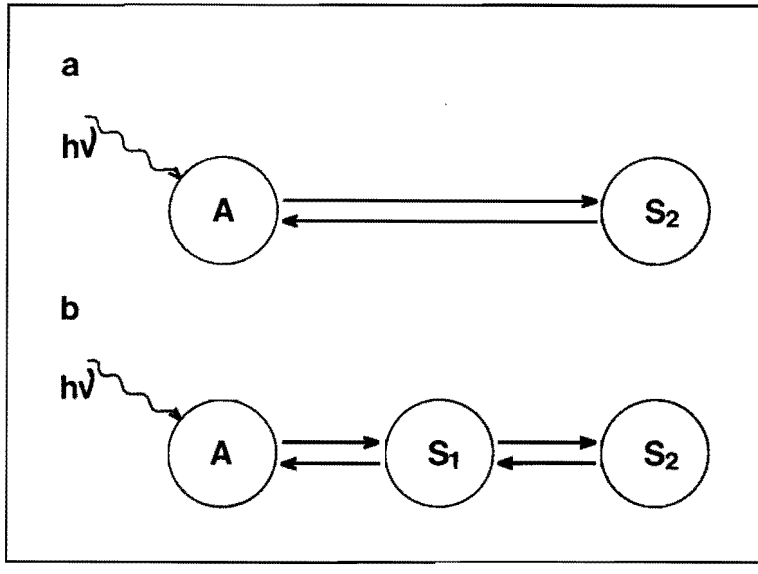

Figure 2.6. (a) Single scattering process; and (b) multiple scattering process. A = absorber atom; S_1, S_2 = scatterer atoms.

for Cu metal and the other fcc metals also a phase shift of approx. π rad is observed with respect to a contribution of the same absorber-scatterer pair not incorporating multiple scattering.

Exact theoretical treatment of the multiple scattering effect is difficult. However, a good approximation is obtained when eq 2.1 is substituted by:[20,21]

$$\chi(k) = \sum_j \Omega_j(\beta,k)\, A_j(k) \sin(2kR_j + \phi_j(k) + \omega_j(\beta,k)) \qquad (2.7)$$

in which both the amplitude correction factor $\Omega_j(\beta,k)$ and the phase correction factor $\omega_j(\beta,k)$ are dependent on k as well as the angle β between absorber A, scatterer S_1, and scatterer S_2.

2.3.2 Use of Experimental References

Just as in the case of single scattering contributions, shells incorporating multiple scattering can be analysed using experimentally determined phase shifts and backscattering amplitudes from references also incorporating multiple scattering. Even then analysis is not as straightforward as in the case of a single scattering contribution, because now phase and amplitude depend both on k and the A-S_1-S_2 angle β (see eq 2.7).

In this Thesis, two types of contributions incorporating multiple scattering have been encountered: (1) the fourth metal-metal shell in small metal particles with the fcc structure (see Chapter 6); and (2) the metal-carbonyl oxygen shell in metal carbonyl clusters (see Chapters 3, 4, and 5).

Analysis of the fourth metal-metal shell is not expected to yield severe problems, because the rather rigid fcc structure ensures that the A-S_1-S_2 angle β will only deviate negligibly from $\beta = 180°$ in the bulk metal, and thus the analysis can proceed essentially angle-independent.

In the metal carbonyls, however, the angle β is not restricted to a fixed value and a method had to be devised to incorporate variation of the angle β in our method of data analysis. Teo[20,21] performed theoretical calculations on the multiple scattering effect. He showed that the behaviour of $\Omega_j(\beta,k)$ and $\omega_j(\beta,k)$ (see eq 2.7) depends on the type of intervening atom *j*. For the case of a system with oxygen as the intervening atom S_1, he

calculated $\Omega_j(\beta,k)$ and $\omega_j(\beta,k)$ for R_{A-S1} = 1.95 Å and R_{S1-S2} = 1.28 Å. Some results are shown in Figure 2.7.

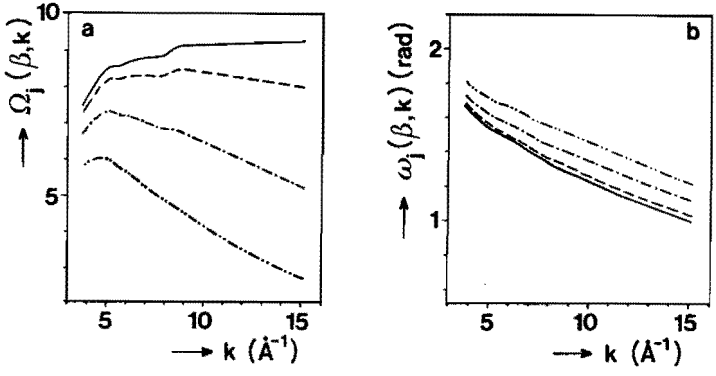

Figure 2.7. (a) Amplitude enhancement factor $\Omega_j(\beta,k)$; and (b) phase modification factor $\omega_j(\beta,k)$ versus k for β = 180° (—), 175° (— —), 170° (— · —), and 165° (— · · —).[20,21]

The system for which Teo performed the multiple scattering calculations, is very much like the metal carbonyl interaction: the coordination distances R_{A-S1} and R_{S1-S2} are very much alike (R_{A-S1} = 1.95 Å and R_{S1-S2} = 1.28 Å in Teo's system, versus R_{M-C} ~ 1.95 Å and R_{C-O} ~ 1.15 Å in a typical metal carbonyl). The behaviour of carbon as the intervening atom S_1 will not significantly differ from that of oxygen. We therefore infer that at least the trends in Teo's results can be applied to the metal carbonyl system.

It appears from the results shown in Figure 2.7 that the behaviour of the phase modification factor versus k is very similar for values of β ranging between 165° and 180°. Therefore it seems appropriate that a variation in angle β with respect to the reference compound will well be accommodated by changing V_0.[1] On the other hand, the behaviour of the amplitude enhancement factor versus k varies significantly between β = 165° and 180°, the differences being smaller at low k values. This behaviour is more equivalent to a change in σ^2 in the single scattering approximation (see Section 2.2.2), than to a change in N, and therefore we have chosen the last option. In Chapter 4 and 5 it is shown that indeed with the use of a change

in V_0 (to approximate the varying phase modification factor) and a change in σ^2 for the metal-carbonyl oxygen shell (to approximate the varying amplitude enhancement factor) good analysis results can be obtained although the angle β in the reference shell and the shell to be analysed may not be exactly the same.

In principle, it should be possible to determine the angle β in the shell to be analysed from the angle β in the reference shell and the observed changes in $\Omega_j(\beta,k)$ and $\omega_j(\beta,k)$. However, this requires a range of reference compounds with different angles β, or excellent theoretically calculated values. The first option is not feasible, in the first place because such a range of compounds usually is not available, and in the second place because the determination of the angle β with XRD often is not accurate enough. With respect to the use of theoretical values, Daresbury's EXCURVE program[22,23] seems the best possibility. However, in a recent publication on Cobalt carbonyl complexes[24] the authors state that a correct bond angle determination with this program still is difficult. Therefore bond angle determination remains a desirable future option.

2.4 References

(1) J. B. A. D. Van Zon, *Thesis;* Eindhoven University of Technology, Eindhoven, the Netherlands, 1984.

(2) J. H. A. Martens, *Thesis;* Eindhoven University of Technology, Eindhoven, the Netherlands, 1988.

(3) J. W. Cook, and D. E. Sayers, *J. Appl. Phys.* **1981**, *52*, 5024.

(4) E. A. Stern, B. A. Bunker, and S. M. Heald, *Phys. Rev. B* **1980**, *21*, 5521.

(5) E. A. Stern, *Phys. Rev. B* **1974**, *10*, 3027.

(6) F. W. Lytle, D. E. Sayers, and E. A. Stern, *Phys. Rev. B* **1975**, *11*, 4825.

(7) P. Eisenberger, and G. S. Brown, *Solid State Commun.* **1979**, *29*, 481.

(8) E. D. Crozier, and A. J. Seary, *Can. J. Phys.* **1980**, *58*, 1388.

(9) E. D. Crozier, and A. J. Seary, *Can. J. Phys.* **1981**, *59*, 876.

(10) C. Bouldin, and E. A. Stern, *Phys. Rev. B* **1982**, *25*, 3462.

(11) E. A. Stern, D. E. Sayers, and F. W. Lytle, *Phys. Rev. B* **1975**, *11*, 4836.

(12) B. K. Teo, and P. A. Lee, *J. Am. Chem. Soc.* **1979**, *101*, 2815.

(13) H. F. J. Van 't Blik, J. B. A. D. Van Zon, T. Huizinga, J. C. Vis, D. C. Koningsberger, and R. Prins, *J. Am. Chem. Soc.* **1985**, *107*, 3139.

(14) P. A. Lee, and G. Beni, *Phys. Rev. B* **1977**, *15*, 2862.

(15) F. W. Lytle, R. B. Greegor, E. C. Marques, D. R. Sandstrom, G. H. Via, and J. H. Sinfelt, *J. Catal.* **1985**, *95*, 546.

(16) J. B. Pendry, *EXAFS for Inorganic Systems* (Proceedings of the Daresbury Study Weekend, 28-29 March 1981); C. D. Garner, and S. S. Hasnain, Eds.; Science and Engineering Research Council, Daresbury Laboratory: Daresbury, England, 1981; p 5.

(17) E. A. Stern, B. A. Bunker, and S. M. Heald, *Phys. Rev. B* **1980**, *21*, 5521.

(18) C. A. Ashley, and S. Doniach, *Phys. Rev. B* **1975**, *11*, 1279.

(19) P. A. Lee, and J. B. Pendry, *Phys. Rev. B* **1975**, *11*, 2795.

(20) B. K. Teo, *J. Am. Chem. Soc.* **1981**, *103*, 3990.

(21) B. K. Teo, *EXAFS: Basic Principles and Data Analysis*; Springer Verlag: New York, 1986; p 196.

(22) S. J. Gurman, N. Binsted, and I. Ross, *J. Phys. C* **1984**, *17*, 143.

(23) S. J. Gurman, N. Binsted, and I. Ross, *J. Phys. C* **1986**, *19*, 1845.

(24) N. Binsted, S. L. Cook, J. Evans, G. N. Greaves, and R. J. Price, *J. Am. Chem. Soc.* **1987**, *109*, 3669.

Chapter Three

The Structure of Alumina-Supported Osmium Clusters after Chemisorption and Decomposition

3.1 Introduction

Supported metal catalysts used in many large-scale processes consist of small (~ 10-1000 Å) aggregates or crystallites of metal dispersed on high-surface-area metal-oxide supports. Since the metal aggregates are non-uniform in size, shape, and catalytic properties, the best attainable relations between structure and catalytic performance have been based on the average structural properties which are inferred -sometimes tenuously- from indirect structure probes. Only for very small aggregates of structurally simple supported metals are structures well-defined; X-ray absorption spectroscopy, combined with other physical methods, has been decisive in the structure determinations.[1-3]

Alternatively, supported organometallic species analogous to molecular structures are attractive as model supported metal catalysts offering several advantages with respect to fundamental understanding of structure and performance: (1) the structure can, in prospect, be determined with precision, on the basis of comparisons of sample spectra and those of fully characterized molecular analogues; (2) the nature of the bonding between the organometallic species and the support can be determined with precision on the basis of comparisons of spectra of surface species with those of analogous molecular structures incorporating ligands similar to those of the functional groups terminating the support surface. Therefore, the often ill-defined issues related to the structure of supported metal catalysts and metal-support interactions can be placed on a firm fundamental foundation.

The supported 'molecular' organometallics that have been characterized most thoroughly are triosmium clusters anchored to silica and alumina.[4-9] The structure has been inferred to be the following

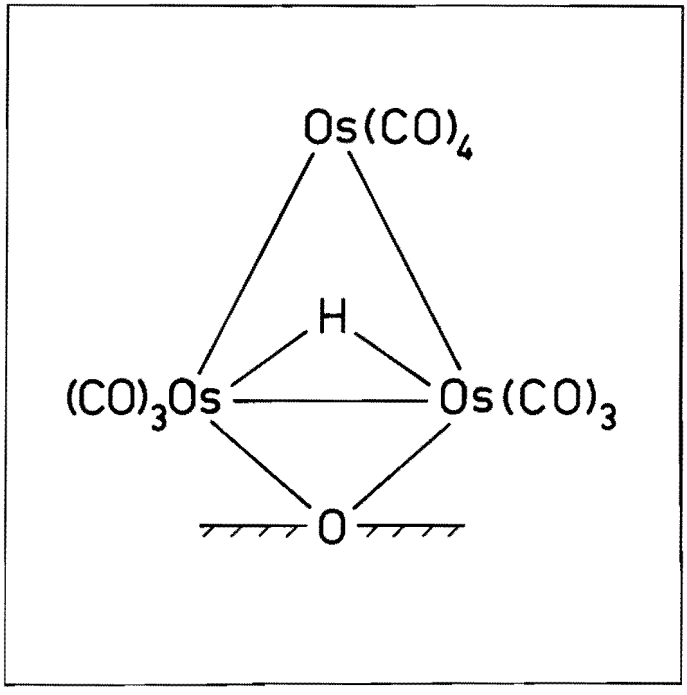

from (1) the stoichiometry of the synthesis from $Os_3(CO)_{12}$ and surface OH groups (splitting off two CO ligands),[5] (2) infrared spectra in the carbonyl region,[5-7] (3) Raman spectra indicating Os-Os bonds,[8] and (4) observations by high-resolution electron microscopy, indicating surface structures with the size of the clusters and no larger metal structures.[9,10] All the spectroscopic results were interpreted by comparison with spectra of analogous compounds with known crystal structures, such as $HOs_3(CO)_{10}(OH)$. Recently, the crystal structure of an excellent analogue of the silica-supported cluster, $HOs_3(CO)_{10}OSiEt_3$, has been reported (Figure 3.1).[11]

This surface structure should perhaps be regarded as well established, but a complete characterization requires a confirmation by X-ray absorption spectroscopy, which can in prospect determine the average interatomic distances and the metal oxidation states in the surface organometallic structures. There are two communications[12,13] reporting EXAFS (Extended X-ray Absorption Fine Structure) spectra of oxide-supported triosmium clusters. The results do not provide clear and convincing confirmation of the

structure suggested above, although they are consistent with this and similar structures.

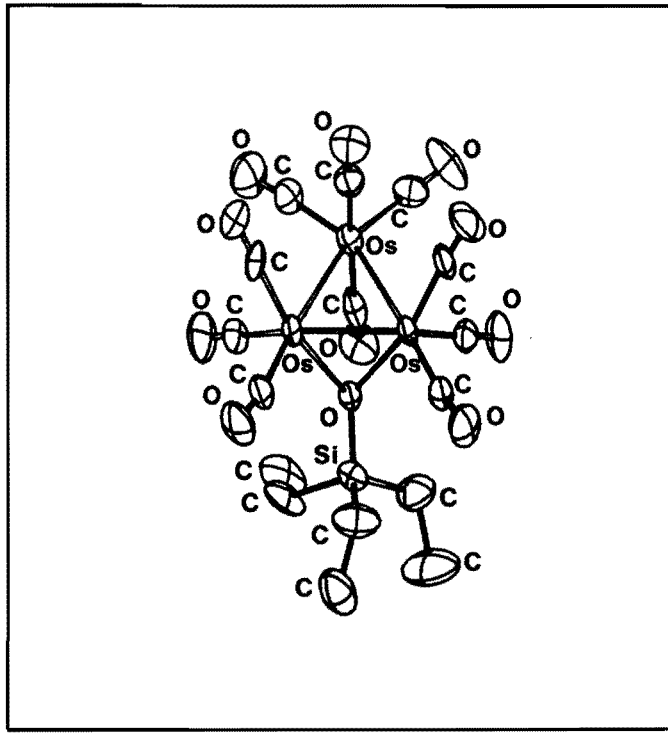

Figure 3.1. Structure of $HOs_3(CO)_{10}OSiEt_3$.[11] with Os-Os distances 2.816, 2.820, and (oxygen bridged) 2.777 Å.

Besson et al.[5,12] reported EXAFS results confirming the presence of triosmium clusters on silica and showing the absence of osmium metal particles. The average Os-Os distance in the supported cluster was inferred to be 2.68 Å, whereas the distance in the presumed molecular analogue $HOs_3(CO)_{10}OSiEt_3$ is 2.777 Å for the oxygen-bridged osmiums, the other osmium-osmium distances being 2.820 and 2.816 Å.[11]

Cook et al.[13] used EXAFS to characterize triosmium clusters supported on γ-Al_2O_3. They fitted their data in k space using theoretically calculated values of the phase shift and backscattering amplitude and a theoretical calculation of the multiple scattering between carbon and oxygen. With these theoretically calculated values, they inferred an average

Os-Os distance of 2.84 Å. They suggested that the surface structure analogous to that shown in Figure 3.1 might be accompanied by a surface structure incorporating two bridging oxygen ions of the surface; this latter structure has not been suggested by other authors.

The reactivity and catalytic activity of the oxide-bound cluster $HOs_3(CO)_{10}\{OAl\}$ have been investigated in some detail.[5-9,14-16] On the basis of the stoichiometry of the reaction,[5] infrared spectra,[5-7] and Raman spectra,[8] it has been inferred that heating of the supported cluster to about 120 °C (the value is support-dependent) in vacuum or He leads to breaking of the Os-Os bonds, oxidation of the osmium to the divalent state, and evolution of CO and H_2. Surface OH groups are the oxidizing agent. The resulting structure has been postulated[5-9] to be $Os^{II}(CO)_n$, where n = 2 or 3. Infrared spectroscopy has been used to establish details of the structure of this mononuclear surface complex and to follow the reversible carbonylation-decarbonylation process.[7] Electron micrographs of these broken-up clusters on γ-alumina suggested the presence of three-atom ensembles of Os; the Os ions were inferred to have remained on the surface very nearly where the clusters were originally bonded.[9,10] The reconstitution of a fraction of the clusters induced by CO was taken as evidence confirming the presence of these ensembles.[14]

To provide a more nearly definitive structural characterization of these surface species, EXAFS experiments have been performed with $Os_3(CO)_{12}$, the alumina-supported triosmium cluster, and the broken-up cluster on alumina. Experimentally determined phases and backscattering amplitudes were used for the analysis of the EXAFS data characterizing the alumina-supported cluster and the broken-up cluster. $Os_3(CO)_{12}$ was used as an experimental reference for the Os-CO coordination. To determine reliably the contributions to the EXAFS spectrum arising from the various groups coordinated to osmium, the difference file technique was applied[1] (see also Chapter 2, Section 2.2.5) together with phase- and/or amplitude-corrected Fourier transforms.

The results confirm the earlier structural conclusions and cast doubt on the EXAFS results published for the alumina-supported osmium cluster. Detailed information has also been obtained that characterizes the structure of the broken-up cluster on alumina, in particular the coordination of osmium with support oxygen ions.

3.2 Experimental

3.2.1 Materials and Catalyst Preparation

$Os_3(CO)_{12}$ was obtained from Strem and used without further purification. n-Octane (Fisher analysed) was freshly dried and redistilled in the presence of metallic sodium under N_2. Dichloromethane (Fisher analysed) was freshly dried and redistilled in the presence of phosphorous pentoxide under nitrogen.

The γ-alumina used as a support was grade D supplied by Ketjen; the BET surface area was about 250 m^2/g. The alumina was treated for 5 h in flowing oxygen at 400 °C, purged with N_2 for 2 h at 400 °C, cooled to room temperature under vacuum, and then transferred under N_2 to a drybox. For the preparation of the catalyst, 4 g of Al_2O_3, 65.3 mg of $Os_3(CO)_{12}$, and 200 ml of n-octane were added to a 500 ml flask in the absence of air. The mixture was stirred and refluxed for 90 min. Upon refluxing, the deep yellow solution became colorless and the solid particles yellow. These observations suggest that most of the cluster had been adsorbed on the alumina. The slurry was transferred under nitrogen to a Soxhlet apparatus, where the solid was extracted with dichloromethane for 10 h to remove physisorbed cluster. The extract solutions were pale yellow. The resulting solid, containing about 1 wt% Os, was dried under vacuum for 10 h and then stored under N_2 in a drybox. A fraction of the sample was held for 5 h at 150 °C in a calcining tube for thermal decomposition of the surface-bound cluster; this sample was also handled under N_2.

3.2.2 Infrared Spectroscopy

Infrared spectra were measured with a Nicolet 7199 Fourier transform spectrophotometer. The details of the cell design are reported by Barth et al.[14] The samples were self-supporting wafers. The spectral resolution was 4 cm^{-1}. The spectrum of the sample prepared from $Os_3(CO)_{12}$ and γ-Al_2O_3 compares very well with spectra of previous reports.[5,6] The spectrum of the decomposed cluster on alumina is similar to published spectra,[5-7] indicating the presence of mononuclear osmium complexes on the support.

3.2.3 EXAFS

The experiments were carried out at EXAFS station I-5 at the Stanford Synchrotron Radiation Laboratory (SSRL), with a ring energy of 3 GeV and ring currents between 40 and 80 mA. A Si(220) channel-cut monochromator with a d spacing of 1.92 Å was employed.

The powder was pressed into self-supporting wafers to give samples of good uniformity. The wafer thickness was chosen to give a total X-ray absorbance of about 1. An EXAFS sample cell allowed the measurements at liquid nitrogen temperature and in situ treatments of the sample at elevated temperatures to decompose the supported cluster in a helium atmosphere. The data collection time for each run was about 25 min. Experiments were carried out at the Os L_{III} edge (10871 eV) with the alumina-supported cluster, the decomposed cluster, and a reference material consisting of a physical mixture of approximately 1 wt% crystalline $Os_3(CO)_{12}$ with silica powder.

The data analysis was carried out applying the difference file technique (see Chapter 2). $Os_3(CO)_{12}$ was measured at the Os L_{III} edge, and Pt foil and $Na_2Pt(OH)_6$ were measured at the Pt L_{III} edge (11564 eV). From the $Os_3(CO)_{12}$[17] data, a reference was extracted for the Os-C-O moiety, as outlined below. Pt foil[18] data were used to estimate the Os-Os contributions and $Na_2Pt(OH)_6$[19] data were used to estimate the Os-$O_{support}$ contributions. These references were used because Os metal and Os oxide data measured under the same experimental conditions at the same EXAFS station were not available. The choice of the references is justified in the Discussion (Section 3.4).

3.3 Results

3.3.1 The Os-CO Reference

A physical mixture of $Os_3(CO)_{12}$ and SiO_2 was characterized to provide a reference for the Os-CO shell.

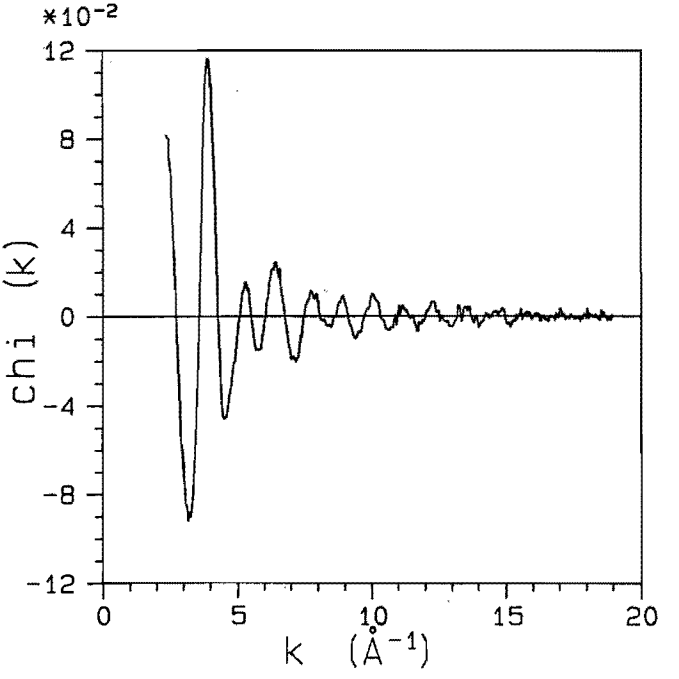

Figure 3.2. Raw EXAFS data of a physical mixture of $Os_3(CO)_{12}$ and SiO_2.

The EXAFS spectrum (Figure 3.2) is a superposition of an Os-Os and an Os-CO contribution. Separation of these contributions is not straightforward because the Os-Os and Os-O^* (O^* refers to the carbonyl oxygen) peaks in r space (after Fourier transformation) are superimposed. Even a k^3-weighted transform, which should separate the Os-Os and Os-O^* peaks as well as possible, is not sufficient (Figure 3.3a).

The best way to separate the contributions was found to be an estimation of the Os-Os contribution in k space. Since C and O cause negligible backscattering at values of k greater than ~ 10-11 $Å^{-1}$,[20] the EXAFS spectrum for $k > 11$ $Å^{-1}$ is almost entirely due to the Os-Os shell. The crystal structure provides the data for the Os-Os coordination:[17] $N_{Os-Os} = 2$, $R_{Os-Os} = 2.88$ Å. With these parameters, a best estimate for the Os-Os shell was calculated. A Debye-Waller factor ($\Delta\sigma^2$) of -0.001 $Å^2$ (relative to Pt foil) was used, which gave the best agreement with the EXAFS data for $k > 11$ $Å^{-1}$ (Figure 3.4).

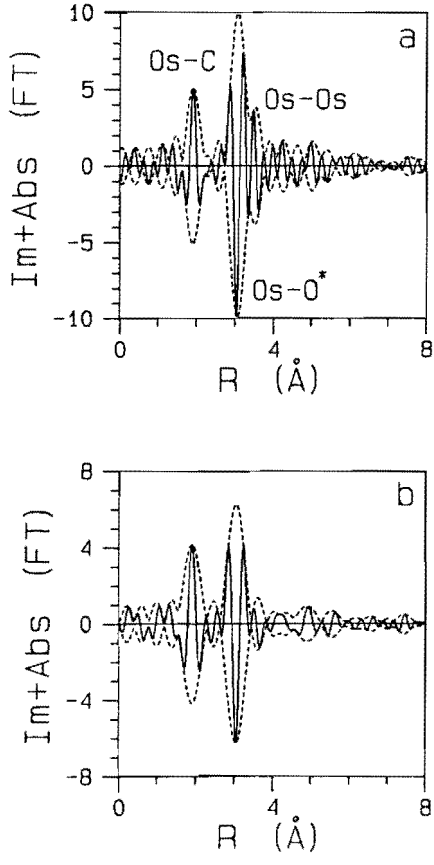

Figure 3.3. k^3-weighted Fourier transform (Os-O phase corrected) of (a) the $Os_3(CO)_{12}$ data (Δk = 3.72-12.55 $Å^{-1}$); and (b) the $Os_3(CO)_{12}$ data minus calculated Os-Os shell (Δk = 3.75-11.89 $Å^{-1}$).

After subtraction of the calculated Os-Os contribution from the experimental results, a Fourier transform was again applied, with a k^3 weighting used to separate the Os-C and Os-O* peaks in r space as well as possible. By use of an Os-O phase correction, a peak pattern should be obtained in r space with two symmetrical imaginary parts, one with a positive peak (the Os-C shell) and one with a negative peak (the Os-O* shell). The negative imaginary part of the Os-O* peak is due to the multiple scattering contribution (see Section 3.4). To get perfectly symmetrical peaks in the k^3-weighted Fourier transform (Δk = 3.75-11.89 $Å^{-1}$, Os-O phase corrected) of the difference spectrum, small V_0 corrections were needed: the

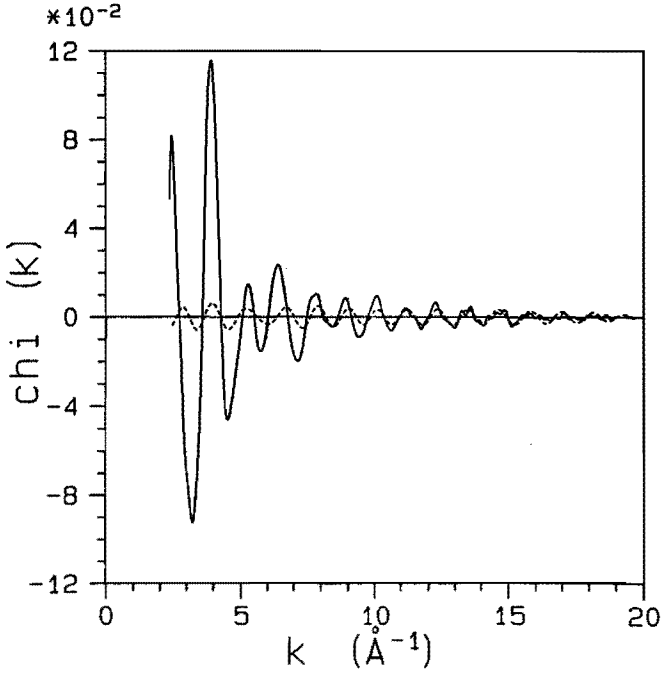

Figure 3.4. EXAFS of $Os_3(CO)_{12}$ (—) and calculated Os-Os shell (N = 2, R = 2.88 Å, $\Delta\sigma^2$ = -0.001 Å^2 relative to Pt foil) (— —).

calculated Os-Os shell had to be corrected with V_0 = -3.3 eV before the subtraction, and the Os-CO difference spectrum required a correction of V_0 = -4.6 eV. The k^3-weighted Fourier transform of the difference spectrum (experimental results minus calculated Os-Os shell) is presented in Figure 3.3b. The sidelobe in the Os-O* peak in Figure 3.3a, caused by the Os-Os contribution, has disappeared. The imaginary part of the Os-C contribution peaks positively at the maximum of its Fourier transform, at R = 1.93 Å, which corresponds within the limits of accuracy to the value obtained from crystallographic data (R = 1.95 Å). The Os-O* peak has an imaginary part which peaks negatively at the maximum of its magnitude. The peak is located at R = 3.08 Å, which is almost equal to the crystallographic distance of 3.09 Å. This negative imaginary part is caused by multiple scattering (see Section 3.4). The resulting spectrum in r space was back

transformed with Δr = 1.20-3.46 Å to give an Os-CO reference. The back transformation spectrum is taken to be reliable as an Os-CO reference only between k = 4.2 and 11 $Å^{-1}$, because of truncation errors in the Fourier transformation procedures.

3.3.2 Triosmium Clusters Chemisorbed on γ-Al_2O_3

The raw EXAFS spectrum of the product formed in the reaction of $Os_3(CO)_{12}$ with the surface of γ-Al_2O_3 is shown in Figure 3.5. It has been reported[5-7] that the $Os_3(CO)_{12}$ cluster loses two CO ligands when it reacts with oxide supports like Al_2O_3, with the Os_3 skeleton remaining intact.

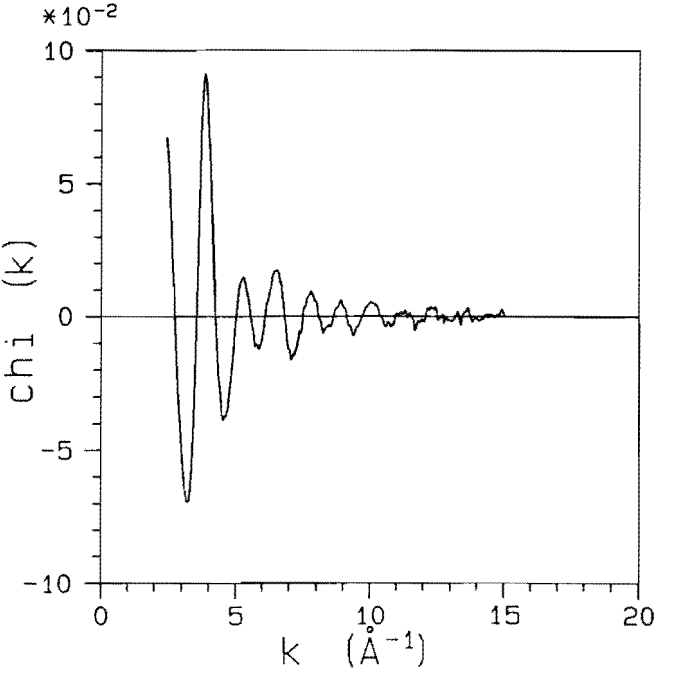

Figure 3.5. Raw EXAFS of the reaction product of $Os_3(CO)_{12}$ and γ-Al_2O_3.

Comparing the imaginary parts of the Fourier transforms of the parent $Os_3(CO)_{12}$ cluster and the supported cluster shows that strong interferences are present between R = 1.8 and 2.7 Å. This result indicates the presence of an additional scatterer, most probably support oxygen. Between R = 0 and 1.8 Å, the Fourier transform for the supported cluster is

very similar to that of the parent $Os_3(CO)_{12}$ cluster. Assuming the commonly accepted structure[5-7] for the supported cluster (shown in Section 3.1) we expect to infer evidence of Os-Os, Os-CO, and Os-$O_{support}$ interactions from the EXAFS data. Of these contributions, the Os-CO contribution is expected to be the greatest and thus the easiest to determine. The loss of two CO ligands per cluster during chemisorption should result in an average EXAFS coordination number N_{Os-CO} = 10/3. With this value for N and the distances R_{Os-C} and R_{Os-O} equal to the values characterizing the unsupported parent cluster (R_{Os-C} = 1.95 Å and R_{Os-O} = 3.09 Å) the EXAFS for an Os-CO shell was calculated. A Debye-Waller factor (relative to the unsupported cluster) of 0.0025 $Å^2$ was found to give the best agreement in r space (between R = 0 and 1.8 Å) with the experimental results. The experimental results for the supported cluster and the calculated Os-CO shell (both after a k^1-weighted Fourier transformation with Δk = 4.2-9.0 $Å^{-1}$, Os-O phase corrected) are shown in Figure 3.6a.

This calculated Os-CO contribution was subtracted from the experimental results. The difference spectrum should contain at least two contributions, namely the Os-Os and Os-$O_{support}$ shells. Since it is entirely possible that the Os_3 skeleton is only negligibly affected by the reaction with Al_2O_3, we took the parameters of the Os-Os shell to be those of the unsupported parent cluster (N_{Os-Os} = 2, R_{Os-Os} = 2.88 Å, $\Delta\sigma^2$ = -0.001 $Å^2$). k^1-weighted Fourier transformations of the difference spectrum and the calculated Os-Os contribution (Δk = 4.2-9.0 $Å^{-1}$, Os-Os phase corrected) showed a good agreement between R = 2.8 and 3.4 Å (Figure 3.6b). The differences at low r values are caused by Os-$O_{support}$ contributions. Within our limits of precision, we could not find better parameters for the Os-Os shell. The Os-Os coordination distance of 2.88 Å gives the best agreement between the imaginary parts of the Fourier transforms of the calculated and difference spectra. This result stands in contrast to the crystallographic data characterizing $HOs_3(CO)_{10}OSiEt_3$,[11] for which an average Os-Os distance of 2.81 Å was observed.

The remainder of the data (experiment minus Os-CO shell minus Os-Os shell) should only contain an Os-$O_{support}$ contribution. One large, symmetrical peak was obtained upon Fourier transformation (k^1-weighted, Δk = 4.2-9.0 $Å^{-1}$, Os-O phase corrected), which is ascribed to an Os-$O_{support}$ interaction (Figure 3.6c). The Fourier transform of an EXAFS function cal-

culated with N_{Os-O} = 0.65, R_{Os-O} = 2.16 Å, and $\Delta\sigma^2$ = -0.004 Å^2 (relative to $Na_2Pt(OH)_6$) gave the best agreement in r space (between R = 1.7 and 2.6 Å) with the corresponding Fourier transform of the remainder of the data (Figure 3.6c).

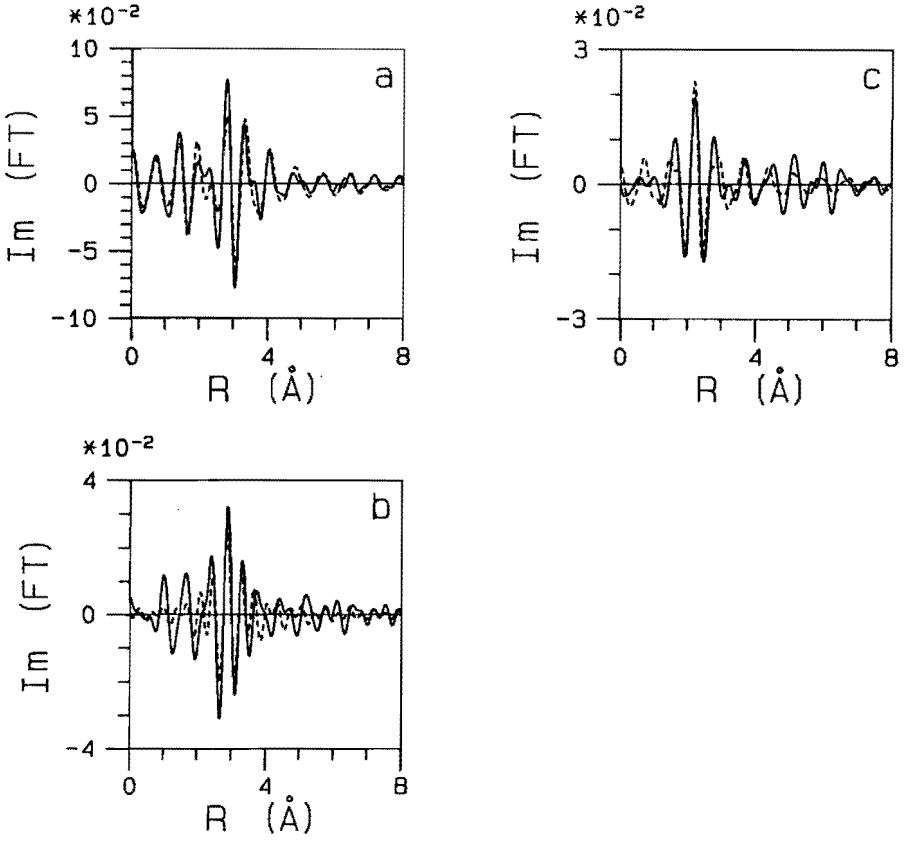

Figure 3.6. k^1-weighted Fourier transforms (Δk = 4.2-9.0 Å^{-1}) of (a) supported cluster from $Os_3(CO)_{12}$ and γ-Al_2O_3 (—) and calculated Os-CO shell (N = 3.35, R_{Os-C} = 1.95 Å, R_{Os-O} = 3.09 Å, $\Delta\sigma^2$ = 0.0025 Å^2 relative to $Os_3(CO)_{12}$) (— —) (Os-O phase corrected); (b) data for supported cluster minus Os-CO shell (—) and calculated Os-Os shell (N = 2, R = 2.88 Å, $\Delta\sigma^2$ = -0.001 Å^2 relative to Pt foil) (— —) (Os-Os phase corrected); and (c) data for supported cluster minus Os-CO and Os-Os shells (—) and calculated Os-$O_{support}$ shell (N = 0.65, R = 2.16 Å, $\Delta\sigma^2$ = -0.004 Å^2 relative to $Na_2Pt(OH)_6$) (— —) (Os-O phase corrected).

The coordination parameters for all calculated shells are summarized in Table 3.1. To further verify the reliability of the full set of coordination parameters, the calculated EXAFS functions of each individual contribution

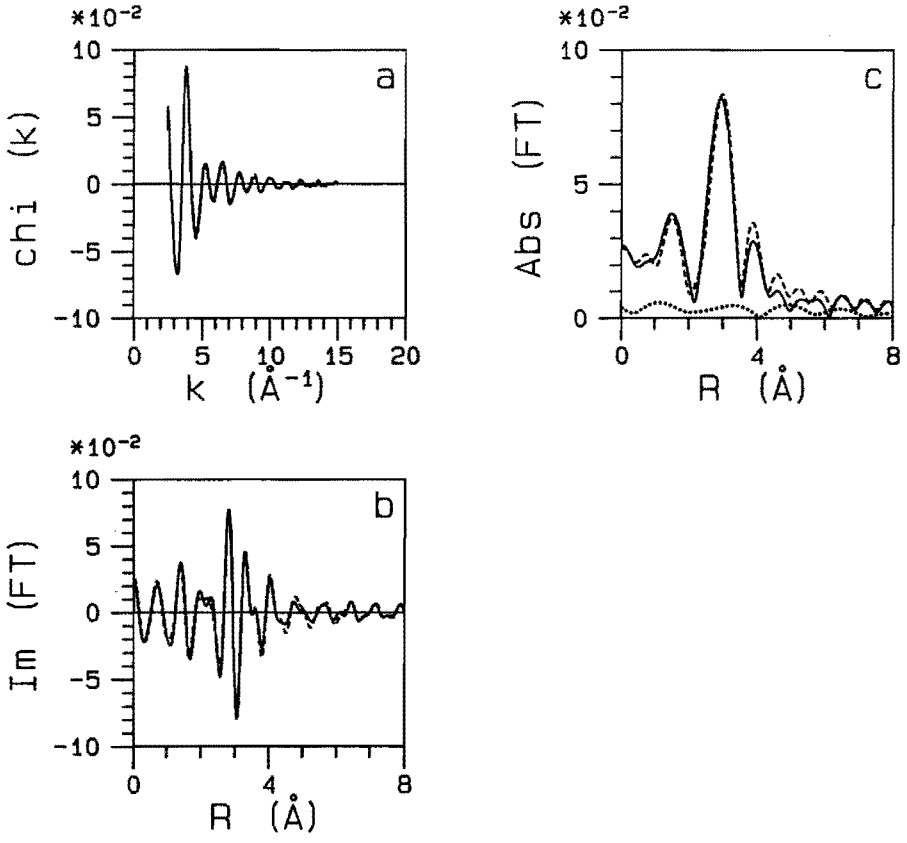

Figure 3.7. Experimental results for supported cluster formed from $Os_3(CO)_{12}$ and γ-Al_2O_3 (—) and sum of the calculated Os-CO, Os-Os, and Os-$O_{support}$ shells (— —) (a) in k space; (b) in r space (imaginary parts, Δk = 4.2-9.0 $Å^{-1}$, Os-O phase corrected); and (c) in r space (magnitude, Δk = 4.2-9.0 $Å^{-1}$, Os-O phase corrected). Also shown in (c) is the magnitude of the difference between experimental and calculated results (Δk = 4.5-7.5 $Å^{-1}$, Os-O phase corrected) (· · ·).

(Os-CO, Os-Os, and Os-$O_{support}$) were added. It can be seen in Figure 3.7a that the sum of the calculated contributions agrees very well with the experimental results in k space. Another highly sensitive check of the reliability of the full set of parameters consists of a comparison of the imaginary parts of the corresponding Fourier transforms. Figure 3.7b shows hardly any differences between the two curves.

Table 3.1. Parameters obtained for the coordination shells in $HOs_3(CO)_{10}\{OAl\}$[a]

Shell	N	R (Å)	$\Delta\sigma^2$ (Å^2)	Ref. Compd.
Os-CO	3.35	1.95 (Os-C) 3.09 (Os-O*)	0.0025	$Os_3(CO)_{12}$
Os-Os	2	2.88	-0.001	Pt foil
Os-$O_{support}$	0.65	2.16	-0.004	$Na_2Pt(OH)_6$

[a]Accuracies: N, ± 15%; R, ± 1%; $\Delta\sigma^2$, ± 15%.

3.3.3 Broken-up Clusters on γ-Al_2O_3

The raw EXAFS data of the decomposed Os cluster are presented in Figure 3.8. Comparing this spectrum with that of the supported cluster (Figure 3.5) shows the absence of EXAFS oscillations (due to osmium neighbours) for values of $k > 10$ Å^{-1}. This result is in agreement with the results of infrared and other experiments, from which it has been concluded that the cluster breakup yields two species, $Os^{II}(CO)_2$ and $Os^{II}(CO)_3$.[5-7] Thus, only Os-CO and Os-$O_{support}$ contributions were expected to be present in the EXAFS of the decomposed cluster.

An Os-CO contribution was calculated by using the reference obtained from the $Os_3(CO)_{12}$ data. This calculated contribution was subtracted from the experimental results and the difference spectrum was analysed for Os-$O_{support}$ contributions. In a recurrent way (described in Section 2.2.5) optimized parameters were found for both coordinations. The best calculation for the Os-CO shell yielded N_{Os-CO} = 2.8, R_{Os-C} = 1.91 Å, R_{Os-O} = 3.05 Å, $\Delta\sigma^2$ = 0 Å^2 (relative to $Os_3(CO)_{12}$). The calculated Os-CO shell and the experimental results were Fourier transformed (k^1-weighted, Δk = 4.2-8.5 Å^{-1}, Os-O phase corrected; see Figure 3.9a).

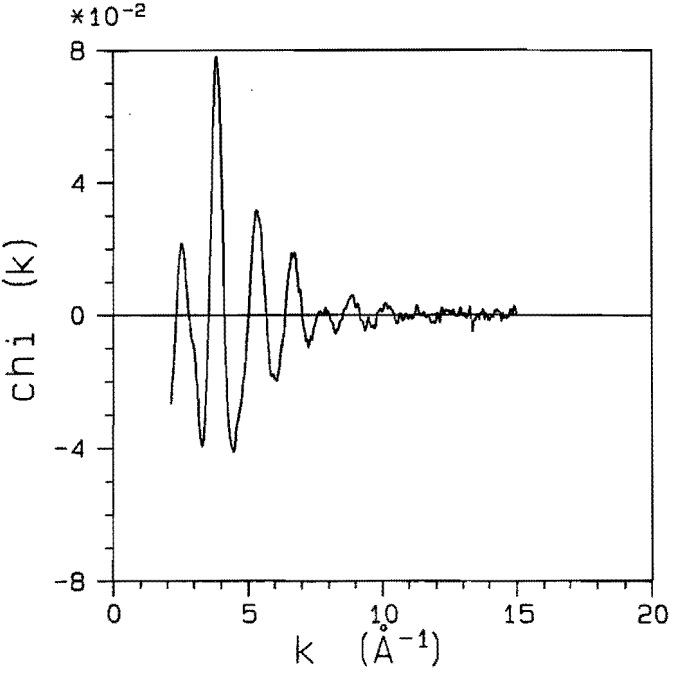

Figure 3.8. Raw EXAFS of the supported clusters formed from $Os_3(CO)_{12}$ and γ-Al_2O_3 after decomposition in He at 150 °C.

The best parameters for the Os-$O_{support}$ shell were found to be N_{Os-O} = 3, R_{Os-O} = 2.17 Å, and $\Delta\sigma^2$ = -0.0025 Å^2 (relative to $Na_2Pt(OH)_6$). The calculated Os-$O_{support}$ shell and the difference spectrum were Fourier transformed (k^1-weighted, Δk = 4.2-8.5 Å^{-1}, Os-O phase corrected; see Figure 3.9b). The difference spectrum showed only one peak. Clearly, no detectable Os-Os shell is present.

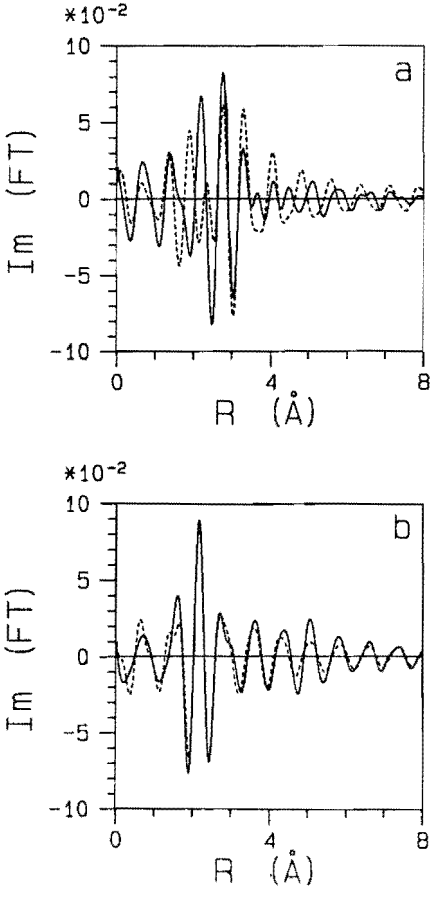

Figure 3.9. k^1-weighted Fourier transforms (Δk = 4.2-8.5 $Å^{-1}$; Os-O phase corrected) of (a) decomposed cluster data (—) and calculated Os-CO shell (N = 2.8, R_{Os-C} = 1.91 Å, R_{Os-O} = 3.05 Å, $\Delta\sigma^2$ = 0 $Å^2$ relative to $Os_3(CO)_{12}$) (— —); and (b) decomposed cluster data minus Os-CO shell (—) and calculated $Os-O_{support}$ shell (N = 3, R = 2.17 Å, $\Delta\sigma^2$ = -0.0025 $Å^2$ relative to $Na_2Pt(OH)_6$) (— —).

The sum of the calculated Os-CO and $Os-O_{support}$ shells was Fourier transformed (k^1-weighted, Δk = 4.2-8.5 $Å^{-1}$, Os-O phase corrected) and compared with the experiment (Figure 3.10). The agreement in k and in r space is rather good. However, deviations appear at low r values, especially between R = 1.5 and 2 Å.

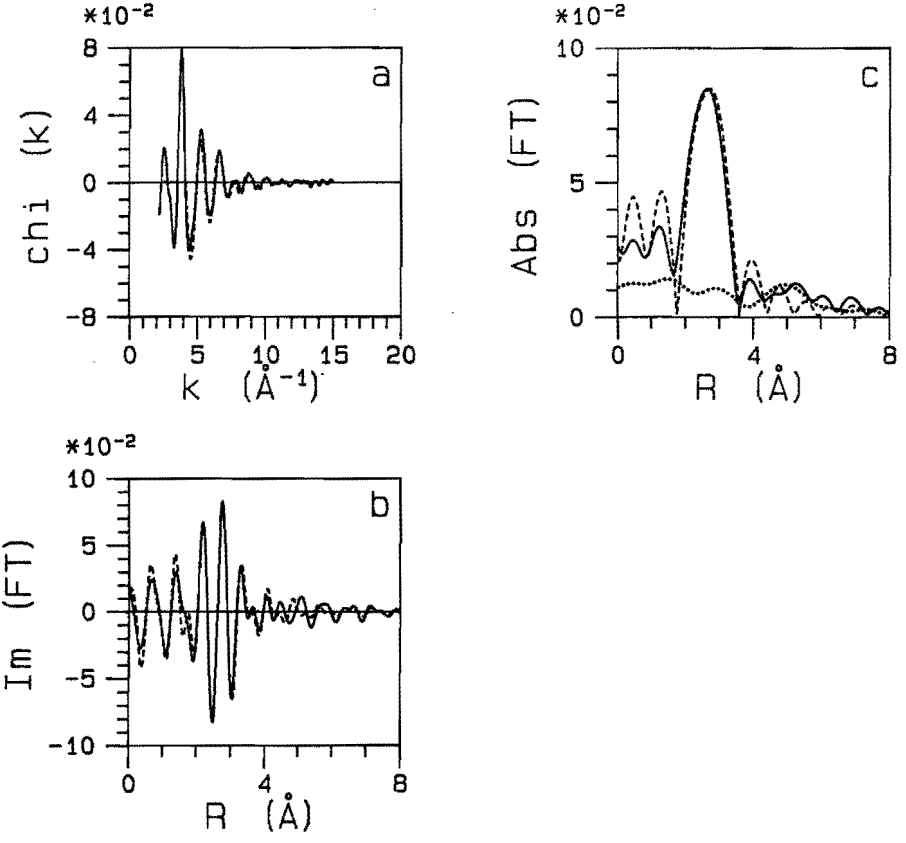

Figure 3.10. Experimental results characterizing the decomposed clusters on γ-Al_2O_3 (—) and the sum of the calculated Os-CO and Os-$O_{support}$ shells (— —) (a) in k space; (b) in r space (imaginary parts, Δk = 4.2-8.5 $Å^{-1}$, Os-O phase corrected); and (c) in r space (magnitude, Δk = 4.2-8.5 $Å^{-1}$, Os-O phase corrected). Also shown in (c) is the magnitude of the difference between experimental and calculated results (Δk = 4.5-7.5 $Å^{-1}$, Os-O phase corrected) (• • •).

These deviations are probably caused by changes in the Os-C-O geometry with respect to the $Os_3(CO)_{12}$ cluster. First, in Os^{II}-C-O the π-backbonding effect is inferred to be weaker, resulting in longer Os-C and shorter C-O distances. Second, we infer that in Os^{II}-C-O the Os-C-O angle is closer to 180°. This leads to a further enhancement of the Os-O^* shell,[21] while the contribution of the Os-C shell is not affected.

Table 3.2. Parameters obtained for the coordination shells in $Os^{II}(CO)_n\{OAl\}_3$ (n = 2 or 3)[a]

Shell	N	R (Å)	$\Delta\sigma^2$ (Å^2)	Ref. Compd.
Os-CO	2.8	1.91 (Os-C) 3.05 (Os-O*)	0	$Os_3(CO)_{12}$
$Os\text{-}O_{support}$	3	2.17	-0.0025	$Na_2Pt(OH)_6$

[a]Accuracies: N, ± 15%; R, ± 1% (Os-C ± 5%); $\Delta\sigma^2$, ± 15%.

The parameters of the calculated shells are summarized in Table 3.2. The average $N_{Os\text{-}CO}$ coordination number of 2.8 supports the results of infrared and other experiments which show that breakup of the supported clusters gives a mixture of $Os^{II}(CO)_2\{OAl\}_3$ and $Os^{II}(CO)_3\{OAl\}_3$ on the Al_2O_3 surface. The analysis shows clear evidence for a coordination of the osmium ion with three oxygen ligands on the γ-Al_2O_3 support.

3.4 Discussion

3.4.1 Methods of Data Analysis and Reference Compounds

Interpretation of EXAFS data is sensitive to assumptions underlying the analysis, and often the assumptions have been less than fully stated in published EXAFS studies; consequently it is difficult to determine the validity of structural models and to compare results presented by different groups. In the next paragraphs the assumptions used in the analysis are evaluated on the basis of the EXAFS technique. Then the results for (1) $Os_3(CO)_{12}$, the reference compound; (2) the supported cluster; and (3) the broken-up cluster on the support are interpreted and compared with data reported in the literature. In the following sections, we evaluate the agreement between the structural models presented in the literature and the EXAFS results, finally drawing some conclusions concerning methodologies for evaluation of EXAFS data and comparing the structures of the supported 'molecular' osmium species with those of other supported metals.

A crucial issue in EXAFS spectroscopy is centered on the need for well-characterized reference compounds and the incorporation of EXAFS data characterizing those reference compounds in the interpretation of spectra of less-well-characterized samples. In this work we have collected and used data for a fully characterized reference compound, $Os_3(CO)_{12}$, to account for the Os-CO interactions. We have also used data for platinum metal to analyse the Os-Os interactions and data for the fully characterized compound $Na_2Pt(OH)_6$ to analyse the Os-O interactions.

Calculations of Teo and Lee[20] show that phase shifts and backscattering amplitudes of nearest and next-nearest neighbours in the periodic table are hardly different. The use of phase shifts and backscattering amplitudes obtained from EXAFS data of reference compounds has been shown to be valid in many cases when the chemical state and local structure of the reference and the sample are comparable. Teo and Lee[20] also showed that shifts in the phase function associated with changes in the electronic configuration or oxidation state can be largely compensated by a variation of inner potential. In our analysis we have used the inner potential V_0 as an adjustable parameter. Variations in V_0 arise from uncertainties in the energy calibration and from real edge shifts between the reference material and sample. Since the values of V_0 used in our analyses were always small (< 5 eV), we infer that the assumptions concerning the phase transferability are correct.[22]

The data analysis carried out in this work involved the use of phase- and/or amplitude-corrected Fourier transforms, the difference file technique, and fitting in k space. A sensitive criterion was used to estimate the reliability of the parameters, which were determined by fitting procedures in k space. This consisted of a comparison of the Fourier transform (the imaginary part as well as the magnitude) of the EXAFS function (calculated with these parameters) with the corresponding Fourier transform of the experimental results.

3.4.2 The Os-CO Reference

The parent cluster $Os_3(CO)_{12}$ has been used as a reference to characterize the Os-CO moiety, since it is expected to be similar in the supported clusters. The Os-CO moiety was estimated by subtracting the calculated Os-Os contributions from the experimental EXAFS results obtained for

$Os_3(CO)_{12}$. The coordination number (N = 2) and Os-Os distance (2.88 Å, determined by X-ray diffraction for $Os_3(CO)_{12}$) were taken as fixed parameters in the analysis. When a coordination distance of 2.88 Å is used for the calculation of the Os-Os contribution the (Os-O phase-corrected) Fourier transform of the difference file (experimental results minus calculated Os-Os EXAFS, thus representing the Os-CO contribution) has an imaginary part which peaks positively at 1.93 Å (Os-C) and negatively at 3.08 Å (Os-O*). These values are equal (within the limits of accuracy) to the corresponding Os-C and Os-O* distances found by X-ray diffraction. This comparison demonstrates that the EXAFS results are in agreement with those obtained by X-ray diffraction. No attempt was made to analyse further the data for the $Os_3(CO)_{12}$ cluster itself. The value of the Debye-Waller factor for the Os-Os bond in the cluster determined in the analysis is 0.001 $Å^2$ smaller than that for the Pt-Pt bond in platinum metal. This result is in agreement with the higher energy of the Os-Os bonds in osmium metal (sublimation energy = 730 kJ/mol) in comparison with that of Pt-Pt bonds in platinum metal (570 kJ/mol).[23]

The occurrence of multiple scattering in the Os-O* interaction is shown in the phase-corrected Fourier transform (Figure 3.3b). The amplitude of the peak at 3 Å is much greater than the value that would be expected on the basis of the simple $1/r^2$ dependence indicated by the EXAFS formula (Chapter 2, eq 2.2). Another indication of multiple scattering is the phase shift of approx. π rad of the Os-O* peak, which results in an imaginary part with a negative peak located at the maximum of the magnitude of the Fourier transform. Similar multiple scattering effects have been observed in the Fourier transforms for $(Rh(CO)_2Cl)_2$,[24] $Na_2Fe(CO)_4$,[21] and $Mo(CO)_6$.[25] The EXAFS function obtained by back transformation (not shown) was found to give an excellent representation of the Os-CO coordination. Those data were therefore used for the analysis of the EXAFS data characterizing the Os-CO moieties in the supported clusters and the broken-up clusters. Since a quantitative theoretical calculation of this multiple scattering process is difficult, even with the best available methods, we expect that experimentally measured values of the phase shift and backscattering amplitude for this moiety will give the most reliable analyses of the EXAFS data.

3.4.3 Assessment of the Structural Models

The starting point in the analysis of the EXAFS data for the supported cluster was the assumption of the $HOs_3(CO)_{10}\{OAl\}$ structure indicated by the stoichiometry of the synthesis from $Os_3(CO)_{12}$ and surface OH groups and the results of infrared, Raman and electron microscopy experiments mentioned in Section 3.1. Therefore, a value of 3.35 (approx. 10/3) was assumed for the number of CO ligands per Os atom, and the number of nearest Os neighbours of each Os atom was taken to be two. The Os-Os distance was taken to be 2.88 Å, which is the distance in crystalline $Os_3(CO)_{12}$. An Os-Os distance of 2.84 Å, as was found in the analysis by Cook et al.[13] of EXAFS data of the triosmium cluster supported on γ-Al_2O_3, leads in our analysis procedure to imaginary parts of the Fourier transforms of the calculated EXAFS contributions which do not match those of the corresponding difference file and experimental results.

The EXAFS results strongly confirm the structural model, being fully consistent with the spectroscopic and stoichiometric data mentioned immediately above. The alumina-supported triosmium cluster is inferred to be one of the best-defined structures on a metal oxide support. The key to the structural determination is the full spectroscopic characterization, with EXAFS being essential, which is based on comparisons with spectra of analogous molecular structures characterized by X-ray crystallography. We recognize that an improved structural determination of the surface-bound cluster could be obtained from EXAFS with the use of better reference compounds (such as, for example, $HOs_3(CO)_{10}OSiEt_3$[11]). We also emphasize that EXAFS results cannot provide any evidence of the bridging hydride ligand; its existence is based entirely on inference.

The most significant new result characterizing the supported cluster is the determination of the coordination number and average length of the bonds involving the surface oxygen of the support. The average coordination distance was determined clearly from the EXAFS data when the structural assumptions for the Os-CO shell (loss of two CO ligands per cluster upon adsorption) and the Os-Os coordination (N = 2, R = 2.88 Å) were built into the analysis. The average $Os\text{-}O_{support}$ coordination number of 0.65 means that two osmium atoms of the Os_3 skeleton are bonded to a surface oxygen of the support. EXAFS cannot distinguish whether one (bridging) oxygen or two oxygen atoms of the support are involved.

Chemical arguments support the former.

The absence of any Os-Os oscillations in the experimental EXAFS spectrum and the average Os-CO coordination number of N = 2.8 provide strong confirmation of the structure of the mononuclear complex formed by breakup of the cluster on the alumina support, $Os^{II}(CO)_n\{OAl\}_3$ (n = 2 or 3).[5-7] The structure determination might be improved by use of a reference compound such as the presumably oligomeric $(Os^{II}(CO)_2I_2)$, which has iodide ligands bridging divalent osmium ions. The influence of the M-C-O angle on the experimentally obtained phase and backscattering amplitude needs to be investigated in more detail.

The striking new results characterizing the broken-up cluster are the determination of the number of surface oxygen ions bonded to the osmium and the distance between the Os atoms and these ligands. These results were determined straightforwardly and with a high degree of confidence from the analysis of the EXAFS data. An analogous structure of a metal ion with two CO ligands bonded to three support oxygen ions with a short oxide-type bond length has been reported by Van 't Blik et al.[24] This type of surface species was formed during CO chemisorption at room temperature upon very small rhodium metal particles supported on γ-Al_2O_3. The CO chemisorption process induced a disruption of the metal particles leading to a $Rh^{I}(CO)_2\{OAl\}_3$ complex.

3.4.4 Perspectives on EXAFS of Supported Organometallics and Small Metal Clusters

One of the central research goals in surface catalysis is to relate catalytic properties to structures of well-defined materials. EXAFS can give exact, detailed information about the structures of supported organometallics and small metal aggregates. As shown in this work, EXAFS also can provide precise structural information characterizing the interface (or bonds) between the organometallic species and the support. It is evident that there is fertile ground for further study of organometallics that can serve as structural analogues of metal-support interfaces (as in typical supported metal catalysts). The results can be expected to lead to a better knowledge of metal-support interactions. Decomposition of the supported organometallic cluster into mononuclear complexes followed by a reduction to ultrahighly dispersed metal particles[10,26] provides the possibility to

follow with EXAFS the formation of the metal-support interface.

In this work we have determined a distance of 2.17 Å between the osmium ion (formed by decomposition of the triosmium cluster) and the oxygen ion of the support. The EXAFS study by Asakura et al.[26] of a decomposed ruthenium cluster on alumina shows a distance of about 2.17 Å between the ruthenium ion and the support oxygen; after reduction in H_2 at 400 °C the formation of small ruthenium entities (consisting of three or four atoms) was observed. Analysis of the EXAFS data by fitting in k space showed the same ionic-type distance between the ruthenium and support oxygen after reduction. A striking feature was the stability of these ruthenium entities at high temperatures, showing a catalytic behavior different from that of typical ruthenium metal particles (d > 10 Å).

Covalent-type coordination distances between metal atoms present in the metal-support interface and oxygen ions of the support have been characterized with EXAFS for very small rhodium and platinum metal aggregates (consisting of 5 to 10 atoms) supported on γ-Al_2O_3[1,27,28] and TiO_2.[29,30] The EXAFS signal arising from the metal-support interface for very small metal particles is large enough in comparison to the EXAFS contribution of the metal-metal coordination to allow a reliable determination of the structure of the metal-support interface. For rhodium, a value of about 2.7 Å was found for the coordination distance between a rhodium metal atom and the oxygen atoms of the support. This distance is much greater than the distances observed between the atoms in the ruthenium entities and the support. The rhodium atoms in the small rhodium aggregates were certainly metallic, as determined by XPS,[24] hydrogen chemisorption,[24] and catalytic experiments.[31] On the basis of the results of the catalytic experiments and the EXAFS structural studies reported here and in the literature, we infer that the oxidation state of the ruthenium atoms in the small ruthenium entities[26] is different from zero. More EXAFS investigations are needed to characterize further the bonds present in the metal-support interface.

In summary, the results of this work show the unique value of the well-defined surface-bound organometallics as models of supported metal catalysts. The results provide a firm basis for further EXAFS studies of metal-support interfaces, which will lead to a better understanding of metal-support interactions.

3.5 References

(1) J. B. A. D. Van Zon, D. C. Koningsberger, H. F. J. Van 't Blik, and D. E. Sayers, *J. Chem. Phys.* **1985**, *82*, 5742.

(2) G. H. Via, J. H. Sinfelt, and F. W. Lytle, *J. Chem. Phys.* **1979**, *71*, 690.

(3) J. H. Sinfelt, G. H. Via, F. W. Lytle, and R. B. Greegor, *J. Chem. Phys.* **1981**, *75*, 5527.

(4) R. Psaro, and R. Ugo, *Metal Clusters in Catalysis;* B. C. Gates, L. Guczi, and H. Knözinger, Eds.; Elsevier: Amsterdam, 1986; p 427.

(5) R. Psaro, R. Ugo, G. M. Zanderighi, B. Besson, A. K. Smith, and J. M. Basset, *J. Organomet. Chem.* **1981**, *213*, 215.

(6) M. Deeba, and B. C. Gates, *J. Catal.* **1981**, *67*, 303.

(7) H. Knözinger, and Y. Zhao, *J. Catal.* **1981**, *71*, 337.

(8) M. Deeba, B. J. Streusand, G. L. Schrader, and B. C. Gates, *J. Catal.* **1981**, *69*, 218.

(9) H. Knözinger, Y. Zhao, B. Tesche, R. Barth, R. Epstein, B. C. Gates, and J. P. Scott, *Faraday Discuss.* **1981**, *72*, 53.

(10) J. Schwank, L. F. Allard, M. Deeba, and B. C. Gates, *J. Catal.* **1983**, *84*, 27.

(11) L. D'Ornelas, A. Choplin, J. M. Basset, L.-Y. Hsu, and S. Shore, *Nouv. J. Chim.* **1985**, *9*, 155.

(12) B. Besson, B. Moraweck, A. K. Smith, J. M. Basset, R. Psaro, and A. Fusi, *J. Chem. Soc., Chem. Commun.* **1980**, 569.

(13) S. L. Cook, J. Evans, and G. N. Greaves, *J. Chem. Soc., Chem. Commun.* **1983**, 1287.

(14) R. Barth, B. C. Gates, Y. Zhao, H. Knözinger, and J. Hulse, *J. Catal.* **1983**, *82*, 147.

(15) X. J. Li, and B. C. Gates, *J. Catal.* **1983**, *84*, 55.

(16) X. J. Li, J. H. Onuferko, and B. C. Gates, *J. Catal.* **1984**, *85*, 176.

(17) E. R. Corey, and L. F. Dahl, *Inorg. Chem.* **1962**, *1*, 521.

(18) R. W. G. Wyckoff, *Crystal Structure*, 2nd ed.; Wiley: New York, 1963; Vol. I, p 10.

(19) M. Troemel, and E. Lupprich, *Z. Anorg. Allg. Chem.* **1975**, *414*, 160.

(20) B. K. Teo, and P. A. Lee, *J. Am. Chem. Soc.* **1979**, *101*, 2815.

(21) B. K. Teo, *J. Am. Chem. Soc.* **1981**, *103*, 3990.

(22) F. W. Lytle, personal communication. Having both Os metal and Pt metal data available, Dr. Lytle has kindly ascertained that the phase and amplitude of Pt can indeed be used for the analysis of Os data.

(23) C. S. G. Phillips, and R. J. P. Williams, *Inorganic Chemistry*; Clarendon: Oxford, 1966; Part II, p 20.

(24) H. F. J. Van 't Blik, J. B. A. D. Van Zon, T. Huizinga, J. C. Vis, D. C. Koningsberger, and R. Prins, *J. Am. Chem. Soc.* **1985**, *107*, 3139.

(25) S. P. Cramer, K. O. Hodgson, E. I. Stiefel, and W. E. Newton, *J. Am. Chem. Soc.* **1978**, *100*, 2748.

(26) K. Asakura, M. Yamada, Y. Iwasawa, and H. Kuroda, *Chem. Lett.* **1985**, 511.

(27) D. C. Koningsberger, J. B. A. D. Van Zon, H. F. J. Van 't Blik, G. J. Visser, R. Prins, A. N. Mansour, D. E. Sayers, D. R. Short, and J. R. Katzer, *J. Phys. Chem.* **1985**, *89*, 4075.

(28) D. C. Koningsberger, and D. E. Sayers, *Solid State Ionics* **1985**, *16*, 23.

(29) D. C. Koningsberger, J. H. A. Martens, R. Prins, D. R. Short, and D. E. Sayers, *J. Phys. Chem.* **1986**, *90*, 3047.

(30) D. C. Koningsberger, H. F. J. Van 't Blik, J. B. A. D. Van Zon, and R. Prins, *Proc. 8th Int. Congress on Catalysis* (Berlin, 1984); Verlag Chemie: Weinheim, 1985; Vol. V, p 123.

(31) H. F. J. Van 't Blik, *Thesis*; Eindhoven University of Technology, Eindhoven, the Netherlands, 1984.

Chapter Four

Structural Characterization of $[H_xRe_3(CO)_{12}]^{x-3}$ (x = 2 or 3) by Extended X-ray Absorption Fine Structure Spectroscopy

4.1 Introduction

Extended X-ray Absorption Fine Structure (EXAFS) spectroscopy is a powerful technique for determination of structure of solids, but application to metal carbonyls and other compounds incorporating linear arrays of atoms is restricted by the difficulty of accounting for the multiple scattering effects. Here we demonstrate the use of EXAFS for structural characterization of metal carbonyls, taking advantage of experimental reference compounds to account for the multiple scattering effects.

The crystal structure of $H_3Re_3(CO)_{12}$ has not been reported; attempts to grow crystals suitable for structural analysis by X-ray diffraction (XRD) have been unsuccessful.[1] A full structural analysis of $[H_2Re_3(CO)_{12}]^-$ is also lacking; only the Re-Re distances are known.[2] We have characterized these clusters structurally by EXAFS spectroscopy.

EXAFS measurements were performed on the Re L_{III} edge, providing information about the coordination environment of the Re atoms in the clusters. EXAFS analysis of compounds such as metal carbonyls, in which the metal is in an almost linear array with the C and O atoms of the carbonyl ligands, presents difficulties because the multiple scattering effect is prominent.[3] The analysis calls for a reference (theoretical or experimental) taking account of the multiple scattering, and the methods are illustrated by the use of experimental references to analyse the EXAFS spectra characterizing alumina-supported crystallites of Rh with chemisorbed CO[4,5] and alumina-supported triosmium carbonyl clusters.[6] The Os-CO contribution from $Os_3(CO)_{12}$[7] in a physical mixture serves very well as a reference, being preferable to theoretical references because the values of the coordination parameters determined with the Os-CO reference are physically more realistic.[8,9] In the present research, we have used the Os-C and Os-O^* (O^* refers to the carbonyl oxygen) shells from $Os_3(CO)_{12}$ as a reference for the

Re-C and Re-O* contributions, since no structurally well-defined Re carbonyl compound was available having approximately the same geometry as the complexes to be analysed. The use of an Os reference for the analysis of Re data has been justified both theoretically and experimentally.[6,10,11]

The detailed structural characterization with EXAFS affords a comparison of the structures of $H_3Re_3(CO)_{12}$ and $[H_2Re_3(CO)_{12}]^-$ with that of $[HRe_3(CO)_{12}]^{2-}$, for which an XRD structure has been determined.[12] The results demonstrate the trends associated with the changing negative charge in the series of clusters.

4.2 Experimental

$H_3Re_3(CO)_{12}$ was prepared from $Re_2(CO)_{10}$ (Strem) by the method of Huggins et al.[1] $[(C_6H_5)_4As]$ $[H_2Re_3(CO)_{12}]$ was prepared by the method of Churchill et al;[2] the synthesis procedure was slightly modified by the addition of a 50% excess of KOH; the anion was recrystallized from a dry solution of CH_2Cl_2, ethanol, and pentane.[13] The infrared spectrum of $H_3Re_3(CO)_{12}$ in cyclohexane and that of $[(C_6H_5)_4As]$ $[H_2Re_3(CO)_{12}]$ in acetone agree well with the reported spectra.[1,2]

EXAFS measurements were performed to characterize solid $H_3Re_3(CO)_{12}$ and $[(C_6H_5)_4As]$ $[H_2Re_3(CO)_{12}]$. Each sample was mixed with inert BN and pressed into a thin self-supporting wafer having optimal X-ray absorbance. Each sample was mounted in a controlled atmosphere EXAFS cell and characterized in helium at liquid nitrogen temperature at the Re L_{III} edge (10535 eV). The measurements were performed on X-ray beam line X-11 (equipped with a Si (111) monochromator, estimated resolution 3 eV) at the Brookhaven National Synchrotron Light Source with a ring energy of 2.48 GeV and a ring current between 40 and 120 mA. The monochromator was detuned to 20% of the primary intensity, in order to reduce the higher harmonics content of the incoming X-ray beam.

As experimental references for the EXAFS data analysis, $Os_3(CO)_{12}$[7] (Strem, in a physical mixture with SiO_2) and Re metal powder[14] (Aesar, 99.999% pure) were chosen for the Re-CO and Re-Re contributions, respectively. Also ReO_3[15] data (Morton Thiokol) were used in the data analysis procedure. The data characterizing the Re powder and the Re carbonyl

clusters were collected at Brookhaven. The data characterizing $Os_3(CO)_{12}$ (L_{III} edge: 10871 eV) and ReO_3 were measured on beam line I-5 (equipped with a Si (220) monochromator, estimated resolution 3 eV) at the Stanford Synchrotron Radiation Laboratory with a ring energy of 3 GeV and a ring current between 40 and 80 mA. The gas fillings of the ionization chambers were chosen in such a way that they were made transparent for the higher harmonics in the incoming X-ray beam.

Since different experimental conditions were used for the carbonyl clusters and Re powder, and $Os_3(CO)_{12}$ and ReO_3, it was possible that a different higher harmonics content for the two sets of measurements might influence the accuracy of the data analysis results. Afterwards, we checked this for an $Os_3(CO)_{12}$ sample measured both in Brookhaven and in Stanford. No serious differences were observed between the two spectra. Small differences (less than 10% in amplitude) were present but these could entirely be attributed to a small difference in sample temperature during the measurement (the sample was cooled with liquid nitrogen using different types of dewars).

The structural data for Re metal, ReO_3, and $Os_3(CO)_{12}$ are given in Table 4.1.

4.3 Data Analysis and Results

4.3.1 Data Reduction

The EXAFS data were obtained from the X-ray absorption spectrum by a cubic spline background subtraction,[16] followed by division by the edge height.[17]

The $H_3Re_3(CO)_{12}$ data are of very good quality, but the $[(C_6H_5)_4As][H_2Re_3(CO)_{12}]$ data contain an artifact at $k > 10.3$ Å^{-1}, and the data in this range were not used. The raw data characterizing the two samples are shown in Figure 4.1, together with their k^3-weighted Fourier transforms.

The data characterizing the reference compounds are all of excellent quality; the raw EXAFS data are shown elsewhere.[6,18]

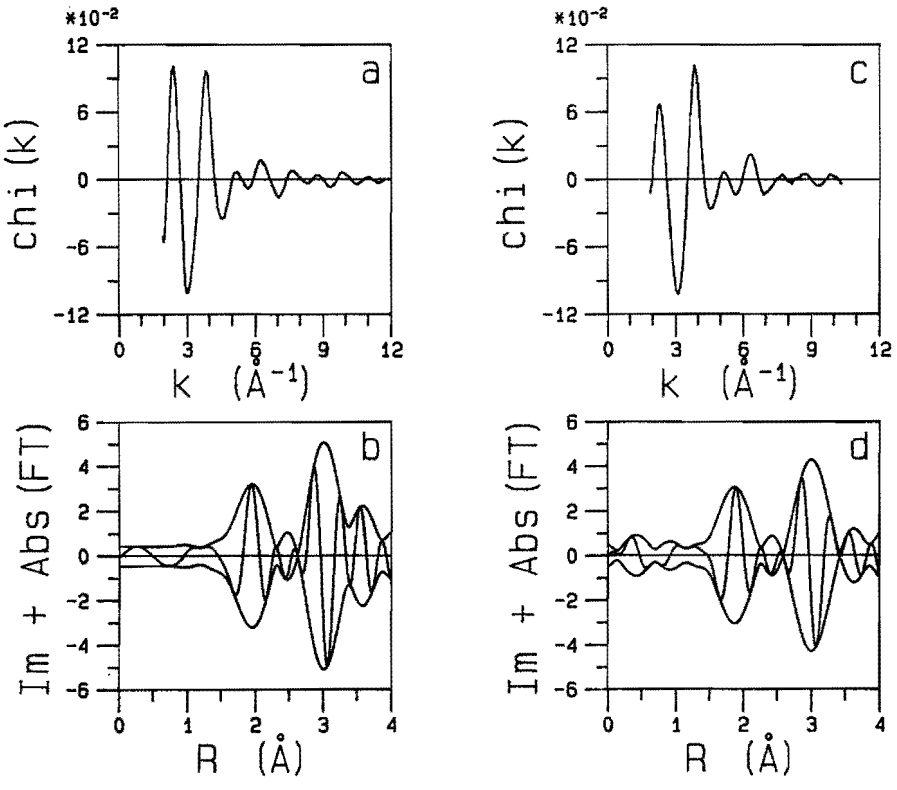

Figure 4.1. (a) Raw EXAFS data characterizing $H_3Re_3(CO)_{12}$; and (b) k^3-weighted Fourier transform (Δk = 3.51-11.14 $Å^{-1}$, Re-O phase corrected). (c) Raw EXAFS data characterizing $[H_2Re_3(CO)_{12}]^-$; and (d) k^3-weighted Fourier transform (Δk = 3.49-10.23 $Å^{-1}$, Re-O phase corrected).

4.3.2 Reference Compounds

In the data analysis procedure, only experimentally determined phases and backscattering amplitudes were used. To obtain these, each particular contribution of interest in the EXAFS data characterizing a reference compound (with accurately known coordination number and coordination distance) had to be isolated from the other contributions; this was done by taking a k^3-weighted Fourier transform (in which the peaks due to the different contributions are separated as well as possible) and then taking an

inverse Fourier transform isolating the peak of interest. This straightforward procedure was used to determine a Re-Re reference from the first Re-Re shell in Re powder.[14]

Table 4.1. Structural data for Re powder,[14] ReO_3,[15] and $Os_3(CO)_{12}$[7] and data ranges used to extract the experimental references.

Sample	Shell	N	R (Å)	Δk (Å^{-1})	Δr (Å)
Re powder	1st Re-Re	12	2.751	3.11-18.33	1.66-3.40
ReO_3	1st Re-O	6	1.867	2.54-11.04	0.66-2.08
$Os_3(CO)_{12}$[a]	Os-Os	2	2.88	-	-
	Os-C[b]	4	1.95	2.90-12.44	0.88-1.98
	Os-O*,[b]	4	3.09	2.90-12.44	1.98-3.30

[a]Os-C-O angle = 169°.

[b]After subtraction of the Os-Os contribution: coordination number N = 2, interatomic distance R = 2.88 Å, Debye-Waller factor $\Delta\sigma^2$ = -0.001 Å^2, inner potential correction V_0 = -3.3 eV; and an inner potential correction of V_0 = -4.4 eV on the difference file.

Care was taken to select a good reference for the Re-CO contributions. Structural similarity between the compounds to be analysed and the reference was a primary criterion. And since the multiple scattering effect in the Re-O* shell is crucial,[6] it was deemed essential to fit with a Re-O reference that exhibits multiple scattering. $Os_3(CO)_{12}$ was found to be a good choice: its structure is accurately known,[7] and although no hydrogen is incorporated in the cluster its structure is otherwise very similar to that proposed for $[HRe_3(CO)_{12}]^{2-}$;[12] each has a triangular metal skeleton, the same number of CO ligands per metal atom, and the same ratio of axial to equatorial carbonyl ligands. The metal-carbon distances in the two compounds are similar, as are the carbon-oxygen distances. Os is adjacent to Re in the

periodic table of the elements, and thus Os components can be used for the analysis of Re spectra,[6,10,11] if small changes in V_0 are allowed in the EXAFS data analysis procedure. In this case, however, a straightforward isolation of the Os-C and Os-O* contributions was not possible because the Os-O* contribution shows overlap with the Os-Os contribution in r space. This Os-Os contribution was first subtracted from the experimental results (as shown elsewhere,[6,18] see also Chapter 3), leaving a spectrum in which the phase of the imaginary part of the Os-O* peak is shifted approx. π rad with respect to the Os-C peak as a consequence of the multiple scattering effect.[3] As shown elsewhere,[6,18] the Os-C and Os-O* peaks seem well separated after a k^3-weighted Fourier transform, and therefore an inverse transform was applied to each in order to determine references for the Re-C and Re-O* contributions.

The first Re-O shell in ReO_3[15] was used as a Re-O reference. This reference was not used for fitting of the Re carbonyl spectra, but only to determine Re-O phase-corrected Fourier transforms.

Data ranges used in the extraction of the references and important structural parameters characterizing the reference compounds are given in Table 4.1.

4.3.3 Analysis of the Data Characterizing $H_3Re_3(CO)_{12}$ and $[H_2Re_3(CO)_{12}]^-$

The data analysis was performed with phase-corrected Fourier transforms. The use of such transforms aids in the attribution of the peaks in r space to shells of the proper neighbours.[6,17] For example, with a Re-Re phase correction, the imaginary part of the Re-Re contribution peaks positively, and with a Re-O phase correction, the imaginary part of the Re-C contribution peaks positively, whereas that of the Re-O* contribution peaks negatively (as a consequence of the multiple scattering effect in the M-O* shell of metal carbonyls[6]).

Re-O phase-corrected Fourier transforms of the data characterizing $H_3Re_3(CO)_{12}$ and $[(C_6H_5)_4As][H_2Re_3(CO)_{12}]$ are shown in Figure 4.2. It is immediately clear that the two clusters are very much alike in structure, but some differences are apparent: in $[H_2Re_3(CO)_{12}]^-$ the Re-C distance is less and the Re-O* distance is slightly greater than in $H_3Re_3(CO)_{12}$. Both peaks are somewhat smaller in the $[H_2Re_3(CO)_{12}]^-$ spectrum, and the small

peak on the right-hand side of the Re-O* peak (partly due to the Re-Re contribution) is much smaller in the spectrum characterizing this cluster.

In the further analysis of the EXAFS data the difference file technique was used[6,17] (see also Chapter 2, Section 2.2.5). First, a Re-C contribution was calculated that agreed as well as possible with the Re-C peak of the data in a Re-O phase-corrected k^3-weighted Fourier transform, with the Re-C coordination number held constant and equal to 4. This contribution was then subtracted from the data and fitting was done to find coordination parameters for the combined Re-O* + Re-Re peak. As a first guess, a Re-O* contribution was calculated with coordination number (N), disorder ($\Delta\sigma^2$), and inner potential correction (V_0) equal to the values in the Re-C contribution and with a coordination distance which resulted in the best agreement with the imaginary part of the experimental peak in r space.

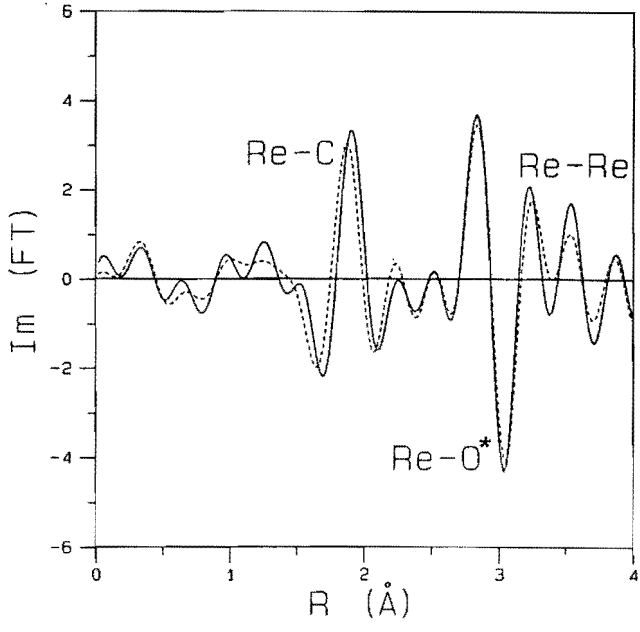

Figure 4.2. Comparison of the imaginary parts of a Re-O phase-corrected k^3-weighted Fourier transform for $H_3Re_3(CO)_{12}$ (Δk = 3.51-10.26 $Å^{-1}$) (—) and for $[H_2Re_3(CO)_{12}]^-$ (Δk = 3.49-10.23 $Å^{-1}$) (– –).

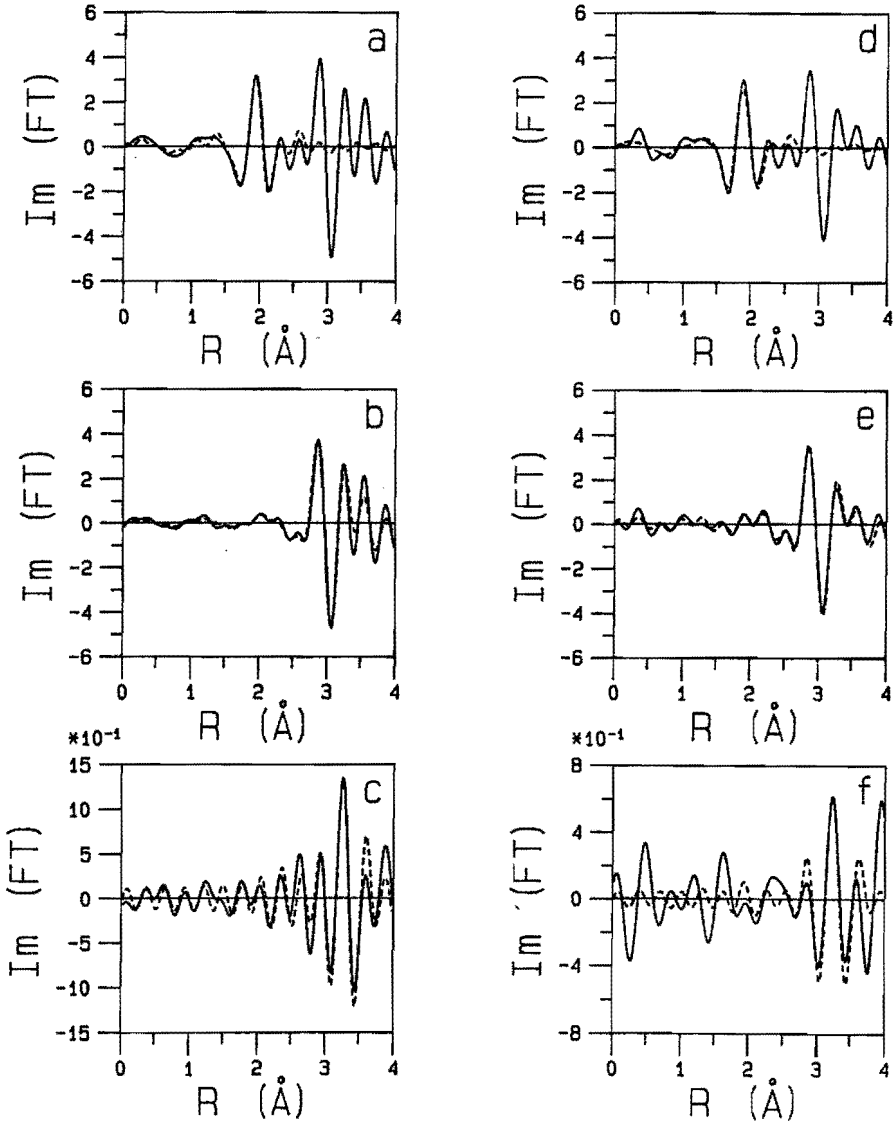

Since as a first approximation no important differences are expected between the CO ligands in the Re and Os carbonyls, N, $\Delta\sigma^2$, and V_0 should be almost equal for the Re-C and Re-O* contributions. After subtraction of this first-guess Re-O* contribution, the best Re-Re parameters were determined. For the Re-Re contribution, the coordination number was held constant and equal to 2. Subsequently, all three contributions were added and compared with the data in k space and in r space after a k^3-weighted Fourier transform.

← **Figure 4.3.** Illustration of the subsequent steps used in the difference file technique for EXAFS data analysis. (a) k^3-weighted Fourier transform (Δk = 3.51-11.14 $Å^{-1}$) of the experimental results (—) and best Re-C contribution (— —) for $H_3Re_3(CO)_{12}$ (Re-O phase corrected); (b) experimental results minus Re-C contribution (—), and best Re-O* contribution (— —) (Re-O phase corrected); and (c) experimental results minus Re-C and Re-O* contributions (—), and best Re-Re contribution (— —) (Re-Re phase corrected). (d) k^3-weighted Fourier transform (Δk = 3.49-10.23 $Å^{-1}$) of the experimental results (—) and best Re-C contribution (— —) for $[H_2Re_3(CO)_{12}]^-$ (Re-O phase corrected); (e) experimental results minus Re-C contribution (—), and best Re-O* contribution (— —) (Re-O phase corrected); and (f) experimental results minus Re-C and Re-O* contributions (—), and best Re-Re contribution (— —) (Re-Re phase corrected).

Usually, such a first cycle in the difference file technique does not yield the best agreement possible, and therefore the previously calculated Re-O* and Re-Re contributions were subtracted from the data, and better parameters were sought for the Re-C shell. This procedure was repeated for each of the contributions until a good overall agreement had been obtained. At this stage the only constraints were (1) that the coordination numbers of the Re-C, Re-O*, and Re-Re shells were fixed at 4, 4, and 2, respectively, and (2) that the inner potential corrections for the Re-C and Re-O* shells were kept equal. The subsequent steps in the difference file technique are shown in Figure 4.3 for $H_3Re_3(CO)_{12}$ and for $[(C_6H_5)_4As]$ $[H_2Re_3(CO)_{12}]$. The Re-C, Re-O*, and Re-Re contributions have been calculated with the best parameters. The final results are shown in Figure 4.4. The best parameters determined in the analysis are given in Table 4.2.

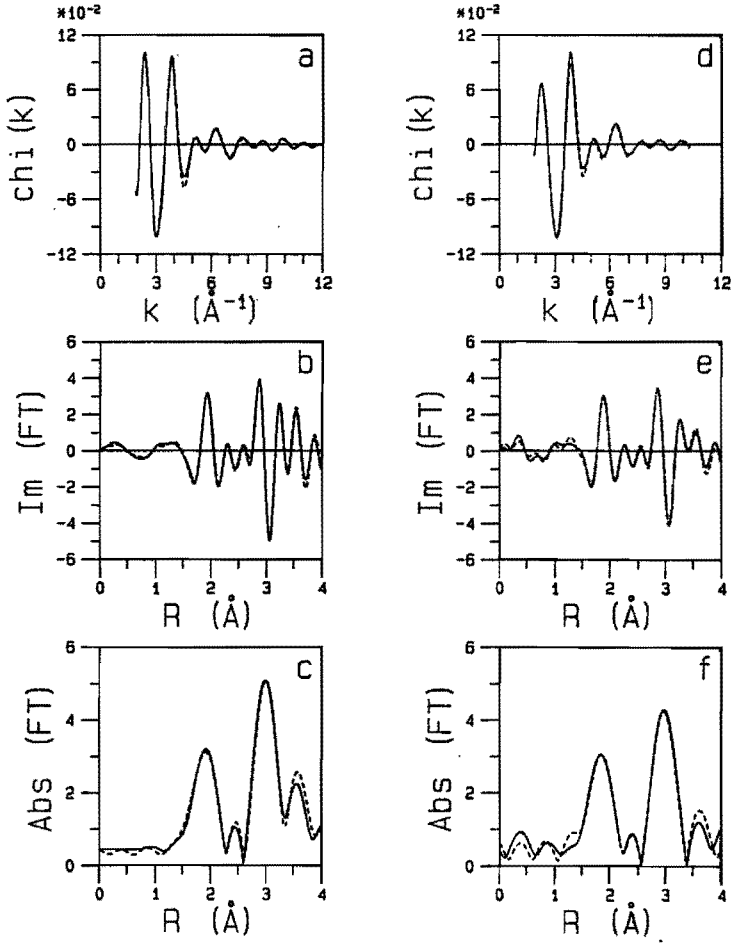

Figure 4.4. EXAFS analysis results obtained with the best calculated coordination parameters. Experimental results (—) and sum of the calculated Re-C, Re-O*, and Re-Re contributions (– –) in k space for (a) $H_3Re_3(CO)_{12}$; (b) imaginary part after a k^3-weighted Fourier transform (Δk = 3.51-11.14 $Å^{-1}$, Re-O phase corrected); and (c) magnitude. Experimental results (—) and sum of the calculated Re-C, Re-O*, and Re-Re contributions (– –) in k space for (d) $[H_3Re_3(CO)_{12}]^-$; (e) imaginary part after a k^3-weighted Fourier transform (Δk = 3.49-10.23 $Å^{-1}$, Re-O phase corrected); and (f) magnitude.

Table 4.2. Structural data for $H_3Re_3(CO)_{12}$ and $[(C_6H_5)_4][H_2Re_3(CO)_{12}]$ (from EXAFS) and for $[Et_4N]_2[HRe_3(CO)_{12}]$ (from XRD[12]).

Sample	Shell[a]	N	R (Å)	$\Delta\sigma^2$ (Å^2)
$H_3Re_3(CO)_{12}$	Re-Re	2	3.285	-0.0003
	Re-C	4	1.976	0.0015
	Re-O*	4	3.102	0.0013
$[H_2Re_3(CO)_{12}]^-$	Re-Re	2	3.246	0.0038
	Re-C	4	1.934	0.0024
	Re-O*	4	3.112	0.0018
$[HRe_3(CO)_{12}]^{2-}$	Re-Re	1.33	3.016	-
		0.67	3.125	-
	Re-C	4	1.83	-
	Re-O*	4	3.07	-

[a]For EXAFS results: Re-Re parameters with respect to the first Re-Re shell in Re powder, Re-C parameters with respect to the Os-C shell in $Os_3(CO)_{12}$, and Re-O* parameters with respect to the Os-O* shell in $Os_3(CO)_{12}$.

Accuracies: R ± 0.05 Å (Re-Re), ± 0.02 Å (Re-C, Re-O*); $\Delta\sigma^2$ ± 0.001 Å^2.

4.4 Discussion

A triangular metal framework has been proposed for each of the clusters $H_3Re_3(CO)_{12}$ and $[H_2Re_3(CO)_{12}]^-$;[1,2] in the neutral cluster, each of the Re-Re bonds is bridged with a hydride ligand, and in the anionic cluster, two of the three Re-Re bonds are bridged with hydride ligands. The EXAFS results corroborate these models; a nearly linear Re-Re-Re skeleton can be ruled out because in r space no Re-Re peak is observed at ~ 6.5 Å (data not shown); such a peak should be prominent because the intermediate Re atom would cause multiple scattering.[3] Structures of $H_3Re_3(CO)_{12}$ and $[H_2Re_3(CO)_{12}]^-$ are shown in Figure 4.5.

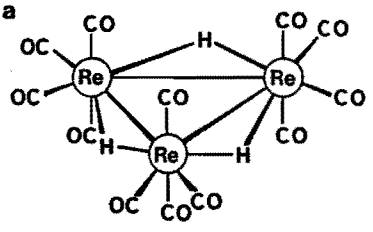

$R_{Re-Re} = 3.285$ Å
$R_{Re-C} = 1.976$ Å
$R_{C-O} = 1.126$ Å

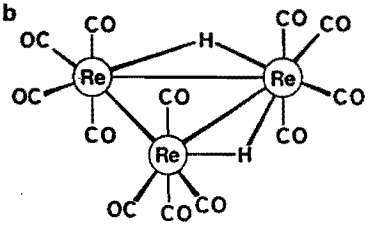

$R_{Re-Re} = 3.246$ Å
$R_{Re-C} = 1.934$ Å
$R_{C-O} = 1.178$ Å

Figure 4.5. Structural models for (a) $H_3Re_3(CO)_{12}$; and (b) $[H_2Re_3(CO)_{12}]^-$. The presence of the bridging H ligands is inferred from chemical arguments only.

The Re-Re distances determined for $H_3Re_3(CO)_{12}$ and $[H_2Re_3(CO)_{12}]^-$ are typical of Re-Re bonds.[19] The mean Re-Re distance in $H_3Re_3(CO)_{12}$ is greater than that in $[H_2Re_3(CO)_{12}]^-$, which is expected because in the neutral cluster all three Re-Re bonds have bridging hydride ligands, and these bridged Re-Re bonds are usually longer than non-bridged Re-Re bonds.[19] Also, the Debye-Waller term (an indication of the disorder in a coordination shell) is larger in the case of the $[H_2Re_3(CO)_{12}]^-$ cluster. This result indicates a range of Re-Re distances rather than a single well-defined one.

However, there is some difference between the mean value for the Re-Re bond in $[H_2Re_3(CO)_{12}]^-$ determined by EXAFS (3.246 ± 0.05 Å) and that determined by XRD (3.13 ± 0.02 Å).[2] Since from the cluster structure no other contributions are expected around R ~ 3.2 Å (the nearest contribution being an interaction between Re and C from the CO ligands on the other Re atoms at R ~ 3.8 Å), this discrepancy can not be explained by interference with other contributions in the EXAFS spectrum. It must be kept in mind, however, that in calculating the mean bond length from XRD, all Re-Re bonds are weighted equally. (The bridged Re-Re bonds are 3.170 Å and 3.181 Å, and the non-bridged Re-Re bond is 3.035 Å.[2]) In contrast, in determining the mean bond length by EXAFS, the bonds with the smallest $\Delta\sigma^2$ are weighted more heavily. Thus the larger value of the mean Re-Re bond length determined with EXAFS is consistent with the fact that the hydrogen-bridged Re-Re bonds have a smaller Debye-Waller factor (i. e., are less affected by lattice vibrations) than the non-bridged Re-Re bond.

Table 4.3. Comparison of Re-C and C-O bond distances in the $[H_xRe_3(CO)_{12}]^{x-3}$ (x = 1,2, or 3) clusters.

Sample	Re-C (Å)	C-O (Å)
$H_3Re_3(CO)_{12}$	1.976	1.126
$[H_2Re_3(CO)_{12}]^-$	1.934	1.178
$[HRe_3(CO)_{12}]^{2-}$ [12]	1.83	1.24

A comparison of the Re-C and C-O bond distances in the $[H_xRe_3(CO)_{12}]^{x-3}$ (x = 1,2, or 3) clusters obtained from EXAFS and XRD (Table 4.3) shows that as the cluster becomes more negatively charged, the Re-C distance decreases and the C-O distance increases. This trend can be explained by increased π-backbonding in the case of the more negatively charged clusters, because then the Re atoms can donate more electrons to the π^* orbitals of the CO ligands, thus increasing the Re-C bond strength and decreasing the C-O bond strength.

The high quality of the EXAFS data obtained in this work allows more than a determination of differences in C-O distance with respect to the reference compound; the data also provide information about the differences in the M-C-O angles. As the enhancement of the M-O* contribution is a function of M-C-O angle (the enhancement being stronger when the M-C-O angle approaches 180° [3]) enlargement of the M-C-O angle with respect to the Os-C-O angle in the reference compound $Os_3(CO)_{12}$ is indicated in the EXAFS data analysis by a larger N and/or a smaller $\Delta\sigma^2$ for the M-O* contribution with respect to the M-C contribution. From theoretical calculations[3] it may be concluded that in the case of low-Z scatterers like oxygen, a change in M-C-O angle may well be approximated by a change in $\Delta\sigma^2$ only (see also Chapter 2, Section 2.3).

For both the $H_3Re_3(CO)_{12}$ and the $[H_2Re_3(CO)_{12}]^-$ clusters, the Debye-Waller factors characterizing the Re-C and Re-O* shells do not differ beyond the accuracy (± 0.001 Å^2) (Table 4.2). This result implies that the mean Re-C-O angle in these complexes is approximately equal to the Os-C-O angle in $Os_3(CO)_{12}$, viz. 169°. In the XRD structure determination of $[HRe_3(CO)_{12}]^{2-}$ a mean Re-C-O angle of 169° was found as well.[12] Thus we infer that there is only very little influence of the overall charge on the cluster (and thus the extent of π-backbonding) on the Re-C-O angle.

In summary, with the aid of good reference compounds, it is well possible to do a rather complete structure determination of a metal carbonyl with EXAFS. Special attention must be paid to the choice of references for the metal-carbonyl contributions because of the multiple scattering effect.

4.5 References

(1) D. K. Huggins, W. Fellmann, J. M. Smith, and H. D. Kaesz, *J. Am. Chem. Soc.* **1964**, *86*, 4841.

(2) M. R. Churchill, P. H. Bird, H. D. Kaesz, R. Bau, and B. Fontal, *J. Am. Chem. Soc.* **1968**, *90*, 7135.

(3) B. K. Teo, *J. Am. Chem. Soc.* **1981**, *103*, 3990.

(4) H. F. J. Van 't Blik, J. B. A. D. Van Zon, D. C. Koningsberger, and R. Prins, *J. Mol. Catal.* **1984**, *25*, 379.

(5) H. F. J. Van 't Blik, J. B. A. D. Van Zon, T. Huizinga, J. C. Vis, D. C. Koningsberger, and R. Prins, *J. Am. Chem. Soc.* **1985**, *107*, 3139.

(6) F. B. M. Duivenvoorden, D. C. Koningsberger, Y. S. Uh, and B. C. Gates, *J. Am. Chem. Soc.* **1986**, *108*, 6254.

(7) E. R. Corey, and L. F. Dahl, *Inorg. Chem.* **1962**, *1*, 521.

(8) S. L. Cook, J. Evans, and G. N. Greaves, *J. Chem. Soc., Chem. Commun.* **1983**, 1287.

(9) N. Binsted, S. L. Cook, J. Evans, G. N. Greaves, and R. J. Price, *J. Am. Chem. Soc.* **1987**, *109*, 3669.

(10) B. K. Teo, and P. A. Lee, *J. Am. Chem. Soc.* **1979**, *101*, 2815.

(11) B. Lengeler, *J. de Phys. C8* **1986**, *47*, 75.

(12) G. Ciani, G. D'Alfonso, M. Freni, P. Romiti, and A. Sironi, *J. Organomet. Chem.* **1978**, *157*, 193.

(13) P. S. Kirlin, F. A. DeThomas, J. W. Bailey, H. S. Gold, C. Dybowski, and B. C. Gates, *J. Phys. Chem.* **1986**, *90*, 4882.

(14) R. W. G. Wyckoff, *Crystal Structures*, 2nd ed.; Wiley: New York, 1963; Vol. I, p 11.

(15) R. W. G. Wyckoff, *Crystal Structures*, 2nd ed.; Wiley: New York, 1964; Vol. II, p 52.

(16) J. W. Cook, and D. E. Sayers, *J. Appl. Phys.* **1981**, *52*, 5024.

(17) J. B. A. D. Van Zon, D. C. Koningsberger, H. F. J. Van 't Blik, and D. E. Sayers, *J. Chem. Phys.* **1985**, *82*, 5742.

(18) P. S. Kirlin, F. B. M. Van Zon, D. C. Koningsberger, and B. C. Gates, to be published.

(19) G. Ciani, A. Sironi, and V. G. Albano, *J. Organomet. Chem.* **1977**, *136*, 339.

Chapter Five

An EXAFS Study of the Structure of $Ir_4(CO)_{12}$ Adsorbed on Partially Dehydrated γ-Al_2O_3: Applicability as a Model for Reduced Ir/γ-Al_2O_3 Catalysts

5.1 Introduction

Metal particles in supported metal catalysts usually are non-uniform in size and shape. This may cause differences in the catalytic performance of the particles. Clearly it is not simple to acquire a direct relationship between the catalytic activity and the structural properties of such a catalyst. It is thus attractive to use supported organometallic species as model systems for supported metal catalysts[1-7] (see also Chapter 3). They have the important advantage that a system can be obtained in which the metal aggregates are uniform in size and shape, allowing a more accurate determination of the structural properties. Knowledge of these properties makes it possible to establish the important relation between structural and catalytic properties. Another advantage of a system with uniform metal entities, is that the metal-support interaction also will be uniquely defined. This makes it easy to quantify the metal-support contribution.

In this study we have characterized the $Ir_4(CO)_{12}$ cluster, adsorbed on partially dehydrated γ-Al_2O_3. Also, this system has been compared with a reduced Ir/γ-Al_2O_3 catalyst prepared by the conventional incipient wetness technique,[8] in order to determine to what extent the supported cluster resembles the metal particles in the reduced Ir/γ-Al_2O_3 system. Characterization of the supported $Ir_4(CO)_{12}$ cluster was mainly done with the EXAFS (Extended X-ray Absorption Fine Structure) technique, while IR spectroscopy and TPD/MS (Temperature Programmed Decomposition combined with Mass Spectrometry) were used as auxiliary techniques.

5.2 Experimental

5.2.1 Sample Preparation

$Ir_4(CO)_{12}$ was obtained from Alfa Products, and used without further purification. γ-Al_2O_3 (Ketjen, 000-1.5E, surface area 200 m^2/g, particle size 250-425 μ) was partially dehydroxylated by calcining in vacuum at 773 K for 8 h. Cyclohexane was dried over a sodium/benzophenone mixture and used freshly distilled. The metal carbonyl was dissolved in the dried cyclohexane and stirred with γ-Al_2O_3 under N_2 for 4 h. After filtration and drying overnight in vacuum, the final Ir loading was 0.8% by weight. EXAFS, IR, and TPD/MS experiments were done with this sample. Difficulties in the quantification of the TPD/MS results, mainly due to a broad background superposed on the CO evolution signal (see Section 5.4), made it necessary to prepare a slightly different sample. In this case larger γ-Al_2O_3 particles were used (425-500 μ) in order to avoid pressure build-up in the reactor bed. Benzene (pretreated in the same way as cyclohexane) was used as a solvent in order to reduce interference of the signal from decomposition products of the solvent, and the final Ir loading was 1.4% by weight in order to obtain a larger $Ir_4(CO)_{12}$ CO evolution peak with respect to the background signal. Judging from the IR spectra, the changed preparation procedure has no influence on the structure of the adsorbed clusters.

5.2.2 IR Measurements

IR spectra of Nujol mulls between KBr windows were measured with a Hitachi 270-30 Infrared Spectrophotometer. The spectral resolution was approx. 6 cm^{-1}. Measurements were carried out on samples of a physical mixture with approx. 2 wt% $Ir_4(CO)_{12}$ and dehydrated γ-Al_2O_3, and of $Ir_4(CO)_{12}$ adsorbed on γ-Al_2O_3.

5.2.3 TPD/MS Measurements

In order to follow the chemisorption of $Ir_4(CO)_{12}$ on γ-Al_2O_3, and to obtain information about the loss of CO ligands in this process, we compared the temperature programmed decomposition of a physical mixture of approx. 2 wt% $Ir_4(CO)_{12}$ and dehydrated γ-Al_2O_3 with that of $Ir_4(CO)_{12}$ adsorbed on γ-Al_2O_3. Evolution of H_2, CH_4, H_2O, CO, and CO_2 were

monitored with a Leybold Heraeus Quadruvac PGA 100 Mass Spectrometer. TPD experiments were performed in He, at $1 \cdot 10^5$ Pa, with a maximum temperature of 573 K and a heating rate of 5 or 10 K/min.

5.2.4 EXAFS Measurements

The EXAFS measurements were performed on Wiggler station 9.2 at the SRS at Daresbury, U. K. The samples were pressed into thin self-supporting wafers with an absorbance of approximately 2.5, and mounted in an in situ EXAFS cell. The Ir L_{III} edge (11215 eV) of the supported $Ir_4(CO)_{12}$ sample was measured in helium at 77 K. As reference compounds were used Pt foil[9] and $Na_2Pt(OH)_6$[10] (Pt L_{III} edge at 11564 eV), both measured at 77 K. Reference data of a physical mixture of $Ir_4(CO)_{12}$[11] and dehydrated SiO_2 (Ir L_{III} edge) were collected in helium at 77 K. Pt foil was used as a reference for the Ir-Ir interactions in the supported cluster, $Na_2Pt(OH)_6$ for the Ir-O bonds, and the physical mixture with $Ir_4(CO)_{12}$ both for the Ir-C and Ir-O^* (O^* denoting carbonyl oxygen) contributions. It has been shown theoretically[12] and experimentally[7,13] (see also Chapter 3) that Pt references can be used for Ir contributions.

5.3 Results

5.3.1 IR Experiments

The IR spectra taken of $Ir_4(CO)_{12}$ in a physical mixture with γ-Al_2O_3, or adsorbed on γ-Al_2O_3, are shown in Figure 5.1. Peak positions obtained for $Ir_4(CO)_{12}$ in the physical mixture agree well with literature.[14] After adsorption, some differences in peak positions and relative magnitude are observed between the data for the physical mixture and those for the adsorbed cluster. From the fact that for the adsorbed complex no peaks are observed in the region of 1950-1750 cm^{-1}, it can be concluded that the surface complex contains no bridging carbonyl ligands. Because only few molecular substituted $Ir_4(CO)_{12}$ complexes without bridging CO ligands are known,[15,16] it is difficult to infer the surface structure from comparison with IR spectra of molecular analogues. The fact that no bridging CO ligands are present in the adsorbed complex, makes it possible to reliably

carry out the EXAFS data analysis.

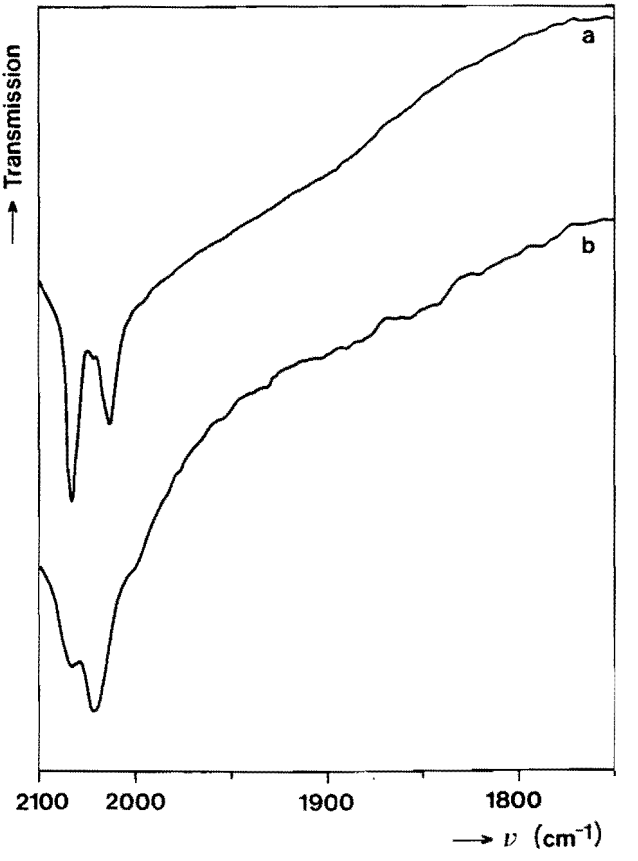

Figure 5.1. IR spectra of (a) $Ir_4(CO)_{12}$ in a physical mixture with partially dehydrated γ-Al_2O_3; and (b) $Ir_4(CO)_{12}$ adsorbed on partially dehydrated γ-Al_2O_3.

5.3.2 TPD/MS Experiments

The TPD curves for $Ir_4(CO)_{12}$ in a physical mixture with γ-Al_2O_3 are shown in Figure 5.2a. It is evident from the TPD that CO is the dominant decomposition product at low temperatures. CH_4 is not detected at all, and CO_2 mainly above 573 K. Quantification of the CO signal resulted in the

evolution of 4.4 ($\pm$ 0.4) molecules CO per $Ir_4(CO)_{12}$ cluster, thus a probable overall composition of the decomposition product of $Ir_4(CO)_8$. Presumably isolated $Ir^I(CO)_2$ entities[17] are formed on the γ-Al_2O_3 surface.

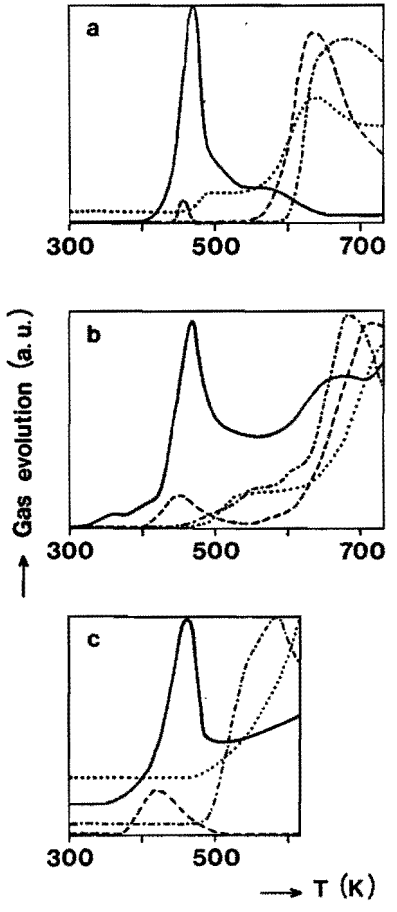

Figure 5.2. TPD (Temperature Programmed Decomposition) curves for (a) $Ir_4(CO)_{12}$ in a physical mixture with γ-Al_2O_3; (b) $Ir_4(CO)_{12}$ adsorbed on γ-Al_2O_3 from cyclohexane; and (c) $Ir_4(CO)_{12}$ adsorbed on γ-Al_2O_3 from benzene. (—) CO, (– –) CO_2, (• • •) H_2, and (– • –) H_2O evolution signal.

Also for $Ir_4(CO)_{12}$ adsorbed on γ-Al_2O_3, CO is the dominant decomposition product at low temperatures. In this case, however, quantification is more difficult. As can be seen in Figure 5.2b, the CO evolution curve (solid line) consists of a sharp peak located at almost the same position as the CO evolution peak in the TPD of the physical mixture, superposed on a broad background. Decomposition of the adsorbed cluster is expected at lower or equal temperature than that of the physical mixture, viz. below 545 K. Quantification of the CO produced up to 545 K (i. e. until after the sharp CO evolution peak) resulted in the evolution of more than 12 CO molecules per cluster. Clearly, not all CO detected originates from the decomposition of the adsorbed cluster. This can be caused by decomposition of the solvent to CO, or pressure build-up in the reactor bed. Therefore the TPD was recorded of a chemisorbed $Ir_4(CO)_{12}$ sample prepared with larger γ-Al_2O_3 particles in benzene as a solvent. Quantification of the sharp CO evolution peak now yielded 1.8 ($\pm$ 0.2) CO molecules per cluster. Assuming that the same decomposition product is formed as in the case of the physical mixture (which is supported by the fact that CO evolution takes place at almost the same temperature), TPD/MS results indicate that adsorption of $Ir_4(CO)_{12}$ occurs with the loss of 2 CO ligands.

5.3.3 EXAFS Results and Data Analysis

Standard procedures[18,19] were used to extract the raw EXAFS data from the measured spectrum. The raw EXAFS data for $Ir_4(CO)_{12}$ in a physical mixture and $Ir_4(CO)_{12}$ adsorbed on γ-Al_2O_3 are shown in Figure 5.3a and 5.3b, respectively. The data were of excellent quality, and could be reliably used up to k = 16 $Å^{-1}$.

5.3.3.1 Reference Compounds

Analysis of the EXAFS data was performed using experimentally determined phases and backscattering amplitudes.[7,18,20,21] Phase and backscattering amplitude were determined from the EXAFS spectra of the reference compounds as follows: a k^3-weighted Fourier transform was applied to the data over an interval in k space as large as possible. As k_{min} the value was chosen at which the first node occurred, and as k_{max} a node was chosen up to which the spectrum was judged reliable (i. e. no artifacts or excessive noise). In the resulting spectrum in r space the peak of interest

(usually representing the first coordination shell) was isolated by an inverse transformation. As r_{min} and r_{max} nodes in the imaginary part were chosen, preferably at positions at which the magnitude is as low as possible. This straightforward procedure was used to manufacture references from the data for Pt foil and $Na_2Pt(OH)_6$. Theoretically[12] and experimentally[7,13] (see also Chapter 3) it is allowed to use Pt references for Ir contributions. The first shell structural parameters for the reference compounds and the data ranges used in obtaining the reference data are given in Table 5.1.

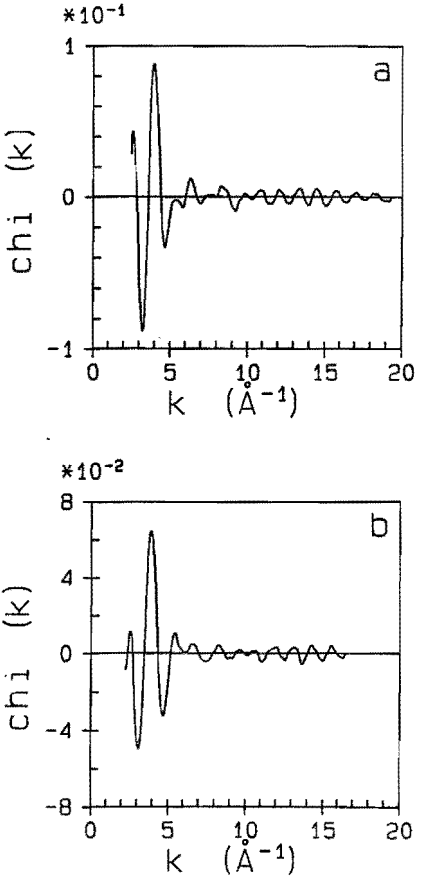

Figure 5.3. Raw EXAFS data for (a) $Ir_4(CO)_{12}$ in a physical mixture with γ-Al_2O_3; and (b) $Ir_4(CO)_{12}$ adsorbed on γ-Al_2O_3.

Table 5.1. Some structural parameters of the reference compounds and ranges in k and in r space used to extract the references from the experimental EXAFS data.

Sample	Shell	N	R (Å)	Δk (Å^{-1})	Δr (Å)
Pt foil[9]	Pt-Pt	12	2.77	1.95-19.77	1.90-3.02
$Na_2Pt(OH)_6$[10]	Pt-O	6	2.05	1.43-17.69	0.50-2.02
$Ir_4(CO)_{12}$[11]	Ir-Ir	3	2.69	-	-
	Ir-C[a]	3	1.87	2.80-16.45	1.06-1.98
	Ir-O*, [a]	3	3.01	2.80-16.45	1.98-3.30

[a]After subtraction of the Ir-Ir contribution: N = 3, R = 2.69 Å, $\Delta\sigma^2$ = -0.001 Å^2, V_0 = 2.5 eV.

For the Ir-C and Ir-O* references the procedure was more complex due to interference with the Ir-Ir contribution. It was necessary to eliminate this contribution from the spectrum prior to the manufacture of the Ir-C and Ir-O* references. This was done as follows: the high-k part of the spectrum (k > 11 Å^{-1}), which is almost exclusively due to Ir-Ir contributions, was fitted with the coordination number fixed at N = 3 (the actual Ir-Ir coordination number in the metal skeleton[11]). With N = 3 and R, $\Delta\sigma^2$ and V_0 from the fit procedure, an Ir-Ir contribution was calculated and subsequently subtracted from the data. The difference file was Fourier transformed with a Pt-O phase correction. Such a phase-corrected Fourier transform causes the imaginary part of the Ir-C contribution to peak positively, while the imaginary part of the Ir-O* contribution peaks negatively due to the multiple scattering contribution in this shell[7,22,23] (see also Chapters 3 and 4). We applied as a criterion for the correct removal of the Ir-Ir contribution that in a Pt-O phase-corrected Fourier transform of the difference file (experimental data minus calculated Ir-Ir contribution) the imaginary part of both the Ir-C and Ir-O* contributions should be symmetrical. Experimentally, good results were obtained for $Os_3(CO)_{12}$ using this criterion[7] (see also Chapter 3). Symmetrical imaginary parts could be

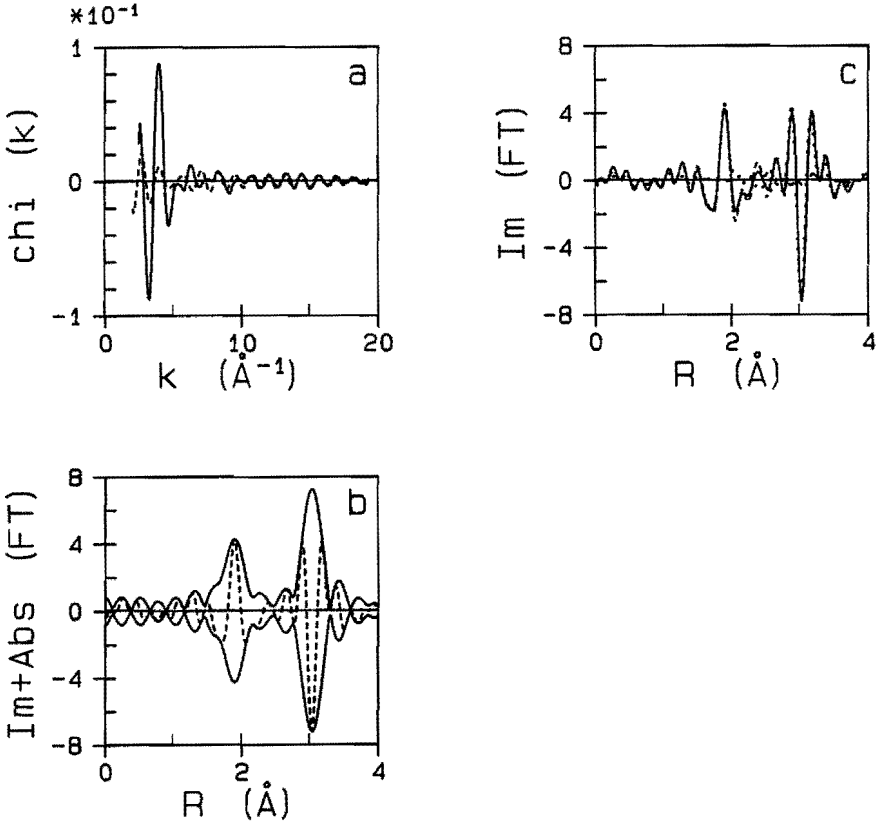

Figure 5.4. Manufacture of Ir-C and Ir-O* references from the EXAFS data for $Ir_4(CO)_{12}$. (a) Raw EXAFS data for $Ir_4(CO)_{12}$ (—), and Ir-Ir contribution calculated with the best fit parameters (— —) (see Table 5.1); (b) imaginary part (— —) and magnitude (—) of the k^3-weighted, Pt-O phase-corrected Fourier transform (Δk = 3.8-15.6 $Å^{-1}$) of the EXAFS data for $Ir_4(CO)_{12}$ minus the best Ir-Ir contribution; and (c) k^3-weighted, Pt-O phase-corrected Fourier transform (Δk = 3.8-15.6 $Å^{-1}$) of the EXAFS data for $Ir_4(CO)_{12}$ minus the best Ir-Ir contribution (—), the isolated Ir-C shell (— —), and the isolated Ir-O* shell (• • •) (all data corrected with V_0 = -5.9 eV).

obtained when we slightly varied the V_0 value found in the fit procedure for the Ir-Ir contribution. This best contribution was thus subtracted from the data, the residue was Fourier transformed over an interval as large as possible, and an inverse transform was applied to isolate the Ir-C and Ir-O* peaks, respectively. The manufacture of the Ir-C and Ir-O* references is illustrated in Figure 5.4. The intervals in k and in r space used in the manufacture of the references are given in Table 5.1.

5.3.3.2 $Ir_4(CO)_{12}$ Adsorbed on γ-Al_2O_3

Comparison of the spectra of $Ir_4(CO)_{12}$ in a physical mixture, and adsorbed on γ-Al_2O_3 (see Figure 5.3) shows several important characteristics. First, the signal above k = 11 $Å^{-1}$ is very similar in both spectra. The signal due to Ir-Ir contributions is very dominant in this region.[12] It is thus expected that the Ir-Ir contribution will be very much alike in both clusters, i. e. the metal skeleton has not changed essentially upon adsorption. On the other hand clear differences are observed at low k values both in amplitude and in phase. This can be caused by exchange of CO ligands for other types of ligands emanating from the support; loss of CO ligands results in a decreased amplitude, while the introduction of new ligands affects the phase.

With the help of the references the EXAFS spectrum of the organometallic cluster adsorbed on γ-Al_2O_3 was analysed. First, the parameters for the Ir-Ir contribution were estimated, being the largest contribution in a k^3-weighted Fourier transform of the EXAFS spectrum. A good estimate for the coordination parameters could be obtained by fitting the high-k region of the EXAFS spectrum ($11 < k < 16$ $Å^{-1}$); the coordination number obtained was very close to N = 3. Therefore the other parameters were determined fixing the coordination number at N = 3. Subsequently an Ir-Ir contribution calculated with these parameters was subtracted from the data. Next, the best parameters were sought for the Ir-C contribution. The coordination number was fixed at N = 2.5 (the mean number of CO ligands per Ir atom in the cluster after adsorption, as determined by TPD/MS) and the other parameters were varied so as to get the best coincidence possible with the difference spectrum after a k^3-weighted Fourier transform. Also, this first guess Ir-C contribution was subtracted from the experimental data, and the Ir-O* contribution was tried. For the Ir-O* con-

tribution, both N and V_0 were fixed: N at 2.5, and V_0 at the same value as was determined for the Ir-C contribution. The Ir-O^* contribution with R and $\Delta\sigma^2$ for which the k^3-weighted Fourier transform agreed best with the difference file, was subtracted. A k^3-weighted Fourier transform of the remainder still showed a considerable contribution at R ~ 2.55 Å, which can be attributed to an Ir-$O_{support}$ contribution. Also for this contribution

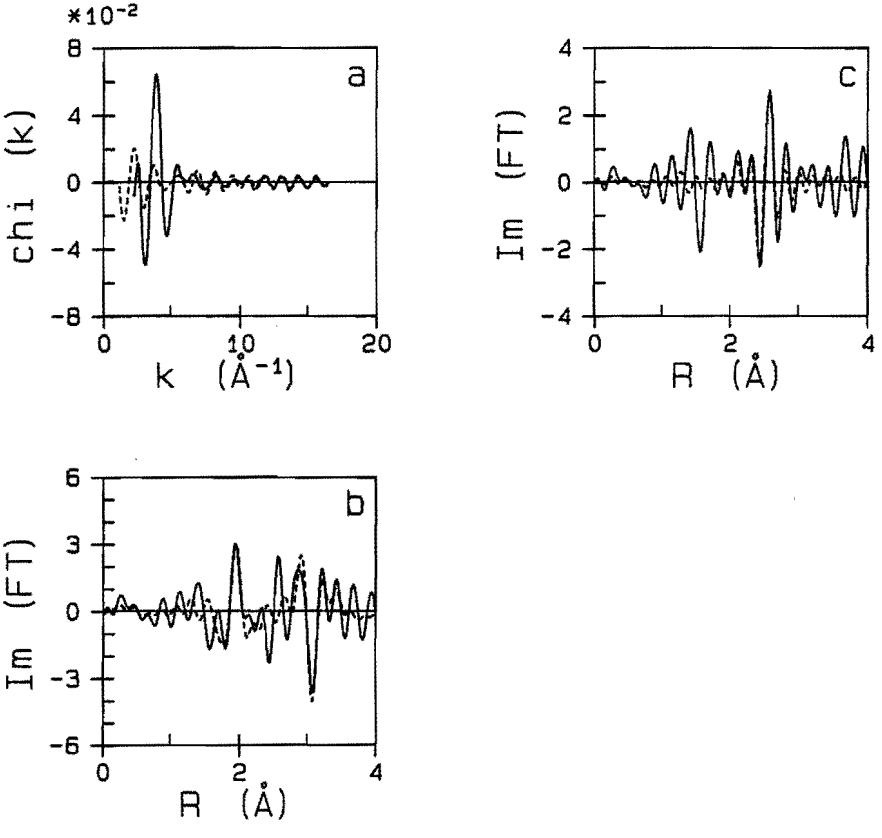

Figure 5.5. Analysis of the EXAFS data for $Ir_4(CO)_{12}$ adsorbed on γ-Al_2O_3. (a) Experimental data (—), and Ir-Ir contribution calculated on the basis of the best fit parameters (— —); k^3-weighted, Pt-O phase-corrected Fourier transform (Δk = 3.5-15.6 $Å^{-1}$) of (b) experimental data minus best Ir-Ir contribution (—), and best calculated Ir-C plus Ir-O^* contributions (— —); and (c) experimental data minus best Ir-Ir, Ir-C, and Ir-O^* contributions (—), and best calculated Ir-$O_{support}$ contribution (— —).

the best parameters were determined based upon the best agreement between the difference file and the calculated contribution in a k^3-weighted Fourier transform.

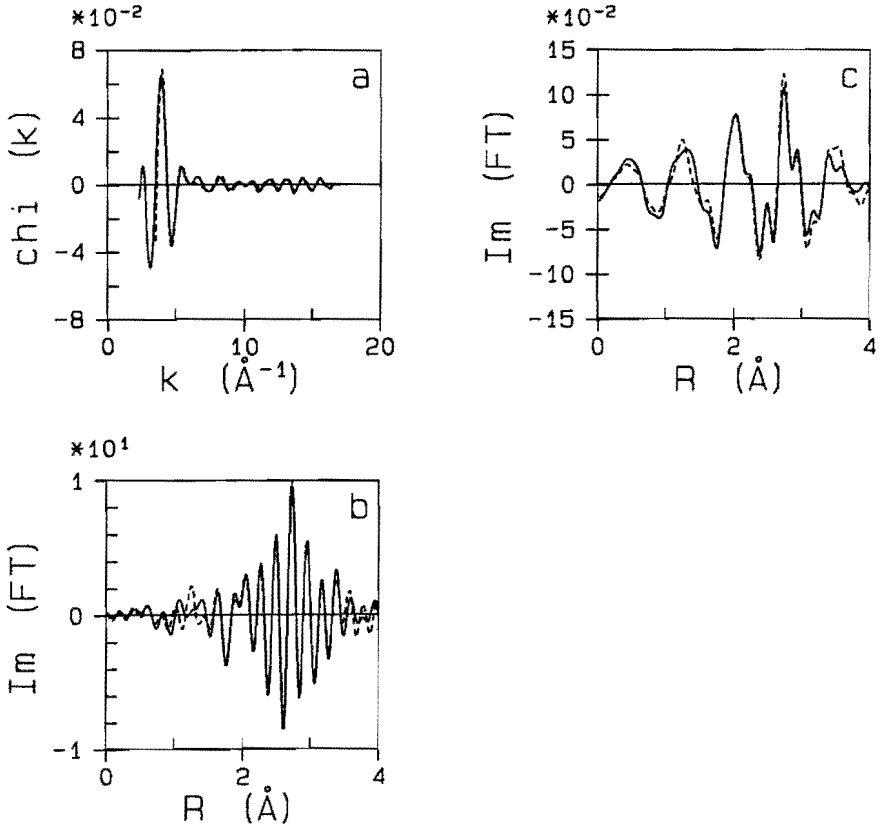

Figure 5.6. Analysis of the EXAFS data for $Ir_4(CO)_{12}$ adsorbed on γ-Al_2O_3. Experimental data (—), and sum of the best calculated contributions (— —) (see Table 5.2) (a) in k space; (b) after a k^3-weighted, Pt-Pt phase-corrected Fourier transform (Δk = 3.5-15.6 $Å^{-1}$); and (c) after a k^1-weighted, Pt-Pt phase-corrected Fourier transform (range used as in (b)).

For the Ir-$O_{support}$ contribution coordination numbers ranging from N ~ 0.5 to N ~ 1.5 are possible without affecting the quality of the fit in k space. However, for the lowest coordination numbers very low values for

$\Delta\sigma^2$ were obtained ($\Delta\sigma^2 \sim$ -0.009 Å^2) when compared with the results for supported $Os_3(CO)_{12}$ (here $\Delta\sigma^2$ = -0.004 Å^2 was obtained for the Os-$O_{support}$ shell,[7] see also Chapter 3). Using chemical arguments, several models can be drawn for the surface structure in which the presence of an Ir_4 skeleton and ten CO ligands is incorporated (see Section 5.4.2). Depending on the model, a coordination number of N = 0.5 or N = 1 has to be used; a coordination number of N = 1 yields a more reasonable value for the Debye-Waller factor, and thus we further used this value in the data analysis procedure. All calculated contributions (Ir-Ir, Ir-C, Ir-O*, and Ir-$O_{support}$) were added and compared with the data in k space and in r space after k^1- and k^3-weighted Fourier transforms. Better agreement was possible, and thus all calculated contributions, except the Ir-Ir contribution, were subtracted from the data, and better Ir-Ir coordination parameters were sought. This procedure was repeated for each of the other contributions until an optimum overall agreement had been obtained; in this process the coordination numbers were fixed at 3, 2.5, 2.5, and 1 for the Ir-Ir, Ir-C, Ir-O*, and Ir-$O_{support}$ contributions, respectively. Also the V_0 correction for both the Ir-C and Ir-O* contributions was restricted to the same value. k^3-weighted Fourier transforms of the EXAFS spectra of the different stages in this process are shown in Figure 5.5. The final results, both in k space and in r space after k^1- and k^3-weighted Fourier transforms, are shown in Figure 5.6. The best coordination parameters are given in Table 5.2.

Table 5.2. Structural parameters determined for the $Ir_4(CO)_{12}$ cluster adsorbed on γ-Al_2O_3.

Shell	N[a]	R (Å)	$\Delta\sigma^2$ (Å^2)	Ref. Compd.
Ir-Ir	3	2.70	0.0000	Pt foil
Ir-C	2.5	1.91	0.0007	$Ir_4(CO)_{12}$
Ir-O*	2.5	3.03	0.0020	$Ir_4(CO)_{12}$
Ir-$O_{support}$	1	2.54	-0.0040	$Na_2Pt(OH)_6$

[a]Fixed in the EXAFS data analysis.

Accuracies: R ± 0.02 Å (Ir-Ir, Ir-C, Ir-O*), ± 0.04 Å (Ir-$O_{support}$); $\Delta\sigma^2$ ± 10-15%.

5.4 Discussion

5.4.1 Structural Changes in $Ir_4(CO)_{12}$ upon Adsorption

When the coordination parameters determined for the parent $Ir_4(CO)_{12}$ cluster (see Table 5.1) are compared with those determined for the adsorbed cluster (see Table 5.2) it appears that, apart from the loss of two CO ligands, no striking changes have taken place in the Ir-Ir and Ir-CO interactions.

This is very clear for the Ir-Ir contribution: N, R, and $\Delta\sigma^2$ differ only slightly (within the range of experimental accuracy) for the parent $Ir_4(CO)_{12}$ and the adsorbed cluster. Some differences are expected because the Ir_4 skeleton will be somewhat distorted upon adsorption. The fact that the differences are so small, makes it very unlikely that part of the $Ir_4(CO)_{12}$ clusters has decomposed to e. g. $Ir^I(CO)_2$ entities,[17] whereas the remainder is only physically adsorbed. However, in view of the TPD/MS results, which showed that on the average two CO ligands are lost per adsorbed $Ir_4(CO)_{12}$ cluster, this may be the case, if one assumes that approximately 50% of the cluster is only physisorbed (thus losing four CO ligands during decomposition), whereas the remainder has already decomposed to $Ir^I(CO)_2$ (thus not losing any more CO ligands). We tested this hypothesis on the EXAFS data. Assuming that no Ir-Ir bonds of 2.70 Å exist between the $Ir^I(CO)_2$ entities, only 50% of the Ir atoms (the physically adsorbed clusters) will be responsible for the Ir-Ir signal between k = 11 and 16 $Å^{-1}$. In EXAFS only average coordination numbers can be determined. Hence, in this case we have 50% of the Ir atoms with $N_{Ir-Ir} = 3$ (the $Ir_4(CO)_{12}$ clusters), and 50% of the Ir atoms with $N_{Ir-Ir} = 0$ (the $Ir^I(CO)_2$ entities), leading to an expected average EXAFS coordination number of $N_{Ir-Ir} = 1.5$. With this coordination number we performed the same fitting procedure as for the adsorbed cluster. We obtained values of R = 2.70 Å and $\Delta\sigma^2 = -0.0025$ $Å^2$. If indeed physisorbed clusters had been present, this value should have been equal to $\Delta\sigma^2 = -0.001$ $Å^2$, the value for the parent complex (see Table 5.1). Therefore, we conclude that most of the adsorbed clusters still have an intact Ir_4 skeleton, surrounded by ten CO ligands.

The Ir-CO interactions (see Table 5.3) are also much alike in the parent complex and the adsorbed cluster, both exhibit multiple scattering in the Ir-O* contribution.[22] Also, the Ir-O* coordination distances are equal within the limits of accuracy. The Ir-C distance in the adsorbed cluster, however, is significantly larger than in the physical mixture. This effect was also observed in $H_xRe_3(CO)_{12}^{x-3}$ (x = 2 or 3) complexes[23] (see also Chapter 4) and can very well be attributed to a change in π-backbonding: in a more positively charged cluster the donation of electrons from the metal atom to the π^* orbitals of the CO ligands is weaker, resulting in a longer Ir-C, and a shorter C-O distance than in the parent (neutral) cluster. Indeed, in the adsorbed cluster also the C-O distance is somewhat smaller than in the parent cluster. In conclusion, the changes in Ir-C and C-O distances indicate a positive charge on the adsorbed cluster.

Table 5.3. Comparison of Ir-C and C-O bond distances in $Ir_4(CO)_{12}$ in a physical mixture, and adsorbed on γ-Al_2O_3.

Sample	Ir-C (Å)	C-O (Å)
$Ir_4(CO)_{12}$ + SiO_2	1.87	1.14
$Ir_4(CO)_{12}$ on γ-Al_2O_3	1.91	1.12

Another difference in the Ir-CO interactions of the parent and the adsorbed cluster is the difference in disorder, $\Delta\sigma^2$, observed in the Ir-C and Ir-O* shells. By definition, $\Delta\sigma^2$ is always determined with respect to the reference compound. Therefore, no difference in $\Delta\sigma^2$ is present for the Ir-C and Ir-O* shells in the physical mixture. Significant differences in Debye-Waller factor are observed, however, for the Ir-C and Ir-O* shells in the adsorbed cluster, the values being 0.0007 and 0.0020 $Å^2$ for the Ir-C and Ir-O* shell, respectively. This difference may be caused by a larger disorder in the Ir-O* shell with respect to the Ir-C shell, e. g. due to inhomogeneous distribution of the positive charge over the Ir atoms in the Ir_4 skeleton. However, a difference in charge on the metal skeleton did not produce this type of effect in the $[H_xRe_3(CO)_{12}]^{x-3}$ (x = 2 or 3) complexes[23] (see also Chapter 4). Theoretical calculations concerning the multiple scattering effect[22] show that the enhancement of a shell including multiple scattering

such as Ir-O*, depends on the Ir-C-O angle. The enhancement is maximal at an angle of 180°. Also, from the calculations of the enhancement of the backscattering as a function of k, it can be concluded that at these large Ir-C-O angles ($165° < \alpha < 180°$), differences in bond angle may result in an apparent change in the Debye-Waller factor with respect to the reference (see Chapter 2, Figure 2.7). It thus seems from the EXAFS results that the mean Ir-C-O angle is smaller in the adsorbed cluster than in the parent complex.

5.4.2 Model of the Surface Structure

On the basis of the IR and TPD/MS results several conclusions on the structure of the adsorbed complex can be drawn: all models consist of an $Ir_4(CO)_{10}L_x$ cluster (L being a ligand emanating from the support) with no bridging CO ligands. Several classes of models are possible (see Figure 5.7): (A) models in which the two CO ligands are removed from one Ir atom; and (B) models in which two Ir atoms lose one CO ligand each. The last class can then be subdivided in (B1) models in which no Ir-Ir bonds are broken; and (B2) models in which the bond between the two Ir atoms that lose a CO ligand is disrupted. Assuming that the ligand exchanged for CO is exclusively surface oxygen, class A and class B1 yield surface structures in which the metal skeleton (consisting of four Ir atoms) is coordinated to the support by two Ir-O bonds, thus resulting in an average EXAFS coordination number of $N_{Ir-O} = 2/4 = 0.5$. In class B2, the cluster is coordinated to the support by four Ir-O bonds, leading to an average EXAFS coordination number of $N_{Ir-O} = 4/4 = 1$.

In the EXAFS data analysis, $N_{Ir-O} = 1$ yielded more reasonable values for $\Delta\sigma^2$ [7] (see also Chapter 3). Therefore, we believe that class B2 (for which $N_{Ir-O} = 1$) represents the surface structure of the adsorbed $Ir_4(CO)_{12}$ cluster best. On the basis of EXAFS results both bridging and non-bridging surface oxygen ligands have been postulated for the surface structure of $Os_3(CO)_{12}$ adsorbed on γ-Al_2O_3[7,24,25] (see also Chapter 3). A model with no bridging ligands at all is highly improbable in our opinion, since in that case the non-bonding Ir-Ir coordination is expected to be very 'loose', which will result in an increased Debye-Waller factor for the Ir-Ir shell in the adsorbed cluster with respect to that in the parent cluster and a larger Ir-Ir distance. This is not observed. On the other hand it is very difficult to

decide whether bridging or non-bridging oxygen ligands are present from EXAFS results alone: in principle, EXAFS does detect only neighbours, and not the bonds (nor the bonding direction) between the central atom and those neighbours. (In fact, also non-bonded neighbours can be detected.) Both surface models left (one in which a double oxygen bridge is present, and one in which a single bridge plus two non-bridging oxygen ligands are incorporated) yield the same expected coordination numbers. Therefore we can only infer that the $Ir_4(CO)_{10}$ entity is bonded by at least one bridging surface oxygen ligand.

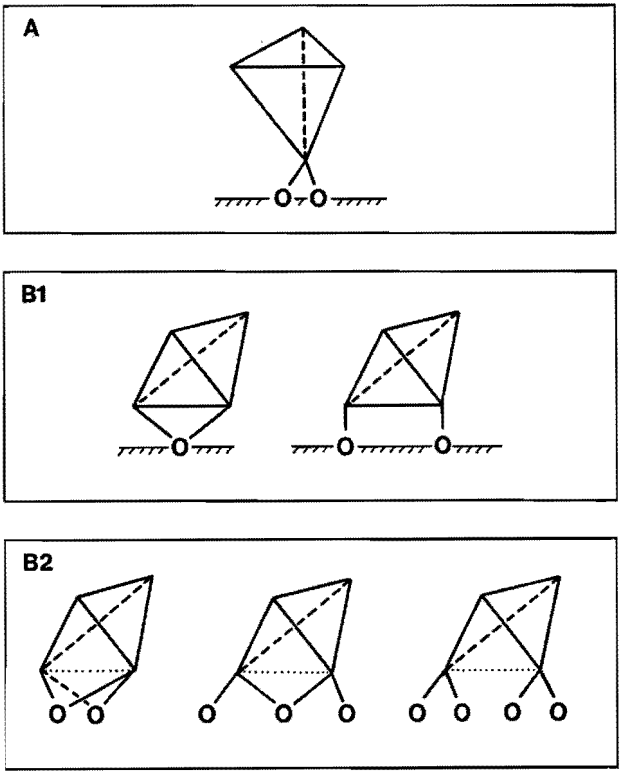

Figure 5.7. Several surface structure models possible for the $Ir_4(CO)_{12}$ cluster adsorbed on γ-Al_2O_3. (A) $Ir_4(CO)_{10}L_2$, both CO ligands exchanged from one Ir atom; (B1) $Ir_4(CO)_{10}L_2$, exchange of two CO ligands from different Ir atoms; and (B2) $Ir_4(CO)_{10}L_4$, as (B1), but with cleavage of one Ir-Ir bond. For clarity, the CO ligands have been omitted.

5.4.3 Applicability of $Ir_4(CO)_{10}/\gamma$-Al_2O_3 as a Model for Reduced Ir/γ-Al_2O_3

One of the reasons to investigate $Ir_4(CO)_{12}$ adsorbed on γ-Al_2O_3 with EXAFS, was to obtain a system in which the metal entities are uniquely defined, so that especially the metal-support coordination can be quantified with precision. Indeed we believe such a system has been prepared, and we were able to determine the number of $Ir\text{-}O_{support}$ bonds per cluster. It is now possible to compare the metal-support coordination in the supported metal carbonyl system with that in reduced Ir/γ-Al_2O_3. In Table 5.4 the metal-support coordination parameters of a reduced 0.8 wt% Ir/γ-Al_2O_3 system, prepared by the incipient wetness technique, are given[8] (see also Chapter 6).

Table 5.4. Structural parameters determined for the first coordination shells in reduced 0.8 wt% Ir/γ-Al_2O_3.

Shell	N	R (Å)	$\Delta\sigma^2$ (Å^2)	Ref. Compd.
Ir-Ir	4.9	2.71	0.0020	Pt foil
$Ir\text{-}O_{support}$	1.8	2.55	0.0050	$Na_2Pt(OH)_6$

Accuracies: N ± 10-15% (Ir-Ir), ± 15-20% (Ir-O); R ± 0.02 Å (Ir-Ir), ± 0.04 Å (Ir-O); $\Delta\sigma^2$ ± 10-15% (Ir-Ir), ± 15-20% (Ir-O).

When the coordination parameters for the Ir-Ir and $Ir\text{-}O_{support}$ contributions are compared, it can be seen that although the metal entities in the reduced system are much larger ($N_{Ir\text{-}Ir}$ = 4.9, i. e. particles consisting of approx. 12 Ir atoms[8] (see also Chapter 6)) than those in the system with the adsorbed cluster ($N_{Ir\text{-}Ir}$ = 3, i. e. clusters consisting of 4 Ir atoms) the coordination number for the $Ir\text{-}O_{support}$ shell in the reduced system is not smaller: usually, the larger particles, the smaller the $Ir\text{-}O_{support}$ coordination number is.[18] This is a clear indication that the type of oxygen coordination is not the same. Indeed, from modelling it was inferred that in the reduced system the Ir atoms in the interface are threefold coordinated to support oxygen (see Figure 5.8[8]), whereas in adsorbed $Ir_4(CO)_{12}$ the Ir

atoms in contact with the support are twofold coordinated. Nevertheless, it is demonstrated from the data of the adsorbed cluster, that Ir atoms can be multiply coordinated to the support.

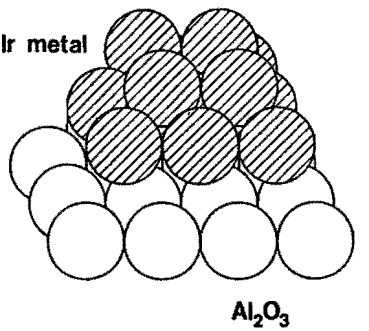

Figure 5.8. Model for the average Ir particle (consisting of 12 atoms) in reduced $Ir/\gamma\text{-}Al_2O_3$.

An $Ir\text{-}O_{support}$ coordination in the adsorbed cluster with a long distance (R = 2.54 Å) had not been expected, because short metal-oxygen distances were observed for supported $Os_3(CO)_{12}$[7,24,25] (see also Chapter 3) and $Ru_3(CO)_{12}$[25] clusters. For reduced systems several explanations can be found to account for the long metal-oxygen distance in the interface. It is possible that this interaction is a metal-hydroxyl rather than a metal-oxide contribution.[26] Also, electronic changes in the supported metal particles due to adsorbed hydrogen, or hydrogen present in the metal-support interface may be responsible. However, neither explanation can be used for the case of the supported $Ir_4(CO)_{12}$ complex: hydrogen gas is not present in the system, and in molecular analogues of the supported $Os_3(CO)_{12}$ cluster Os-O, and not Os-(OH) bonds are detected by XRD.[27] Chemisorption of metal carbonyls, resulting in surface structures incorporating support oxygen, is thought to procede via insertion of the carbonyl cluster in a surface hydroxyl group. In the case of the adsorbed cluster, the long $Ir\text{-}O_{support}$ bond might be partly due to steric hindrance, which is in accord with the observation that the average Ir-C-O angle decreases upon adsorption when compared with the parent cluster. On the other hand, it is known that Ir is much more easily reduced that Ru and Os. Therefore it is possible that the

reducibility of the metal atom in the metal-oxygen bond also has a large influence on the metal-oxygen bond length. More research has to be carried out in order to elucidate this.

5.5 Conclusions

With a combination of IR, TPD/MS, and EXAFS a rather complete surface structure model of $Ir_4(CO)_{12}$ adsorbed on partially dehydroxylated γ-Al_2O_3 was obtained. From TPD/MS and IR experiments it was concluded that two CO ligands are removed upon adsorption, and that the surface complex contains no bridging carbonyl ligands.

From the EXAFS experiments accurate coordination parameters were determined. The Ir_4 skeleton hardly changes upon adsorption. With respect to the parent $Ir_4(CO)_{12}$ cluster, in the adsorbed cluster the Ir-C distance is larger, and the C-O distance is somewhat smaller, which can be explained by diminished π-backbonding, due to a positive charge on the Ir_4 skeleton.

The cluster is bonded to the γ-Al_2O_3 support via two Ir atoms, by 4 Ir-O bonds of 2.54 Å. At least one bridging oxygen is present. The Ir-$O_{support}$ bond length observed in the adsorbed cluster is equal to that for a reduced Ir/γ-Al_2O_3 system. Because the Ir-O bonds in both systems are thought to have a different origin, we infer that the reducibility of the metal atom in the metal-oxygen bond must have a large influence on the bond length. The fact that the average Ir-C-O angle has decreased after adsorption, indicates that also steric hindrance may partly explain the large Ir-$O_{support}$ bond length.

5.6 References

(1) R. Psaro, and R. Ugo, *Metal Clusters in Catalysis*; B. C. Gates, L. Guczi, and H. Knözinger, Eds.; Elsevier: Amsterdam, 1986; p 427.

(2) R. Psaro, R. Ugo, G. M. Zanderighi, B. Besson, A. K. Smith, and J. M. Basset, *J. Organomet. Chem.* **1981**, *213*, 215.

(3) M. Deeba, and B. C. Gates, *J. Catal.* **1981**, *67*, 303.

(4) H. Knözinger, and Y. Zhao, *J. Catal.* **1981**, *71*, 337.

(5) M. Deeba, B. J. Streusand, G. L. Schrader, and B. C. Gates, *J. Catal.* **1981**, *69*, 218.

(6) H. Knözinger, Y. Zhao, B. Tesche, R. Barth, R. Epstein, B. C. Gates, and J. P. Scott, *Faraday Discuss.* **1981**, *72*, 53.

(7) F. B. M. Duivenvoorden, D. C. Koningsberger, Y. S. Uh, and B. C. Gates, *J. Am. Chem. Soc.* **1986**, *108*, 6254.

(8) F. B. M. Van Zon, and D. C. Koningsberger, *J. Chem. Phys.* submitted.

(9) R. W. G. Wyckoff, *Crystal Structures*, 2nd ed.; Wiley: New York, 1963; Vol. I, p 10.

(10) M. Trömel, and E. Lupprich, *Z. Anorg. Chem.* **1975**, *414*, 160.

(11) M. R. Churchill, and J. P. Hutchinson, *Inorg. Chem.* **1978**, *17*, 3528.

(12) B. K. Teo, and P. A. Lee, *J. Am. Chem. Soc.* **1979**, *101*, 2815.

(13) B. Lengeler, *J. de Phys. C8* **1986**, *47*, 75.

(14) F. Cariati, V. Valenti, and G. Zerbi, *Inorg. Chim. Acta* **1969**, *3*, 378.

(15) G. F. Stuntz, *Thesis*; University of Illinois at Urbana Champaign, 1978.

(16) R. Della Pergola, L. Garlaschelli, S. Martinengo, F. Demartin, M. Manassero, and M. Sansoni, *Gazz. Chim. Ital.* **1987**, *117*, 245.

(17) K. Tanaka, K. L. Watters, and R. F. Howe, *J. Catal.* **1982**, *75*, 23.

(18) J. B. A. D. Van Zon, D. C. Koningsberger, H. F. J. Van 't Blik, and D. E. Sayers, *J. Chem. Phys.* **1985**, *82*, 5742.

(19) J. W. Cook, and D. E. Sayers, *J. Appl. Phys.* **1981**, *52*, 5024.

(20) D. C. Koningsberger, J. B. A. D. Van Zon, H. F. J. Van 't Blik, G. J. Visser, R. Prins, A. N. Mansour, D. E. Sayers, D. R. Short, and J. R. Katzer, *J. Phys. Chem.* **1985**, *89*, 4075.

(21) D. C. Koningsberger, J. H. A. Martens, R. Prins, D. R. Short, and D. E. Sayers, *J. Phys. Chem.* **1986**, *90*, 3047.

(22) B. K. Teo, *J. Am. Chem. Soc.* **1981**, *103*, 3990.

(23) F. B. M. Van Zon, P. S. Kirlin, B. C. Gates, and D. C. Koningsberger, *J. Phys. Chem.* accepted.

(24) S. L. Cook, J. Evans, G. S. McNulty, and G. N. Greaves, *J. Chem. Soc., Dalton Trans.* **1986**, 7.

(25) V. D. Alexiev, N. Binsted, J. Evans, G. N. Greaves, and R. J. Price, *J. Chem. Soc., Chem. Commun.* **1987**, 395.

(26) J. H. A. Martens, R. A. Van Santen, D. C. Koningsberger, and R. Prins, *Catalysis Lett.* submitted.

(27) L. D'Ornelas, A. Choplin, J. M. Basset, L. Y. Hsu, and S. Shore, *Nouv. J. Chim.* **1985**, *9*, 155.

Chapter Six

Metal Particle Morphology and Structure of the Metal-Support Interface in $Ir/\gamma\text{-}Al_2O_3$ Catalysts Studied by EXAFS Spectroscopy

6.1 Introduction

The nature of the metal-support interface in supported metal catalysts recently has received much attention. Knowledge of the interface is important because the metal-support bonding plays an important role in the stability (e. g. against sintering) of the catalytic system. EXAFS (Extended X-ray Absorption Fine Structure) is an excellent tool to study supported metal catalysts, because in this technique the often large fraction of support in the sample does not obscure the structural information about the metal particles. Systems with very small particles are preferable for EXAFS measurements: in small supported metal particles a large fraction of the metal atoms is in contact with the support, resulting in a relatively large metal-support contribution. Hence, the coordination parameters of the metal-support contribution can be determined more accurately. To obtain small metal particles various techniques are used, among which incipient wetness, ion exchange, and the urea method are well known.[1-3]

In model systems, the metal-support interface can also be studied very accurately with EXAFS. As an example, we investigated $Os_3(CO)_{12}$ clusters chemisorbed on $\gamma\text{-}Al_2O_3$ after preparation and after decomposition,[4] and $H_3Re_3(CO)_{12}$ clusters chemisorbed on MgO after preparation, decomposition and reduction,[5] in order to follow the formation of the metal-support interface. The use of supported organometallic clusters as model systems for supported metal catalysts has the important advantage that uniform, well-defined entities are bonded to the support and, consequently, structural and catalytic information can be quantified accurately. In contrast, in supported metal catalysts a range of metal particle sizes exists, resulting in the determination of only average structural and catalytic properties.

In order to compare the metal-support interaction in supported organometallic clusters with that interaction in supported reduced metal catalysts, we prepared a sample in which $Ir_4(CO)_{12}$ was chemisorbed on γ-Al_2O_3.[6] In a preliminary communication we showed that upon reduction of this supported cluster a system with small reduced Ir metal particles was obtained. This system appeared to be very suited for obtaining information about the metal-support interaction.[7] Ir-O bonds with a bond length of 2.58 Å were distinctly observed and attributed to an Ir-$O_{support}$ contribution. The same type of bonds, i. e. with metal-oxygen bond lengths of 2.6-2.7 Å, had been observed previously in Rh/γ-Al_2O_3,[8,9] Rh/TiO_2,[10,11] and Pt/γ-Al_2O_3.[12] Recently, this long metal-oxygen bond has been interpreted on the basis of theoretical calculations[13] as arising from an interaction between a metal atom in the metal-support interface and hydroxyl groups of the support. Also electronic changes in the supported metal particles due to adsorbed hydrogen, or the presence of adsorbed hydrogen in the metal-support interface may be responsible for the long metal-oxygen distance. The most striking result obtained with the reduced $Ir_4(CO)_{12}$/γ-Al_2O_3 system was, however, the presence of an unexpectedly large Ir-$O_{support}$ contribution in the EXAFS spectrum; a coordination number of almost three was determined. A coordination number of three is the maximal value for epitaxy on the most frequently occurring fcc (111) face of γ-Al_2O_3. The EXAFS technique yields coordination numbers which are averaged over all Ir atoms in the sample. Thus the fact that the coordination number determined for the Ir-$O_{support}$ contribution is virtually equal to the maximum expected, shows that almost all Ir atoms must be in the metal-support interface. This points to the presence of raft-like particles.

In this Chapter a comparison is presented between Ir/γ-Al_2O_3, prepared from $Ir_4(CO)_{12}$, and an Ir/γ-Al_2O_3 sample prepared from $IrCl_3$ by the incipient wetness technique.[14] In both samples a metal-support interaction with a long Ir-$O_{support}$ coordination distance has been detected. Marked differences are observed when the EXAFS results obtained for these systems are compared, especially for the higher Ir-Ir shells. Analysis of these higher shells (R $\sim$ 3.5-5.5 Å) yields conclusive evidence that the particle shape is different in both systems, i. e. in the reduced $Ir_4(CO)_{12}$-derived system the Ir metal particles are flat rather than three-dimensional in shape. Apart from the higher Ir-Ir shells, also higher shell Ir-$O_{support}$

contributions were detected for both samples. On the basis of the EXAFS results, a model can be constructed for the metal-support interface, in which the Ir atoms are threefold coordinated by support oxygen atoms, preferentially on those threefold sites on the fcc (111) face of γ-Al_2O_3 which have an oxygen atom directly underneath the Ir atoms in the one-but-topmost oxygen layer (hcp-type of epitaxy).

6.2 Experimental

6.2.1 Catalyst Preparation

$IrCl_3 \cdot xH_2O$ was supplied by Drijfhout (50.9 wt% Ir). An accurately determined amount of this metal salt was dissolved in such an amount of water that the volume of the solution could just fill the pores of the γ-Al_2O_3 support (Ketjen, 000-1.5E, surface area 200 m^2/g, pore volume 0.6 ml/g). The solution was added dropwise to the support under vigorous shaking. After the impregnation the catalyst was dried at 397 K for 16 h. The final Ir loading was 0.8% by weight. The catalyst was prereduced in flowing H_2 at 623 K for 1 h (after heating at a rate of 5 K/min) and passivated in air at room temperature afterwards.

$Ir_4(CO)_{12}$ was obtained from Alfa Products, and used without further purification. γ-Al_2O_3 was partially dehydroxylated by calcining in vacuum at 773 K for 8 h; cyclohexane was dried over a sodium/benzophenone mixture and used freshly distilled. The metal carbonyl was dissolved in the cyclohexane and stirred with γ-Al_2O_3 under N_2 for 4 h. After filtration and drying overnight in vacuum, the final Ir loading was 0.8% by weight. The impregnated system was decomposed in vacuum at 473 K for 2 h, and prereduced in flowing H_2 at 623 K for 15 h (after heating at a rate of 5 K/min). After reduction the catalyst was passivated in air at room temperature.

Hydrogen chemisorption (extensively described previously[15]) was used to determine the dispersion in the reduced catalysts. Due to desorption of cyclohexane or its decomposition products, the H/M value for the $Ir_4(CO)_{12}$-derived system could not be determined. For the $IrCl_3$-derived system H/M = 2.8 was obtained.

6.2.2 EXAFS Measurements

EXAFS measurements were performed on Wiggler station 9.2 at the SRS at Daresbury, U. K., equipped with a double crystal Si(220) monochromator. The samples were pressed into thin self-supporting wafers with an absorbance of log $(I_0/I) \sim 2.5$, and mounted in an in situ EXAFS cell. The passivated $IrCl_3$-derived sample was first heated in flowing He to 423 K (after heating at a rate of 5 K/min), to remove physisorbed water. After 1 h in He at 423 K, the sample was cooled to room temperature and reduced in flowing H_2 at 623 K for 1 h (after heating at a rate of 5 K/min). The passivated $Ir_4(CO)_{12}$-derived sample was reduced in flowing H_2 at 623 K for 1 h (after heating at a rate of 5 K/min). EXAFS measurements were

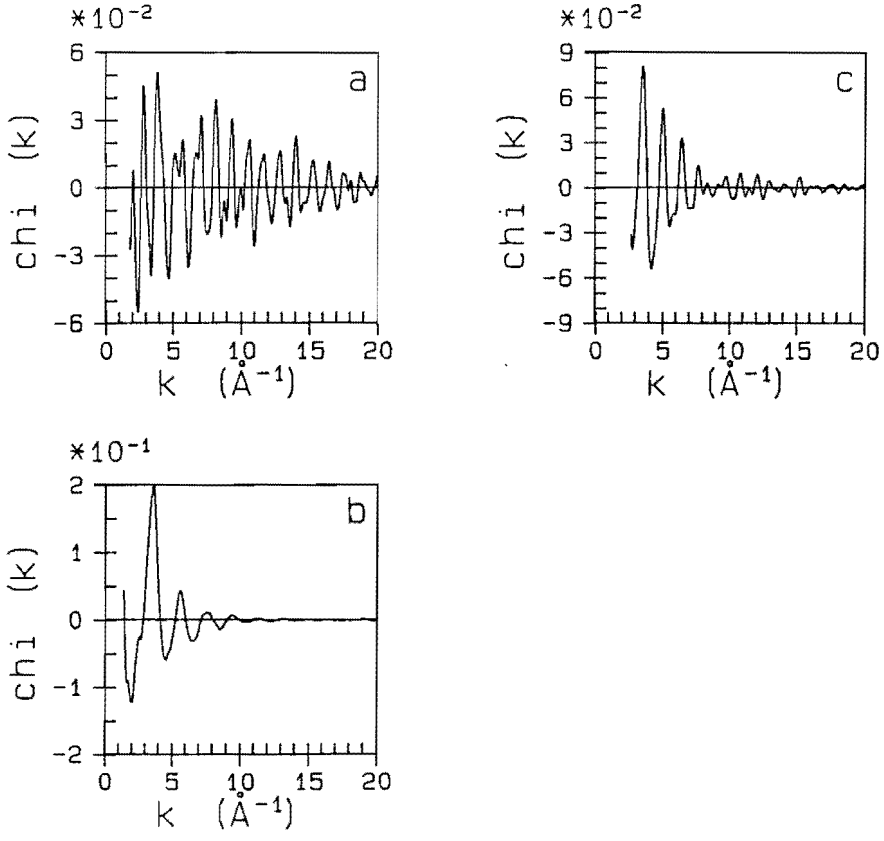

Figure 6.1. Raw EXAFS data of the reference compounds (a) Pt foil; (b) $Na_2Pt(OH)_6$; and (c) IrAl alloy.

done on the Ir L_{III} edge (11215 eV) at liquid nitrogen temperature. The monochromator was 50% detuned in order to avoid contamination of the incoming beam with higher harmonics.

As reference compounds Pt foil[16] and $Na_2Pt(OH)_6$[17] were measured on the Pt L_{III} edge (11564 eV), and IrAl alloy[18] on the Ir L_{III} edge, all at liquid nitrogen temperature. Pt foil was used as a reference for Ir-Ir interactions, $Na_2Pt(OH)_6$ was used as a reference for Ir-O, and the alloy as a reference for Ir-Al contributions. The raw EXAFS data for the reference compounds are shown in Figure 6.1. It has been shown theoretically[19] and experimentally[4,20] that Pt references can be used for Ir contributions. The first shell structural parameters for the reference compounds are given in Table 6.1. Also in Table 6.1 the ranges in k and r space are given which were used to extract the first shell data from the raw EXAFS data. For k_{min} and k_{max}, nodes in the raw EXAFS data were chosen, and likewise for r_{min} and r_{max}, nodes in the imaginary part of a k^3-weighted Fourier transform. In this way truncation effects are minimized.

Table 6.1. Some structural parameters of the reference compounds used, and the ranges in k and r space used to isolate the references (k^3-weighted Fourier transforms were used).

Compound	Shell		N	R (Å)	Δk ($Å^{-1}$)	Δr (Å)
Pt foil[16]	1st	Pt-Pt	12	2.77	1.95-19.77	1.90-3.02
	4th	Pt-Pt	12	5.54	1.95-19.77	5.00-5.66
$Na_2Pt(OH)_6$[17]	1st	Pt-O	6	2.05	1.43-17.69	0.50-2.02
IrAl alloy[18]	1st	Ir-Al[a]	8	2.58	3.02-12.32	0.88-2.48

[a]After subtraction of the Ir-Ir contribution: N = 6, R = 2.99 Å, $\Delta\sigma^2 = 0.0033$ $Å^2$, $V_0 = -3.5$ eV.

The references were reliable at least between $k = (k_{min} + 0.5)$ $Å^{-1}$ and $k = (k_{max} - 0.5)$ $Å^{-1}$ (k_{min} and k_{max} as given in Table 6.1). In this range a good coincidence is obtained both in imaginary part and in magnitude between the k^3-weighted Fourier transforms of the experimental and back transformed data.

6.3 Results

EXAFS spectra were recorded of the $IrCl_3$- and $Ir_4(CO)_{12}$-derived reduced catalyst samples. Standard procedures[8,21] were used to extract the raw EXAFS data from the measured spectrum. The raw data (see Figure 6.2) were of excellent quality; k^3-weighted Fourier transforms are also shown in Figure 6.2.

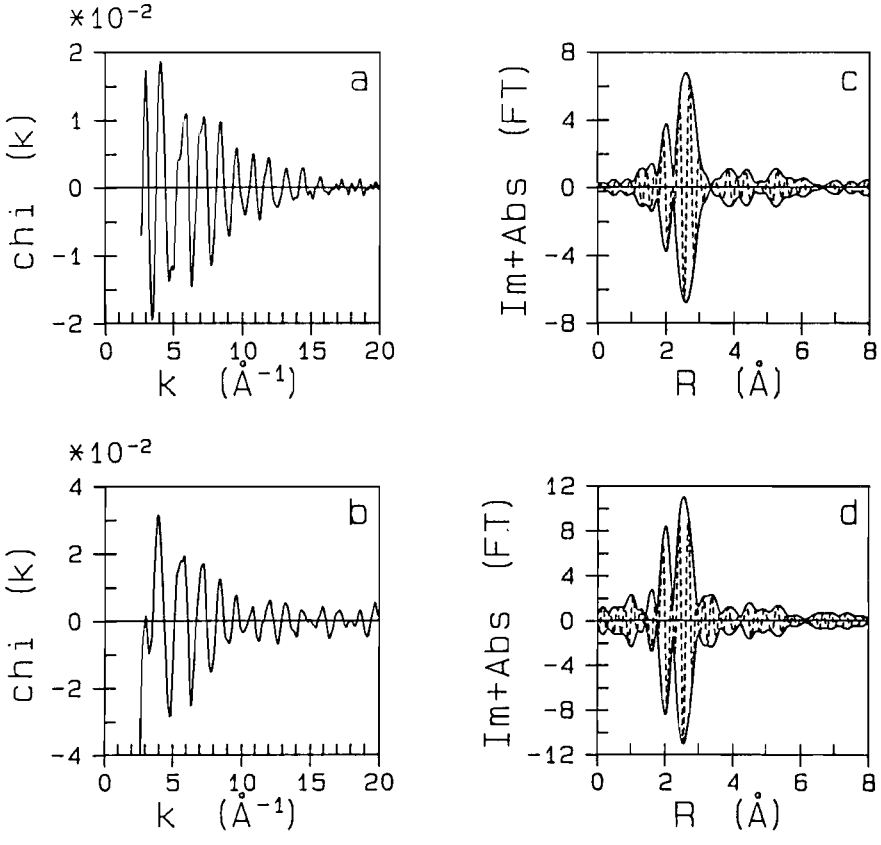

Figure 6.2. Raw EXAFS data of reduced 0.8 wt% Ir/γ-Al_2O_3 (a) ex $IrCl_3$; and (b) ex $Ir_4(CO)_{12}$; k^3-weighted Fourier transform of the EXAFS data of (c) the $IrCl_3$-derived sample (Δk = 3.16-13.49 $Å^{-1}$); and (d) the $Ir_4(CO)_{12}$-derived sample (Δk = 3.60-14.18 $Å^{-1}$).

EXAFS data analysis was performed using experimentally determined phase shifts and backscattering amplitudes for the various contributions. Phase corrected Fourier transforms together with the difference file technique were used. Our data analysis procedures have been extensively described elsewhere.[4,8-11]

6.3.1 Analysis of the First Shell Data

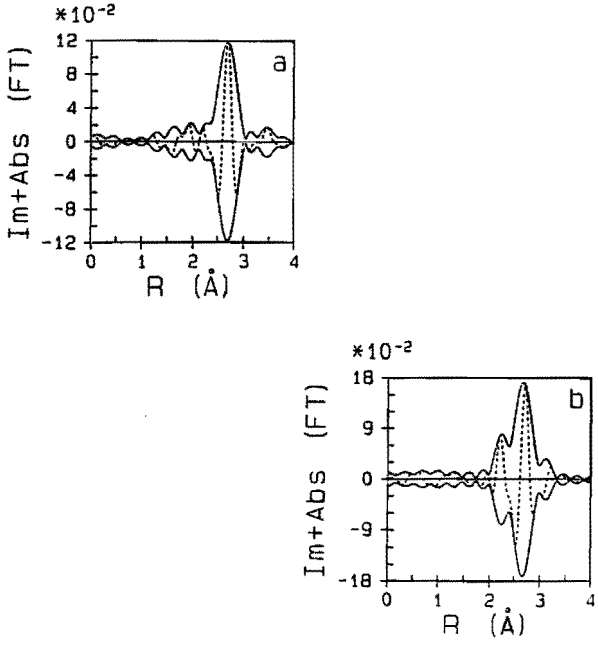

Figure 6.3. Imaginary part (— —) and magnitude (—) of the k^1-weighted, Pt-Pt phase-corrected Fourier transform of the EXAFS of (a) the isolated first shell data of the $IrCl_3$-derived sample (Δk = 3.10-13.57 $Å^{-1}$) (data isolated by a k^1-weighted Fourier transform with Δk = 2.72-14.18 $Å^{-1}$ and an inverse transform with Δr = 1.24-3.16 Å); and (b) the isolated first shell data of the $Ir_4(CO)_{12}$-derived sample (Δk = 3.60-14.18 $Å^{-1}$) (data isolated by a k^1-weighted Fourier transform with Δk = 2.94-14.75 $Å^{-1}$ and an inverse transform with Δr = 1.28-3.22 Å).

In the difference file technique, first the Ir-Ir contribution, being the largest component in the EXAFS spectrum, was estimated in k space using only the high-k data.[15] An EXAFS function calculated with the first-guess parameters was then subtracted from the experimental data. In the Fourier transform of the difference file metal-support contributions are expected below 3 Å, most probably an Ir-$O_{support}$ interaction. When compared with the first shell Ir-Ir contribution, this Ir-O contribution is usually much smaller. In order to obtain reliable parameters, it is therefore imperative that good quality data are used (otherwise the noise will dominate the difference file), and that highly dispersed catalysts are used (otherwise the metal-support contribution will be too small). The difference file was analysed by calculating an Ir-O contribution which agreed with the difference spectrum in r space as well as possible. The first-guess Ir-Ir and Ir-$O_{support}$ contributions were then added and compared with the experimental data in k and in r space. Usually, the agreement between experiment and sum of the contributions can be considerably improved. Therefore, the Ir-$O_{support}$ contribution was subtracted from the experimental data and better parameters for the Ir-Ir contribution were sought. This process was repeated until a good agreement had been obtained.

In Figures 6.3a and 6.3b, the k^1-weighted, Pt-Pt phase-corrected Fourier transforms are shown of the isolated first shell data for both samples. The imaginary part as well as the magnitude of both Fourier transforms are asymmetric at the low-r side of the Ir-Ir peak at R ~ 2.7 Å in the EXAFS spectrum. This indicates the presence of additional scatterers, because with a proper phase correction (i. e. Pt-Pt for Ir-Ir contributions) the Ir-Ir peak in the Fourier transform should be symmetric if no other contributions are present.[8-11] In Figures 6.4a and 6.4d again the imaginary part of the k^1-weighted, Pt-Pt phase-corrected Fourier transform is shown for the $IrCl_3$- and $Ir_4(CO)_{12}$-derived sample, respectively. The best calculated Ir-Ir contribution is shown in these graphs for each sample. Large deviations are observed between R ~ 1.8 and 2.6 Å, which are caused by the presence of additional contributions.

The difference between the isolated first shell data and the best calculated Ir-Ir contribution is shown for the $IrCl_3$- and $Ir_4(CO)_{12}$-derived samples in Figures 6.4b and 6.4e (in k space), and Figures 6.4c and 6.4f (after a k^1-weighted, Pt-O phase-corrected Fourier transform). An Ir-$O_{support}$ con-

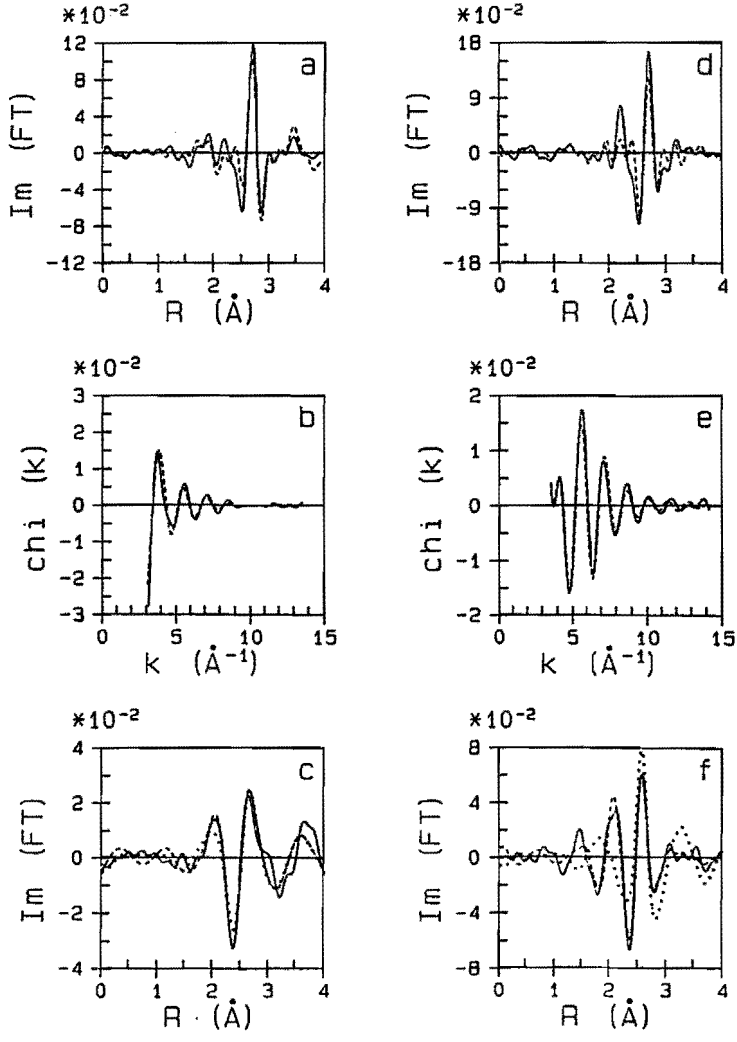

tribution was sought which agreed as well as possible with the difference spectrum after a k^1-weighted, Pt-O phase-corrected Fourier transform, but this did not yield satisfactory results. In Figures 6.4c and 6.4f the best calculated Ir-$O_{support}$ contributions are shown; in both cases deviations are observed at R $\sim$ 2.0-2.4 Å. Therefore, a second contribution of a low-Z scatterer was incorporated. In the case of the $IrCl_3$-derived sample, we

← **Figure 6.4.** Analysis of the isolated first shell data of the $IrCl_3$-derived sample. (a) k^1-weighted, Pt-Pt phase-corrected Fourier transform (Δk = 3.10-13.57 $Å^{-1}$) of the isolated first shell data (—), and the best calculated Ir-Ir contribution (– –); (b) first shell data minus Ir-Ir contribution (—), and sum of the best calculated Ir-$O_{support}$ and Ir-O contributions (– –) in k space; and (c) first shell data minus Ir-Ir contribution (—), best Ir-$O_{support}$ contribution (· · ·), and sum of the best Ir-$O_{support}$ and Ir-O contributions (– –) after a k^1-weighted, Pt-O phase-corrected Fourier transform (Δk = 3.10-13.57 $Å^{-1}$). Analysis of the isolated first shell data of the $Ir_4(CO)_{12}$-derived sample. (d) k^1-weighted, Pt-Pt phase-corrected Fourier transform (Δk = 3.60-14.18 $Å^{-1}$) of the isolated first shell data (—), and the best calculated Ir-Ir contribution (– –); (e) first shell data minus Ir-Ir contribution (—), and sum of the best calculated Ir-$O_{support}$ and Ir-C contributions (– –) in k space; and (f) first shell data minus Ir-Ir contribution (—), best Ir-$O_{support}$ contribution (· · ·), and sum of the best Ir-$O_{support}$ and Ir-C contributions (– –) after a k^1-weighted, Pt-O phase-corrected Fourier transform (Δk = 3.60-14.18 $Å^{-1}$).

think this contribution is caused by an Ir-O interaction, which may be due to a small amount of unreduced Ir or to an Ir-$O_{support}$ interaction other than the dominant one. For the $Ir_4(CO)_{12}$-derived sample, it was argued before[7] that the contribution at R ~ 2.1 Å is most likely caused by an Ir-C interaction. In this case Ir-C contributions can well be attributed to the presence of decomposition products of cyclohexane or the CO ligands on the Ir metal surface. The sum of the two contributions (Ir-$O_{support}$ plus Ir-O in the case of the $IrCl_3$-derived sample, and Ir-$O_{support}$ plus Ir-C in the case of the $Ir_4(CO)_{12}$-derived sample) agrees much better with the difference spectrum in r space (see Figures 6.4c and 6.4f); also in k space good agreement is obtained (see Figures 6.4b and 6.4e).

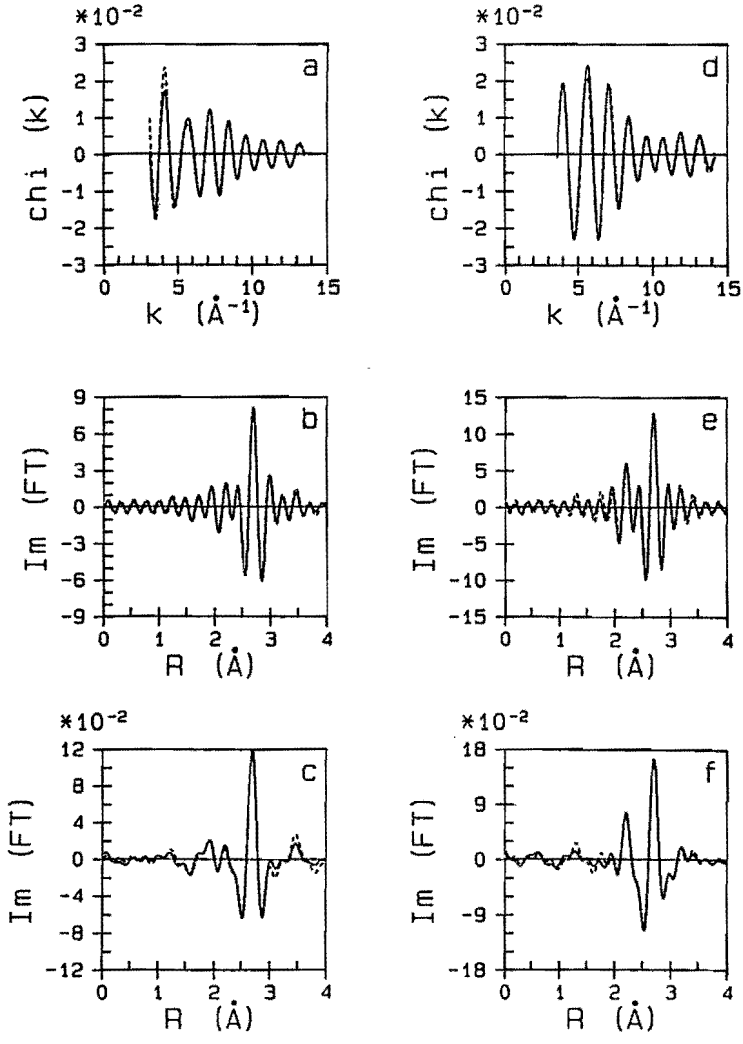

In Figure 6.5 the isolated first shell data for both samples are compared with the sum of the calculated contributions. In k space as well as in r space (both after k^1-weighted and k^3-weighted Fourier transforms) the agreement is good. The parameters used in the final calculations are given in Table 6.2. For lack of a better reference, the Ir-C shell in the $Ir_4(CO)_{12}$-derived sample was analysed using the Pt-O reference. This yields good coordination distances, but larger errors are to be expected in the coordination number and Debye-Waller factor than for the Ir-O contributions.[22]

← **Figure 6.5.** EXAFS of the isolated first shell data of the $IrCl_3$-derived sample (—), and sum of best calculated contributions (— —) (see Table 6.2) (a) in k space; (b) after a k^3-weighted, Pt-Pt phase-corrected Fourier transform (Δk = 3.10-13.57 $Å^{-1}$); and (c) after a k^1-weighted, Pt-Pt phase-corrected Fourier transform, with conditions as in (b). EXAFS of the isolated first shell data of the $Ir_4(CO)_{12}$-derived sample (—), and sum of best calculated contributions (— —) (see Table 6.2) (d) in k space; (e) after a k^3-weighted, Pt-Pt phase-corrected Fourier transform (Δk = 3.60-14.18 $Å^{-1}$); and (f) after a k^1-weighted, Pt-Pt phase-corrected Fourier transform, with conditions as in (e).

Table 6.2. Structural parameters determined for the first coordination shells in reduced $Ir/\gamma\text{-}Al_2O_3$.

Sample	Shell	N_{unc}	N	R (Å)	$\Delta\sigma^2$ ($Å^2$)
Ir/Al_2O_3	Ir-Ir	4.9	4.9	2.71	0.0020
ex $IrCl_3$	Ir-$O_{support}$	1.5	1.8	2.55	0.0050
	Ir-O	0.3	0.3	2.16	0.0060
Ir/Al_2O_3	Ir-Ir	4.7	4.7	2.68	0.0004
ex $Ir_4(CO)_{12}$	Ir-$O_{support}$	2.4	2.9	2.58	-0.0010
	Ir-C	3.0	3.0	2.10	0.0107

Accuracies: N ± 10-15% (Ir-Ir), ± 15-20% (Ir-O), ± 50% (Ir-C); R ± 0.02 Å (Ir-Ir), ± 0.04 Å (Ir-O and Ir-C); σ^2 ± 10-15% (Ir-Ir), ± 15-20% (Ir-O), ± 50% (Ir-C).

In Table 6.2 there are two columns with coordination numbers, viz. one with uncorrected coordination numbers N_{unc} that were used in the EXAFS calculations, and one with the actual (average) coordination numbers in the sample N. For the long Ir-$O_{support}$ contributions N_{unc} is smaller than the actual N, because of the factor $\exp(-2R/\lambda)$ in the EXAFS formula.[23-25] This factor is usually taken to be equal in the reference shell and the shell to be analysed. However, when the coordination distance of the analysed shell differs considerably from that of the reference,

coordination numbers will deviate. Therefore $N_{unc}/\exp[-2(R-R_{ref})/\lambda]$ is the real coordination number N; λ was assumed to be equal to 6 Å [25,26] (to be discussed later).

6.3.2 Analysis of the Higher Shell Data

The k^3-weighted Fourier transforms of the isolated higher shell data for the $IrCl_3$- and $Ir_4(CO)_{12}$-derived samples, with a Pt-Pt phase correction, are shown in Figure 6.6. Without analysis already two important differences between the spectra can be observed: the imaginary part and the magnitude of the Fourier transforms show large differences below R = 4.4 Å, and the relative magnitude of the peaks at R ~ 4.7 Å and at R ~ 5.3 Å has changed. Note that below R ~ 3.4 Å especially the magnitude may be unreliable due to overlap of the first coordination shells with shells in that region. Therefore this part of the spectrum was not used in the data analysis.

The higher shell data were analysed for two different kinds of contributions: higher Ir-Ir shells (which provide information about the particle shape), and higher Ir-$O_{support}$ and Ir-$Al_{support}$ shells (in order to acquire information about the metal-support interface). Because of the large disorder already observed in the first Ir-C shell of the $Ir_4(CO)_{12}$-derived sample, it is expected that higher Ir-C shells will not contribute significantly to the higher shell data. In the analysis it was first tried to determine which Ir-Ir shells are present in the Fourier transform. From the coordination distance determined for the first Ir-Ir shell (2.71 and 2.68 Å for the $IrCl_3$- and $Ir_4(CO)_{12}$-derived catalyst, respectively) and the fcc structure for Ir metal,[16] the distances for the higher Ir-Ir shells can be calculated directly (see Table 6.5). With the calculated distances from Table 6.5 the presence of the various Ir-Ir coordination shells in the EXAFS spectrum was verified: after a k^3-weighted Fourier transform, corrected for the Pt-Pt phase shift, the imaginary part should show a positively peaking maximum at approximately the calculated distances for the second and third Ir-Ir shells, and a negatively peaking imaginary part (due to the multiple scattering effect[27]) should be observed at approximately the expected distance for the fourth Ir-Ir shell. Due to the low backscatttering amplitude at high k values for light elements like O and Al,[19] the metal-support contributions are strongly suppressed in a k^3-weighted Fourier transform.

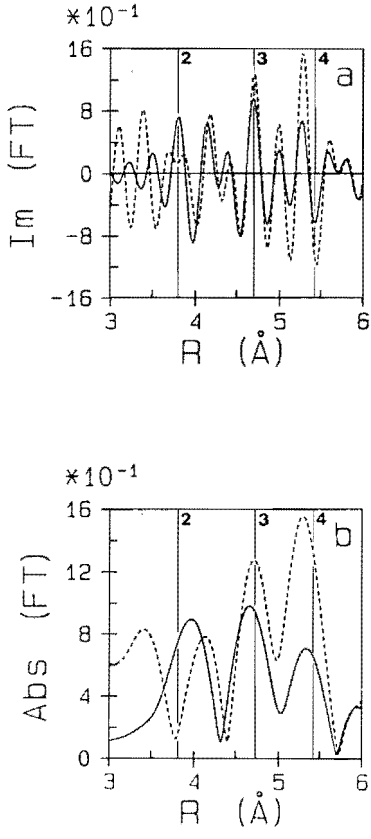

Figure 6.6. k^3-weighted, Pt-Pt phase-corrected Fourier transforms of the isolated higher shell data for the $IrCl_3$-derived sample (Δk = 4.21-12.11 $Å^{-1}$) (—), and for the $Ir_4(CO)_{12}$-derived sample (Δk = 4.25-12.04 $Å^{-1}$) (— —) (a) imaginary part; and (b) magnitude. Indicated are the positions of the higher Ir-Ir shells, based on calculations using the first shell Ir-Ir distance determined with EXAFS. Data for the $IrCl_3$-derived sample are isolated by a k^3-weighted Fourier transform with Δk = 2.72-13.49 $Å^{-1}$ and an inverse transform with Δr = 3.18-8.00 Å. Data for the $Ir_4(CO)_{12}$-derived sample are isolated by a k^3-weighted Fourier transform with Δk = 2.94-14.18 $Å^{-1}$ and an inverse transform with Δr = 2.90-7.98 Å.

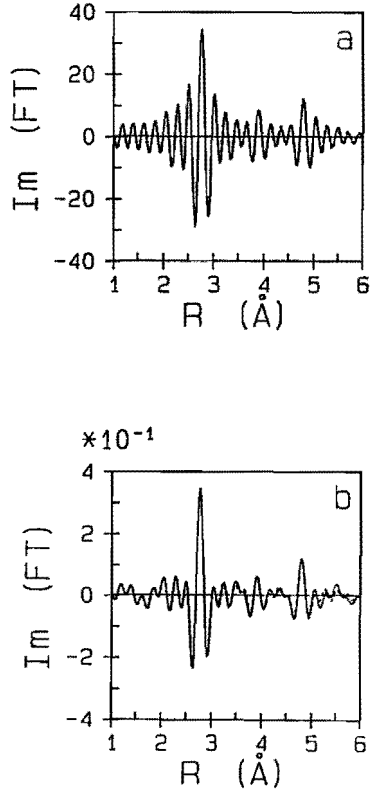

Figure 6.7. EXAFS of the isolated first three shells data of Pt foil (data isolated by a k^3-weighted Fourier transform with Δk = 1.95-19.77 $Å^{-1}$ and an inverse transform with Δr = 1.90-5.00 Å) (—), and best three-shell fit using the first Pt-Pt shell as a reference, and λ = 6 Å (— —) (see Table 6.3) (a) after a k^3-weighted, Pt-Pt phase-corrected Fourier transform (Δk = 3.60-14.30 $Å^{-1}$); and (b) after a k^1-weighted, Pt-Pt phase-corrected Fourier transform, with conditions as in (a).

The approximate positions at which higher Ir-Ir shells are expected, are indicated in Figure 6.6. For the $IrCl_3$-derived catalyst the imaginary part peaks at approximately the calculated distances (see Figure 6.6a); also the coincidence of the maxima in the magnitude of the Fourier transform and the distances calculated for the higher Ir-Ir shells is satisfactory: thus all

these shells are present. However, for the $Ir_4(CO)_{12}$-derived catalyst, the second Ir-Ir shell is absent: at the expected position a dip in the imaginary part is observed (see Figure 6.6a), and the magnitude shows a minimum (see Figure 6.6b). Instead, a peak is observed at R ~ 4.2 Å. In view of the large first shell Ir-$O_{support}$ contribution (N = 2.9) it is very probable that this peak is caused by a higher metal-support contribution.

Parameters for the higher shells were determined as follows: coordination parameters were first sought for the shell with the smallest R (viz. Ir-Ir for the $IrCl_3$-derived sample, and Ir-$O_{support}$ for the $Ir_4(CO)_{12}$-derived sample); depending on the type of contribution expected (Ir-Ir or Ir-$O_{support}$), a first-guess Debye-Waller factor was chosen equal to that determined for the first shell of the same atom type; N, R, and V_0 were chosen so as to get the best agreement possible between the calculated peak and the experimental data in a k^3-weighted Fourier transform. This contribution was then subtracted from the experimental data, and the procedure was repeated for the next coordination shell. Thus in the analysis of the $IrCl_3$-derived catalyst first the second Ir-Ir shell was calculated, followed by the third and fourth Ir-Ir shells; for the $Ir_4(CO)_{12}$-derived system first an Ir-$O_{support}$ contribution was calculated, and then the third and fourth Ir-Ir shells.

Table 6.3. Structural parameters determined for the first three Pt-Pt shells in Pt foil, using the first Pt-Pt shell as a reference and λ = 6 Å.

Shell		XRD results		EXAFS analysis			
		N	R (Å)	N_{unc}[a]	R (Å)	$\Delta\sigma^2$ (Å^2)	V_0 (eV)[a]
1st	Pt-Pt	12	2.770	12	2.770	0	0
2nd	Pt-Pt	6	3.917	4.1	3.901	-0.0006	0
3rd	Pt-Pt	24	4.798	12.2	4.782	0.0002	0

[a]Fixed in the analysis procedure.

EXAFS accuracies: R ± 0.02 Å; $\Delta\sigma^2$ ± 0.001 Å^2.

For the second and third Ir-Ir shells we used the first Pt-Pt shell as a reference. In this case, like for the first shell Ir-$O_{support}$ contribution, the coordination numbers N_{unc} that are determined in the EXAFS data analysis will significantly deviate from the actual ones in the sample due to the factor $\exp(-2R/\lambda)$ in the EXAFS formula.[23-25] Since the difference between the coordination distances in the reference shell and the shells to be analysed is so large, accurate determination of the actual coordination numbers in the sample will strongly depend on a correct choice for the mean free path λ. For values of $k > 3$ Å^{-1}, λ may be approximated by $\lambda \sim 6$ Å.[25,26] We checked this assumption for Pt foil. The first shell data (which were used to analyse the Ir-Ir contributions) were used to analyse the second and third Pt-Pt shells. A straightforward two-shell fit was applied; for the coordination numbers N_{unc} values were taken which were calculated on the basis of the real coordination numbers N in bulk Pt metal and $\lambda = 6$ Å; V_0 corrections were taken equal to zero. Good agreement was obtained in r space after k^1-weighted and k^3-weighted Fourier transforms (see Figure 6.7); the parameters obtained are given in Table 6.3. The values for R agree very well with those determined by XRD.[16] Therefore we are confident that using the first Pt-Pt shell in Pt foil as a reference with $\lambda = 6$ Å, accurate values are obtained for the coordination numbers of the higher Ir-Ir shells. Because it is reported that the value of λ does not depend very much on the type of compound under study,[26] we also used the first Pt-O shell in $Na_2Pt(OH)_6$ as a reference for the higher Ir-$O_{support}$ shells, and corrected the determined coordination numbers N_{unc} also using $\lambda = 6$ Å. For the fourth Ir-Ir shell we used a reference manufactured from the fourth Pt-Pt shell in Pt foil. Due to the multiple scattering contribution in the fourth shell of the fcc structure,[27] analysis of the fourth Ir-Ir shell with a reference made from the first Pt-Pt shell yields numerically erroneous results.

All first-guess contributions were added and compared with the experimental data after k^1-weighted and k^3-weighted Fourier transforms. The overall agreement obtained in this first cycle was not very good, especially not after the k^1-weighted Fourier transform. Therefore all contributions except that of the starting shell (the shell with the smallest R) were subtracted from the experimental data and better parameters were sought for the first contribution after a k^3-weighted Fourier transform, varying all parameters. This was done for each contribution in turn. After one or two

of these cycles usually a better agreement was obtained after a k^3-weighted Fourier transform. However, large differences remained in the k^1-weighted Fourier transforms. This strongly indicated that additional shells of low-Z

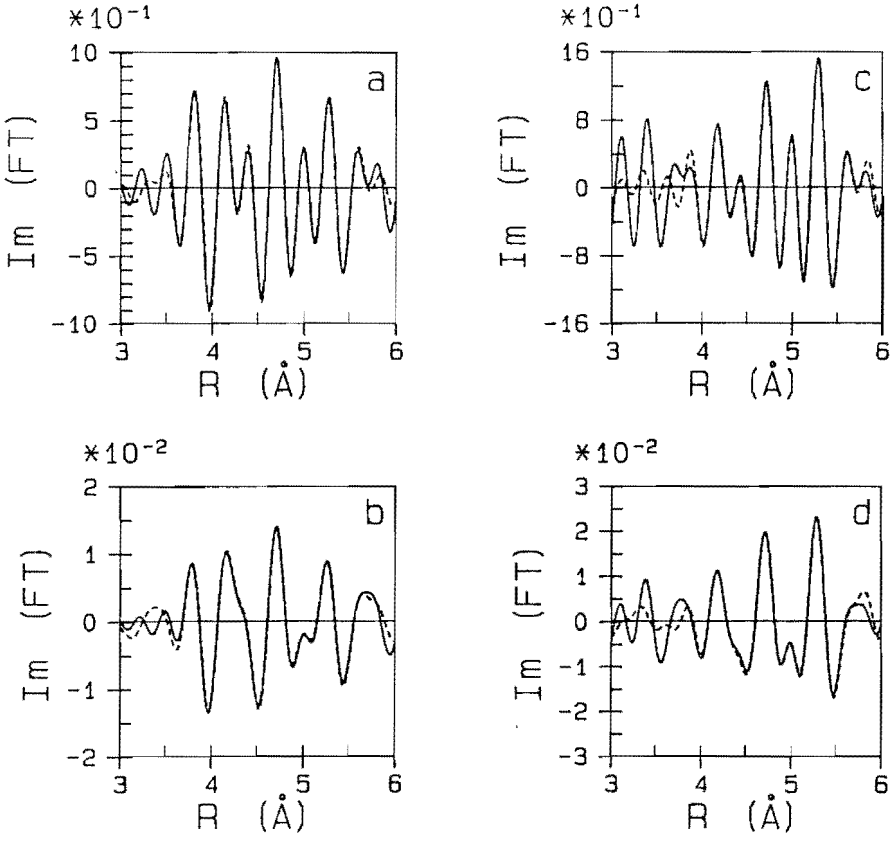

Figure 6.8. EXAFS data for the isolated higher shells of the $IrCl_3$-derived sample (—), and sum of the best calculated higher shell contributions (— —) (see Table 6.4) (a) after a k^3-weighted Fourier transform (Δk = 4.21-12.11 $Å^{-1}$, Pt-Pt phase corrected); and (b) after a k^1-weighted Fourier transform, with conditions as in (a). EXAFS data for the isolated higher shells of the $Ir_4(CO)_{12}$-derived sample (—), and sum of the best calculated higher shell contributions (— —) (see Table 6.4) (c) after a k^3-weighted Fourier transform (Δk = 4.25-12.04 $Å^{-1}$, Pt-Pt phase corrected); and (d) after a k^1-weighted Fourier transform, with conditions as in (c).

scatterers had to be incorporated: low-Z scatterer shells are expected to be more prominent in a k^1-weighted, than in a k^3-weighted Fourier transform.[19] Thus, in the analysis of the $IrCl_3$-derived system additional $Ir-O_{support}$ shells were incorporated at R ~ 4.1 Å and at R ~ 5.1 Å; in the case of the $Ir_4(CO)_{12}$-derived catalyst an additional shell at R ~ 5.1 Å was needed. These additional $Ir-O_{support}$ shells provide valuable information about the structure of the metal-support interface.

Table 6.4. Coordination parameters determined for the higher coordination shells in reduced $Ir/\gamma-Al_2O_3$.

Sample	Shell	N_{unc}	N	R (Å)	$\Delta\sigma^2$ (Å^2)
Ir/Al_2O_3	Ir-Ir	1.3	1.8	3.84	0.0022
ex $IrCl_3$	Ir-O	1.5	3.0	4.11	0.0080
	Ir-Ir	2.1	3.9	4.70	0.0022
	Ir-O	1.6	4.5	5.17	0.0090
	Ir-Ir[a]	0.9	0.9	5.39	-0.0009
Ir/Al_2O_3	Ir-O	2.4	5.3	4.46	0.0000
ex $Ir_4(CO)_{12}$	Ir-Ir	1.6	3.1	4.69	0.0005
	Ir-O	1.3	3.6	5.09	0.0030
	Ir-Ir[a]	3.0	3.0	5.35	0.0010

[a]Multiple scattering contribution.

Accuracies: N ± 20-30%; R ± 0.06 Å; σ^2 ± 20-30%.

We are aware of the fact that the number of shells that is incorporated in the EXAFS data analysis has become rather large. However, with the help of the difference file technique, and with deliberate use of both k^1- and k^3-weighted Fourier transforms, we think that it is possible to determine the coordination parameters of all these shells with reasonable accuracy. The best coordination parameters for the higher shells are given in Table 6.4; k^1-weighted and k^3-weighted Fourier transforms of the experimental data and the sum of the calculated contributions are shown in Figure 6.8.

6.4 Discussion

6.4.1 Nature of the Metal-Support Bonding

Analysis of the first shell EXAFS data shows that small metal particles have been obtained in the $IrCl_3$-derived system as well as in the $Ir_4(CO)_{12}$-derived system. Also, a significant Ir-$O_{support}$ contribution has been observed for both systems, with a long Ir-O coordination distance. Previously, such long metal-oxygen bonds were reported for the metal-support interface in reduced Rh/γ-Al_2O_3,[8,9] Rh/TiO_2,[10,11] and Pt/γ-Al_2O_3[12] systems.

For the Rh/γ-Al_2O_3 catalysts, the Rh-$O_{support}$ coordination number of the Rh atoms in the interface was determined to be between two and three on the basis of the coordination numbers determined for the Rh-Rh and Rh-$O_{support}$ contributions and assuming a half-spherical particle shape for the supported metal particles.[8] The rather large inaccuracy in the number of Rh-$O_{support}$ bonds for the interface Rh atoms is partly caused by the fact that with EXAFS average coordination numbers are determined (thus the Rh-$O_{support}$ coordination number that is determined straightforwardly in the data analysis procedure, is averaged over those Rh atoms that are in contact with the support, and those that are not) while the correction procedure introduces an additional inaccuracy.

In this study we have used $Ir_4(CO)_{12}$ adsorbed on γ-Al_2O_3, to follow the formation of the metal-support interface. After reduction, we obtained an Ir/γ-Al_2O_3 system in which an Ir-$O_{support}$ coordination number of almost three was determined, without correcting for the particle shape (this will be discussed below). Therefore, if we assume that in both the reduced Rh/γ-Al_2O_3 and Ir/γ-Al_2O_3 systems the type of epitaxy is the same, it must be concluded that the metal-oxygen coordination number in the interface is equal to three.

ASED (Atom Superposition Electron Delocalization) MO theoretical calculations[13] performed on the Rh/γ-Al_2O_3 system, yielded the following results. On a hydroxylated (111) γ-Al_2O_3 surface (thus bounded by OH groups) a threefold coordination of the interface Rh atoms by surface OH groups is the most stable situation. In this case, a Rh^0-OH^- coordination distance of R = 2.55 Å is calculated. On a dehydroxylated (111) γ-Al_2O_3

surface, interface Rh atoms singly coordinated by surface oxygen are most stable, with a Rh^0-O^{2-} coordination distance of R = 2.10 Å.

The results of the calculations for Rh/γ-Al_2O_3 agree very well with the experimental EXAFS results for Ir/γ-Al_2O_3: after reduction, an Ir-$O_{support}$ contribution is detected with long Ir-O bonds (R ~ 2.5-2.6 Å) and a threefold coordination in the interface, whereas after subsequent evacuation (after which the γ-Al_2O_3 surface is presumably partially dehydroxylated) the Ir-$O_{support}$ coordination distance contracts to R ~ 2.1 Å.[28,29]

Still more experimental evidence is needed in order to decide unambiguously whether the long metal-support oxygen coordination distance is caused by a metal-hydroxyl interaction, by electronic effects, or by the presence of adsorbed hydrogen in the metal-support interface. Future experiments including evacuation/rehydrogenation are expected to yield conclusive information.

6.4.2 The Carbonaceous Overlayer in Ir/γ-Al_2O_3 ex $Ir_4(CO)_{12}$

In Ir/γ-Al_2O_3 ex $Ir_4(CO)_{12}$ a low-Z scatterer shell was observed at R ~ 2.10 Å. This shell was attributed to an Ir-C interaction, because no realistic model could be devised in which two Ir-O contributions, at a long (R ~ 2.6 Å) coordination distance as well as at a short (R ~ 2.1 Å, thus oxidic) distance, are present. Because carbon is present in the precursor system in the CO ligands from $Ir_4(CO)_{12}$ and the cyclohexane solvent, an Ir-C contribution seems very likely.

Since the Ir-C coordination number is large (N = 3 from the EXAFS data analysis; the actual coordination number very likely being larger[22]) it is possible that an ordered carbonaceous overlayer has been formed. Stable interfaces are reported for the (0001) basal plane of graphite, and the (111) and (110) faces of Pt,[30-33] although there is a mismatch in lattice parameters. With dynamical LEED the graphite/Pt (111) interface was studied,[33] and a distance between the Pt surface and the graphite (0001) basal plane of 3.70 Å was determined. In between these layers, C atoms were observed at R_{Pt-C} = 2.03 ± 0.07 Å. It is stated that these C atoms can be present both at hcp and fcc hollow sites, and a regular arrangement does not follow necessarily from the experimental data. It is very likely that the carbon neighbours observed with EXAFS are of the same type as the intercalated C

atoms observed with LEED: the coordination distance determined is equal in both cases, and also the large Debye-Waller factor determined with EXAFS for the Ir-C shell shows that the carbonaceous overlayer is not very well defined. From EXAFS, no indications are obtained that a full graphitic overlayer is present at a larger distance. In view of the lattice mismatch (2.68 Å for the Ir-Ir coordination distance, vs. 2.46 Å for the distance between the centers of the hexagons in the graphitic (0001) basal plane) a large spread in Ir-C distances is expected, and it is not very probable that such an Ir-C interaction will be observed in the EXAFS spectrum.

6.4.3 Determination of the Particle Morphology

When comparing the coordination numbers determined for the first Ir-Ir and Ir-$O_{support}$ shells, it is clear that from the view of the Ir-Ir coordination numbers (4.9 and 4.7 for the $IrCl_3$- and $Ir_4(CO)_{12}$-derived system, respectively), particle sizes are almost equal. The particle shape being equal, a larger Ir-Ir coordination number means a larger average particle size, and hence a smaller fraction of the metal atoms in the metal-support interface. Since in EXAFS coordination numbers are averaged over all metal atoms, this means that for larger metal particles a smaller Ir-$O_{support}$ coordination number will be determined.[8] Thus we expected that for the $IrCl_3$-derived system the Ir-$O_{support}$ coordination number might be somewhat smaller. This was found indeed, but the difference observed between the two systems (Ir-$O_{support}$ coordination numbers of 1.8 and 2.9 determined in the EXAFS analysis for the $IrCl_3$- and $Ir_4(CO)_{12}$-derived system, respectively) is very large in view of the small difference in the Ir-Ir coordination numbers.

By modelling, under the assumption of half-spherical metal particle shape, a relationship was determined between the measured metal-metal and metal-oxygen coordination numbers,[8] from which the actual metal-oxygen coordination number for the atoms in the interface has been derived. Applying this relationship to the parameters determined for our Ir/γ-Al_2O_3 systems, we found an Ir-O interface coordination number just over three for the $IrCl_3$-derived system, and a coordination number of more than four for the $Ir_4(CO)_{12}$-derived system.

Both from modelling[34] and HREM (High-Resolution Electron Microscopy) observations[35,36] it appears that small γ-Al_2O_3 particles predominantly exhibit fcc (111) faces. Therefore, we expect that the metal-support interface will preferentially consist of a (111) oxygen (or hydroxyl) layer on the side of the γ-Al_2O_3 support. In order to get a good epitaxial fit, also the metal particles will then be bounded by a (111) face in the metal-support interface. A (111) interface only allows up to three Ir-$O_{support}$ bonds per Ir interface atom. Assuming a half-spherical particle shape, the model calculations yielded more than four Ir-$O_{support}$ bonds per interface atom for the $Ir_4(CO)_{12}$-derived sample. We therefore conclude that in the $Ir_4(CO)_{12}$-derived system the metal particles are not half-spherical in shape. Because the Ir-$O_{support}$ coordination number as determined in the EXAFS analysis is equal to three within the limits of accuracy, all metal atoms must be in the metal-support interface, thus leading to a (111) flat particle shape. Such a particle shape is not very common in supported metal catalysts. We think that the shape is strongly influenced by the presence of carbon on the metal particle (with EXAFS, a significant Ir-C contribution is determined with N = 3 and R = 2.10 Å); a carbon overlayer may effectively prevent three-dimensional growth of the metal particles, or stabilize two-dimensional particles.

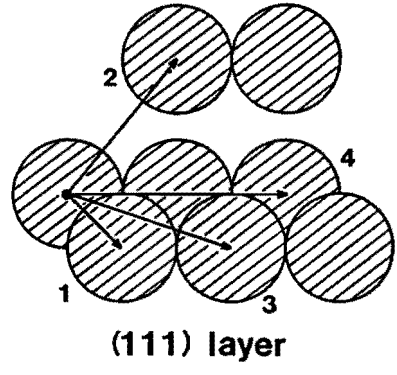

Figure 6.9. Illustration of the various Ir-Ir distances occurring in the fcc structure (see also Table 6.5).

Assuming that the metal-support epitaxy in the $IrCl_3$-derived system is the same as in the $Ir_4(CO)_{12}$-derived system, approximately 2/3 of the metal atoms will be in contact with the support in the former.

When the results of the higher shell analysis obtained for both systems are compared, it is clear from the parameters of the Ir-Ir shells that the particle shape in both systems is different. The absence of the second Ir-Ir shell in the $Ir_4(CO)_{12}$-derived system constitutes conclusive evidence that the Ir particles are flat, and consist of a single Ir layer with (111)-like geometry, because the second Ir-Ir coordination is only found between the Ir atoms of adjacent (111) layers, and not within a layer (see Figure 6.9).

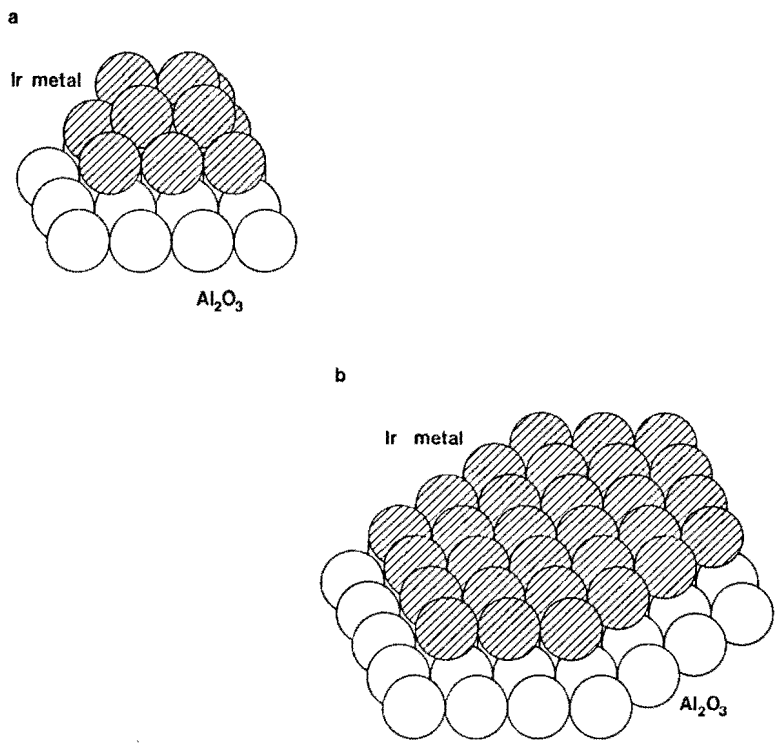

Figure 6.10. (a) Model for the average Ir particle (consisting of 12 atoms) in $IrCl_3$-derived Ir/γ-Al_2O_3; and (b) model for the average Ir particle (consisting of 30 atoms) in $Ir_4(CO)_{12}$-derived Ir/γ-Al_2O_3.

Table 6.5. Comparison of the parameters obtained for the Ir-Ir shells in the EXAFS data analysis, and those calculated on the basis of the coordination number and distance for the first shell assuming half-spherical particles (for the $IrCl_3$-derived system, see Figure 6.10a) or flat particles (for the $Ir_4(CO)_{12}$-derived system, see Figure 6.10b).

Sample	Shell		EXAFS analysis N	EXAFS analysis R (Å)	Model calculation N	Model calculation R (Å)
Ir/Al_2O_3 ex $IrCl_3$	1st	Ir-Ir	4.9	2.71	5.1	2.71
	2nd	Ir-Ir	1.8	3.84	1.2	3.83
	3rd	Ir-Ir	3.9	4.70	3.0	4.69
	4th	Ir-Ir	0.9	5.39	0.9	5.42
Ir/Al_2O_3 ex $Ir_4(CO)_{12}$	1st	Ir-Ir	4.7	2.68	4.7	2.68
	2nd	Ir-Ir	-	-	-	3.79
	3rd	Ir-Ir	3.1	4.69	3.7	4.64
	4th	Ir-Ir	3.0	5.35	3.5	5.36

In the $IrCl_3$-derived sample a significant contribution of the second Ir-Ir shell is observed, indicating that three-dimensional metal particles are present, presumably half-spherical in shape.

The assumptions concerning the particle shape were checked by modelling. The EXAFS coordination numbers for both the first Ir-Ir shell and the higher Ir-Ir shells were consistent with an approximately half-spherical particle consisting of 12 atoms (diameter $\sim$ 9 Å) in the case of the $IrCl_3$-derived system, and an approximately round, flat particle consisting of 30 atoms (diameter $\sim$ 16 Å) in the case of the $Ir_4(CO)_{12}$-derived system. The metal particles for which the model parameters were calculated, are shown in Figure 6.10. The coordination numbers determined with EXAFS and those calculated for the model metal particles are compared in Table 6.5. Also in Table 6.5 the coordination distances determined for the higher Ir-Ir shells from the first shell distance and the fcc structure, are compared with those from the EXAFS data analysis. As can be seen in Table 6.5, the higher shell EXAFS results compare very well with the calculated parameters. Judging from the agreement between EXAFS results

and model calculations for the Ir-Ir shells, we infer that the assumptions concerning the metal particle shape are valid.

6.4.4 Structure of the Metal-Support Interface

γ-Al_2O_3 may be described as a defect spinel,[37-39] that is, an fcc packed oxygen lattice with Al atoms distributed over the octahedral and tetrahedral sites. Approximately 25% of the Al cations occupy tetrahedral sites.[40] This means that with respect to the spinel structure, all octahedral and 2/3 of the tetrahedral positions are filled. Two different types of epitaxy can be imagined: one in which the Ir atoms lie directly above the oxygen atoms of the second layer in γ-Al_2O_3 (hcp-type epitaxy, see Figure 6.11a), and one in which the Ir atoms lie above the oxygen atoms of the third layer in γ-Al_2O_3 (fcc-type epitaxy, see Figure 6.11b). Information about the occurrence of either type of epitaxy may be obtained from the position of the higher Ir-O shells (see Figure 6.11a and 6.11b), but more reliably from the positions of the Ir-Al shells.

Unfortunately, we did not observe contributions that could be attributed to Ir-Al shells, possibly due to a large spread in Ir-Al distances. Several explanations can be found for this disorder: intrinsic disorder in the Al positions of the γ-Al_2O_3 lattice, a poorly defined Ir-Al_2O_3 interface, or reconstruction of the γ-Al_2O_3 surface. Disorder in the tetrahedral Al positions has been reported[37] but this can not fully account for the missing Ir-Al signal since most of the Al atoms (75%) are located at octahedral sites. A non-perfect epitaxy might provide an explanation: the O-O distance in γ-Al_2O_3 is approximately 2.80 Å,[39] while the first shell Ir-Ir distance determined for the $Ir_4(CO)_{12}$-derived system is 2.68 ± 0.02 Å. However, the disorder does not occur in the Ir-O interface, since for the Ir-$O_{support}$ shells large contributions with small Debye-Waller factors are observed (see Tables 6.2 and 6.4). Therefore, we conclude that at least in the $Ir_4(CO)_{12}$-derived sample the metal-support interface is a well-defined one. Of course it is possible that the hcp- and fcc-type interface coexist, but the Ir-$O_{support}$ interactions are well-defined. We believe that reconstruction of the γ-Al_2O_3 surface might explain the absence of the Ir-Al signal.

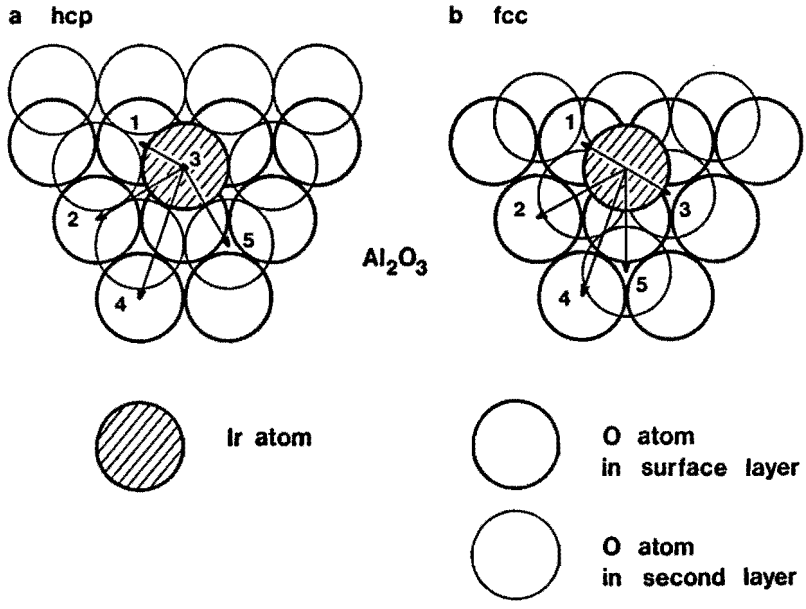

Shell	Hcp model		Fcc model		EXAFS results	
	N	R (Å)	N	R (Å)	N	R (Å)
1	3	2.58	3	2.58	2.9	2.58
2	3	3.72	3	3.72	n.d.	n.d.
3	1	4.25	3	4.52	5.3	4.46
4	6	4.58	6	4.58		
5	6	5.03	3	5.26	3.6	5.09

Figure 6.11. (a) Epitaxial model for $Ir_4(CO)_{12}$-derived Ir/γ-Al_2O_3 in which the Ir atoms lie directly above the second layer of γ-Al_2O_3 oxygen atoms (hcp-type); and (b) epitaxial model in which the Ir atoms lie above the third layer of γ-Al_2O_3 oxygen atoms (fcc-type).

It has been shown with HREM[35,36] that the surface of small Al_2O_3 particles is significantly reconstructed. In view of the well-ordered Ir-O interface inferred above, we assume that the oxygen atoms in the Ir-O interface are displaced, the more since the Ir-Ir distance determined in the EXAFS data analysis of the $Ir_4(CO)_{12}$-derived system (2.68 Å [7]) is actually shorter than the first shell Ir-Ir distance in bulk Ir metal (2.71 Å [16]). From the fact that the O-O distance in γ-Al_2O_3 is approx. 2.80 Å,[39] it was expected that in order to get a good epitaxial fit, the Ir-Ir distance should increase rather than decrease. Remarkably, in the case of the $IrCl_3$-derived system the Ir-Ir distance does not decrease and a much larger disorder has been determined in the first Ir-$O_{support}$ shell although the number of Ir atoms in the interface per particle is smaller in this system than in the $Ir_4(CO)_{12}$-derived system. Also in supported Rh/γ-Al_2O_3 systems, with a Rh-Rh distance of approx. 2.68 Å, Rh-$O_{support}$ contributions were found with small Debye-Waller factors.[8,9] In conclusion, we suggest that the O-O distance in the Ir-Al_2O_3 interface is contracted to $\sim$ 2.68 Å, or perhaps even less. Reconstructed domains of about the size of the metal particles in the $Ir_4(CO)_{12}$-derived sample will exist on the (111) faces of the γ-Al_2O_3 crystallites.

Notwithstanding the lack of information on the Ir-Al coordination, it still is possible to obtain information on the type of epitaxy from the higher Ir-O shells. In Figure 6.11 the occurrence of some Ir-$O_{support}$ shells is illustrated for two types of epitaxy, together with the number of oxygen atoms in each shell and the approximate coordination distance. In view of the rather inaccurate information on the γ-Al_2O_3 crystal structure, and the presumed surface reconstruction, it is very difficult to give good estimates of the actual distances. The values in Figure 6.11 are calculated on the following assumptions: the O-O distance in the first two (111) oxygen layers is equal to the first shell Ir-Ir distance in the $Ir_4(CO)_{12}$-derived sample (2.68 Å), and the first shell Ir-$O_{support}$ distance is equal to 2.58 Å, as determined with EXAFS. We think that the accuracy of the calculated distances is about 0.2 Å. This means that presumably the third and fourth Ir-O shell in the fcc-type epitaxial model must be added, so that the parameters of the third Ir-O shell will be N = 9, R = 4.56 Å.

In the EXAFS data analysis we did not take into account the second Ir-O shell at 3.72 Å. This contribution might be reduced in amplitude due

to the range in r space used to extract the higher shell data making the coordination parameters inaccurate. Fortunately, two other Ir-O contributions were very outspoken in the spectrum of the $Ir_4(CO)_{12}$-derived sample. The coordination numbers and distances determined point to the hcp-type of epitaxy: the contribution at R = 4.46 Å can be attributed to the fourth shell Ir-O contribution, while the contribution at R = 5.05 Å is caused by the fifth shell Ir-O interaction (see Figure 6.11a). The coordination number of the third shell Ir-O interaction in this model (N = 1) is so small that we think this contribution can not be significantly detected. In case of an fcc-type of epitaxy, a combined third and fourth shell Ir-O contribution were to be expected, and thus a large coordination number of the Ir-O shell at R ~ 4.5 Å (N = 9). This was not observed. Also for the $IrCl_3$-derived system the parameters determined for the $Ir\text{-}O_{support}$ shells point to the same type of epitaxy, although the agreement of the parameters with those calculated from the interface model is less, probably due to the contribution of the Ir atoms which are not in direct contact with the support.

6.5 Conclusions

The EXAFS spectra of reduced $Ir/\gamma\text{-}Al_2O_3$ catalysts, prepared either from $Ir_4(CO)_{12}$ or $IrCl_3$, show a distinct contribution from the metal-support interface. The Ir atoms in the interface are coordinated to three support oxygen atoms, at R ~ 2.6 Å.

Comparison of the EXAFS spectra of the differently prepared $Ir/\gamma\text{-}Al_2O_3$ catalysts shows clearly that the method of preparation has a large influence on the shape of the reduced metal particles. The preparation method with $IrCl_3$ yields three-dimensional (most likely half-spherical) particles consisting of approx. 12 atoms, whereas preparation with $Ir_4(CO)_{12}$ yields a system with flat particles, consisting of approx. 30 atoms.

The $Ir/\gamma\text{-}Al_2O_3$ system ex $Ir_4(CO)_{12}$ is an excellent system to study the metal-support interface in detail. (111) epitaxy is clearly established, with a threefold first shell $Ir\text{-}O_{support}$ coordination in the interface. Most probably reconstruction of the $\gamma\text{-}Al_2O_3$ surface ensures a good epitaxial fit.

The coordination parameters determined for the higher Ir-$O_{support}$ shells indicate a model in which the Ir atoms lie directly above the oxygen atoms of the second layer in γ-Al_2O_3 (hcp-type of epitaxy).

6.6 References

(1) J. C. Vis, H. F. J. Van 't Blik, T. Huizinga, J. Van Grondelle, and R. Prins, *J. Mol. Catal.* **1984**, *25*, 367.

(2) T. Huizinga, J. Van Grondelle, and R. Prins, *Appl. Catal.* **1984**, *10*, 199.

(3) J. W. Geus, *Preparation of Catalysts III*; G. Poncelet, P. Grange, and P. A. Jacobs, Eds.; Elsevier: Amsterdam, 1983; p 1.

(4) F. B. M. Duivenvoorden, D. C. Koningsberger, Y. S. Uh, and B. C. Gates, *J. Am. Chem. Soc.* **1986**, *108*, 6254.

(5) P. S. Kirlin, F. B. M. Van Zon, D. C. Koningsberger, and B. C. Gates, to be published.

(6) F. B. M. Van Zon, A. D. Van Langeveld, J. Van Grondelle, and D. C. Koningsberger, to be published.

(7) F. B. M. Van Zon, G. J. Visser, and D. C. Koningsberger, *Proc. 9th Int. Congress on Catalysis* (Calgary, 1988); M. J. Phillips, and M. Ternan, Eds.; Chemical Institute of Canada: Ottawa, 1988; Vol. III, p 1386.

(8) J. B. A. D. Van Zon, D. C. Koningsberger, H. F. J. Van 't Blik, and D. E. Sayers, *J. Chem. Phys.* **1985**, *82*, 5742.

(9) D. C. Koningsberger, J. B. A. D. Van Zon, H. F. J. Van 't Blik, G. J. Visser, R. Prins, A. N. Mansour, D. E. Sayers, D. R. Short, and J. R. Katzer, *J. Phys. Chem.* **1985**, *89*, 4075.

(10) D. C. Koningsberger, J. H. A. Martens, R. Prins, D. R. Short, and D. E. Sayers, *J. Phys. Chem.* **1986**, *90*, 3047.

(11) J. H. A. Martens, R. Prins, H. Zandbergen, and D. C. Koningsberger, *J. Phys. Chem.* **1988**, *92*, 1903.

(12) D. C. Koningsberger, and D. E. Sayers, *Solid State Ionics* **1985**, *16*, 23.

(13) J. H. A. Martens, R. A. Van Santen, D. C. Koningsberger, and R. Prins, *Catalysis Lett.* submitted.

(14) B. J. Kip, J. Van Grondelle, J. H. A. Martens, and R. Prins, *Appl. Catal.* **1986**, *26*, 353.

(15) B. J. Kip, F. B. M. Duivenvoorden, D. C. Koningsberger, and R. Prins, *J. Catal.* **1987**, *105*, 26.

(16) R. W. G. Wyckoff, *Crystal Structures*, 2nd ed.; Wiley: New York, 1963; Vol. I, p 10.

(17) M. Trömel, and E. Lupprich, *Z. Anorg. Chem.* **1975**, *414*, 160.

(18) P. Esslinger, and K. Schubert, *Z. Metallk.* **1957**, *48*, 126.

(19) B. K. Teo, and P. A. Lee, *J. Am. Chem. Soc.* **1979**, *101*, 2815.

(20) B. Lengeler, *J. de Phys. C8* **1986**, *47*, 75.

(21) J. W. Cook, and D. E. Sayers, *J. Appl. Phys.* **1981**, *52*, 5024.

(22) K. I. Pandya, and D. C. Koningsberger, *Proc. XAFS V Conference* (Seattle, 1988) accepted.

(23) E. A. Stern, *Phys. Rev. B* **1974**, *10*, 3027.

(24) F. W. Lytle, D. E. Sayers, and E. A. Stern, *Phys. Rev. B* **1975**, *11*, 4825.

(25) E. A. Stern, B. A. Bunker, and S. M. Heald, *Phys. Rev. B* **1980**, *21*, 5521.

(26) M. P. Seah, and W. A. Dench, *Surf. Interf. Anal.* **1979**, *1*, 2.

(27) B. K. Teo, *J. Am. Chem. Soc.* **1981**, *103*, 3990.

(28) D. C. Koningsberger, F. B. M. Duivenvoorden, B. J. Kip, and D. E. Sayers, *J. de Phys. C8* **1986**, *47*, 255.

(29) F. W. H. Kampers, and D. C. Koningsberger, to be published.

(30) J. Santiesteban, S. Fuentes, and M. Yacaman, *J. Mol. Catal.* **1983**, *20*, 213.

(31) R. Vanselow, and M. Mundschau, *Surf. Sci.* **1986**, *176*, 701.

(32) H. Zi-pu, D. F. Ogletree, M. A. Van Hove, and G. A. Somorjai, *Surf. Sci.* **1987**, *180*, 433.

(33) N. L. Wu, and J. Phillips, *Surf. Sci.* **1987**, *184*, 463.

(34) S. Soled, *J. Catal.* **1983**, *81*, 252.

(35) S. Iijima, *Jap. J. Appl. Phys.* **1984**, *23*, L347.

(36) S. Iijima, *Surf. Sci.* **1985**, *56*, 1003.

(37) B. C. Lippens, and J. H. De Boer, *Acta Cryst.* **1964**, *23*, 1003.

(38) H. Knözinger, *Catalysis by Acids and Bases*; B. Imelik, C. Naccache, G. Coudurier, Y. Ben Taarit, and J. C. Vedrine, Eds.; Elsevier: Amsterdam, 1985; p 111.

(39) S. J. Wilson, *J. Solid State Chem.* **1979**, *30*, 247.

(40) C. S. John, N. C. M. Alma, and G. R. Hays, *Appl. Catal.* **1983**, *6*, 341.

Chapter Seven

A Structural Characterization of the Metal-Support Interface in Reduced Ir/MgO and Rh/MgO Catalyst Systems with EXAFS

7.1 Introduction

Chemical reactions are exclusively catalysed by the metal surface of metal-on-support catalysts. Therefore it is usually tried to prepare catalysts in such a way that after reduction the metal surface area per amount of metal is as large as possible. This is attained if the metal particles on the support are very small. These particles must be stabilized by interaction with the support; bonding to the support will prevent the particles to move freely on the support surface, which would eventually result in the coalescence of the small particles, and thus the loss of available surface area. Knowledge of the metal-support interaction may enable us to design more stable catalysts.

In the past we have extensively studied with EXAFS the metal-support interface in catalyst systems with Rh and Ir as metals and γ-Al_2O_3 and TiO_2 as supports.[1-6] From these studies we concluded that the reduced metal particles are bonded to the support via long metal-oxygen bonds (R $\sim$ 2.5-2.8 Å). The EXAFS experiments were carried out in a H_2 atmosphere, after in situ reduction. Theoretical calculations have shown that the long metal-oxygen bonds may be attributed to metal-surface hydroxyl interactions,[7] implying that the metal particles are resting on the hydroxyl groups of the support. Other explanations for the long metal-oxygen bonds may be that hydrogen adsorbed onto the supported metal particles induces electronic changes in the metal, or that adsorbed hydrogen is present between the metal particle and the supporting oxide.

In Rh/MgO catalysts, Rh-O bonds have been reported to be present, but with a short Rh-O distance (R $\sim$ 1.95 Å).[8] These bonds were attributed to a metal-support interaction. This should mean that the nature of the MgO support is very much different from that of the γ-Al_2O_3 and TiO_2

supports, because in the reduced Rh/γ-Al_2O_3[1,2] and Rh/TiO_2[3,4] systems we detected long Rh-$O_{support}$ bonds. Differences in the nature of the metal-support interaction may arise from the type of plane which is preferentially engaged in the metal-support epitaxy. Contrary to γ-Al_2O_3 and TiO_2, MgO (which has the rocksalt structure) almost exclusively exhibits (100) faces.[9] This makes MgO a very suitable support to study the metal-support interaction with EXAFS, because the metal-support interface probably will be uniquely defined.

In this work, we studied the metal-support interface of a highly dispersed Ir/MgO catalyst, in order to compare the types of metal-oxygen bonds present in Al_2O_3- and MgO-supported Ir catalysts. The Ir/MgO catalyst was prepared from $Ir_4(CO)_{12}$ in order to obtain a highly dispersed system. Only EXAFS data of high quality obtained for highly dispersed systems allow a reliable detection of the contribution of the metal-support interface, since in highly dispersed systems the fraction of the metal atoms, present in the metal-support interface, is relatively high. Also, we reanalysed previously published EXAFS data of a reduced Rh/MgO catalyst,[8] using a Rh_2O_3 reference compound which was checked by XRD in order to exclude the presence of a mixture of oxides. EXAFS data analysis was performed using fitting in k space as well as the difference file technique combined with phase-corrected Fourier transforms.[1]

7.2 Experimental

7.2.1 Catalyst Preparation

The Ir/MgO catalyst was prepared by impregnation of MgO with a solution of $Ir_4(CO)_{12}$ in cyclohexane. MgO was prepared as follows: 88 g of $Mg(NO_3)_2{\cdot}6H_2O$ was dissolved in 400 ml of distilled water. This solution was added dropwise under vigorous stirring to a 1000 ml water/ice mixture in which 200 ml of concentrated ammonia had been dissolved. After all $Mg(NO_3)_2$ solution had been added, and the ice had melted, the precipitate was filtrated. The precipitate was then suspended again in 500 ml of water/ice mixture, and subsequently filtrated. This was repeated until the pH of the suspension was equal to 7. After the last filtration, the precipitate was dried overnight at 393 K, and powdered. The white powder was

calcined in N_2 at 673 K for 2 h (heating rate 5 K/min), in order to remove nitrogen-containing residues. The resulting MgO powder has a surface area of 119 m^2/g (determined by N_2 adsorption). The MgO was partly dehydroxylated by calcining in vacuum at 873 K for 8 h (heating rate 5 K/min). $Ir_4(CO)_{12}$ was obtained from Alfa Products and used without further purification. Cyclohexane was dried over a sodium/benzophenone mixture and used freshly distilled. The metal carbonyl was dissolved in the cyclohexane and stirred with MgO under N_2 for 4 h. After filtration and drying overnight in vacuum at room temperature, the final Ir loading was 0.8% by weight. The impregnated system was decomposed in N_2 at 473 K for 2 h, prereduced in flowing H_2 at 623 K for 8 h (heating rate 5 K/min), and passivated in air at room temperature prior to storage.

The Rh/MgO catalyst was prepared from $Rh(NO_3)_3$ by a modified ion-exchange procedure, as described previously.[8] The Rh loading was 3 wt%.

7.2.2 EXAFS measurements

EXAFS measurements on the Ir/MgO system were performed on Wiggler station 9.2 at the SRS at Daresbury, U. K. The sample was pressed into a thin self-supporting wafer with an absorbance of approx. 2.5, and mounted in an in situ EXAFS cell. The sample was reduced in flowing H_2 at 623 K for 1 h (heating rate 5 K/min). EXAFS measurements were done on the Ir L_{III} edge (11215 eV) at liquid nitrogen temperature, in a H_2 atmosphere. As reference compounds Pt foil[11] and $Na_2Pt(OH)_6$[12] were measured on the Pt L_{III} edge (11564 eV), and IrAl alloy[13] on the Ir L_{III} edge, all at liquid nitrogen temperature. Pt foil was used as a reference for Ir-Ir interactions, $Na_2Pt(OH)_6$ was used for Ir-O, and the alloy as a reference for Ir-Mg interactions. It has been shown theoretically[14] and experimentally[15] that the use of these references for the mentioned contributions is justified. The crystallographic first shell coordination parameters for the reference compounds, and the ranges in k and r space used to extract the reference data from the experimental EXAFS data, are given in Table 7.1. The data analysis procedures used to obtain these reference data are extensively described previously.[6]

Table 7.1. First shell structural parameters of the reference compounds, and the ranges in k and r space used to extract the references from the EXAFS data (k^3-weighted Fourier transforms were used).

Sample	Shell	N	R (Å)	Δk ($Å^{-1}$)	Δr (Å)
Pt foil[11]	Pt-Pt	12	2.77	1.95-19.77	1.90-3.02
$Na_2Pt(OH)_6$[12]	Pt-O	6	2.05	1.43-17.69	0.50-2.02
IrAl alloy[13]	Ir-Al[a]	8	2.58	3.02-12.32	0.88-2.48
Rh foil[11]	Rh-Rh	12	2.69	2.76-18.21	1.62-2.74
Rh_2O_3[16]	Rh-O	6	2.05	2.80-17.38	0.18-2.06

[a]After subtraction of the Ir-Ir contribution: N = 6, R = 2.99 Å, $\Delta\sigma^2$ = 0.0033 $Å^2$, V_0 = -3.5 eV.

EXAFS measurements of the Rh/MgO system were performed on X-ray beam line I-5 at the SSRL at Stanford, U. S. A, as described previously.[8] Measurements on the Rh K edge (23220 eV) were done on the Rh/MgO system after in situ reduction at 473 and 673 K. As reference compounds Rh foil[11] and Rh_2O_3[16] were used. The Rh foil data shown previously[1,8] were used, but for Rh_2O_3 we used the data of a sample that had been checked with XRD, in order to exclude a mixture of oxides.[1] The first shell parameters for the reference compounds, and the ranges in k and r space used to extract the references from the EXAFS data, are given in Table 7.1.

7.3 Data Analysis and Results

Standard procedures[1,17] were used to extract the raw EXAFS data from the measured spectrum. The high quality of the raw data (see Figure 7.1) made it possible to reliably separate the contribution of the metal-support interface from the dominating metal-metal contribution. EXAFS data analysis was performed using the experimentally determined phase shifts and backscattering amplitudes for the various contributions. The

difference file technique was applied together with phase-corrected Fourier transforms. Our data analysis procedure has been extensively discussed elsewhere.[1-4]

In some cases coordination numbers (N_{unc}) obtained in the data analysis, had to be corrected for the difference in the absorber-scatterer distance between the reference shell and the shell to be analysed. This is due to the factor $\exp(-2R/\lambda)$ in the EXAFS formula.[18] The real coordination number N therefore is $N_{unc}/\exp(-2(R-R_{ref})/\lambda)$. λ was taken to be equal to 6 Å, which is a reasonable approximation above k = 3 $Å^{-1}$.[6,18]

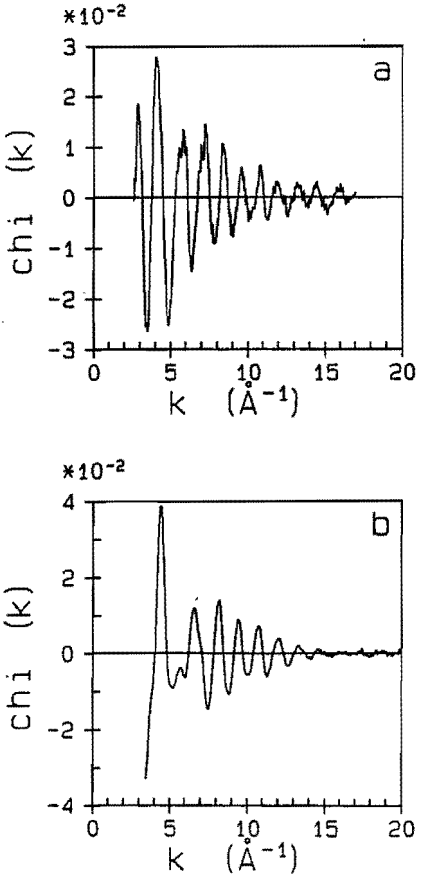

Figure 7.1. Raw EXAFS data of (a) reduced Ir/MgO; and (b) Rh/MgO reduced at 473 K.

7.3.1 Analysis of the Ir/MgO Data

EXAFS data analysis of the reduced Ir/MgO sample was performed on an isolated part of the spectrum. First, the data were Fourier transformed with a Pt-Pt phase correction (k^3-weighted, Δk = 2.57-13.62 $Å^{-1}$), and on the resulting spectrum in r space an inverse transform was applied with Δr = 1.42-3.30 Å. The Ir-Ir contribution, being the largest component in the EXAFS spectrum, was estimated in k space using only the data above k = 9

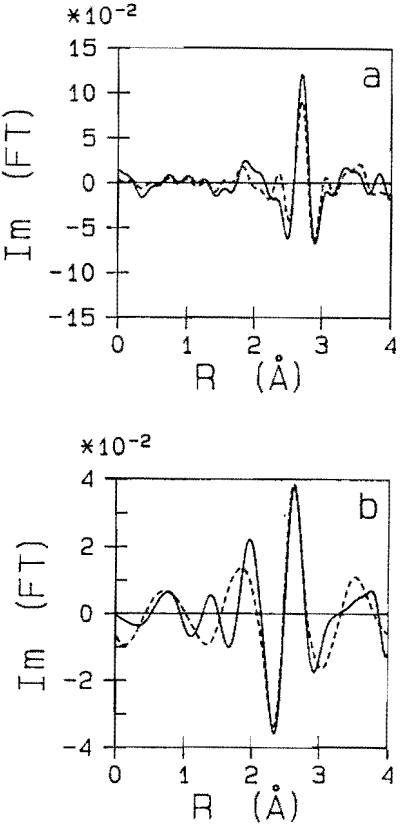

Figure 7.2. EXAFS analysis of the Ir/MgO sample. k^1-weighted Fourier transforms (Δk = 3.11-11.56 $Å^{-1}$) of (a) isolated first shell data (—), and best calculated Ir-Ir contribution (— —) (Pt-Pt phase-corrected); and (b) isolated first shell data minus best Ir-Ir contribution (—), and best calculated Ir-$O_{support}$ contribution (— —) (Pt-O phase-corrected).

$Å^{-1}$.[19] An EXAFS function was calculated with the first guess parameters. This Ir-Ir contribution was subtracted from the experimental data, and the resulting difference file was analysed for Ir-O contributions. This was done by selecting a calculated Ir-O contribution which agreed best with the difference file in a k^1-weighted, Pt-O phase-corrected Fourier transform.

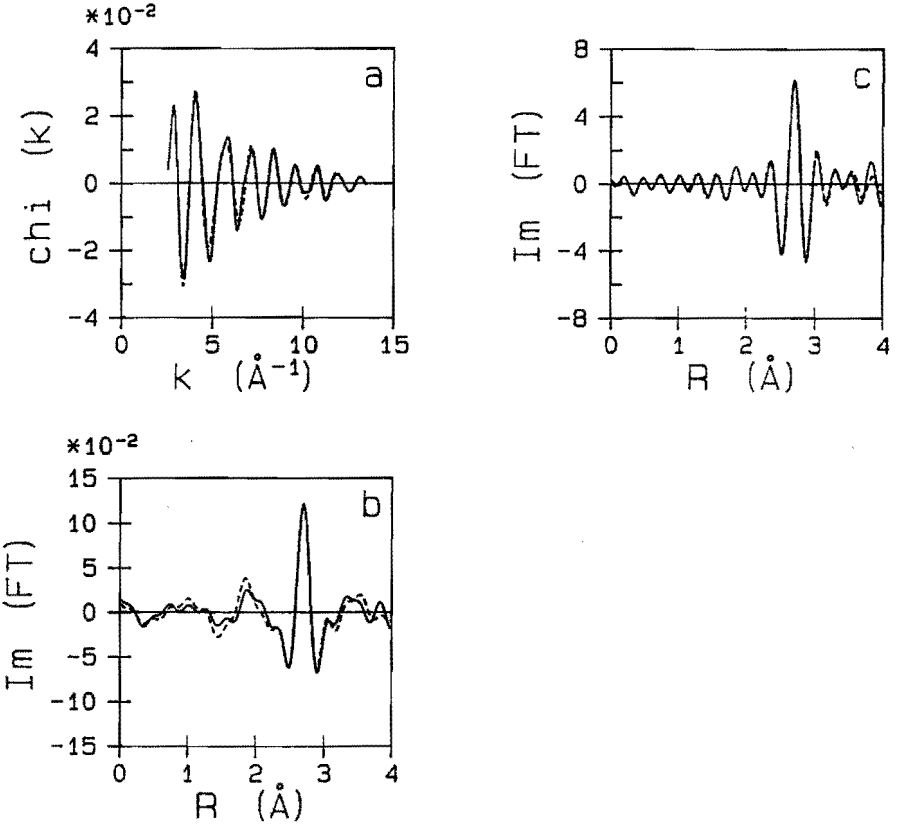

Figure 7.3. EXAFS analysis of the Ir/MgO sample. Isolated first shell data (—) and sum of the best calculated Ir-Ir and Ir-$O_{support}$ contributions (– –) (a) in k space; (b) after a k^1-weighted, Pt-Pt phase-corrected Fourier transform (Δk = 3.11-11.56 $Å^{-1}$); and (c) after a k^3-weighted, Pt-Pt phase-corrected Fourier transform over the same range as used in (b).

The calculated Ir-Ir and Ir-O contributions were added and compared with the experimental data after k^1- and k^3-weighted Fourier transforms. Checking both these Fourier transforms is essential, since in a k^1-weighted Fourier transform the Ir-O contribution is more prominent, and therefore a k^1-weighted Fourier transform is much more sensitive to the presence of Ir-O contributions, and thus to small deviations from the best coordination parameters for that contribution. In a k^3-weighted Fourier transform the metal-metal contribution is dominant, and information about the Ir-O contribution is lost. Better agreement could be obtained when a new Ir-Ir contribution was calculated based upon agreement with a k^1-weighted, Pt-Pt phase-corrected Fourier transform of the difference between experimental data and the calculated Ir-O contribution. After several cycles (alternately recalculating the Ir-Ir and Ir-O contributions) very good agreement was obtained in the region R = 2.2-3.2 Å, both after k^1- and k^3-weighted Fourier transforms. The best Ir-Ir and Ir-O contributions calculated with the technique described above, are shown in Figures 7.2a and 7.2b, respectively. Small deviations are still observed between R = 1.7 and 2.2 Å.

Further analysis showed that a small low-Z scatterer contribution was still present at R ~ 1.7 Å. Good results were obtained when this shell was attributed to an Ir-Mg interaction. However, it can not be excluded that this contribution is due to an Ir-C interaction.[5,6] The amplitude of this contribution is so small that a reliable assignment is difficult. Therefore it was not taken into account in the data analysis procedure.

Table 7.2. First shell structural parameters determined for the Ir/MgO sample.

Shell	N_{unc}	N	R (Å)	$\Delta\sigma^2$ (Å^2)
Ir-Ir	4.6	4.6	2.71	0.0013
Ir-$O_{support}$	1.8	2.1	2.54	0.0044

Accuracies: N ± 10-15% (Ir-Ir), ± 20-25% (Ir-O); R ± 0.02 Å (Ir-Ir), ± 0.05 Å (Ir-O); $\Delta\sigma^2$ ± 10-15% (Ir-Ir), ± 20-25% (Ir-O).

7.3.2 Analysis of the Rh/MgO Data

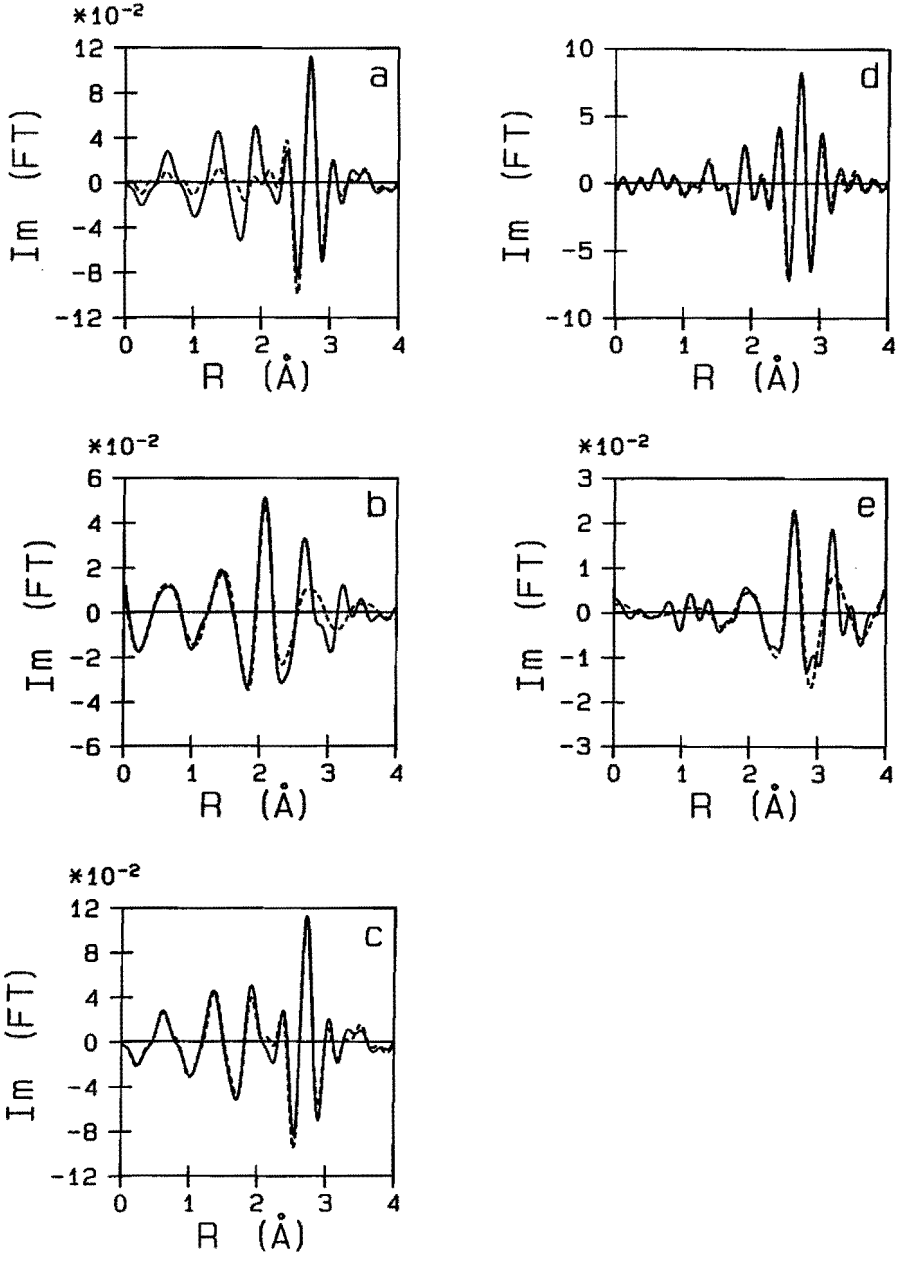

← **Figure 7.4.** EXAFS analysis of the Rh/MgO sample. k^1-weighted Fourier transforms (Δk = 4.02-12.38 Å^{-1}) of (a) isolated first shell data (—), and best calculated Rh-Rh contribution (— —) (Rh-Rh phase-corrected); (b) isolated first shell data minus best Rh-Rh contribution (—), and best calculated Rh-O_{oxide} contribution (— —) (Rh-O phase-corrected); (c) isolated first shell data (—), and sum of the best calculated Rh-Rh and Rh-O_{oxide} contributions (— —) (Rh-Rh phase-corrected); (d) as (c), but after a k^3-weighted Fourier transform; and (e) isolated first shell data minus best Rh-Rh and Rh-O_{oxide} contributions (—), and best calculated Rh-$O_{support}$ contribution (— —) (Rh-O phase-corrected).

Previously,[8] the analysis of two Rh/MgO samples has been described, one reduced at 473 K and one reduced at 673 K. For the sample reduced at 673 K a coordination number of N_{Rh-Rh} = 7.9 was determined. For a system in which the particles are already so large, it is not possible to detect the metal-support interaction with accuracy. Therefore it was decided not to reanalyse this system.

The results obtained for the sample reduced at 473 K showed that in that case much smaller metal particles had been obtained, and in this system the metal-support interaction might be reliably determined. This sample was reanalysed using as references the same Rh foil data as before, but different Rh_2O_3 data from a sample that had been checked with XRD.[1] Apart from the usual technique of fitting in k space, we also applied the difference file technique together with phase-corrected Fourier transforms.[1] Like for the Ir/MgO sample, the use of a k^1-weighted Fourier transform, which is more sensitive for the detection of low-Z scatterers, was essential to detect and subsequently to reliably separate the metal-support contribution from the dominating metal-metal contribution.

The first shell range of the data was isolated by a k^3-weighted Fourier transform (Δk = 3.43-13.77 Å^{-1}) and an inverse transform with Δr = 0-3.04 Å. In the same way as described for the Ir/MgO sample, the first guess parameters were determined for the Rh-Rh contribution, followed by the Rh-O contribution. Indeed, for this Rh-O contribution we found R ~ 2.0 Å, and just like before this contribution was assigned to an oxidic Rh-O bond.[8] Refinement was again done by alternately recalculating the different

contributions, and comparing them in a k^1-weighted Fourier transform with the appropriate difference file. The procedure followed is illustrated in Figures 7.4a and 7.4b for the best Rh-Rh and Rh-O contributions. A good agreement could be obtained between the experimental data and the sum of the Rh-Rh and Rh-O contributions in a k^3-weighted Fourier transform (see Figure 7.4d), but in the k^1-weighted Fourier transform a significant difference remained between the Rh-Rh and Rh-O peaks (see Figure 7.4c).

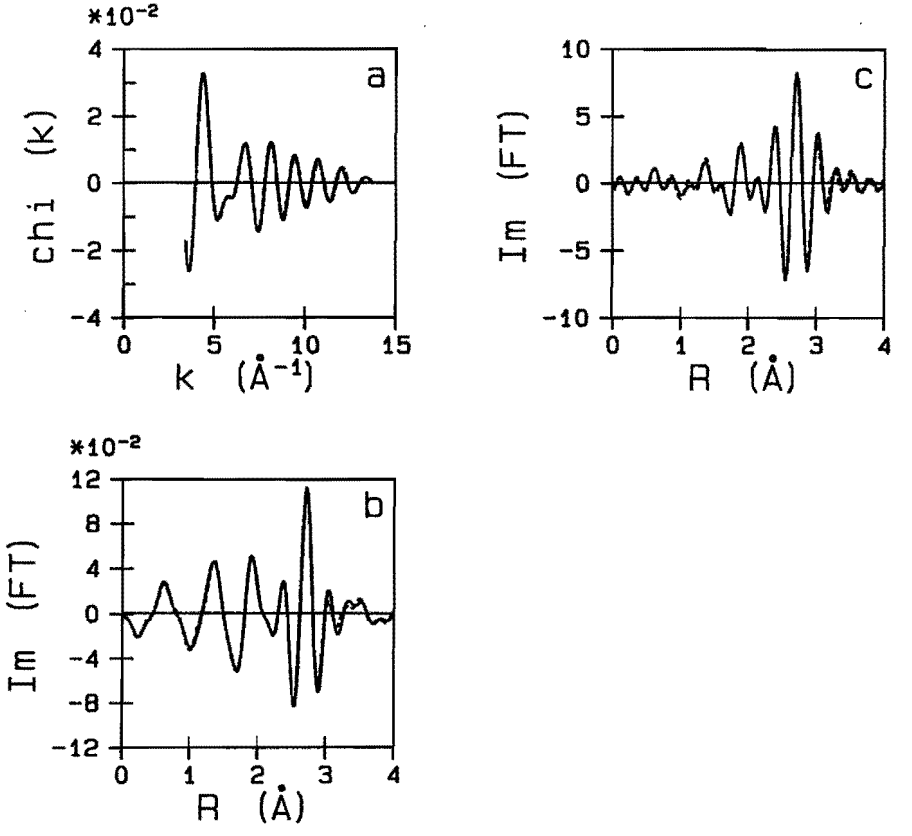

Figure 7.5. EXAFS analysis of the Rh/MgO sample. Isolated first shell data (—) and sum of the best calculated Rh-Rh, Rh-O_{oxide}, and Rh-$O_{support}$ contributions (— —) (a) in k space; (b) after a k^1-weighted, Rh-Rh phase-corrected Fourier transform (Δk = 4.02-12.38 $Å^{-1}$); and (c) after a k^3-weighted, Rh-Rh phase-corrected Fourier transform over the same range as used in (b).

Upon subtraction of the Rh-Rh and Rh-O contributions from the experimental data, a difference file was obtained which after a k^1-weighted, Rh-O phase-corrected Fourier transform still showed a peak at R ~ 2.7 Å, with a positively peaking imaginary part. Thus this additional contribution was attributed to a second Rh-O contribution (see Figure 7.4e). Because of the agreement of the coordination distance for this second contribution with those determined in other supported Rh systems,[1-4] we assign this contribution to a $Rh\text{-}O_{support}$ interaction, whereas we think the Rh-O contribution at R ~ 2.0 Å is caused by unreduced Rh. Refinement of the three contributions resulted in the coordination parameters given in Table 7.3. In this Table, also the coordination parameters determined previously[8] are given. The final results are shown in Figure 7.5.

Table 7.3. Coordination parameters for the first shells in Rh/MgO, reduced at 473 K.

Shell	EXAFS results				Previous results[8]		
	N_{unc}	N	R (Å)	$\Delta\sigma^2$ (Å^2)	N	R (Å)	$\Delta\sigma^2$ (Å^2)
Rh-Rh	3.6	3.6	2.69	0.0016	2.8	2.70	0.0008
$Rh\text{-}O_{oxide}$	2.1	2.1	2.06	0.0004	1.7	1.93	0.0059
$Rh\text{-}O_{support}$	1.5	1.9	2.68	0.0003	-	-	-

Accuracies: N ± 10-15% (Rh-Rh), ± 20-25% (Rh-O); R ± 0.02 Å (Rh-Rh), ± 0.05 Å (Rh-O); $\Delta\sigma^2$ ± 10-15% (Rh-Rh), ± 20-25% (Rh-O).

7.4 Discussion

7.4.1 Particle Size in the Reduced Systems

In the Ir/MgO system no contribution of oxidic Ir (i. e. an Ir-O contribution with a short Ir-O distance) can be observed. Therefore it can be assumed that almost all Ir is in the metallic state. Usually it is assumed that the small metal particles in reduced metal catalysts are three-dimensional in shape, e. g. half-spherical. Indeed, from the higher shells in

the spectrum in r space (see Figure 7.6a) it can be concluded that the metal particles are three-dimensional: both second and third metal-metal shells are present.[6] The average Ir metal particle size can be calculated easily on the basis of the Ir-Ir coordination number determined with EXAFS and assuming half-spherical particles with fcc structure:[1] d ~ 9 Å (approx. 10 atoms per particle).

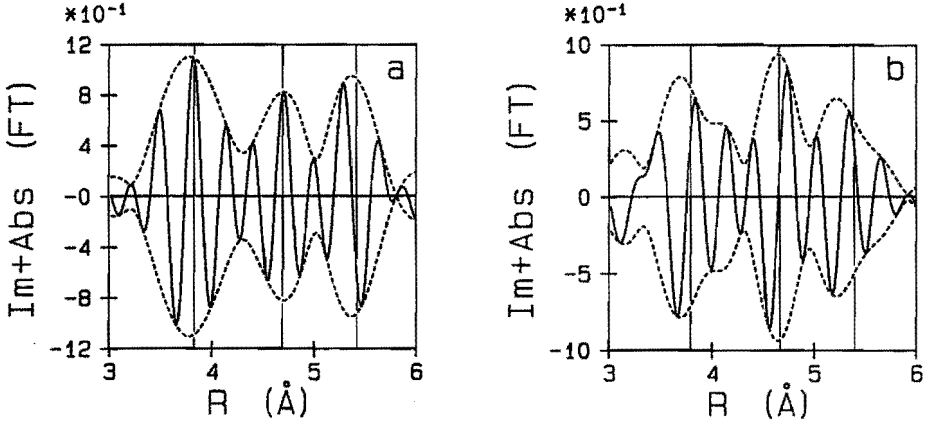

Figure 7.6. (a) k^3-weighted, Pt-Pt phase-corrected Fourier transform (Δk = 3.29-11.42 $Å^{-1}$) of the isolated higher shells in the Ir/MgO sample; shells isolated by a k^3-weighted, Pt-Pt phase-corrected Fourier transform with Δk = 2.57-13.62 $Å^{-1}$, and an inverse transform with Δr = 3.30-6.08 Å. (b) k^3-weighted, Rh-Rh phase-corrected Fourier transform (Δk = 3.29-11.42 $Å^{-1}$) of the isolated higher shells in the Rh/MgO sample; shells isolated by a k^3-weighted Fourier transform with Δk = 3.43-13.77 $Å^{-1}$, and an inverse transform with Δr = 2.92-5.52 Å. Positions of the second, third, and fourth metal-metal shells are indicated.

In the case of the Rh/MgO system, however, determination of the average metal particle size is not straightforward, because part of the Rh still seems to be in the oxidic state. This is strongly indicated by the Rh-O contribution at R = 2.06 Å, thus with a Rh-O distance almost equal to that in the Rh_2O_3 reference compound. In Figure 7.6b the k^3-weighted Fourier transform of the higher shells in the Rh/MgO sample is shown; when this is compared with the higher shells in Ir/MgO (see Figure 7.6a) it is immediately clear that in Rh/MgO extra contributions are present besides the higher metallic Rh-Rh shells: these must be higher oxidic Rh-Rh shells. We thus conclude that the Rh/MgO system is only partly reduced. Therefore the coordination numbers applying to the reduced phase (viz. Rh-Rh and $Rh\text{-}O_{support}$) must be corrected, because in the EXAFS data analysis only coordination numbers averaged over all Rh atoms in the sample (i. e. those in the reduced phase as well as those in the oxidic phase) can be determined. In the correction procedure[1,4,20] it is assumed that in the oxidic phase the real coordination number is $N_{Rh\text{-}O} = 6$. From the EXAFS data analysis we obtained $N_{Rh\text{-}O} = 2.1$, thus 2.1/6 = 35% of the Rh atoms is in the oxidic phase. The coordination numbers of the Rh atoms in the reduced phase (65% of the total number of Rh atoms) must then be corrected with a factor 1/0.65. Thus in the reduced phase we obtain $N_{Rh\text{-}Rh} = 5.5$, and $N_{Rh\text{-}O(support)} = 2.9$. On the basis of this Rh-Rh coordination number, and assuming half-spherical fcc metal particles, the average Rh metal particle size is d ~ 12 Å (approx. 18 atoms per particle).

7.4.2 The Metal-Support Interface

Long metal-support bonds (R ~ 2.5-2.8 Å) had already been detected for reduced $Rh/\gamma\text{-}Al_2O_3$,[1,2] Rh/TiO_2,[3,4] and $Ir/\gamma\text{-}Al_2O_3$.[5,6] These bonds may be attributed to $M^0\text{-}OH^-$ interactions on the basis of theoretical calculations,[7] to electronic changes in the supported metal particles due to adsorbed hydrogen, or to adsorbed hydrogen in the metal-support interface. Now we have also found the same type of metal-support oxygen bonds for Ir/MgO and Rh/MgO.

The metal particles in the supported metal catalysts usually are three-dimensional in shape. Thus only a fraction of the metal atoms are present in the metal-support interface. Since the EXAFS coordination parameters are averaged over all metal atoms in the sample, the metal-

support oxygen coordination number determined in a straightforward EXAFS analysis has to be corrected in order to yield the metal-oxygen coordination number for the metal atoms in the interface only. For the case of reduced Rh/γ-Al_2O_3, model calculations were performed assuming half-spherical particles.[1] On the basis of the coordination numbers determined for the Rh-Rh and Rh-$O_{support}$ interactions, the Rh-O coordination number for the Rh atoms in the metal-support interface could then be determined. Using this type of calculations we here determined a metal-oxygen coordination number of $N_{Ir-O} \sim 3.5$ for the Ir/MgO catalyst, and $N_{Rh-O} \sim 4.5$ for the Rh/MgO catalyst (see Figure 7.7). Assuming that the same type of epitaxy is present in the Ir/MgO and Rh/MgO systems, and taking the accuracy into account, the metal-MgO interface can be modelled with a metal-oxygen coordination number of four.

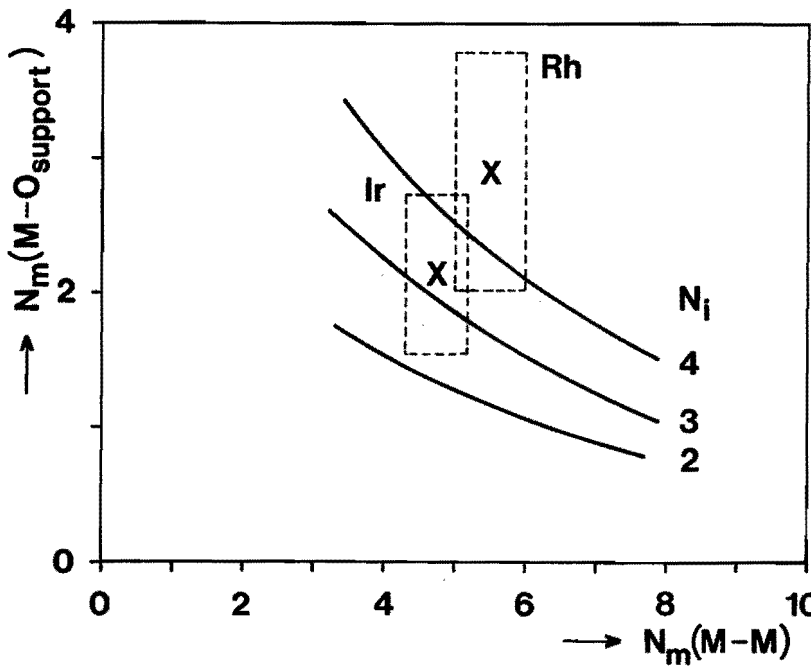

Figure 7.7. The measured metal-support coordination number $N_m(M\text{-}O_{support})$ versus the measured metal-metal coordination number $N_m(M\text{-}M)$. The lines indicated by A, B, and C reflect the situations for which the metal-support interface coordination number $N_i(M\text{-}O_{support})$ is equal to 4, 3, and 2, respectively.[1] X = data point, with an accuracy within the (— —) bounds.

Using a metal-oxygen coordination number of four in the interface, two models can be devised for the metal-support epitaxy, as shown in Figure 7.8. Assuming that the support surface has no hydroxyl groups in contact with the metal particles, the metal atoms are positioned directly above the Mg atoms in the (100) surface (Figure 7.8a). The small contribution at R ~ 1.7 Å mentioned in Section 7.3.1 can then be attributed to an Ir-Mg interaction. With hydroxyl groups present in the metal-support interface, a similar arrangement is possible (see Figure 7.8b) in which each metal atom in the interface rests on four OH^- groups which are positioned on top of the Mg atoms in the (100) surface. In this case, at R ~ 1.7 Å an Ir-C contribution may be present.

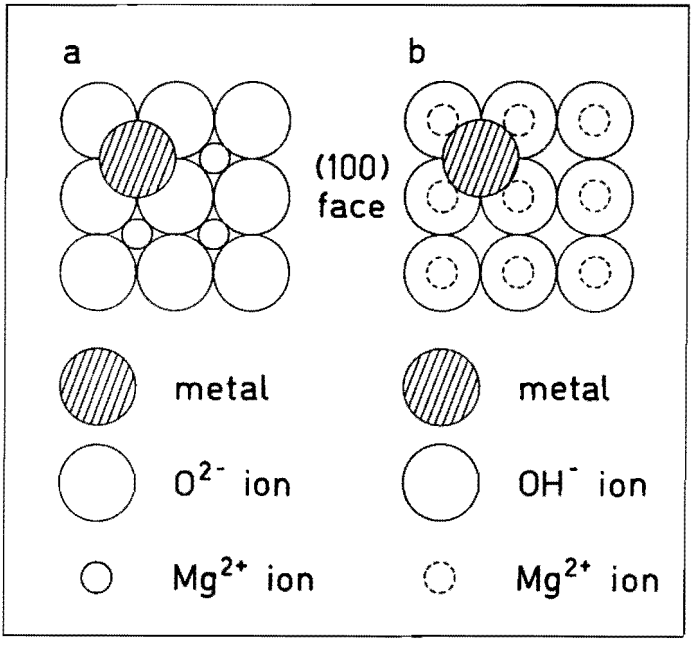

Figure 7.8. Illustration of the proposed site for the metal atoms in the metal-MgO (100) interface. (a) Dehydroxylated (100) face; and (b) hydroxylated (100) face.

Also for the Rh/MgO system, the Rh-$O_{support}$ coordination number agrees well with a Rh-MgO interface in which the Rh atoms are fourfold coordinated by surface oxygen.

7.5 Conclusions

With EXAFS it has proved possible to detect the metal-support interface in both reduced Ir/MgO and Rh/MgO catalyst systems. Even in the case of Rh/MgO, which was not fully reduced, the presence of an oxidic Rh-O contribution did not severely hamper the analysis of the metal-support interface.

Metal-support oxygen bonds with a M-O bond length of R$\sim$ 2.6 Å were detected, just like for supported Rh/γ-Al_2O_3, Rh/TiO_2, and Ir/γ-Al_2O_3. Thus it can be concluded that the metal-support interaction on MgO does not differ significantly from the interaction with γ-Al_2O_3 and TiO_2.

Assuming that the metal particles are half-spherical in shape, a metal-support interface can be modelled in which the interface metal atoms are fourfold coordinated to support oxygen. This type of coordination can very well be visualized on the most frequently occurring (100) face of MgO.

7.6 References

(1) J. B. A. D. Van Zon, D. C. Koningsberger, H. F. J. Van 't Blik, and D. E. Sayers, *J. Chem. Phys.* **1985**, *82*, 5742.

(2) D. C. Koningsberger, J. B. A. D. Van Zon, H. F. J. Van 't Blik, G. J. Visser, R. Prins, A. N. Mansour, D. E. Sayers, D. R. Short, and J. R. Katzer, *J. Phys. Chem.* **1985**, *89*, 4075.

(3) D. C. Koningsberger, J. H. A. Martens, R. Prins, D. R. Short, and D. E. Sayers, *J. Phys. Chem.* **1986**, *90*, 3047.

(4) J. H. A. Martens, R. Prins, H. Zandbergen, and D. C. Koningsberger, *J. Phys. Chem.* **1988**, *92*, 1903.

(5) F. B. M. Van Zon, G. J. Visser, and D. C. Koningsberger, *Proc. 9th Int. Congress on Catalysis* (Calgary, 1988); M. J. Phillips, and M. Ternan, Eds.; Chemical Institute of Canada: Ottawa, 1988; Vol. III, p 1386.

(6) F. B. M. Van Zon, and D. C. Koningsberger, *J. Chem. Phys.* submitted.

(7) J. H. A. Martens, R. A. Van Santen, D. C. Koningsberger, and R. Prins, *Catalysis Lett.* submitted.

(8) R. J. Emrich, A. N. Mansour, D. E. Sayers, S. T. McMillan, and J. R. Katzer, *J. Phys. Chem.* **1985**, *89*, 4261.

(9) V. C. Henrich, *Rep. Progr. Phys.* **1985**, *48*, 1481.

(10) F. B. M. Van Zon, A. D. Van Langeveld, J. Van Grondelle, and D. C. Koningsberger, to be published.

(11) R. W. G. Wyckoff, *Crystal Structures*, 2nd ed.; Wiley: New York, 1963; Vol. I, p 10.

(12) M. Trömel, and E. Lupprich, *Z. Anorg. Chem* **1975**, *414*, 160.

(13) P. Esslinger, and K. Schubert, *Z. Metallk.* **1957**, *48*, 126.

(14) B. K. Teo, and P. A. Lee, *J. Am. Chem. Soc.* **1979**, *101*, 2815.

(15) B. Lengeler, *J. de Phys. C8* **1986**, *47*, 75.

(16) J. M. Coey, *Acta Cryst. B* **1970**, *26*, 1876.

(17) J. W. Cook, and D. E. Sayers, *J. Appl. Phys.* **1981**, *52*, 5024.

(18) E. A. Stern, B. A. Bunker, and S. M. Heald, *Phys. Rev. B* **1980**, *21*, 5521.

(19) B. J. Kip, F. B. M. Duivenvoorden, D. C. Koningsberger, and R. Prins, *J. Catal.* **1987**, *105*, 26.

(20) P. W. J. G. Wijnen, F. B. M. Van Zon, and D. C. Koningsberger, *J. Catal.* accepted.

Chapter Eight

Determination of the Metal Particle Size in Rh, Ir, and Pt Catalysts by Hydrogen Chemisorption and EXAFS

8.1 Introduction

Selective chemisorption of gaseous molecules, especially hydrogen, has been extensively used to estimate the degree of dispersion of group VIII metal catalysts.[1-27] Chemisorption methods are of special importance for highly dispersed metal catalysts, since it is often difficult to establish the degree of dispersion by other techniques such as X-ray diffraction or electron microscopy measurements.[1] Moreover, the chemisorption technique is relatively quick and cheap. Hydrogen chemisorption data can be directly used to compare dispersions of a metal in different samples in a relative way. However, when it is required to calculate metal surface areas in an absolute way the hydrogen-to-metal stoichiometry must be known. Usually a H/M stoichiometry of one has been used. Surface science studies proved that a maximum of one hydrogen atom per metal atom could be chemisorbed on the (111) faces of fcc metal single crystals.[8] Assuming that the surface of metal particles larger than ~ 2 nm consists largely of (111) faces, it is clear that the empirical assumption of a H/M = 1 stoichiometry was rather successful in many studies.

However, as early as 1960 data began to appear in the literature about stoichiometries exceeding one. H/Pt = 1.5-1.65 has been measured for Pt/Al_2O_3 catalysts[9,10] and H/Pt = 1.3-1.6 has been quoted for Pt/SiO_2 catalysts,[11,12] while a value of H/Pt = 2 has been observed by Rabo et al. for Pt deposited on a zeolite.[13] Recently, Sato[14] has described a Pt/TiO_2 system made by photo impregnation of hexachloroplatinic acid with H/Pt = 2.5, while Frennet and Wells[15] have reported H/Pt values around 1.2 for 6.3 wt% Pt/SiO_2. Wanke and Dougharty[16] have reported the adsorption of more than one hydrogen atom per surface rhodium atom for Rh/Al_2O_3 catalysts. For supported Ir catalysts even values near 3.0 have been measured. McVicker et al.[17] have found an upper limit of two adsorbed

hydrogen atoms per Ir atom for Ir/Al_2O_3 systems, only using the strongly bonded hydrogen. When the total amount of adsorbed hydrogen is taken into account, they have reported H/Ir values exceeding two. Krishnamurthy et al.[18] have shown that 0.48 wt% Ir/Al_2O_3 adsorbs up to 2.72 hydrogen atoms per iridium atom, part of which is weakly bound (H/Ir = 0.28).

In literature, several explanations have been given for H/M values exceeding unity. Often a distinction has been made between reversibly and irreversibly adsorbed hydrogen, and in many cases only the irreversibly adsorbed hydrogen has been assumed to be important for the determination of the metal surface area.[17-22] Several authors have ascribed the high H/M values to hydrogen spillover to the support,[14,28-30] or to an increased hydrogen-to-metal stoichiometry for metal atoms situated at the corners and edges of the small metal particles.[16-18] Another explanation given for high H/M values has been the positioning of part of the hydrogen under the surface of the metal particle.[31-33]

In our laboratory, Pt, Rh, and Ir catalysts supported on Al_2O_3, SiO_2, and TiO_2 have been studied in the hydrogenation of carbon monoxide to hydrocarbons and oxygenated products. Hydrogen chemisorption has been used to characterize the highly dispersed supported metal catalysts and H/M values exceeding unity have been obtained for supported Rh and Pt catalysts[34-36] and H/M values even exceeding 2.0 have been observed for supported Ir systems.[37] Because of a lack of information on the hydrogen-to-metal stoichiometry for very small metal particles, it was impossible to calculate the dispersion from the chemisorption results. Therefore, another technique has been used to obtain information about the particle size: Extended X-ray Absorption Fine Structure (EXAFS). With this technique, it is possible to determine the metal coordination number of a metal atom (N) in a particle and thus to get information about the particle size.[36,38-43]

In this Chapter, the results of hydrogen chemisorption and EXAFS measurements are compared for Pt, Rh, and Ir catalysts supported on SiO_2 and Al_2O_3. Several hypotheses for the observed high H/M values are discussed and it will be shown that multiple adsorption of hydrogen on surface metal atoms is the only one which can explain all experimental observations.

8.2 Experimental

8.2.1 Preparation of the Catalysts

Pt, Ir, and Rh catalysts were prepared from $RhCl_3$ and $IrCl_3$ via the incipient wetness technique,[34,35,37] from $Pt(NH_3)_4(OH)_2$ and $Rh(NO_3)_3$ via the ion exchange technique,[36,44] and from $IrCl_3$ via the urea method.[37,45] The following supports were used: γ-Al_2O_3 from Ketjen (000-1.5E, surface area 200 m^2/g, pore volume 0.60 ml/g), γ-Al_2O_3 obtained by heating boehmite (Martinswerk, GmbH, surface area 150 m^2/g, pore volume 0.65 ml/g), and SiO_2 (Grace, S.D. 2-324.382, surface area 290 m^2/g, pore volume 1.2 ml/g). The metal precursors ($IrCl_3 \cdot xH_2O$, $RhCl_3 \cdot xH_2O$ and $Pt(NH_3)_4(OH)_2$) were supplied by Drijfhout, Amsterdam. All catalysts were dried in air at 395 K for 16 h (heating rate 2 K/min).

8.2.2 Hydrogen Chemisorption Measurements

Volumetric hydrogen chemisorption measurements were performed in a conventional glass system at 298 K. Hydrogen was purified by passing through a palladium diffusion cell. Before measuring the H_2 chemisorption isotherm the dried catalysts were reduced for 1 h (heating rate 5-8 K/min) and evacuated (10^{-2} Pa) for 30 min. The reduction temperatures, at which evacuation was also performed, are presented in Table 8.1. After hydrogen admission at 473 K, $P(H_2)$ = 93 kPa, desorption isotherms were measured at room temperature. The total amount of chemisorbed H atoms was obtained by extrapolating the linear high pressure part (20 kPa < P < 80 kPa) of the isotherm to zero pressure.[2] Correction for chemisorption on the bare support was not necessary, because the extrapolated values of the desorption isotherms for the bare supports, pretreated in the same way as the catalysts, were zero within the uncertainty of the measurements.

8.2.3 EXAFS Measurements

Catalyst samples were measured at 77 K as thin self-supporting wafers in H_2, after in situ reduction. The Rh and Pt measurements were performed on beam line I-5 at the Stanford Synchrotron Radiation Laboratory (SSRL) in Stanford, U. S. A. (3 GeV, 40-80 mA) at the Rh K edge (23220 eV) and Pt L_{III} edge (11564 eV), respectively. The data were

analysed with the use of reference compounds.[38-40] In the case of the Rh catalysts, Rh foil and Rh_2O_3 were used. For the Pt data, Pt foil and $Na_2Pt(OH)_6$ were used.[36] The Ir measurements were done on Wiggler station 9.2 at the Synchrotron Radiation Source (SRS) in Daresbury, U. K. (2 GeV, 80-250 mA) at the Ir L_{III} edge (11215 eV). As reference compounds Pt foil and $Na_2Pt(OH)_6$ were used. Both theoretically[46] and experimentally[47] the choice of Pt references for the analysis of Ir data can be justified.

The results of the analysis of the Rh data have been published before,[38-40] as well as the results for the Pt catalyst with H/M = 1.14.[46]

The metal-metal coordination parameters of the Ir and other Pt catalysts were determined as follows. A k^3-weighted Fourier transform (Δk = 2.7-15 $Å^{-1}$) was applied to the EXAFS data. (Above k ~ 15 $Å^{-1}$, the signal-to-noise ratio is rather low for the most disperse systems, and therefore the EXAFS data are not used beyond this limit.) In the resulting spectrum in r space, the peak representing the first M-M shell (but also including $M\text{-}O_{support}$ contributions) was back transformed (Δr = 1.9-3.5 Å) to k space. In the resulting spectrum the $M\text{-}O_{support}$ contributions are only significant below k = 8 $Å^{-1}$, because a low-Z element like oxygen does not scatter very much at high k values. Therefore, the M-M coordination parameters were determined by fitting the data between k = 7.9 and 13.8 $Å^{-1}$, in such a way that a good agreement was obtained in k and in r space.

8.3 Results

8.3.1 Hydrogen Chemisorption Measurements

Since hydrogen chemisorption can be performed in many, slightly different ways, with often (slightly) different results, it is imperative to start with a description of our own hydrogen chemisorption procedure. After in situ reduction and evacuation a certain amount of hydrogen is admitted at 473 K, as hydrogen adsorption at room temperature is a slow process. Subsequently, the sample is cooled to 298 K under hydrogen and the amount of adsorbed hydrogen is measured ($P_{equilibrium}$ ~ 80 kPa). Thereafter a desorption isotherm is measured at room temperature by

lowering the pressure step by step ($\Delta P \sim 13$ kPa per step), while measuring the amount of desorbed hydrogen. The total amount of chemisorbed hydrogen is obtained by extrapolation of the linear high pressure part (20 kPa $< P <$ 80 kPa) in the isotherm to zero pressure. The H/M values obtained in this way are slightly higher than those obtained by admission at room temperature and waiting for 3 h. As an example, H/Ir values of 2.68 and 2.49 were obtained for a 0.81 wt% Ir/Al_2O_3 catalyst, after admission of H_2 at 473 K and 298 K, respectively. The H/M values obtained for our catalysts are presented in Table 8.1 (and Table 8.2).

Other, often lower, hydrogen pressures have been used in the literature. According to Crucq et al. the hydrogen adsorption isotherms of supported Pt[49] and Rh[50] catalysts are Temkin-like (showing a linear relation between log (P) and H/M over a wide pressure range) due to a strongly decreasing heat of adsorption with coverage. Therefore they recommended the measurement of a single adsorption point at $P > 13$ kPa at room temperature, to obtain the amount of adsorbed hydrogen close to monolayer coverage. However, our measurements were always extrapolated to zero pressure. In that case, the intercept is independent of the dead volume of the adsorption apparatus.[16] Consequently, it is possible to use an arbitrarily chosen dead volume or to ignore the dead volume entirely, since the zero-pressure condition implies no residual adsorbate in the gas phase, and there is thus no necessity for experimental determination of dead volumes.

Several authors have reported increasing H/M values with decreasing temperature. For instance Boronin et al.[12] reported that for Pt catalysts H/M increased to a value of 2 as the temperature of chemisorption was lowered to 77 K. Most likely different metals will have different H/M temperature dependencies and there is no a priori reason why all metals should have the same H/M stoichiometry at a particular temperature. Furthermore, as also shown in this paper, the H/M stoichiometry is dependent on the metal particle size. For these reasons, and also to measure the H/M stoichiometries under identical conditions, a fixed chemisorption temperature is used for all three metals under study. For experimental reasons the desorption isotherms have been measured at 298 K. As a consequence, it should be kept in mind that the resulting calibration of the H/M values is only valid for chemisorption at 298 K.

Table 8.1. Hydrogen chemisorption results for supported Rh, Ir, and Pt catalysts.

Catalyst[a,b]	Reduction Temp. (K)	H/M[c]
4.2% Pt/Al_2O_3, k, A	1100	0.23
4.2% Pt/Al_2O_3, k, A	1058	0.43
4.2% Pt/Al_2O_3, k, A	573	0.77
1.06% Pt/Al_2O_3, k, A	673	1.14
2.00% Rh/Al_2O_3, b, B	673	1.20
2.4% Rh/Al_2O_3, b, A	473	1.20
1.04% Rh/Al_2O_3, k, B	773	1.65
0.47% Rh/Al_2O_3, k, B	773	1.70
0.57% Rh/Al_2O_3, b, B	573	1.98
7.0% Ir/SiO_2, g, B	773	0.43
1.5% Ir/SiO_2, g, B	773	0.83
5.3% Ir/SiO_2, g, C	773	1.24
1.5% Ir/SiO_2, g, C	773	1.70
2.4% Ir/Al_2O_3, k, B	773	1.96
1.5% Ir/Al_2O_3, k, B	773	2.40
0.8% Ir/Al_2O_3, k, B	773	2.68

[a]Support: γ-Al_2O_3 Ketjen (k), γ-Al_2O_3 boehmite (b), SiO_2 Grace (g).

[b]Preparation method: ion exchange (A), incipient wetness (B), urea method (C).

[c]Experimental error in H/M: ± 5%.

No distinction has been made between reversibly and irreversibly adsorbed hydrogen, as is often done in the literature.[17-22] All chemisorption is reversible and one can only distinguish between weakly and strongly adsorbed hydrogen. The only difference between them is the heat of adsorption, which is a function of coverage. Goodwin et al.[21,22] have shown that hydrogen which is weakly adsorbed on supported Ru catalysts is nevertheless associated with the metal, and not with the support. De

Menorval and Fraissard,[51] and Sanz and Rojo[52] have shown that the NMR chemical shifts of hydrogen atoms adsorbed on Pt/Al_2O_3 and Rh/TiO_2 catalysts, respectively, decrease with increasing hydrogen pressure, even at $P > 40$ kPa. This proves that even at these pressures additional hydrogen is still adsorbed on the metal if the hydrogen pressure is increased. Subtraction of the amount of 'reversibly' adsorbed hydrogen therefore does not result in a correction for the adsorption on the support, but instead to the elimination of part of the hydrogen adsorbed on the metal.

Moreover, the amount of weakly adsorbed hydrogen is difficult to determine objectively, as it depends on the apparatus, pump, and evacuation time used.[49] To obtain an idea of the amount of hydrogen which is relatively weakly bound to the metal under the conditions used, measurements were done for the 0.81 wt% Ir/Al_2O_3 catalyst. After 20 minutes of pumping at 298 K, 23% of the original amount of adsorbed hydrogen could be readsorbed ($H/Ir_{strong} = 2.07$, $H/Ir_{weak} = 0.61$). It is obvious that even if only the strongly bonded hydrogen was considered, our H/M values would still exceed unity in many cases.

8.3.2 EXAFS Measurements

In order to obtain the metal particle size of our highly dispersed catalysts, the EXAFS technique was used. Details about the EXAFS data analysis of some of the catalysts have been reported earlier.[36,38-40,47,48] The quality of the fit obtained for the first metal-metal shell in the EXAFS data was always good. As an example the fits in r space and in k space are shown in Figure 8.1 for the 4.2 wt% Pt/Al_2O_3 sample with an H/M value of 0.77. The fit has been obtained between k = 7.9 (below this limit Pt-O contributions are present) and 13.8 $Å^{-1}$. In k space a clear deviation is observed for $k < 7$ $Å^{-1}$ between the Pt-Pt spectrum calculated on the basis of the fit parameters, and the experimental spectrum. This deviation is caused by Pt-O contributions which cannot be neglected in this region.[36]

The average metal-metal coordination numbers N obtained from the EXAFS analysis are presented in Table 8.2 and Figure 8.2. As can be seen in Tables 8.1 and 8.2, two supports and a variety of preparation methods

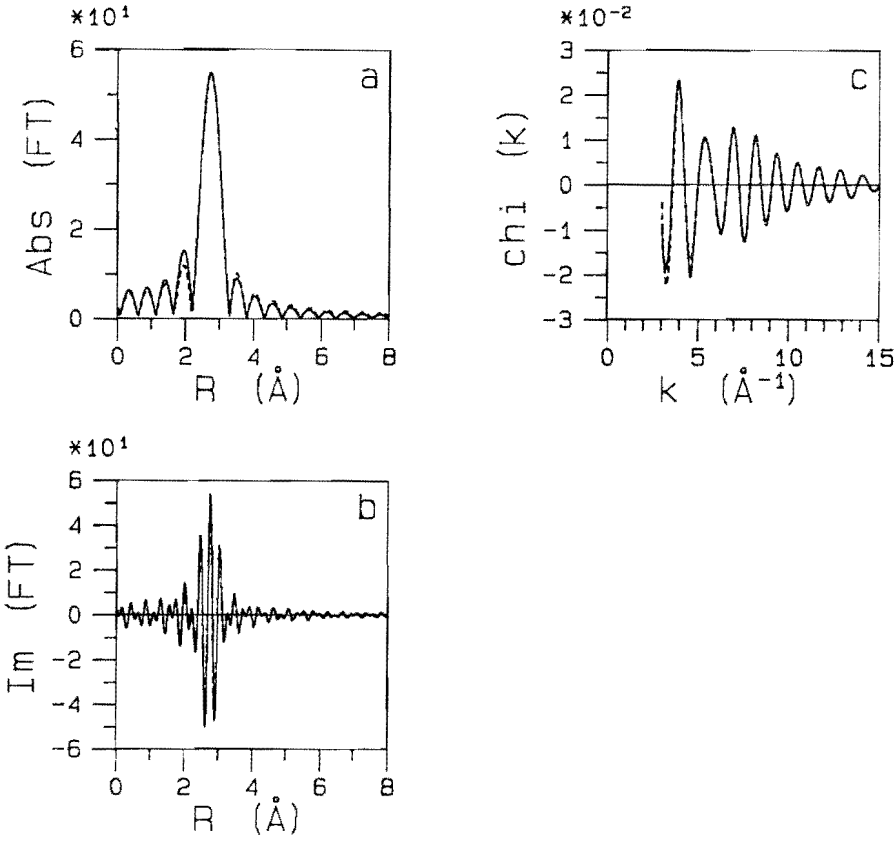

Figure 8.1. EXAFS of the back transformed first Pt-Pt shell (+ Pt-O shell) in 4.2 wt% Pt/Al_2O_3 with H/Pt = 0.77 (—), and calculated Pt-Pt contribution (— —) (a) amplitude of the k^3-weighted Fourier transform (Δk = 7.9-13.8 $Å^{-1}$); (b) imaginary part; and (c) fit in k space. The Pt-Pt spectrum has been calculated on the basis of the fit for $7.9 < k < 13.8$ $Å^{-1}$, with N = 7.6, R = 2.75 Å, and $\Delta\sigma^2 = 0.0035$ $Å^2$ (with respect to Pt foil).

have been used. However, if any of these parameters has an effect on the hydrogen-to-metal stoichiometry, it can only be a minor one since the metal-metal coordination number versus H/M relationship can be described by a single straight line for each metal. Rather unexpectedly a large difference is observed between the three metals. This difference is very marked and experimentally significant above H/M = 1, but still exists at lower H/M values. For a given particle size (equal metal-metal coordination number) the H/M values increase in the sequence H/Pt < H/Rh < H/Ir.

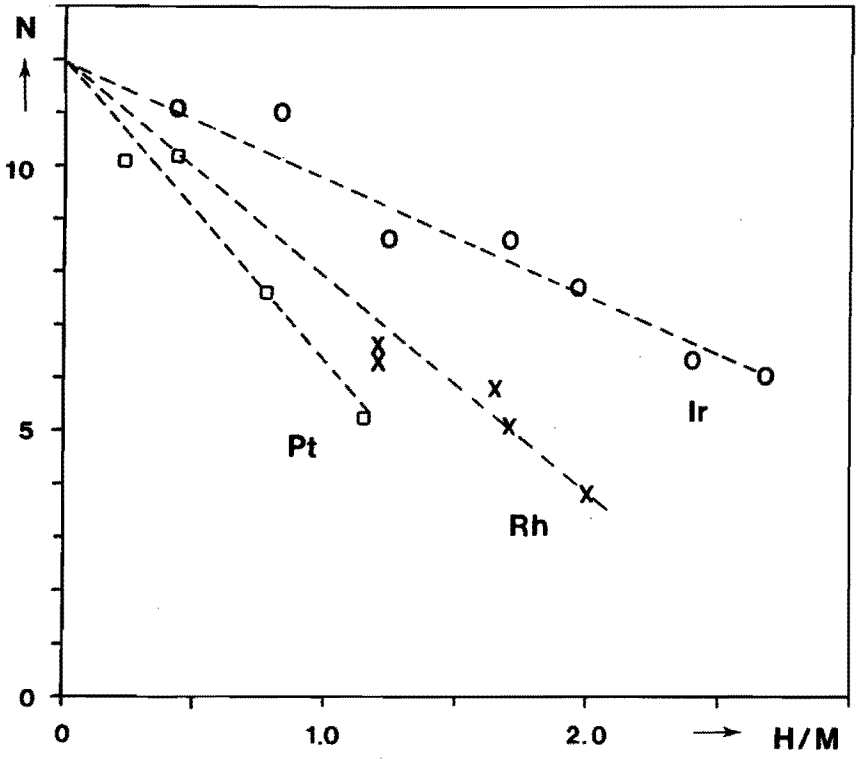

Figure 8.2. Metal-metal coordination number N from EXAFS versus H/M from chemisorption, for Pt (□), Rh (x), and Ir (o).

Table 8.2. EXAFS results for supported Rh, Ir, and Pt catalysts.

Catalyst	H/M[a]	N[b]	R (Å)[c]	$\Delta\sigma^2$ (Å)^2 [d]
4.2% Pt/Al_2O_3	0.23	10.0	2.75	0.0030
4.2% Pt/Al_2O_3	0.43	10.2	2.75	0.0033
4.2% Pt/Al_2O_3	0.77	7.6	2.75	0.0035
1.06% Pt/Al_2O_3	1.14	5.2	2.76	0.0033
2.00% Rh/Al_2O_3	1.20	6.6	2.69	0.0032
2.4% Rh/Al_2O_3	1.20	6.3	2.69	0.0053
1.04% Rh/Al_2O_3	1.65	5.8	2.68	0.0050
0.47% Rh/Al_2O_3	1.70	5.1	2.68	0.0051
0.57% Rh/Al_2O_3	1.98	3.8	2.68	0.0050
7.0% Ir/SiO_2	0.43	11.1	2.71	-0.0019
1.5% Ir/SiO_2	0.83	11.0	2.70	-0.0020
5.3% Ir/SiO_2	1.24	8.6	2.70	-0.0006
1.5% Ir/SiO_2	1.70	8.6	2.70	-0.0006
2.4% Ir/Al_2O_3	1.96	7.7	2.70	-0.0007
1.5% Ir/Al_2O_3	2.40	7.3	2.70	-0.0006
0.8% Ir/Al_2O_3	2.68	6.0	2.70	0.0005

[a]Experimental error in H/M: ± 5%.

[b]Experimental error in N: ± 10%.

[c]Experimental error in R: ± 1%.

[d]With respect to Pt foil at 77 K (Pt catalysts), Rh foil at 77 K (Rh catalysts), and Pt foil at 298 K (Ir catalysts); experimental error in $\Delta\sigma^2$: ± 10%.

8.3.3 Model Calculations

To investigate if the high H/M values can be explained by adsorption at the surface metal atoms, model calculations were performed. A computer programme was made to determine the area available for chemisorption around a supported small metal particle. In the spirit of Wynblatt and Gjostein[53] the shape of the metal particle was calculated as a function of the

relative magnitude of the metal-metal and metal-support interaction energy by minimizing the total energy. We assumed the support to consist of a flat (111) layer of oxygen anions, the size of which was taken equal to that of the metal atoms. The metal atoms were assumed to be fcc packed, and to fit epitaxially on the support surface. The shape of a metal particle with n+1 atoms was obtained from that of a particle with n atoms by putting the extra metal atom at the position of minimum energy. Such calculations were carried out over a whole range of α-values, with α being the ratio of the metal atom-oxygen anion interaction E(M-O^{2-}) and the metal atom-metal atom interaction E(M-M).

Table 8.3. Results of the computer calculations on small metal particles.

α[a]	0.5				
Number of atoms per particle	4	10	30	100	800
Empty positions[b]:					
1 neighbour	9	15	16	19	36
2 ,,	9	8	21	35	81
3 ,,	0	5	10	33	125
4 ,,	0	2	4	15	113
5 ,,	0	0	2	2	15
Dispersion	1.0	1.0	0.80	0.62	0.36
H/M[c]	4.5	3.0	1.8	1.0	0.46
H/M[d]	2.3	1.5	1.2	0.85	0.42
N[e]	3.0	4.8	6.8	8.5	10.2
d[f]	2.1	3.3	4.4	7.0	12.9

Table 8.3. (continued)

α[a]	2.0				
Number of atoms per particle	4	10	30	100	800
Empty positions[b]:					
1 neighbour	11	13	14	14	39
2 ,,	6	10	21	41	85
3 ,,	1	4	10	23	129
4 ,,	0	1	6	21	92
5 ,,	0	1	0	0	18
Dispersion	1.0	1.0	0.80	0.60	0.35
H/M[c]	4.5	2.9	1.7	1.0	0.45
H/M[d]	1.8	1.6	1.2	0.85	0.41
N[e]	2.5	4.2	6.5	8.3	10.2
d[f]	2.8	3.7	5.1	7.4	14.0

[a] $\alpha = E(M\text{-}O^{2-})/ E(M\text{-}M)$.

[b] Vacant fcc positions around the metal particle which have at least one metal neighbour, and which can be occupied by H atoms.

[c] Assuming that all vacant fcc positions around the particle are filled by hydrogen.

[d] Assuming that only vacant positions with more than one metal neighbour are filled by hydrogen.

[e] Metal-metal coordination number.

[f] Diameter of the particle expressed in metal atom diameters.

To obtain an estimate of the number of hydrogen atoms that can be placed around such a metal particle, it was assumed that the hydrogen atoms will occupy the free fcc positions around the metal particle and that only one hydrogen atom per vacant fcc position is allowed. Although

diffraction results for metal hydride complexes point to a hydrogen atom radius which is much smaller than that of the Pt, Rh, or Ir atoms,[54] these same results also show that H-H distances smaller than M-M distances are rarely observed. Similarly, in line with results obtained in surface science,[8] our model predicts that the maximum number of hydrogen atoms which can adsorb on the (111) surface of an fcc metal single crystal is equal to the number of metal atoms in that surface. Our assumptions therefore seem reasonable. They lead to a lower limit for the number of hydrogen atoms that geometrically can be put around a supported metal cluster.

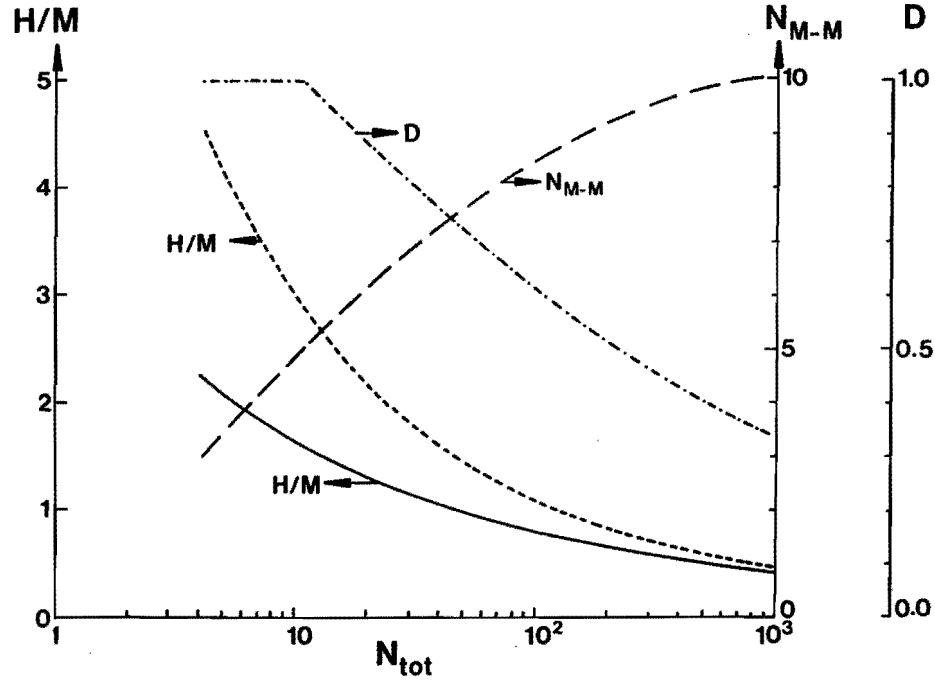

Figure 8.3. Results of model calculations for α = 0.5 (spherical metal particles). Calculated H/M, assuming that all free positions around the metal particle are filled with hydrogen (— —), or that only the free positions with at least two metal neighbours are filled (—), versus total number of metal atoms in a single particle N_{tot}. Calculated dispersion D (- • -) and calculated metal-metal coordination number N_{M-M} (— —) versus N_{tot}.

Table 8.3 summarizes the results of the calculations for two situations. One in which the interaction between metal and oxygen is half that of the metal-metal interaction, $E(M\text{-}O^{2-})/E(M\text{-}M) = \alpha = 0.5$, which results in spherical particles, and one in which $\alpha = 2$, resulting in raft-like particles. Dispersions (defined as the surface fraction of the metal atoms), metal-metal coordination numbers, diameters of the particles (expressed in metal atom diameters) and H/M values are presented as a function of the number of atoms per particle. In each case, two H/M values were calculated. Very high H/M values (up to 4.5) were obtained if hydrogen was allowed to occupy all vacant fcc positions, even those where the hydrogen atom is bonded to only one metal atom. Alternatively, if only vacant positions were considered, where the hydrogen atom is bonded to at least two metal atoms, H/M values up to 2.3 could be obtained. In Figure 8.3 the two series of H/M values have been plotted as a function of the total number of atoms in a metal particle, using $\alpha = 0.5$. In the same figure also the corresponding calculated coordination number N, to be compared with the EXAFS results, and the dispersion D are presented.

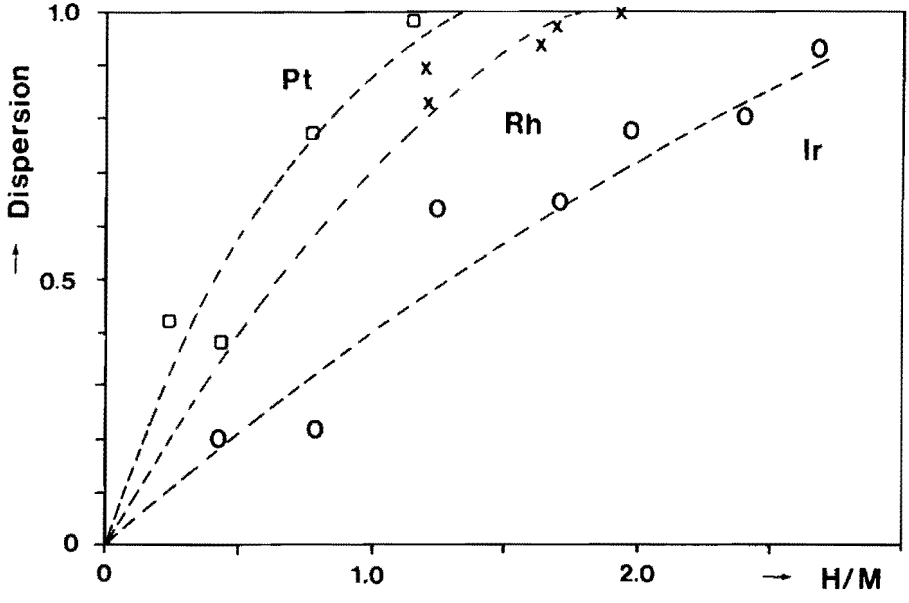

Figure 8.4. Dispersion ($M_{surface}/M_{total}$) obtained on the basis of model calculations ($\alpha = 0.5$, spherical metal particles) for Pt (□), Rh (x), and Ir (o), versus H/M.

With the aid of these calculations, the metal-metal coordination numbers determined by EXAFS were used to calculate dispersions. These dispersions versus the measured H/M values are shown in Figure 8.4. It is clear from this figure that the $H/M_{surface}$ stoichiometry cannot be taken as equal to one, and varies among the group VIII metals studied.

8.4 Discussion

First of all, several trivial effects are to be excluded which could explain the high H/M values:

- unreduced M^{n+} was not present, as can be concluded from TPR experiments.[34-37] Within the experimental error (5%), all metal was reduced to M^0.
- contamination of the catalysts with carbon did not occur. Elemental analysis (using a Perkin Elmer Element Analyzer Model 240) showed that initially no carbon residues existed on the catalysts. Carbon residues could be produced by grease or oil vapours during evacuation. However, TPD experiments, which are absolutely free of grease and oil vapour, resulted in similarly high H/M values.[37]
- partial reoxidation during outgassing at high temperature, mentioned by Martin et al. for Fe[55] and Ni,[56] can be excluded, because oxygen consumption during oxidation at 773 K after reduction and evacuation at 773 K was measured to be O/Ir = 1.96 for 1.5 wt% Ir/Al_2O_3. As IrO_2 is the most stable oxide of iridium, these results prove that Ir was in the zero-valent state after reduction and evacuation.

In the literature several explanations have been proposed for high H/M values. A common explanation is that in fact not all hydrogen is adsorbed by the small particles but that part of the hydrogen is adsorbed by the support through hydrogen spillover from the metal particles. Kramer and Andre[28] have reported the spillover of atomic hydrogen (formed by dissociation of H_2 on platinum) on alumina and calculated a maximum surface capacity of their alumina for atomic hydrogen of $2 \cdot 10^{16}$ atoms/m^2. Cavanagh and Yates[29] have studied hydrogen spillover on alumina by exchange of D_2 with OH-groups and have shown that near 300 K, the rate

of the exchange process is high in the presence of Rh particles on Al_2O_3. However, this experiment does not constitute proof for hydrogen spillover because the occurrence of exchange of hydrogen on the metal with hydrogen of the OH-groups on the support is a necessary but not sufficient condition for spillover to take place. Hydrogen spillover has also been reported on SiO_2, especially by Teichner and coworkers.[30]

We do not believe that spillover can explain our results. In the first place, it is not expected that the extent of spillover will differ greatly among the group VIII metals, and thus it cannot explain the observed differences between Pt, Rh, and Ir. Besides, it is often said that spillover depends on the type of support used. In the case of Ir we have used two supports, SiO_2 and Al_2O_3, and the H/Ir versus N values were found to lie on a straight line, independent of the support. Moreover, the reported number of sites on Al_2O_3, available for hydrogen spillover, $2 \cdot 10^{16}$ atoms/m^2,[28] can only account for a fraction of the hydrogen chemisorbed by our catalysts. We can not imagine any trap for hydrogen on alumina or silica (what can be reduced?) besides defects or impurities. The amounts of adsorbed hydrogen are far too high to be compatible with the concentration of impurities or defects.

Thus, it is concluded that the main reason for the observed large H/M values must be an adsorption stoichiometry larger than one. There are two ways to achieve such a high adsorption stoichiometry:

- adsorption beneath the metal surface, or
- multiple adsorption on (parts of) the metal surface.

Both explanations have been proposed in the literature.[16-18,31-33] In fact the difference is not that great, subsurface hydrogen can be considered as being bound to subsurface metal atoms, or alternatively as being bound to surface atoms. In the latter case the metal surface atom is multiply coordinated by hydrogen.

Subsurface hydrogen has already been observed for e.g. Pt(111), Ni(111), and Pd(111) by surface characterization techniques like XPS.[32] Also, Yates et al.[33] have invoked subsurface hydrogen to explain the delayed desorption of H_2 from a H_2/D_2 covered Ru (0001) surface, while Konvalinka and Scholten[31] have explained the TPD results of Pd/C with subsurface hydrogen. Because the hydrogen solubility in the bulk of Pt, Rh,

and Ir is rather low[57] the hydrogen can only be located just below the surface. Wells[58] has given an explanation for the different hydrogen absorption characteristics of the group VIII metals. He has related the degree of internal perfection of a metal particle to the amount of subsurface hydrogen (as determined by butadiene titration and deuterium exchange) and has stated that the degree of perfection is determined by the height of the reduction temperature, relative to the Hüttig temperature. The Hüttig temperature is taken as one third of the melting temperature, and thought to be the temperature at which surface mobility becomes possible. For Pt this Hüttig temperature is 682 K, for Rh 746 K, and for Ir 894 K. Especially in the case of Ir, the Hüttig temperature is not reached during reduction, and thus the existence of internal defects is expected. These defects might accommodate subsurface hydrogen atoms.

While for large particles it is difficult to attribute the differences in H/M for Ir, Rh, and Pt to multiple adsorption or subsurface adsorption exclusively, it is much easier to make a choice for the small metal particles. In the small metal particles almost all metal atoms occupy a surface position, and the number of subsurface atoms is not sufficient to accommodate a large number of extra hydrogen atoms. Besides, subsurface hydrogen can never explain a hydrogen-to-metal stoichiometry above one, because subsurface adsorption sites need subsurface metal atoms in order to exist.

Therefore, it is concluded that multiple adsorption on exposed metal atoms must be the main reason for the high H/M values observed by ourselves and others. For very small particles almost all metal atoms will have an edge or corner position, independent of the type of metal and thus we are left with the conclusion, that certainly in the case of very small particles, high H/M values must be explained by high $H/M_{surface}$ stoichiometries.

Multiple hydrogen adsorption has mostly been considered for edge and corner metal atoms, and a H/M stoichiometry of 2 has been assumed.[16-18] The results of our model calculations demonstrate that from a geometrical point of view high H/M values are acceptable, even those for the highly dispersed Ir catalysts with H/M > 2.0. Easing up our assumptions (no fcc structure for the smallest metal particles and more than one hydrogen atom filling an fcc vacancy at the surface of the metal particle), only results in still higher calculated hydrogen-to-metal ratios. The

calculations show that high H/M values can indeed be caused by multiple adsorption at the corners and edges of the metal particle. The extremely high H/M values found for the Ir catalysts lead to two possibilities on the basis of these calculations. Either a relatively large proportion of the metal surface atoms occupies a corner or edge position (irregular particle shape), or the H/M stoichiometry for corner and edge iridium atoms is relatively high. The first possibility is unlikely since in the EXAFS analysis no higher Debye-Waller factor has been found for the metal-metal contribution in the iridium systems,[48] while a metal particle with many edges and corners is expected to have a high degree of disorder and thus a high Debye-Waller factor for the metal-metal first shell contribution.

Although the model calculations indicate that there is room enough around the metal particles to accommodate a large number of hydrogen atoms, they do in fact not constitute proof that all these hydrogen atoms can really be bonded strong enough to stay adsorbed at room temperature at a pressure of tens of kPa. Recently Christmann et al.[59] performed studies of hydrogen adsorption on the Ni(110) and Rh(110) surfaces and found that at higher hydrogen pressure the Ni, respectively Rh atoms in the exposed rows all adsorb 1.5, respectively 2 hydrogen atoms. This proves that for Ni a stoichiometry of H/Ni = 1.5 and for Rh a stoichiometry of H/Rh = 2.0 is at least possible.

The calculations do not make clear either why there is such a difference in H/M values for Pt, Rh, and Ir catalysts with the same dispersion, as is shown in Figure 8.4. The explanation for these questions must come from electronic arguments. The most simple explanation, differences in heats of adsorption for hydrogen on Pt, Rh, or Ir, does not seem to be valid, because these heats do not differ markedly.[60] However, the reported spread in the heats of adsorption is large and no real comparison for similar metal crystal surfaces at the same hydrogen coverage has been published yet. Theoretically one would indeed expect platinum to adsorb the lowest number of H atoms, because Pt has one (antibonding) electron more than Rh and Ir. The fact that Ir has a higher hydrogen adsorption capacity than Rh can be related to the larger size of 5d orbitals, which gives better overlap and stronger bonding.

The difference in H/M values between Pt, Rh, and Ir can also be explained by taking a closer look at the analogy between the hydrogen-

covered small metal particles (d < 15 Å) and transition-metal polyhydride complexes. This can be justified by the fact that these very small particles are not truly metallic, because they consist of too few atoms. By using ^1H NMR, Sanz and Rojo[52] have observed the similarity between the chemical shifts of chemisorbed hydrogen on Rh/TiO_2 at hydrogen pressures above 40 kPa, and of diamagnetic non-metallic hydride coordination compounds of the transition-metal elements.

In the case of Pt, hydride complexes with H/Pt > 2 are rarely mentioned in the literature.[54] Recently Minot et al.[61] performed extended Hückel calculations on the hydrogenation of small Pt_n (n = 2-13) clusters and they reported stable complexes with rather high numbers of bonded hydrogen atoms and dihydrogen molecules. Thus for Pt_4 and Pt_6 clusters the maximum amount of hydrogen which could be bonded corresponded to the $Pt_4H_{16}(H_2)_2$ and $Pt_6H_{12}(H_2)_4$ complexes, respectively. These calculations indicated that in all cases the hydrogen atoms (hydride ions) were stronger bonded than the dihydrogen molecules and that dissociation of the dihydrogen molecules in the complexes with maximum number of hydrogen and dihydrogen would lead to an increase, rather than a decrease in total energy.

While these theoretical results already suggest that dihydrogen molecules are much weaker bonded to a metal atom than hydrogen atoms, experimental results in the field of organometallics have presented convincing proof for this. Kubas et al.[62] were the first to demonstrate that transition-metal complexes containing a coordinated dihydrogen molecule, bonded side-on in the η^2 mode, could be prepared. But the H_2 in their $M(CO)_3(PR_3)_2(H_2)$ complexes (M = Mo, W and R = cyclohexyl, i-propyl) is extremely labile. Others have in the past years followed up on Kubas' work and have prepared other complexes in which one or two dihydrogen molecules are coordinated to a transition metal atom.[63-68] In all cases the dihydrogen molecules are readily lost from these complexes and only a few complexes were isolated in crystalline form. For that reason we have assumed that in our case, with small metal particles on a support at room temperature under a pressure of a few tens of kPa, the bonding of dihydrogen molecules to the metal particles is very weak and that the experimentally observed H/M values have to be explained in terms of hydrogen atoms (hydride ions) bonded to metal particles only.

Besides direct quantum mechanical calculations such as the ones published by Minot et al.[61] also rules based on (semi-empirical) theory might shed a light on the number of hydrogen atoms which can be bonded to a particular metal cluster. Based on a topological approach and coupled with chemical intuition backed up by semi-empirical MO calculations, Wade,[69] Mingos,[70] Lauher,[71] and Teo[72] developed rules to explain the existence of boron hydrides and metal carbonyl clusters. These rules have been very successful and can even explain the existence of high-nuclearity clusters. Applying these rules to our metal particles, the binding of many hydrogen atoms to small metal clusters, with a resultant H/M stoichiometry above 1, is no surprise. Stoichiometries above 2 for Pt and above 3 for Rh and Ir are easily explained, if it is assumed that every H atom donates one electron. As examples we quote the existence of the $Pt_{38}(CO)_{44}H_{12}^{2-}$ and $Rh_{13}(CO)_{24}H^{4-}$ clusters, in which each CO molecule donates two electrons and each H atom one electron. According to the rules of Mingos, Lauher, or Teo this means that complexes like $Pt_{38}H_{100}^{2-}$ and $Rh_{13}H_{49}^{2-}$ might be stable, resulting in stoichiometries of H/Pt = 2.6 and H/Rh = 3.8, respectively.

Independent of the size of the metal cluster, all rules predict that all things being equal the H/M stoichiometry for a Pt atom should be smaller by one than for Rh and Ir particles, and that Rh and Ir should have equal stoichiometry. In essence the reason for that is the same as for mononuclear complexes, for which the 18 electron rule holds for octahedral and trigonal bipyramidal symmetry and the 16 electron rule for square planar symmetry. Since Rh and Ir atoms have one valence electron less than Pt atoms, they can coordinate one one-electron donating ligand more than Pt can. Therefore Pt is expected to have the lowest H/M value, and indeed it has. When Rh and Ir atoms or ions have the same valency, they have an equal number of valence electrons and therefore they are expected to coordinate an equal number of ligands. A difference between Rh and Ir is that Ir can reach a higher valency than Rh, Ir^{4+} ions are more stable than Rh^{4+} ions. As the M-H band can formally be described as M^{+}-H^{-}, we expect higher polyhydrides for Ir. Indeed many higher Ir polyhydrides are known, with H/Ir even as high as 6, while Rh polyhydrides are more rare, and are only known up to H/Rh = 5.[54] This tendency is very clear in complexes of Ir and Rh that have the same ligands besides hydride ions. Garlaschelli et

al.[73] prepared $H_5Ir[P(i\text{-}Pr)_3]_2$ (i-Pr = isopropyl) from $HIrCl_2[P(i\text{-}Pr)_3]_2$, while the analogous procedure for Rh yielded only $H_2RhCl[P(i\text{-}Pr)_3]_2$. So the H/M stoichiometries in polyhydride complexes increase in the order Pt < Rh < Ir.

In conclusion, the very high H/M values for the group VIII metals Pt, Rh, and Ir are due to multiple adsorption of hydrogen on metal surface atoms. Differences in H/M values are due to different valencies of the three metals and are completely in line with the observed order of stability of corresponding metal polyhydride complexes. Hydrogen spillover or subsurface hydrogen can not be fully excluded as an explanation, but they give only minor contributions to the high H/M values observed.

The results of this study clearly show that hydrogen chemisorption measurements cannot be used directly to determine particle sizes of highly dispersed metals, because of the uncertainty in the hydrogen-to-surface metal stoichiometry. Of course, for a particular metal the hydrogen chemisorption results can always be used to compare metal particle sizes in a qualitative way. However, by means of the EXAFS technique a calibration can be made, and by using this calibration measured H/M values can be quantitatively related to the percentage of exposed metal atoms as shown in Figure 8.4. At the moment, this calibration is based on assumptions with regard to the metal particle shape. Thus in this work model calculations were used to determine dispersion from metal coordination number. EXAFS analysis of the higher metal-metal shells might give better information on the particle shape.

8.5 References

(1) J. H. Sinfelt, *Ann. Rev. Mat. Sci.* **1972**, *2*, 641.

(2) J. E. Benson, and M. Boudart, *J. Catal.* **1965**, *4*, 704.

(3) J. H. Sinfelt, and D. J. C. Yates, *J. Catal.* **1967**, *8*, 82.

(4) J. H. Sinfelt, *J. Catal.* **1973**, *29*, 308.

(5) H. A. Benesi, R. M. Curtis, and H. P. Studer, *J. Catal.* **1968**, *10*, 328.

(6) T. A. Dorling, M. J. Eastlake, and R. L. Moss, *J. Catal.* **1969**, *14*, 23; T. A. Dorling, B. W. J. Lynch, and R. L. Moss, *J. Catal.* **1971**, *20*, 190.

(7) G. R. Wilson, and W. K. Hall, *J. Catal.* **1972**, *24*, 306.

(8) K. Christmann, G. Ertl, and T. Pignet, *Surface Sci.* **1976**, *54*, 365.

(9) S. F. Adler, and J. J. Keavney, *J. Phys. Chem.* **1960**, *64*, 208.

(10) R. A. Herrmann, S. F. Adler, M. S. Goldstein, and R. M. De Baun, *J. Phys. Chem.* **1961**, *65*, 2189.

(11) V. S. Boronin, V. S. Nikulina, and O. M. Poltorak, *Russ. J. Phys. Chem.* **1963**, *37*, 1174.

(12) V. S. Boronin, O. M. Poltorak, and A. O. Turakulova, *Russ. J. Phys. Chem.* **1974**, *48*, 156.

(13) J. A. Rabo, V. Schomaker, and P. E. Pickert, *Proc. 3rd Int. Congress on Catalysis* (Amsterdam, 1964); Elsevier: Amsterdam, 1964; Vol. II, p 1264.

(14) S. Sato, *J. Catal.* **1985**, *92*, 11.

(15) A. Frennet, and P. B. Wells, *Appl. Catal.* **1985**, *18*, 243.

(16) S. E. Wanke, and N. A. Dougharty, *J. Catal.* **1972**, *24*, 367.

(17) G. B. McVicker, R. T. K. Baker, G. L. Garten, and E. L. Kugler, *J. Catal.* **1980**, *65*, 207.

(18) S. Krishnamurthy, G. R. Landolt, and H. J. Schoennagel, *J. Catal.* **1982**, *78*, 319.

(19) J. H. Sinfelt, Y. L. Lam, J. A. Cusumano, and A. E. Barnett, *J. Catal.* **1976**, *4*, 227.

(20) J. H. Sinfelt, and G. H. Via, *J. Catal.* **1979**, *56*, 1.

(21) C. Yang, and J. R. Goodwin Jr., *J. Catal.* **1982**, *78*, 182.

(22) A. Sayari, H. T. Wang, and J. R. Goodwin Jr., *J. Catal.* **1985**, *93*, 368.

(23) M. A. Vannice, *J. Catal.* **1975**, *37*, 449.

(24) R. M. J. Fiederow, B. S. Chabor, and S. E. Wanke, *J. Catal.* **1978**, *51*, 193.

(25) D. J. C. Yates, L. L. Murrell, and E. B. Prestridge, *J. Catal.* **1979**, *57*, 41.

(26) P. R. Watson, and G. A. Somorjai, *J. Catal.* **1981**, *72*, 3.

(27) T. P. Wibon, P. H. Kasai, and P. C. Ellgen, *J. Catal.* **1981**, *69*, 193.

(28) R. Kramer, and M. Andre, *J. Catal.* **1979**, *58*, 287.

(29) R. R. Cavanagh, and J. T. Yates Jr., *J. Catal.* **1981**, *68*, 22.

(30) D. Bianchi, M. Lacroix, G. Pajonk, and S. J. Teichner, *J. Catal.* **1979**, *59*, 467.

(31) J. A. Konvalinka, and J. J. F. Scholten, *J. Catal.* **1977**, *48*, 374.

(32) W. Eberhardt, F. Greuter, and E. W. Plummer, *Phys. Rev. Lett.* **1981**, *46*, 1085.

(33) J. T. Yates Jr., C. H. F. Peden, J. E. Houston, and D. W. Goodman, *Surface Sci.* **1985**, *160*, 37.

(34) J. C. Vis, H. F. J. Van 't Blik, T. Huizinga, J. Van Grondelle, and R. Prins, *J. Catal.* **1985**, *95*, 333.

(35) J. C. Vis, H. F. J. Van 't Blik, T. Huizinga, J. Van Grondelle, and R. Prins, *J. Molec. Catal.* **1984**, *25*, 367.

(36) D. C. Koningsberger, and D. E. Sayers, *Solid State Ionics* **1985**, *16*, 23.

(37) B. J. Kip, J. Van Grondelle, J. H. A. Martens, and R. Prins, *Appl. Catal.* **1986**, *26*, 353.

(38) J. B. A. D. Van Zon, D. C. Koningsberger, H. F. J. Van 't Blik, and D. E. Sayers, *J. Chem. Phys.* **1985**, *82*, 5742.

(39) D. C. Koningsberger, J. B. A. D. Van Zon, H. F. J. Van 't Blik, G. J. Visser, R. Prins, A. N. Mansour, D. E. Sayers, D. R. Short, and J. R. Katzer, *J. Phys. Chem.* **1985**, *89*, 4075.

(40) D. C. Koningsberger, H. F. J. Van 't Blik, J. B. A. D. Van Zon, and R. Prins, *Proc. 8th Int. Congress on Catalysis* (Berlin, 1984); Verlag Chemie: Weinheim, 1985; Vol. V, p 123.

(41) F. W. Lytle, R. B. Greegor, E. C. Marques, D. R. Sandstrom, G. H. Via, and J. H. Sinfelt, *J. Catal.* **1985**, *95*, 546.

(42) G. H. Via, J. H. Sinfelt, and F. W. Lytle, *J. Chem. Phys.* **1979**, *71*, 690.

(43) G. H. Via, G. Meitzner, F. W. Lytle, and J. H. Sinfelt, *J. Chem. Phys.* **1983**, *79*, 1527.

(44) T. Huizinga, J. Van Grondelle, and R. Prins, *Appl. Catal.* **1984**, *10*, 199.

(45) J. W. Geus, *Preparation of Catalysts III*; G. Poncelet, P. Grange, and P. A. Jacobs, Eds.; Elsevier: Amsterdam, 1983; p 1.

(46) B. K. Teo, and P. A. Lee, *J. Am. Chem. Soc.* **1979**, *101*, 2815.

(47) F. B. M. Duivenvoorden, D. C. Koningsberger, Y. S. Uh, and B. C. Gates, *J. Am. Chem. Soc.* **1986**, *108*, 6254.

(48) D. C. Koningsberger, F. B. M. Duivenvoorden, B. J. Kip, and D. E. Sayers, *J. de Phys. C8* **1986**, *47*, 255.

(49) A. Crucq, L. Degols, G. Lienard, and A. Frennet, *Acta Chim. Acad. Sci. Hung.* **1982**, *111*, 547.

(50) A. Crucq, G. Lienard, L. Degols, and A. Frennet, *Appl. Surf. Sci.* **1983**, *17*, 79.

(51) L. C. X. De Menorval, and J. P. Fraissard, *Chem. Phys. Lett.* **1981**, *77*, 309.

(52) J. Sanz, and J. M. Rojo, *J. Phys. Chem.* **1985**, *89*, 4974.

(53) P. Wynblatt, and N. A. Gjostein, *Progr. Solid State Chem.* **1975**, *9*, 21.

(54) G. G. Hlatky, and R. H. Crabtree, *Coord. Chem. Rev.* **1985**, *65*, 1.

(55) R. Dutartre, P. Bussiere, J. A. Dalmon, and G. A. Martin, *J. Catal.* **1979**, *59*, 382.

(56) J. A. Dalmon, C. Mirodatos, P. Turlier, and G. A. Martin, *Spillover of adsorbed species* (Studies in Surface Science and Catalysis); G. M. Pajonk, S. J. Teichner, and J. E. Germain, Eds.; Elsevier: Amsterdam, 1983; Vol. XVII, p 169.

(57) R. B. McLellan, and W. A. Oates, *Acta Met.* **1973**, *21*, 181.

(58) P. B. Wells, *J. Catal.* **1978**, *52*, 498.

(59) R.J. Behm, K. Christmann, G. Ertl, V. Penka, and R. Schwankner, *The structure of surfaces*; M. A. van Hove, and S. Y. Tong, Eds.; Springer Verlag: Berlin, 1985; p 257.

(60) I. Toyoshima, and G. A. Somorjai, *Catal. Rev.* **1979**, *19*, 105.

(61) C. Minot, B. Bigot, and A. Hariti, *J. Am. Chem. Soc.* **1986**, *108*, 196.

(62) G. J. Kubas, R. R. Ryan, B. I. Swanson, P. J. Vergamini, and H. J. Wasserman, *J. Am. Chem. Soc.* **1984**, *106*, 451.

(63) R. K. Upmacis, G. E. Gadd, M. Poliakoff, M. B. Simpson, J. J. Turner, R. Whyman, and A. F. Simpson, *J. Chem. Soc., Chem. Commun.* **1985**, 27.

(64) S. P. Church, F. W. Grevels, H. Hermann, and K. Schaffner, *J. Chem. Soc., Chem. Commun.* **1985**, 30.

(65) R. H. Crabtree, and M. Lavin, *J. Chem. Soc., Chem. Commun.* **1985**, 794.

(66) R. L. Sweany, *J. Am. Chem. Soc.* **1985**, *107*, 2374.

(67) R. H. Morris, J. F. Sawyer, M. Shiralian, and J. D. Zubkowski, *J. Am. Chem. Soc.* **1985**, *107*, 5581.

(68) Compare also the abstracts of the papers presented at the 191st Meeting of the American Chemical Society, New York, April 1986: Symposium on hydrogen-rich organometallic and inorganic complexes.

(69) K. Wade, *Chem. Britain* **1975**, *11*, 177; *Adv. Inorg. Chem. Radiochem.* **1976**, *18*, 1.

(70) D. M. P. Mingos, *J. Chem. Soc., Dalton Trans.* **1974**, 133; *J. Chem. Soc., Dalton Trans.* **1976**, 1173.

(71) J. W. Lauher, *J. Am. Chem. Soc.* **1978**, *100*, 5305; *J. Am. Chem. Soc.* **1979**, *101*, 2604.

(72) B. K. Teo, *J. Chem. Soc., Chem. Commun.* **1983**, 1362; *Inorg. Chem.* **1984**, *23*, 1251.

(73) L. Garlaschelli, S. I. Khan, R. Bau, G. Longini, and T. F. Koezle, *J. Am. Chem. Soc.* **1985**, *107*, 7212.

Chapter Nine

Determination of Metal Particle Size in Partly Reduced Ni Catalysts by Hydrogen/Oxygen Chemisorption and EXAFS

9.1 Introduction

Hydrogen chemisorption is commonly used to determine the degree of dispersion of group VIII metal catalysts.[1-5] In the determination of the metal surface area usually a hydrogen-to-metal stoichiometry of one has been used. However, increasingly more publications have appeared in which H/M values exceeding unity are reported.[3-6] Thus to overcome the apparent difficulties in determining the metal surface area in these highly dispersed systems by the hydrogen chemisorption technique we have recently presented a calibration of H/M values by EXAFS (Extended X-ray Absorption Fine Structure) for the group VIII metals Rh, Ir, and Pt[7] (see also Chapter 8). Our results have clearly shown that the high H/M values are caused by high $H/M_{surface}$ stoichiometries (exceeding unity), with H/Pt < H/Rh < H/Ir. In this previous study we have used only fully reduced systems.

However, in practice often supported metal catalysts are studied which are only partly reduced. Therefore we present here hydrogen chemisorption and EXAFS measurements on Ni/SiO_2 systems with different degrees of reduction due to the application of different preparation methods.[8]

9.2 Experimental

9.2.1 Catalyst Preparation

The catalysts were prepared using SiO_2 (Degussa aerosil 200) and $Ni(NO_3)_2 \cdot 6H_2O$ (p. a. Merck) according to the incipient wetness technique or the urea method.[6,9] Nickel loadings were determined using Atomic

Absorption Spectroscopy.

9.2.2 Chemisorption Measurements

Hydrogen chemisorption was carried out as described in Chapter 8:[7] volumetric chemisorption measurements were performed in a conventional glass system at 298 K. Hydrogen was purified by passing through a palladium diffusion cell. The dried catalyst samples were first reduced in flowing H_2 at 723 K for 30 min (heating rate 5 K/min) and then evacuated (10^{-2} Pa) at the same temperature for 30 min. Hydrogen ($P(H_2)$ = 93 kPa) was admitted at 473 K, as hydrogen adsorption at room temperature is a slow process. Subsequently, the sample was cooled to 298 K under hydrogen and the amount of adsorbed hydrogen was measured ($P_{equilibrium} \sim 80$ kPa). Thereafter a desorption isotherm was measured at room temperature by lowering the pressure step by step ($\Delta P \sim 13$ kPa per step), while measuring the amount of desorbed hydrogen. The total amount of chemisorbed H atoms was obtained by extrapolating the linear high-pressure part (20 kPa < P < 80 kPa) of the isotherm to zero pressure.[1] Correction for chemisorption on the bare support was not necessary, because extrapolation of the desorption isotherm for the bare support, pretreated in the same way as the catalysts, yielded zero within the uncertainty of the measurements.

Oxygen chemisorption experiments were carried out immediately after hydrogen chemisorption. The sample was evacuated at 298 K and then heated to 473 K (heating rate 5 K/min). At this temperature evacuation was prolonged for 30 min (10^{-2} Pa), to remove all adsorbed hydrogen from the metal particles. The sample was cooled to 298 K under vacuum, a certain amount of oxygen was admitted ($P \sim 40$ kPa) and the sample again heated to 473 K (heating rate 5 K/min). At this temperature the sample was held for 1 h, after which all reduced Ni had been converted to NiO, and then cooled to 298 K. Subsequently a desorption isotherm was measured in the same way as in the case of hydrogen. The O/Ni values thus obtained were used to correct the hydrogen chemisorption results for the amount of unreduced Ni in the sample:

$$H/M_{corr} = \frac{1}{O/M_{meas}} H/M_{meas} \qquad (9.1)$$

The preparation details and chemisorption results are presented in Table 9.1. It is clear that the sample prepared according to the incipient wetness technique is more easily reduced than those prepared according to the urea method.

Table 9.1. Preparation characteristics and chemisorption results for the Ni/SiO_2 catalysts.

Catalyst[1]	H/M	H/M_{corr}	Degree of reduction	
			O/M	1-f (EXAFS)
1.9% Ni/SiO_2, I	0.29	0.32	0.90	1
2.4% Ni/SiO_2, U	0.17	0.36	0.47	0.42
5.2% Ni/SiO_2, U	0.30	0.43	0.69	0.53

[1]prepared by the incipient wetness technique (I) or the urea method (U).

Accuracies: H/M: ± 5%; O/M: ± 10%; 1-f (EXAFS): ± 15%.

9.2.3 EXAFS Measurements

The EXAFS measurements were performed on the laboratory EXAFS spectrometer at Eindhoven University,[10,11] equipped with a Si(111) Johansson crystal. Measurements were done at the Ni K edge (8333 eV). The catalyst samples were pressed into self-supporting wafers with $\mu x \sim 2.7$. The wafers were mounted in an in situ EXAFS cell[12] and EXAFS spectra were taken at room temperature in H_2 after in situ reduction in flowing H_2 at 723 K (heating rate 5 K/min). EXAFS data analysis was performed using experimentally determined phases and backscattering amplitudes. Therefore, the reference compound Ni foil[13] was measured and the first Ni-Ni coordination shell was extracted from the EXAFS data in order to provide phase and backscattering amplitude information on Ni-Ni contributions. Likewise, NiO[14] was measured to provide that information on Ni-O contributions.

9.3 Data Analysis Results

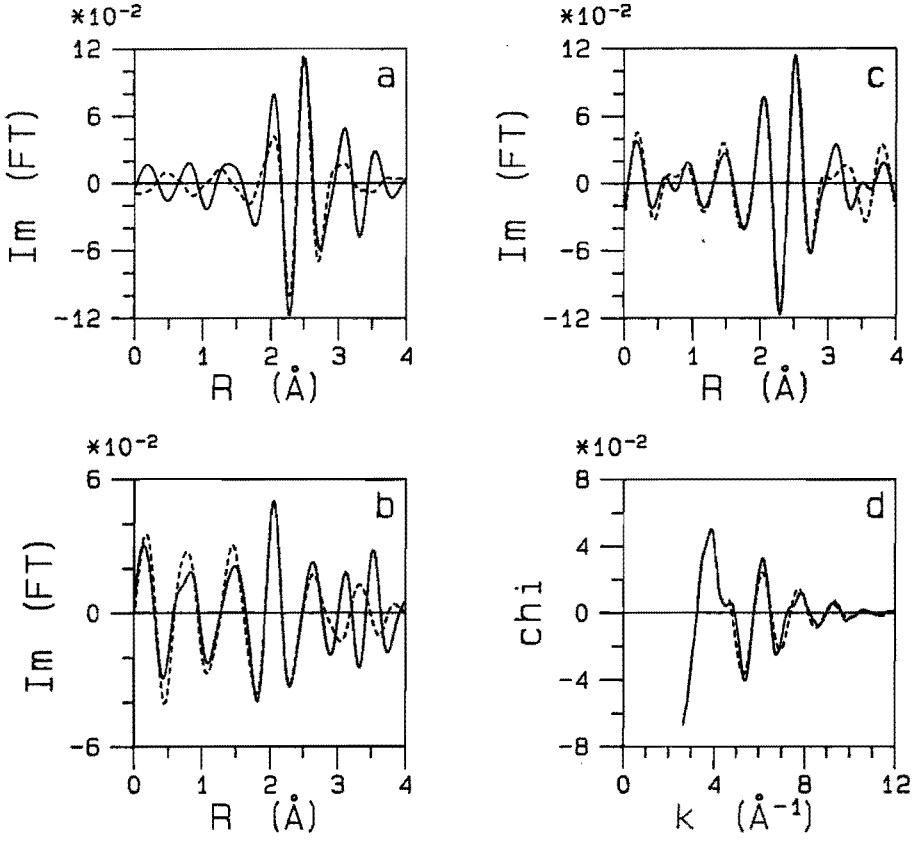

Figure 9.1. (a) Imaginary part of the k^1-weighted Fourier transform (4.3-11.3 $Å^{-1}$, Ni-Ni phase corrected) of experimental EXAFS data for 5.2 wt% Ni/SiO_2 after reduction (—) and calculated Ni-Ni contribution (— —); (b) imaginary part of the k^1-weighted Fourier transform (4.3-11.3 $Å^{-1}$, Ni-O phase corrected) of experimental data minus Ni-Ni contribution (—) and calculated Ni-O contribution (— —); (c) imaginary part of the k^1-weighted Fourier transform (4.3-11.3 $Å^{-1}$, Ni-O phase corrected) of experimental data (—), and sum of the calculated Ni-O and Ni-Ni contributions (— —); and (d) experimental data (—), and sum of the calculated Ni-O and Ni-Ni contributions (— —) in k space.

In the partly reduced systems four contributions are expected with R < 3.5 Å: Ni-Ni of the reduced phase, and Ni-O, Ni-Ni, and Ni-Si of the hydrosilicate phase.[15] Of these, the reduced Ni-Ni and the oxidic Ni-O coordination parameters (coordination number N, coordination distance R, and Debye-Waller factor $\Delta\sigma^2$ with respect to the appropriate reference compound) were determined using the difference file technique[16] (see also Chapter 2, Section 2.2.5). In this technique, first an estimate for the parameters of the largest contribution (viz. Ni-Ni) is made, by fitting the right-hand side in the combined Ni-O + Ni-Ni peak at 1.6-2.8 Å after Fourier transformation in r space (Figure 9.1a). This contribution is subsequently subtracted from the experimental data, and the difference spectrum is Fourier transformed. It is then tried to estimate the coordination parameters of the Ni-O contribution at 1.6-2.6 Å in the same way (Figure 9.1b). As a check both calculated contributions are added and compared with the experimental data in r and in k space. Usually it is repeatedly necessary to adjust the parameters of the Ni-Ni contribution and to calculate a new Ni-O contribution thereupon before good agreement between the experimental and calculated spectrum is obtained (Figures 9.1c and 9.1d). In Figure 9.1d small differences are observed that are due to higher shell contributions (mainly Ni-Ni and Ni-Si shells from the hydrosilicate phase). A full analysis of the EXAFS spectrum of the 5.2 wt% Ni/SiO_2 catalyst, including these higher shell contributions, will be presented elsewhere.[17]

The Ni-Ni coordination number obtained from the EXAFS data analysis is averaged over all Ni atoms in the sample, i. e. those in the metallic phase as well as those in the oxidic hydrosilicate phase. However, the real coordination number of the Ni atoms in the metallic phase only is sought, in order to determine the mean metal particle size in the catalysts. If a fraction f of the Ni atoms in the sample is unreduced, then assuming that the real Ni-O coordination number is 6,[15] f is equal to:[18]

$$f = \frac{N_{meas}(Ni-O)}{N_{real}(Ni-O)} = \frac{N_{meas}(Ni-O)}{6} \qquad (9.2)$$

As a consequence, the fraction of reduced Ni atoms in the sample is equal to 1-f. The real Ni-Ni coordination number in the metallic phase can now be determined as:

$$N_{real}(Ni-Ni) = \frac{N_{meas}(Ni-Ni)}{(1-f)} \qquad (9.3)$$

The results of the EXAFS analysis are presented in Table 9.2 and Figure 9.1. With respect to the accuracies given in Table 9.2, it should be mentioned that, although the absolute accuracy for e. g. EXAFS coordination numbers is ± 0.5, the relative accuracy is much higher. We feel confident that the Ni-O coordination number obtained for the 2.4 wt% Ni/SiO_2 system is significantly higher than that obtained for the 5.2 wt% Ni/SiO_2 catalyst.

Table 9.2. Coordination parameters for the reduced Ni/SiO_2 catalysts.

Sample	Ni-O			Ni-Ni			
	N	R (Å)	$\Delta\sigma^2$ (Å^2)	N	N_{corr}	R (Å)	$\Delta\sigma^2$ (Å^2)
Ni foil[1]	-	-	-	12.0	12.0	2.488	0
NiO[1]	6.0	2.098	0	-	-	-	-
1.9% Ni/SiO_2	n.d.	n.d.	n.d.	9.8	9.8	2.487	0.0000
2.4% Ni/SiO_2	3.5	2.078	-0.0026	3.2	7.7	2.466	0.0020
5.2% Ni/SiO_2	2.8	2.063	-0.0009	4.3	8.1	2.470	0.0013

[1]XRD data[13,14]

Absolute accuracies: N: ± 0.5; R: ± 0.02 Å; $\Delta\sigma^2$: ± 0.001 Å^2.

9.4 Discussion

In literature, the hydrogen chemisorption technique is described in many different ways. Small differences in the experimental details and in

the interpretation of the measurements often yield different results. It must therefore be kept in mind that the numerical results presented here and elsewhere[7] (see also Chapter 8) depend on the method of hydrogen chemisorption. However, we think that our method yields representative results:[7]

- often, the chemisorption process takes place at room temperature instead of a higher temperature (we used 473 K). Both methods were found to differ only 7% in the H/M value determined for an $Ir/\gamma\text{-}Al_2O_3$ catalyst.[7]
- hydrogen adsorption isotherms for supported Pt and Rh catalysts are reported to be Temkin-like (showing a linear relation between log (P) and H/M over a wide pressure range).[19,20] Measuring H/M values at a too high pressure may thus result in values representing a situation in which more than a monolayer has been adsorbed. However in our procedure we extrapolate to zero pressure.
- H/M values are reported to depend on the measurement temperature,[21] being larger at lower temperatures. We used the most convenient temperature of 298 K.
- often, a distinction is made between 'reversibly' and 'irreversibly' adsorbed hydrogen.[5] Only the irreversibly adsorbed hydrogen is then taken into account in the determination of the H/M value. We think it is very difficult to determine the amount of 'irreversibly' adsorbed hydrogen objectively, because the amount of weakly adsorbed hydrogen that can be removed by pumping depends very much on the experimental conditions. Moreover, it has been shown that the NMR chemical shifts of hydrogen atoms adsorbed on Pt/Al_2O_3[22] and Rh/TiO_2[23] catalysts still decrease with increasing H_2 pressure at $P > 40$ kPa, and thus the hydrogen atoms which adsorb at these pressures must still be associated with the metal. Therefore our H/M values are based upon the total amount, rather than the 'irreversibly' adsorbed amount of H_2.

The degrees of reduction from chemisorption (O/M_{meas}) and from EXAFS ($1 - (N_{meas}(Ni\text{-}O)/6)$) are equal within the accuracy of the measurements (see Table 9.1). This shows that slow oxidation of the reduced Ni/SiO_2 samples, a well known problem with this type of catalyst,[24] does not influence our measurements beyond the accuracies given: chemisorption

measurements (hydrogen and oxygen) typically take several hours, while for EXAFS measurements more than a day is needed. Both the chemisorption and EXAFS results show that the incipient wetness technique yields a highly reduced system containing rather large metal particles. The corrected metal-metal coordination number N versus corrected H/M value is presented in Figure 9.2, together with the previously obtained results on Rh, Ir, and Pt[7] (see also Chapter 8).

Just as for the other group VIII elements studied, a linear relationship between H/M and N is observed for Ni. The H/M surface stoichiometry observed is approximately equal to one, as had been expected from literature reports on combined magnetization/chemisorption experiments.[25] Thus we may conclude that there are no systematic errors inherent to our experimental methods, viz. also for the other metals (Pt, Rh, Ir) presented in Figure 9.2 we may have a high degree of confidence in the numerical values emanating from the H/M vs. N curves.

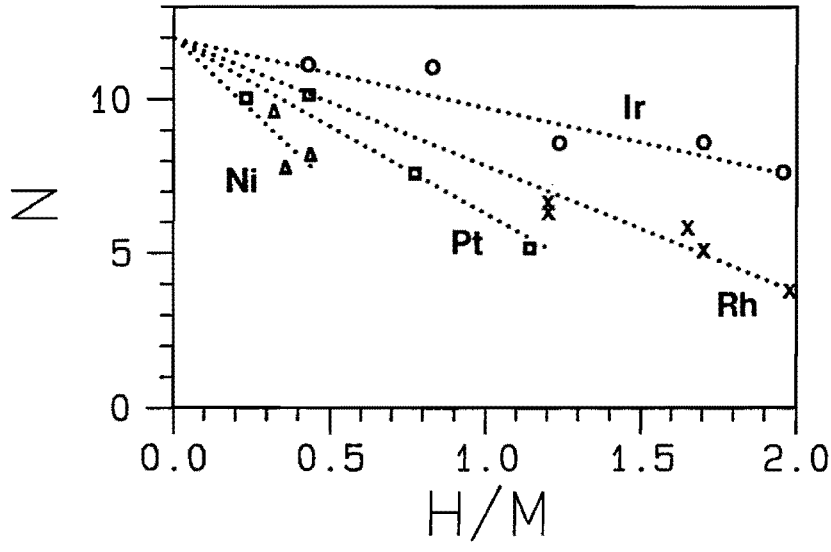

Figure 9.2. Metal-metal coordination number N from EXAFS versus H/M from chemisorption for Ni (Δ), Pt (□), Rh (x), and Ir (o)[7] (see also Chapter 8).

For all metals presented in Figure 9.2 there are 12 first shell neighbours in the bulk due to the fcc structure. Therefore at H/M = 0 a fixed N = 12 is chosen. Also, at N ~ 3, the measured H/M should be virtually equal to the maximal $H/M_{surface}$ stoichiometry for the metal under study, assuming a three-dimensional metal particle shape. We therefore conclude that in highly dispersed systems H/Ni ~ 1, H/Pt ~ 1.5-2, H/Rh ~ 2-2.5, and H/Ir ~ 4.

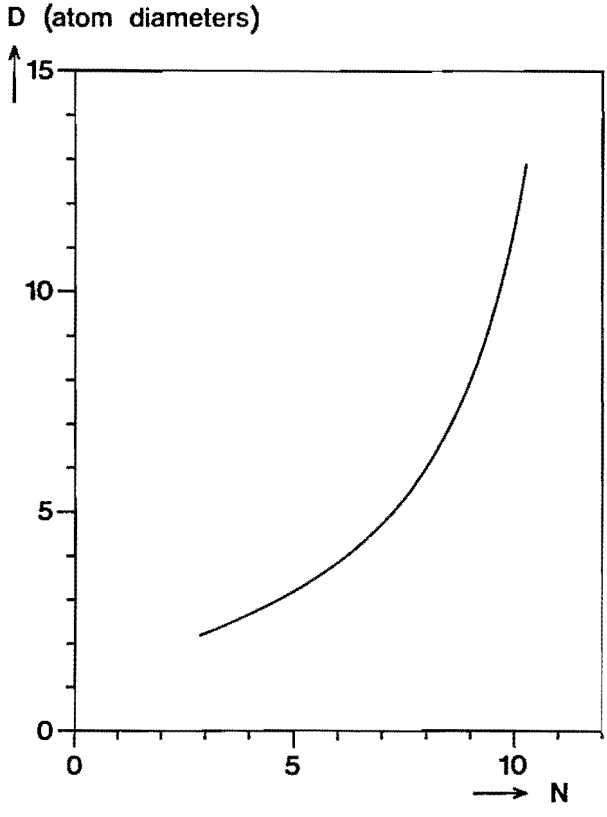

Figure 9.3. Particle diameter D (expressed in atom diameters) calculated from the first shell metal-metal coordination number N from EXAFS, assuming half-spherical metal particles, versus N.[7,16]

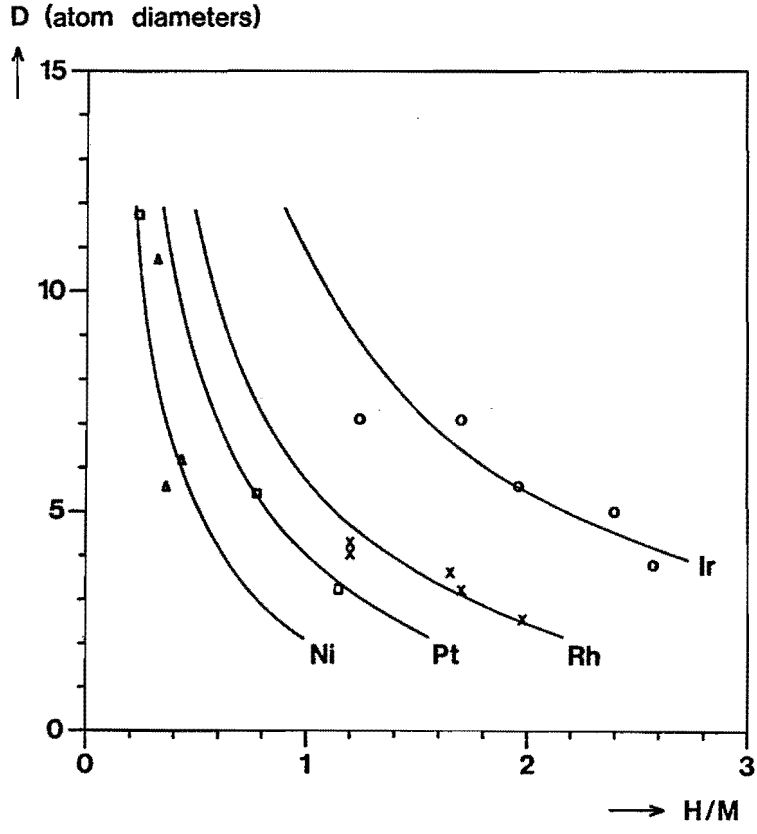

Figure 9.4. Metal particle diameter D (expressed in atom diameters) based upon the metal-metal coordination number N versus H/M from chemisorption for Ni (Δ), Pt (□), Rh (x), and Ir (o).[7] The drawn lines are calculated from the straight lines shown in Figure 9.2.

In order to relate the measured H/M values to particle sizes, assumptions have to be made concerning the particle shape. Usually, it is assumed that the supported metal particles are half-spherical in shape. In that case straightforward calculations yield a relationship between the particle diameter and the first shell metal-metal coordination number as determined with EXAFS.[7,16] This is shown in Figure 9.3. Using the correlation between N and H/M values, as determined in this study and previously[7] for Ni, Pt, Rh, and Ir, we can now relate hydrogen chemisorption results directly to particle sizes (see Figure 9.4), without assuming a value for the H/M surface stoichiometry.

In summary, the EXAFS technique can be used as a method for determining the metal particle size even if the catalysts are not fully reduced. Caution must be taken that the degree of reduction is known when the EXAFS calibration of chemisorption values is used, to avoid assigning a too large mean metal particle size to the sample under study.

9.5 References

(1) J. E. Benson, and M. Boudart, *J. Catal.* **1965**, *4*, 704.

(2) H. A. Benesi, R. M. Curtis, and H. P. Studer, *J. Catal.* **1968**, *10*, 328.

(3) S. F. Adler, and J. J. Keavney, *J. Phys. Chem.* **1960**, *64*, 208.

(4) S. E. Wanke, and N. A. Dougharty, *J. Catal.* **1972**, *24*, 367.

(5) G. B. McVicker, R. T. K. Baker, G. L. Garten, and E. L. Kugler, *J. Catal.* **1980**, *65*, 207.

(6) B. J. Kip, J. Van Grondelle, J. H. A. Martens, and R. Prins, *Appl. Catal.* **1986**, *26*, 353.

(7) B. J. Kip, F. B. M. Duivenvoorden, D. C. Koningsberger, and R. Prins, *J. Catal.* **1987**, *105*, 26.

(8) J. W. E. Coenen, and B. G. Linsen, *Physical and Chemical Aspects of Adsorbents and Catalysts*; B. G. Linsen, Ed.; Academic Press: London, 1970; p 472.

(9) J. W. Geus, *Preparation of Catalysts III*; G. Poncelet, P. Grange, and P. A. Jacobs, Eds.; Elsevier: Amsterdam, 1983; p 1.

(10) P. Brinkgreve, T. M. J. Maas, D. C. Koningsberger, J. B. A. D. Van Zon, M. H. C. Janssen, and A. C. M. E. Van Kalmthout, *EXAFS and Near Edge Structure III*; K. O. Hodgson, B. Hedman, and J. E. Penner-Hahn, Eds.; Springer Verlag: Berlin, 1984; p 517.

(11) J. B. A. D. Van Zon, *Thesis*; Eindhoven University of Technology, Eindhoven, the Netherlands, 1984.

(12) F. W. H. Kampers, T. M. J. Maas, P. Brinkgreve, and D. C. Koningsberger, to be published.

(13) R. W. G. Wyckoff, *Crystal Structures*, 2nd ed.; Wiley: New York, 1963; Vol. I, p 10.

(14) H. P. Rooksby, *Acta Cryst.* **1948**, *1*, 226.

(15) C. B. Ma, *Z. für Krist.* **1975**, *141*, 126.

(16) J. B. A. D. Van Zon, D. C. Koningsberger, H. F. J. Van 't Blik, and D. E. Sayers, *J. Chem. Phys.* **1985**, *82*, 5742.

(17) F. B. M. Van Zon, P. W. J. G. Wijnen, F. W. H. Kampers, and D. C. Koningsberger, to be published.

(18) D. C. Koningsberger, J. B. A. D. Van Zon, H. F. J. Van 't Blik, G. J. Visser, R. Prins, A. N. Mansour, D. E. Sayers, D. R. Short, and J. R. Katzer, *J. Phys. Chem.* **1985**, *89*, 4075.

(19) A. Crucq, L. Degols, G. Lienard, and A. Frennet, *Acta Chim. Acad. Sci. Hung.* **1982**, *111*, 547.

(20) A. Crucq, G. Lienard, L. Degols, and A. Frennet, *Appl. Surf. Sci.* **1983**, *17*, 79.

(21) V. S. Boronin, O. M. Poltorak, and A. O. Turakulova, *Russ. J. Phys. Chem.* **1974**, *48*, 156.

(22) L. C. X. De Menorval, and J. P. Fraissard, *Chem. Phys. Lett.* **1981**, *77*, 309.

(23) J. Sanz, and J. M. Rojo, *J. Phys. Chem.* **1985**, *89*, 4974.

(24) J. A. Dalmon, C. Mirodatos, P. Turlier, and G. A. Martin, *Spillover of Adsorbed Species* (Studies in Surface Science and Catalysis); G. M. Pajonk, S. J. Teichner, and J. E. Germain, Eds.; Elsevier: Amsterdam, 1983; Vol. XVII, p 169.

(25) G. A. Martin, P. De Montgolfier, and B. Imelik, *Surf. Sci.* **1973**, *36*, 675.

Chapter Ten

Concluding Remarks

10.1 Original Scope of this Ph. D. Study

As outlined in Chapter 1, I started my four years of Ph. D. study with the goal to undertake a more close investigation of the metal-support interface in supported metal catalysts, using the EXAFS technique. Especially the study of model systems (i. e. supported metal carbonyls and derived systems) and comparison of new metal-support combinations with those already studied were to be an important part of my investigations.

10.2 The Metal-Support Interaction

10.2.1 Formation of the Metal-Support Interface

In Chapters 5 and 6, the metal-support bonding is studied in Al_2O_3-supported $Ir_4(CO)_{12}$ after adsorption, and after reduction. Detailed EXAFS analysis combined with IR and mass spectrometry results showed that adsorption of $Ir_4(CO)_{12}$ involved exchange of two CO ligands for support oxygen. Four $Ir\text{-}O_{support}$ bonds per cluster were detected with a coordination distance of R = 2.55 Å. To realize this number of $Ir\text{-}O_{support}$ bonds, one Ir-Ir bond must be assumed to be cleaved in the adsorption process. A model for the supported carbonyl has been derived in which the original Ir_4 cluster stays intact. Two of the Ir atoms are each bonded to two support oxygen atoms.

In the case of supported metal carbonyls, it is rather easy to quantify the metal-support bonding, because the metal entities are uniform in size. In most reduced supported metal catalysts, however, the metal particle size is not uniform. The metal crystallites are usually three-dimensional, whereas the metal-support interface is essentially two-dimensional. Variation in particle size will cause a varying fraction of metal atoms in the interface, and hence, difficult quantification of the metal-support

interaction. The difficulties in quantifying the metal-support interactions in supported metal systems can be overcome by studying a catalyst in which the supported metal particles are two-dimensional. Even if the metal particles are non-uniform in size, it is clear that all the metal atoms are present in the metal-support interface. By chance, such a system was obtained by decomposition and reduction of Al_2O_3-supported $Ir_4(CO)_{12}$ (Chapter 6). This Ir/γ-Al_2O_3 system proved to be ideal to study more closely the Ir-Al_2O_3 interface. Ir-$O_{support}$ bonds with R = 2.58 Å were distinctly observed, and also it was established without doubt that per interfacial Ir atom three Ir-$O_{support}$ bonds are present. Since γ-Al_2O_3 mainly exposes (111) faces, a (111)-like interface is clearly present. Theoretical calculations on the Rh-Al_2O_3 interface[1] yield three Rh-$O_{support}$ bonds per interface Rh atom, with a long Rh-O coordination distance (R $\sim$ 2.55 Å) if the Al_2O_3 surface is assumed to be fully hydroxylated. Thus the Ir-$O_{support}$ contribution can be attributed to an Ir^0-OH^- interaction, like the Rh-$O_{support}$ contributions in Rh/γ-Al_2O_3[2,3] and Rh/TiO_2.[4,5] Also, it may be possible that adsorbed hydrogen in the metal-support interface or electronic changes in the supported metal particles due to adsorbed hydrogen cause the long metal-oxygen coordination distance.

The Ir/γ-Al_2O_3 system also proved to be suitable for higher shell analysis. Both higher Ir-Ir and Ir-$O_{support}$ shells were detected. From the higher Ir-$O_{support}$ shells relevant information was obtained about the metal-support epitaxy. A (111) Ir-Al_2O_3 epitaxy was already established, but this still allows two types of epitaxy: (i) with the metal atoms directly above the oxygen atoms of the one-but-topmost layer (hcp-type), and (ii) with the metal atoms above the oxygen atoms of the two-but-topmost layer (fcc-type). These two types are best distinguished by analysing the Ir-$Al_{support}$ contributions. Unfortunately, we could not detect such interactions, presumably caused by a large spread in Ir-Al distances. As is shown in Chapter 6, also from the higher Ir-$O_{support}$ shells it can be decided which type of epitaxy is dominant. Subject to several assumptions (especially concerning the interatomic distances in the outermost γ-Al_2O_3 layers) the hcp-type of interface yields the best agreement with the experimental results.

10.2.2 Metal Carbonyl Clusters as Model Systems

$Os_3(CO)_{12}$, adsorbed on γ-Al_2O_3, has been studied in Chapter 3. Detailed EXAFS analysis showed that adsorption of the carbonyl cluster involved exchange of two CO ligands for support oxygen, just like for supported $Ir_4(CO)_{12}$. In the case of the $Os_3(CO)_{12}$ cluster, however, two Os-$O_{support}$ bonds were formed (with R = 2.17 Å) whereas for the supported $Ir_4(CO)_{12}$ cluster four Ir-$O_{support}$ bonds per cluster were detected. In both systems the M-$O_{support}$ contribution was distinctly detected, in line with the proposition for Rh/γ-Al_2O_3 that metal-oxygen bonds are involved in the metal-support interface.

When the origin of the metal-oxygen bonds is considered, however, it appears that the supported metal and the supported metal carbonyl systems can not be compared exactly. For the $Os_3(CO)_{12}$ metal carbonyl, it is stated that adsorption takes place through insertion of an Os-Os bond in the OH bond of a surface hydroxyl group.[6] The Os-O bonds detected in the EXAFS analysis are thus real Os-O bonds. Presumably, the same process takes place for $Ir_4(CO)_{12}$. The metal-oxygen bonds in supported metal systems are thought to have a different origin. Thus the difference in metal-oxygen bond lengths in the supported $Os_3(CO)_{12}$ system and Rh/γ-Al_2O_3 (R = 2.17 Å versus R $\sim$ 2.70 Å) is not surprising. However, the fact that in supported $Ir_4(CO)_{12}$ the Ir-$O_{support}$ bonds are long, is still puzzling. Possible explanations are steric hindrance (caused by the remaining CO ligands, of which some point towards the γ-Al_2O_3 surface) or more difficult oxidation of Ir (with respect to Os) by the γ-Al_2O_3 surface. Although the metal-support contribution is easily detected in supported metal carbonyls, these carbonyls are thus not entirely satisfactory as model systems for supported metal catalysts.

Supported metal carbonyls can also provide interesting information about the metal-carbonyl coordination. IR measurements of Al_2O_3-supported $Os_3(CO)_{12}$ and $Ir_4(CO)_{12}$ have shown that only singly-coordinated CO ligands are present. In that case, the M-C-O geometry is such that variations in M-C-O bond angle can be distinctly detected, since the multiple scattering contribution in the M-O shell is very susceptible to these variations.

In the most early study on supported $Os_3(CO)_{12}$ (Chapter 3), the CO ligands were treated as a single entity, viz. no changes in C-O distance and Os-C-O angle were allowed. This caused problems in the analysis of the supported cluster after decomposition. Therefore it was tried to treat the M-C and M-O contributions separately.

In Chapter 4 results are presented for $H_3Re_3(CO)_{12}$ and $[H_2Re_3(CO)_{12}]^-$, both having only singly-coordinated CO ligands. In both complexes the Re-C-O coordination could be analysed very well. No differences in Re-C-O angle were observed, but the Re-C and C-O distances varied with the differing charge on the Re_3 skeleton. Both the shortening of the Re-C, and elongation of the C-O bond with a more negative charge, can be explained by decreased π-backbonding in the case of the negatively charged complex.

These promising results led to a separate treatment of the M-C and M-O shells in the case of supported $Ir_4(CO)_{12}$ (Chapter 5). Also here effects of changes in π-backbonding were observed, but now it seems the adsorbed cluster becomes positively charged. Moreover, the magnitude of the Ir-O shell decreased with respect to that of the Ir-C shell, which is a clear indication that the average Ir-C-O bond angle decreases upon adsorption. We think the best possible explanation for this effect is steric hindrance by the support.

Thus in Chapters 3, 4, and 5 important information has been obtained about the metal-carbonyl coordination: changes in C-O distance and M-C-O angle are easily detected with EXAFS, and changes in M-C and C-O distance are indicative of changes in π-backbonding.

10.2.3 Other Metal-Support Combinations

In Sections 10.2.1 and 10.2.2, results concerning Al_2O_3-supported systems were reviewed. In the study of the reduced Ir/γ-Al_2O_3 system, very detailed information about the metal-support epitaxy was obtained. However, it was apparent that γ-Al_2O_3 is not an ideal support from the point of its structure, although it is an excellent support to prepare catalysts with small metal particles. The long metal-support oxygen bond being established for several Al_2O_3-supported systems, it would be very instructive to investigate the metal-support interaction in catalysts with other

supports, in order to ascertain whether the same type of (long) metal-oxygen bond can be detected in those systems.

For Rh/TiO_2, also $Rh\text{-}O_{support}$ bonds with R ~ 2.70 Å were observed.[4,5] It was assumed that the metal particles were present on a mixture of (001) and (101) faces of the TiO_2 anatase support. Although γ-Al_2O_3 is not structurally well-defined, metal crystallites grow almost exclusively on its (111) spinel faces. Anatase is structurally better defined, but metal crystallites seem to be present on both (001) and (101) faces. The most accurate information on the metal-support interaction can be obtained if the support is both well-defined and exhibits one type of face exclusively.

MgO is a support which fulfills both requirements. Its rocksalt structure is accurately known, and the surface of the MgO crystallites consists almost exclusively of (100) faces. In Chapter 7 the Ir/MgO and Rh/MgO systems were studied. Although the Rh/MgO sample was not fully reduced, in both systems a $M\text{-}O_{support}$ contribution was clearly detected (with R = 2.54 Å for Ir/MgO and R = 2.68 Å for Rh/MgO). The type of support apparently does not have much influence on the bond length.

In the case of MgO, the type of epitaxy was established without doubt. The coordination numbers determined are in agreement with an interface model in which the metal atoms are coordinated by four oxygen atoms in the (100) face.

10.3 Particle Morphology

In Section 10.2.1 it was mentioned that a supported metal catalyst with two-dimensional metal particles is ideal for the study of the metal-support interface, and it was also stated there that such a system had been obtained by reduction of Al_2O_3-supported $Ir_4(CO)_{12}$. As described in Chapter 6, this inference was first based on the large $Ir\text{-}O_{support}$ contribution determined for the $Ir_4(CO)_{12}$-derived system. Definite proof was obtained from the higher shell analysis. Two reduced $Ir/\gamma\text{-}Al_2O_3$ systems were compared (one prepared from $Ir_4(CO)_{12}$, and one prepared from $IrCl_3$) and it was immediately observed that the second Ir-Ir shell was absent in

the $Ir_4(CO)_{12}$-derived system. This is possible if only two-dimensional, (111)-like metal particles are present in the system. On the contrary, all higher Ir-Ir shells were observed in the $IrCl_3$-derived system. The coordination numbers of the first four Ir-Ir shells were determined. For the $Ir_4(CO)_{12}$-derived system, they were in good agreement with a model for approximately round, flat metal particles consisting of 30 atoms. For the $IrCl_3$-derived system, a good model proved to be that of half-spherical particles consisting of approx. 12 atoms.

10.4 H_2 Chemisorption

The EXAFS technique normally can not be used to detect adsorbed hydrogen. It has proved to be extremely helpful, however, in calibrating H_2 chemisorption measurements. H_2 chemisorption is an easy technique to obtain qualitative information about the mean metal particle size in supported metal catalysts. To quantify the chemisorption results, an H/M surface stoichiometry of one was widely used. Since doubts existed about the exact H/M surface stoichiometry to be used, especially for the metals Ir and Rh, it was difficult to obtain accurate estimates of the particle size in highly dispersed catalysts.[7]

EXAFS was used to determine the metal particle size in catalysts with known H/M stoichiometries. For supported Pt, Rh, and Ir only fully reduced systems were used (Chapter 8). In the case of Ni, also partly reduced systems were measured (Chapter 9). When the results for the partly reduced systems were corrected for the degree of reduction, consistent results were obtained for all Ni catalysts. The average particle sizes were determined from the first shell metal-metal coordination number, using a half-spherical model for the metal particles. Using the correlation between EXAFS and H_2 chemisorption results, a calibration for the H_2 chemisorption measurements could be obtained. It was found that the surface stoichiometry increases in the order H/Ni < H/Pt < H/Rh < H/Ir, with H/Ni $\sim$ 1, H/Pt $\sim$ 1.5-2, H/Rh $\sim$ 2-2.5, and H/Ir $\sim$ 4. These differences in H/M surface stoichiometry are analogous to those observed in the molecular metal hydrides.

10.5 References

(1) J. H. A. Martens, *Thesis*; Eindhoven University of Technology, Eindhoven, the Netherlands, 1988.

(2) D. C. Koningsberger, J. B. A. D. Van Zon, H. F. J. Van 't Blik, G. J. Visser, R. Prins, A. N. Mansour, D. E. Sayers, D. R. Short, and J. R. Katzer, *J. Phys. Chem.* **1985**, *89*, 4075.

(3) J. B. A. D. Van Zon, D. C. Koningsberger, H. F. J. Van 't Blik, and D. E. Sayers, *J. Chem. Phys.* **1985**, *82*, 5742.

(4) D. C. Koningsberger, J. H. A. Martens, R. Prins, D. R. Short, and D. E. Sayers, *J. Phys. Chem.* **1986**, *90*, 3047.

(5) J. H. A. Martens, R. Prins, H. Zandbergen, and D. C. Koningsberger, *J. Phys. Chem.* **1988**, *92*, 1903.

(6) B. C. Gates, *Metal Clusters in Catalysis*; B. C. Gates, L. Guczi, and H. Knözinger, Eds.; Elsevier: Amsterdam, 1986; p 415.

(7) B. J. Kip, *Thesis*; Eindhoven University of Technology, Eindhoven, the Netherlands, 1987.

Samenvatting

De in dit proefschrift gebruikte techniek EXAFS (Extended X-ray Absorption Fine Structure) is bij uitstek geschikt voor de bestudering van metaal-op-drager katalysatoren. De directe omgeving van de metaalatomen in de katalysatoren wordt bestudeerd. De grote hoeveelheid drager in het monster (normaal zijn slechts enkele procenten metaal aanwezig) stoort nauwelijks bij de meting. Het metaaloppervlak is meestal het katalytisch actieve bestanddeel van de katalysator. Voor de meeste toepassingen is het belangrijk, het metaaloppervlak per hoeveelheid metaal zo groot mogelijk te maken en te houden: metalen als Rh, Ir en Pt zijn duur. Bij het verkrijgen van een goede dispersie (hoog metaaloppervlak) speelt de binding van het metaal aan de drager een grote rol. Met behulp van EXAFS kan men nauwkeurige informatie over het metaal-drager grensvlak krijgen.

Het metaal-drager grensvlak

Eén van de hoofdlijnen van dit proefschrift is de precieze bestudering van de binding tussen metaal en drager in katalysatoren. In de hoofdstukken 5 en 6 is de metaal-drager binding bestudeerd van $Ir_4(CO)_{12}$ op γ-Al_2O_3 na adsorptie en na reductie. Na adsorptie blijkt het metaalcarbonyl 2 CO liganden te hebben verloren. Er zijn 4 $Ir\text{-}O_{drager}$ bindingen ontstaan met R = 2.55 Å (dit houdt in dat er één Ir-Ir binding verbroken is). Er kan een model worden opgesteld waarin de geometrie van de Ir_4 kern intact blijft. Twee van de Ir atomen zijn elk met 2 Ir-O bindingen aan de drager gecoördineerd.

Na reductie van $Ir_4(CO)_{12}$ op γ-Al_2O_3 is een bijzonder systeem ontstaan. De metaaldeeltjes in katalysatoren zijn meestal driedimensionaal. Uit $Ir_4(CO)_{12}$ ontstaan echter platte deeltjes. Deze deeltjesvorm is bij uitstek geschikt om de metaal-drager binding te bestuderen: alle metaalatomen staan in contact met de drager. Uit de data analyse blijkt dat platte (111) deeltjes zijn gevormd. Ieder Ir atoom is drievoudig gecoördineerd aan drager zuurstof met R = 2.58 Å. Soortgelijke metaal-zuurstof afstanden waren al eerder gevonden voor Rh/γ-Al_2O_3 en Rh/TiO_2.

Uit de analyse van de hogere coördinatieschillen kon bovendien nog extra informatie verkregen worden over de epitaxie. (111) epitaxie kan namelijk op twee manieren voorkomen: (i) met de Ir atomen boven de Al_2O_3 zuurstofatomen uit de één-na-bovenste laag (hcp) of (ii) boven zuurstofatomen uit de twee-na-bovenste laag (fcc). De eerste mogelijkheid lijkt preferentieel voor te komen.

Modelsystemen

Bestudering van de metaal-drager binding is ook gebeurd aan de hand van modelsystemen (metaalcarbonylen op drager). Deze kunnen het voordeel hebben dat de metaalkernen in de katalysator éénduidig van vorm en grootte zijn, d. w. z. de oorspronkelijke metaalkern van de carbonylcomplexen blijft bij adsorptie bijhouden.

In hoofdstuk 3 is $Os_3(CO)_{12}$ op γ-Al_2O_3 bestudeerd. 2 CO liganden worden uitgewisseld voor drager zuurstof, met R_{Os-O} = 2.17 Å. Bij de adsorptie van $Ir_4(CO)_{12}$ (hoofdstuk 5) werd ook gevonden dat 2 CO liganden worden uitgewisseld, maar hier ontstaan 4 Ir-O bindingen met R = 2.55 Å. Onverwacht is het feit dat de Ir-O bindingen zo lang zijn. De verwachting was dat de coördinatieafstand vergelijkbaar zou zijn met die voor Os-O, omdat het type binding hetzelfde is. Een reden voor de grote Ir-O afstand zou sterische hindering door de CO liganden kunnen zijn (ze zijn in het geadsorbeerde cluster wat meer gebogen dan in $Ir_4(CO)_{12}$ zelf), maar ook de reduceerbaarheid van het metaal lijkt een rol te spelen.

De metaalcarbonylen op drager leveren ook interessante informatie over de metaal-CO coördinatie. IR metingen van de geadsorbeerde carbonylcomplexen bevestigen dat er alleen eindstandige CO liganden voorkomen. De M-C-O hoek is dan zó groot, dat meervoudige verstrooiing (multiple scattering) optreedt in de metaal-carbonyl zuurstof schil. Dit effect is sterk afhankelijk van de M-C-O hoek. In hoofdstuk 3 ($Os_3(CO)_{12}$ op γ-Al_2O_3) zijn de CO liganden nog als eenheid in de data analyse behandeld, d. w. z. er werd aangenomen dat er geen variatie optreedt in de C-O afstand en de Os-C-O hoek. Het bleek dat dit problemen opleverde bij de analyse van het monster na ontleding.

Zowel in hoofdstuk 5 ($Ir_4(CO)_{12}$ op γ-Al_2O_3) als in hoofdstuk 4 ($H_3Re_3(CO)_{12}$ en $[H_2Re_3(CO)_{12}]^-$) zijn de M-C en M-O bijdragen gescheiden

geanalyseerd. Uit de resultaten voor $H_3Re_3(CO)_{12}$ en $[H_2Re_3(CO)_{12}]^-$ blijkt dat de Re-CO coördinatie gevoelig is voor de lading op het complex: bij meer negatieve lading wordt de Re-C afstand kleiner en de C-O afstand groter, een gevolg van verminderde π-backbonding. In hoofdstuk 5 ($Ir_4(CO)_{12}$ op γ-Al_2O_3) bleek een soortgelijke tendens: de Ir-C afstand is groter, en de C-O afstand iets kleiner in het geadsorbeerd complex dan in $Ir_4(CO)_{12}$ zelf. Dit wijst op een positieve lading van het geadsorbeerd complex. Bovendien bleek dat de Ir-C-O hoek na adsorptie kleiner is. Dit is waarschijnlijk het gevolg van sterische hindering.

Nieuwe metaal-drager combinaties

In Eindhoven waren met EXAFS de Rh/γ-Al_2O_3 en Rh/TiO_2 systemen uitgebreid bestudeerd. In beide gevallen werden lange Rh-O bindingen (R ~ 2.7 Å) in het metaal-drager grensvlak gevonden. Eén van de hoofddoelen van mijn onderzoek was, na te gaan of een dergelijke binding ook bij andere metaal-drager combinaties voorkomt. Dit blijkt inderdaad het geval voor Ir/γ-Al_2O_3 (R_{Ir-O} = 2.55-2.58 Å, zie hoofdstuk 6) en Ir/MgO en Rh/MgO (R_{Ir-O} = 2.54 Å en R_{Rh-O} = 2.68 Å, zie hoofdstuk 7). De metaalatomen in het grensvlak blijken drievoudig aan drager zuurstof gecoördineerd te zijn in Ir/γ-Al_2O_3 ((111) epitaxie), en viervoudig in Ir/MgO en Rh/MgO ((100) epitaxie).

Morfologie van de metaaldeeltjes

EXAFS blijkt informatie te kunnen leveren over de deeltjesvorm van het metaal in katalysatoren. In hoofdstuk 6 zijn twee Ir/γ-Al_2O_3 katalysatoren vergeleken, één bereid uit $Ir_4(CO)_{12}$ en één uit $IrCl_3$. Uit de analyse van de hogere coördinatieschillen bleek dat de tweede Ir-Ir schil ontbreekt in het monster, gemaakt uit $Ir_4(CO)_{12}$. Dit is een duidelijke aanwijzing dat de metaaldeeltjes hier platte (111) deeltjes zijn: de tweede Ir-Ir schil komt alleen voor tussen twee opeenvolgende (111) lagen.

H_2 chemisorptie

EXAFS is een dure techniek en bovendien is meettijd niet altijd beschikbaar. Het is goed mogelijk om met EXAFS de gemiddelde grootte van de metaaldeeltjes in een katalysator te bepalen, maar voor veel metalen is

een chemisorptietechniek (bijv. met H_2) veel eenvoudiger. Echter, bij metalen als Ir, Rh en Pt treden problemen op bij de quantificering van de chemisorptieresultaten omdat de adsorptiestoechiometrie op kleine metaaldeeltjes niet precies bekend is.

In hoofdstuk 8 is voor een aantal Ir, Rh en Pt katalysatoren zowel een H_2 chemisorptiemeting als een EXAFS meting gedaan. Duidelijk blijkt dat er een trend in oppervlaktestoechiometrie is: H/Ir > H/Rh > H/Pt, analoog aan de volgorde in stoechiometrie van hun metaalhydriden. Voor kleine metaaldeeltjes is H/Pt $\sim$ 1.5-2, H/Rh $\sim$ 2-2.5 en H/Ir $\sim$ 4. Dezelfde vergelijking tussen EXAFS en H_2 chemisorptiemetingen is in hoofdstuk 9 getrokken voor Ni katalysatoren. Dit onderzoek wees uit dat de techniek ook bruikbaar is voor gedeeltelijk gereduceerde systemen, als de resultaten voor beide metingen worden gecorrigeerd voor de reductiegraad.

List of Publications

The chapters of this Thesis are based on the following publications:

Chapter 3:

Structures of Alumina-Supported Osmium Clusters ($HOs_3(CO)_{10}\{OAl\}$) and Complexes ($Os^{II}(CO)_{n\,=\,2\ or\ 3}\{OAl\}_3$) Determined by Extended X-ray Absorption Fine Structure Spectroscopy

F. B. M. Duivenvoorden, D. C. Koningsberger, Y. S. Uh, and B. C. Gates, *J. Am. Chem. Soc.* **1986**, *108*, 6254.

Chapter 4:

Structural Characterization of $[H_xRe_3(CO)_{12}]^{x-3}$ ($x = 2,3$) by Extended X-ray Absorption Fine Structure Spectroscopy

F. B. M. Van Zon, P. S. Kirlin, B. C. Gates, and D. C. Koningsberger, *J. Phys. Chem.* accepted.

Chapter 5:

An EXAFS Study of $Ir_4(CO)_{12}$ Adsorbed on Partially Dehydrated γ-Al_2O_3: Applicability as a Model for Reduced Ir/γ-Al_2O_3 Catalysts

F. B. M. Van Zon, A. D. Van Langeveld, J. Van Grondelle, and D. C. Koningsberger, to be published.

Chapter 6:

Study of the Metal-Support Interface in a γ-Al_2O_3 Supported, Reduced $Ir_4(CO)_{12}$ Catalytic System by Extended X-ray Absorption Fine Structure (EXAFS)

F. B. M. Van Zon, G. J. Visser, and D. C. Koningsberger, *Proc. 9th Int. Congress on Catalysis*; M. J. Phillips, and M. Ternan, Eds.; Chemical Institute of Canada: Ottawa, 1988; Vol. III, p 1386.

Metal Particle Morphology and Structure of the Metal-Support Interface in Ir/γ-Al_2O_3 Catalysts Studied by EXAFS Spectroscopy

F. B. M. Van Zon, and D. C. Koningsberger, *J. Chem. Phys.* submitted.

Chapter 7:

A Structural Characterization of the Metal-Support Interface in Reduced Ir/MgO and Rh/MgO Catalyst Systems

F. B. M. Van Zon, L. M. P. Van Gruijthuijsen, D. E. Sayers, and D. C. Koningsberger, to be published.

Chapter 8:

Determination of Metal Particle Size of Highly Dispersed Rh, Ir, and Pt Catalysts by Hydrogen Chemisorption and EXAFS

B. J. Kip, F. B. M. Duivenvoorden, D. C. Koningsberger, and R. Prins, *J. Am. Chem. Soc.* **1986**, *108*, 5633.

Determination of the Metal Particle Size of Supported Pt, Rh, and Ir Catalysts. A Calibration of Hydrogen Chemisorption by EXAFS

F. B. M. Duivenvoorden, B. J. Kip, D. C. Koningsberger, and R. Prins, *J. de Phys. C8* **1986**, *47*, 227.

Determination of Metal Particle Size of Highly Dispersed Rh, Ir, and Pt Catalysts by Hydrogen Chemisorption and EXAFS

B. J. Kip, F. B. M. Duivenvoorden, D. C. Koningsberger, and R. Prins, *J. Catal.* **1987**, *105*, 26.

Chapter 9:

Determination of Metal Particle Size in Partly Reduced Ni Catalysts by Hydrogen/Oxygen Chemisorption and EXAFS

P. W. J. G. Wijnen, F. B. M. Van Zon, and D. C. Koningsberger, *J. Catal.* accepted.

Other publications:

Laboratory EXAFS Spectrometer, Principles and Applications

F. W. H. Kampers, F. B. M. Duivenvoorden, J. B. A. D. Van Zon, P. Brinkgreve, M. P. A. Viegers, and D. C. Koningsberger, *Solid State Ionics* **1985**, *16*, 55.

The Effect of Gas Environment (H_2, O_2) on the Structural Properties of Small Iridium Metal Particles Supported on γ-Al_2O_3 as Determined by EXAFS

D. C. Koningsberger, F. B. M. Duivenvoorden, B. J. Kip, and D. E. Sayers, *J. de Phys. C8* **1986**, *47*, 255.

An EXAFS Study of the Luminescent Bi^{3+} Center in $LaPO_4$-Bi

F. B. M. Van Zon, D. C. Koningsberger, E. W. J. L. Oomen, and G. Blasse, *J. Solid State Chem.* **1987**, *71*, 396.

Design, Synthesis, and Characterization of Surface Catalytic Sites Prepared from $[HRe(CO)_5]$ and $[H_3Re_3(CO)_{12}]$: Mononuclear, Trinuclear, and Metallic Rhenium Catalysts Supported on MgO

P. S. Kirlin, F. B. M. Van Zon, D. C. Koningsberger, and B. C. Gates, to be published.

Dankwoord

Bij deze wil ik graag bedanken:

- mijn ouders, die mij een fijne studie hebben laten volgen en me altijd met hun belangstelling hebben gesteund
- Diek Koningsberger, die door zijn onstuitbaar enthousiasme mijn promotietijd nuttig èn plezierig heeft gemaakt
- Roel Prins, voor de begeleiding tijdens Diek's verblijf in de U. S. A.
- Stephan Bouwens, Joop van Grondelle, Frans Kampers, Bert Kip, Jan Martens en Peter Wijnen (allen TUE), Marjan Botman en Hans den Hartog (RU Leiden), en Jos Steijger voor hun hulp bij de EXAFS metingen in Daresbury (G. B.)
- de groep C/T van de Centrale Technische Dienst, voor het maken en repareren van de EXAFS cellen en toebehoren, die in Daresbury gebruikt werden
- NWO, voor de meettijd in Daresbury en het beschikbaar stellen van reisgeld
- Gert Jan Visser, voor het 'onderhoud' van de data analyse programmatuur, en de hulp bij het lezen van tapes en het implementeren van nieuwe programmatuur
- Adelheid Elemans, Wout van Herpen en Henk van Lieshout, voor de 'gewone' routineklusjes
- de koffieclub, waarvan nog niet genoemd Ad de Koster, Hans Niemantsverdriet, Dick van Langeveld, Leo van Gruijthuijsen en Kumi Pandya, voor alle (klets)koek.

I would like to thank the staff of the SRS at Daresbury for their friendly assistance both at convenient and inconvenient hours. Special thanks are to Greg Diakun, Paul Moir-Riches, Paul Naylor, and Alf Neild.

Also, I would like to thank prof. Gates and his staff for the samples and the EXAFS measurements of the Chapters 3 and 4.

En tot slot, in het bijzonder bedank ik Hans, die als achtereenvolgens collega, vriend, echtgenoot en mede-ouder altijd een steuntje in de rug was.

Curriculum Vitae

Fanny van Zon werd geboren als Francisca Barbara Maria Duivenvoorden op 30 mei 1960 in Voorschoten. Na in Elst (Gld.) de lagere school te hebben doorlopen, volgde zij de VWO-B opleiding aan de R. K. Scholengemeenschap Canisius College-Mater Dei te Nijmegen. Het eindexamen werd behaald in 1978.

In september van dat jaar startte zij met de studie Scheikunde aan de Katholieke Universiteit te Nijmegen. Het kandidaatsexamen (richting S2) werd cum laude behaald op 28 september 1981. Het doctoraalexamen werd, eveneens cum laude, behaald op 16 april 1984, met als hoofdvakken Vaste Stof Chemie (o. l. v. prof. dr. P. Bennema) en Katalyse (o. l. v. prof. dr. ir. J. W. E. Coenen).

Van 1 juni 1984 tot 1 juni 1988 was zij in dienst van de Technische Universiteit Eindhoven, vakgroep Anorganische Chemie en Katalyse, waar zij onder leiding van dr. ir. D. C. Koningsberger het in dit proefschrift beschreven onderzoek verrichtte.

Op 19 juni 1986 trouwde zij met Hans van Zon, en op 22 juni 1988 werd hun zoon Paul geboren.

Stellingen

behorende bij het proefschrift van
Fanny van Zon

Eindhoven, 22 november 1988

1

Liu et al. beweren op grond van XPS metingen dat Cu ionen geen rol spelen in de methanolsynthese over Cu-ZnO-Al_2O_3 katalysatoren. Echter, gezien het ruisniveau van hun spectra kan niet uitgesloten worden dat het monster enkele procenten Cu ionen bevat. Bovendien is niet zeker dat koper oxide stabiel is onder de UHV omstandigheden van de XPS meting.

D. Liu, Q. Zhu en J. Li, *Proc. 9th Int. Congress on Catalysis* (Calgary, 1988); M. J. Phillips en M. Ternan, Eds.; Chemical Institute of Canada: Ottawa, 1988; p 577.

2

Bij reacties van CO over katalysatoren wordt i. h. a. de vorming van CO_2 beschouwd als het bewijs voor de dissociatieve adsorptie van CO (Boudouard reactie), en de afwezigheid van CO_2 ontwikkeling als het bewijs voor het niet optreden ven CO dissociatie. Hierbij worden eenvoudige alternatieven over het hoofd gezien, nl. dat CO_2 vorming ook het gevolg kan zijn van reductie door CO van een promotor oxide, en dat de afwezigheid van CO_2 ontwikkeling kan betekenen dat de reactie van geadsorbeerd CO en O niet verloopt.

3

Mehandru et al. passen hun parameters aan wanneer ASED (Atom Superposition and Electron Delocalization) MO berekeningen van CO op Pt_3Ti verkeerde resultaten opleveren. Deze foutieve resultaten kunnen mogelijk ook verklaard worden door een verkeerde formulering van de repulsieve energie.

S. P. Mehandru, A. B. Anderson en P. N. Ross, *J. Catal.* **1986**, *100*, 210.

A. B. Anderson, *J. Chem. Phys.* **1975**, *62*, 1187.

A. B. Anderson, R. W. Grimes en S. Y. Hong, *J. Phys. Chem.* **1987**, *91*, 4245.

4

Het effect, geconstateerd door Ramsteiner en Wagner, dat het schuiven naar hogere frequentie van de hoofdpiek in het Ramanspectrum van koolstoffilms met toenemende energie van de ingestraalde laserbundel onafhankelijk is van de filmdikte, kan geheel verklaard worden door het feit dat de informatiediepte van Ramanspectroscopie aan koolstof slechts 50 nm is.

M. Ramsteiner en J. Wagner, *Appl. Phys. Lett.* **1987**, *51*, 1355.

I. M. Robinson, M. Zakikhani, R. J. Day, R. J. Young en C. Galiotis, *J. Mat. Sci. Lett.* **1987**, *6*, 1212.

5

Het overgangsgebied zoals dat bij reactief magnetron sputteren gemeten wordt in de curve die de depositiesnelheid weergeeft als functie van de partiële druk van het reactieve gas, wordt ter verklaring gefit aan een theoretisch model. Bij het opstellen van die modellen wordt echter geen rekening gehouden met het feit dat de gemeten druk beïnvloed wordt door diffusie effecten.

T. Abe en T. Yamashima, *Thin Solid Films* **1975**, *30*, 19.

6

Het verschil tussen Pt en Re als verstrooiend atoom is niet voldoende om uit EXAFS metingen aan Pt-Re/Al_2O_3 katalysatoren alleen te concluderen aan welke buren de diverse bijdragen toe te schrijven zijn. Hiervoor moet extra informatie gebruikt worden, bijv. EXAFS metingen aan Re/Al_2O_3 en Pt/Al_2O_3 katalysatoren met vergelijkbare dispersie.

G. Meitzner, G. H. Via, F. W. Lytle en J. H. Sinfelt, *J. Chem. Phys.* **1987**, *87*, 6354.

7

Foutloos kunnen spellen is tegenwoordig meer een teken van een ouderwetse, dan van een goede opleiding.